STRUCTURE-PROPERTY RELATIONS IN SILOXANE-BASED MAIN CHAIN LIQUID CRYSTALLINE ELASTOMERS AND RELATED LINEAR POLYMERS

A Dissertation
Presented to
The Academic Faculty

by

Wanting Ren

In Partial Fulfillment
of the Requirements for the Degree
Doctor of Philosophy in the
School of Polymer, Textile & Fiber Engineering

Georgia Institute of Technology
August 2007

STRUCTURE-PROPERTY RELATIONS IN SILOXANE-BASED MAIN CHAIN LIQUID CRYSTALLINE ELASTOMERS AND RELATED LINEAR POLYMERS

Approved by:

Dr. Anselm C. Griffin, Advisor
School of Polymer, Textile & Fiber Engineering
Georgia Institute of Technology

Dr. David M. Collard
School of Chemistry and Biochemistry
Georgia Institute of Technology

Dr. Satish Kumar
School of Polymer, Textile & Fiber Engineering
Georgia Institute of Technology

Dr. John D. Muzzy
School of Chemical & Biomolecular Engineering
Georgia Institute of Technology

Dr. Mohan Srinivasarao
School of Polymer, Textile & Fiber Engineering
Georgia Institute of Technology

Date Approved: June 26, 2007

ACKNOWLEDGEMENTS

I would like to thank my advisor, Dr. Anselm C. Griffin, for his great guidance, support and encouragement during my PhD study and research.

I would like to thank my committee members, Dr. David M. Collard, Dr. Satish Kumar, Dr. John D. Muzzy and Dr. Mohan Srinivasarao, for their many suggestions for my thesis.

I would like to thank my former group member, Dr. Philip J. McMullan, for his guidance in my synthesis work and constructive suggestions.

I would like to thank my friends, Dr. Huina Guo, Marilyn Minus and Sudhakar Jagannathan, for their kind help during my research.

I would like to thank National Textile Center (M04-G21) for financial support.

I would like to thank my parents, Zhaoying Ren and Jinyu Liu, my brother, Xiankun Ren, my sister-in-law, Ying Su, my lovely niece, Jiawen Ren, my husband, Zheng Li, my parents-in-law, Guilan Qiu and Xiangting Li, for their endless love and support.

TABLE OF CONTENTS

Page

LIST OF TABLES

Page

LIST OF FIGURES

Page

SUMMARY

Soft materials, such as colloids, polymers and liquid crystals, have attracted much scientific and technical interest in recent years. In this thesis, attention has been placed on the underpinning relations between molecular structure and properties of one type of soft matter - main chain liquid crystalline elastomers (MCLCEs), which may have application as shape memory or as auxetic materials. In this work, a number of siloxane-based MCLCEs and their linear polymer analogues (MCLCPs) were synthesized and examined. In addition to the often employed chemical variations, such as siloxane spacer length, crosslinker content, lateral substituents on mesogenic monomers; additional chemical variations, such as rigid *p*-phenylene transverse rod and flat-shaped anthraquinone (AQ) mesogenic monomers were incorporated into MCLCEs and MCLCPs.

Thermal and X-ray analysis found the presence of a smectic C phase in most of the main chain LCEs synthesized in this work. The formation of lamellar structures is due to the strong self-segregation tendency of siloxane spacers, hydrocarbon spacers and mesogenic rods. The smectic C mesophase of the parent LCE was not grossly affected by incorporating terphenyl transverse rods, although they apparently decreased the clearing temperature and broadened the mesophase-isotropic phase transition peak. A smectic A phase was only found in a MCLCE with a *p*-phenylene transverse rod. Strong characteristic π-π stacking was found in both MCLCEs with fluoro substituted mesogenic monomers and MCLCEs with AQ LC monomers.

The relations between chemical structure and mechanical properties were intensively studied in this work. The typical three-region stress-strain curve and a

polydomain-to-monodomain (*P-M*) transition were observed in most of our MCLCEs. It was found that a short hydrocarbon spacer, a short siloxane spacer, high crosslinking content and mesogenic monomer with symmetrical structure generally result in stiffer materials with higher Young's moduli, higher threshold stress to the *P-M* transition, shorter *P-M* transition plateaus, lower elongation at break and higher tensile strength. Specifically, in the strain recovery experiments of MCLCEs a significant dependence of strain retention on the initial strains was found. However, chemical variations such as the crosslinker content and the lateral substitutes on the mesogenic rods do not show much influence on strain retention abilities, although those chemical variations greatly affect the above-mentioned mechanical properties. The combination of elastic and anelastic recovery is discussed with attention drawn to the *P-M* transition and the temperature dependence of the strain recovery process. The MCLCE with *p*-phenylene transverse rod for potential auxetic materials showed a highly ordered smectic A mesophase at room temperature with high stiffness. The unusual molecular architecture of the *p*-phenylene transverse rod provides opportunities for the rod orientation to be parallel or normal to the main chain under uniaxial tension. The model with *p*-phenylene transverse rods normal to the main chain is most likely due to X-ray analysis. Mechanical properties of MCLCEs with AQ monomers exhibit a strong dependence on the specific combination of hydrocarbon spacer and siloxane spacer, which also strongly affects the formation of π-π stacking between AQ monomers. Poisson's ratio measurement over a wide strain range found distinct trends of Poisson's ratio as a function of the crosslinker content as well as terphenyl transverse rod loadings in its parent MCLCEs.

CHAPTER 1

Introduction

1.1 Introduction to Liquid Crystals

The liquid crystalline (LC) state is a separate state of matter from that of a gas, liquid or solid. This term is used to describe a phase showing molecular order similar to a crystal but it can flow like a viscous liquid [1]. The first liquid crystal was observed by a young Austrian botanist, Friedrich Reinitzer, in 1888, when he studied the melting behavior of cholesteryl benzoate and described it as having two melting points [2]. This substance is a cloudy liquid if heated to a temperature between the two melting points, but becomes clear above the upper melting point, typical of the phase behavior for liquid crystals. The cloudy liquid was later named as "liquid crystal" by Lehmann [3] and Vorlander [4]. Lehmann also combined a heating stage with a polarizing microscope to observe the phase behaviors of liquid crystals at elevated temperatures [3]. This technique remains one of the most important methods to study liquid crystals.

To date, a large number of liquid crystals have been synthesized and the structural requirements for giving liquid crystalline phases have generally been well understood [1]. In order to form a liquid crystal phase (also called a mesophase), a molecule is likely to be structurally anisotropic and often will possess a permanent dipole as well as high anisotropy of polarizability.

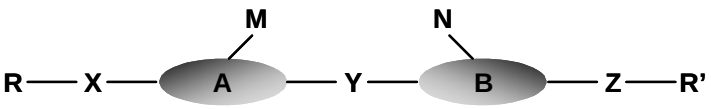

Figure 1-1 Schematic representation of the general structure of a calamitic liquid crystal [5].

Figure 1-1 shows a rigid rod-like molecule, which is the most common feature of liquid crystals [1, 5, 6]. These are also called calamitic LCs. In this structure, A and B are core units that are most often aromatic (e.g., 1,4-phenyl, 2,6-naphthyl, 2,5-pyrimidinyl, etc.). Linearity and polarizability anisotropy of the core is maintained by the linking group Y, which can be an ester group, ethylene group, azo group, imine group, etc. or a direct link. M and N are lateral substituents (e.g. -F, -Cl, $-CH_3$, -CN, etc.) that are often used to modify the mesophase type and physical properties. Lateral substituents can disrupt the molecular packing yet are often advantageous for the formation of liquid crystal phases. The rigid cores themselves usually are not sufficient to generate liquid crystal phases. Flexible terminal groups (R and R') are often introduced to rigid cores directly or through linking groups X and Z in order to lower the melting point and stabilize the molecular alignment in liquid crystalline phase. Alkyl or alkoxy chains are the most often used terminal groups.

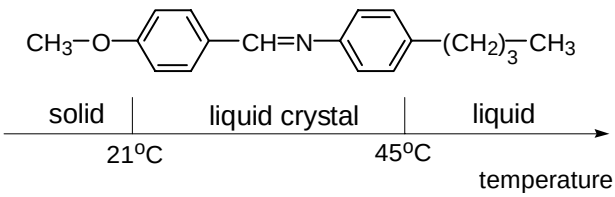

Figure 1-2 Chemical structure of n-(*p*-methoxybenzylidene)-*p*-butylaniline (MBBA) [7].

For example, n-(*p*-methoxybenzylidene)-*p*-butylaniline (MBBA) is a typical calamitic LC as shown in Figure 1-2. In this molecule, an imine group connects two aromatic rings. The linearity of the molecule is preserved by the *1,4-* connections at opposite points on the benzene rings. Two different flexible terminal groups, a methoxy group and a butyl

group, are attached to each end. MBBA exhibits a stable nematic liquid crystalline phase at room temperature [7].

Liquid crystals can be classified into thermotropic LCs [8] and lyotropic LCs [9]. Thermotropic LCs consist of mesogenic molecules by themselves (no solvent) and their mesophase transitions occur as a functional of temperature. Lyotropic LCs contain mesogenic molecules and solvents as well. They exhibit mesophase transitions as a function of concentration and of temperature. In this work, all the LC monomers, LC polymers and elastomers are of the thermotropic type.

In a liquid crystal, the director *n* is often used to describe the preferred molecular orientation. The degree of molecular orientational order is evaluated by the order parameter *S*, which can be calculated by Hermann's equation 1-1 [10].

$$S = \frac{3\left\langle Cos^2\varphi \right\rangle - 1}{2} \tag{1-1}$$

where φ is the angle between the long molecular axis and the director. $<Cos^2\varphi>$ represents the average value of $Cos^2\varphi$ over many LC molecules. S = 1 means a perfect orientation of LC molecules along the director; S = 0 represents a completely random orientation of molecules.

According to the type of mesophase, calamitic LCs can be generally classified into nematic, smectic and cholesteric phases [1] as illustrated schematically in Figure 1-3. The nematic phase has no positional order but does have long range orientational order. A cholesteric LC is also called a chiral nematic LC and has a periodically twisted structure about an axis normal to the director. The chirality typically comes from the

presence of an asymmetric carbon atom in the molecules.

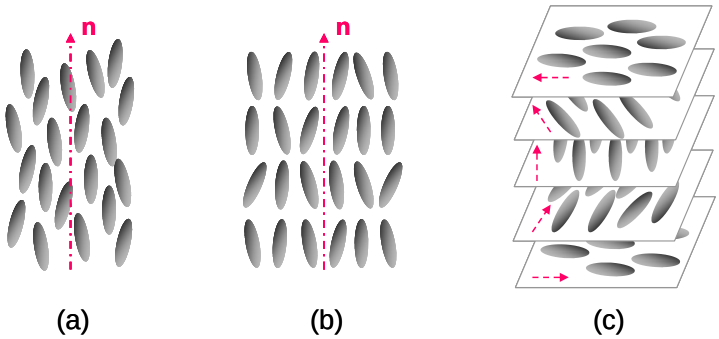

Figure 1-3 A schematic representation of the molecular organization of classical liquid crystals: (a) nematic; (b) smectic; (c) cholesteric or chiral nematic.

The smectic LC phase has a layered structure often resulting from the segregation of terminal chains of rod molecules onto common planes. Furthermore, the smectic LC phase has a number of variations [1, 7]. Among them, smectic A and smectic C are the two most common ones. As shown in Figure 1-4, the director of smectic A is parallel to the layer normal and the director of smectic C tilts at an angle to the layer normal [7].

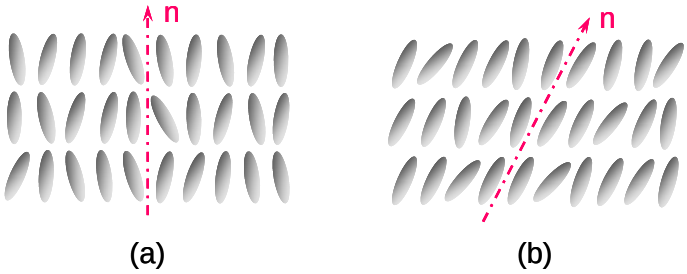

Figure 1-4 Schematic representations of liquid crystalline phases: (a) smectic A; (b) smectic C.

In addition to a rod-like shape, LC molecules can also possess a disc-like shape. These molecules are called discotic LC and often have a flat aromatic core. Figure 1-5 gives an example of a discotic LC molecule which has a rigid and planar center with hydrocarbon terminal chains pointing to all directions [7].

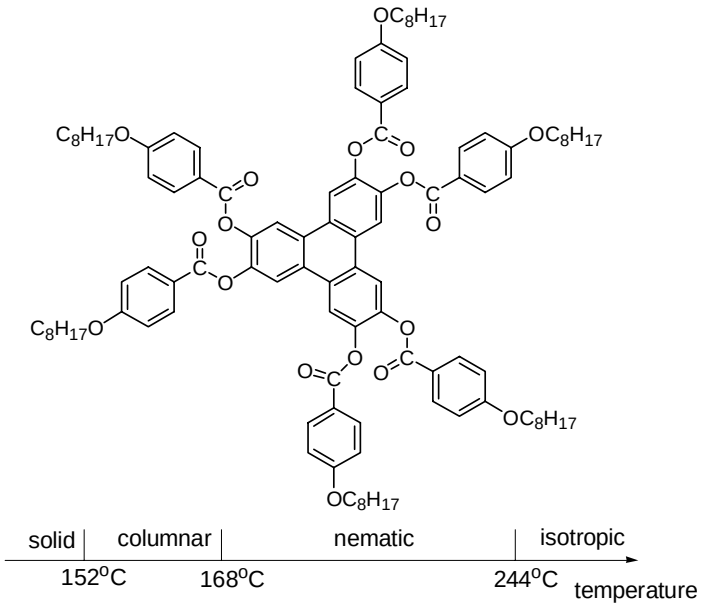

Figure 1-5 Chemical structure and phase diagram of a typical discotic LC molecule [7].

The flat rigid molecules can pack and form a nematic discotic or can pack into stacks and form a columnar discotic phase as illustrated in Figure 1-6 (a) and (b), respectively.

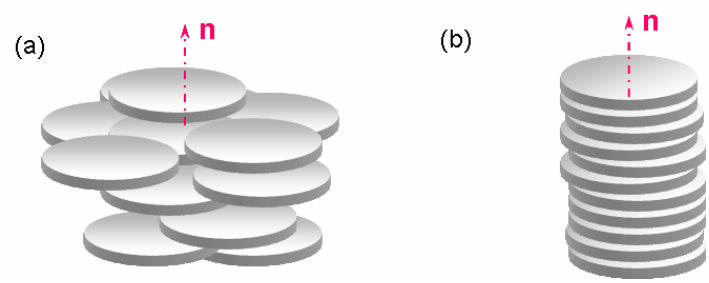

Figure 1-6 A schematic representation of discotic liquid crystals: (a) nematic discotic; (b) columnar discotic [7].

Furthermore, these columns can organize themselves into a more regular structure, such as rectangular columnar arrays in Figure 1-6 (a) or hexagonal arrays in Figure 1-6 (b) [7].

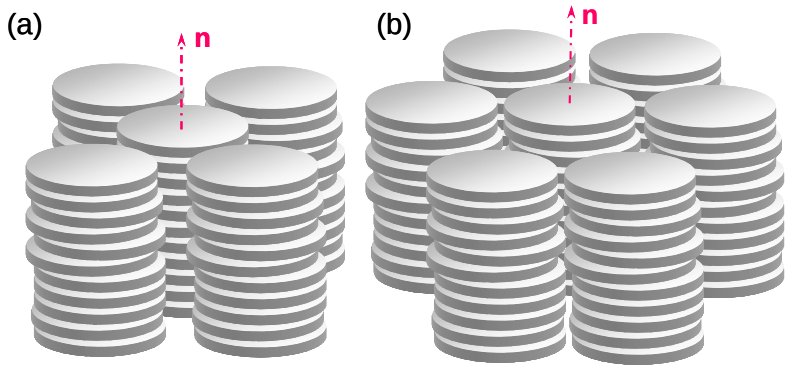

Figure 1-7 A schematic representation of columnar liquid crystals: (a) rectangular columnar; (b) hexagonal columnar [7].

Polarized optical microscopy, differential scanning calorimetry and X-ray diffraction are three main techniques used to identify the liquid crystalline phases. The principles of each technique as well as the examples for LC optical textures, DSC profiles and X-ray diffraction patterns of LC phases will be introduced in detail in Chapter 2.

1.2 Introduction to Liquid Crystalline Polymers

Liquid crystalline polymers (LCPs) combine mesophase features of low molar mass liquid crystals (e.g. high anisotropy, self-assembly and ease of orientation) with versatile properties of polymers (e.g. toughness, ease of processing, light weight). Early in the 1950s, Onsanger [11] and Flory [12] independently predicted in theory that it was possible for a polymer to have liquid crystalline phases.

Incorporating mesogens onto the polymer backbone as pendants or into the polymer main chain produces two types of LCPs, side-chain LCPs (SCLCPs) and main-chain LCEs (MCLCPs). Industrial demands for high-performance polymers inspired the development of all aromatic LCPs. One of the early commercialized main chain LCPs, *Kevlar,* as shown in Figure 1-8 is a LCP exhibiting outstanding heat and flame resistance, ultrahigh strength and modulus [13].

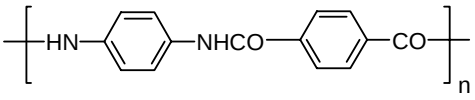

Figure 1-8 Chemical structure of *Kevlar*[13].

However, since the melting point (> 500ºC) of *Kevlar* is higher than its decomposition temperature, the LCP has to be dissolved in a strong solvent, such as sulphuric acid, to form a lyotropic solution for processing.

An effective approach to reduce the transition temperature into a useful working range is adding flexible chains (also called spacers) between rigid mesogens or attaching rigid rods onto a polymer backbone via flexible spacers as illustrated in Figure 1-9 [14].

Figure 1-9 Reducing the transition temperature of liquid crystalline polymers by introducing flexible spacers: (a) main chain liquid crystalline polymers; (b) side chain liquid crystalline polymers [14].

These LCPs can exhibit nematic and smectic phases depending on the organization of mesogenic groups and flexible spacers (as parts of the backbone or as side chains to connect mesogenic units to the backbone). The chemical constitution of these components dictates the way in which they organize [14]. For SCLCPs, long flexible spacers tend to induce smectic phases due to the segregation of flexible spacers forming a layered structure. Short intervals between pendant groups also tend to induce the formation of smectic phases because the rotational and translational motions of mesogenic groups are restricted by short spacers. On the contrary, long intervals encourage nematic phases [14, 15]. For MCLCPs, due to the statistically random

distribution of the rod-like mesogenic units along the backbone, the nematic is the most favorable phase. Formation of a smectic phase is possible if the mesogenic units are regularly distributed on the backbone so that layers can form [1, 14].

1.3 Introduction to Liquid Crystalline Elastomers

Liquid Crystalline Elastomers (LCEs) combine orientational ordering of mesogens with rubber elasticity of polymer networks [15]. In LCEs, the network structure limits the motion of the entire molecule but does not significantly affect the motion of mesogens due to the low crosslinking density. In a lightly crosslinked LCE, the netpoints are far apart so that the motions of chain segments on a smaller length scale are relatively independent from the deformation of netpoints [15, 16]. Therefore, the mesogens in the network have enough freedom to establish liquid crystalline order independently on a microscopic length scale [17].

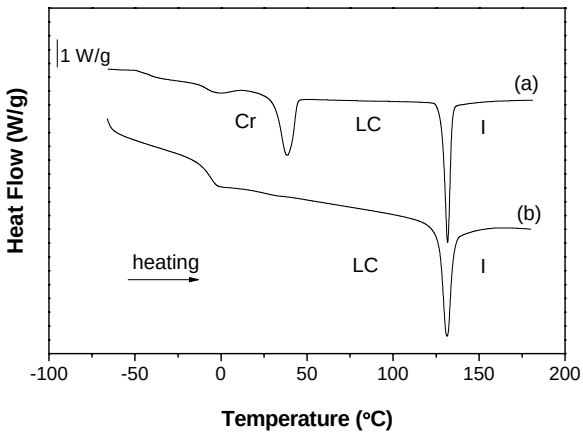

Figure 1-10 DSC traces of two LC materials prepared in this work: (a) a LCP; (b) a LCE with low crosslinking density. Cr: crystalline phase; LC: liquid crystalline phase; I: isotropic phase.

For instance, DSC traces in Figure 1-10 show no significant changes in the mesophase to

isotropic transition temperature of a lightly crosslinked LCE compared with its LCP analogue, although the partial crystallization in the LCP was disrupted by the crosslinking process. Typical rubber elasticity is retained in weakly crosslinked LCEs. Mechanical orientation of polymer chains results in the decrease of entropy of the whole network, which is a thermodynamically unstable condition. After removal of the external stress, the polymer chains tend to go back to the coiled state to increase the entropy of the system. Therefore, the macroscopic elastic response comes from the negative entropy change of polymer chains upon stretching.

Similar to the classification of LCPs, LCEs can also be classified into side chain LCEs and main chain LCEs based on the placement of mesogenic units on the polymer backbone as illustrated in Figure 1-11 [16, 18].

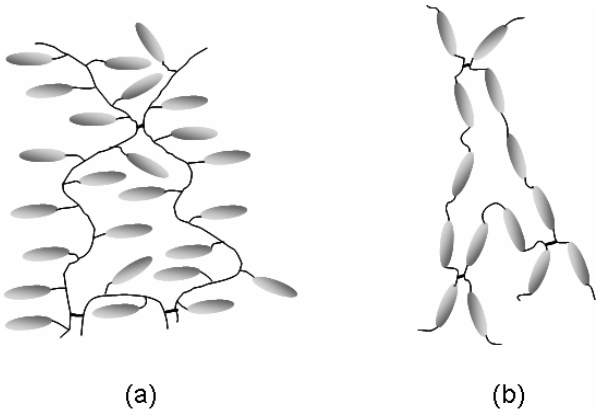

Figure 1-11 Schematic representations of two main types of liquid crystalline elastomers: (a) side-chain LCEs; (b) main-chain LCEs.

Since the pioneering work of Ringsdorf and Finkelmann describing the necessity to decouple pedant groups from the backbone [19], side-chain LC polymers (SCLCPs) and their side-chain LC elastomer (SCLCE) analogues have been designed, synthesized and applied to a variety of scientific and technical interests – from nonlinear- [20, 21]and

electro-optics [22] to tunable lasing media [23] to large photo- [24, 25] and thermo-mechanical actuations [26, 27] over the past two decades. Early in 1975, de Gennes predicted that main-chain LCEs are potential candidates to effectively couple orientational order and mechanical strain because of the direct incorporation of mesogens into the polymer main chains [28]. However, due to the low solubility and high transition temperature of main-chain LC polymers, it has proved difficult to produce the corresponding MCLCEs by crosslinking, which has limited the exploitation of MCLCEs. Recently, Finkelmann *et al.* reported a facile route to prepare MCLCEs having a low glass transition temperature through a hydrosilylation reaction [29].

1.4 Synthesis and Properties of Liquid Crystalline Elastomers

1.4.1 Synthesis of Liquid Crystalline Elastomers

There are two basic approaches to form crosslinks in liquid crystalline polymers. One is forming crosslinks during a polymerization process via the introduction of polyfunctional crosslinkers. The other is crosslinking a preformed polymer backbone. Since the preformed polymer can be easily cast into an appropriate form before crosslinking, the second method was an often used approach [16, 30].

1.4.1.1 Synthesis of Side-chain Liquid Crystalline Elastomers

Over the last two decades, side-chain liquid crystalline elastomers have been intensively studied [19, 31-34]. In fact, the first synthesized liquid crystalline elastomer was a siloxane-based side-chain LC elastomer [19]. This type of material could be synthesized in one step, in which both the monofunctional mesogenic monomer and bifunctional crosslinking agent were added onto the backbone simultaneously. It was

assumed that the monomer and crosslinker were statistically distributed along the polysiloxane backbone [19].

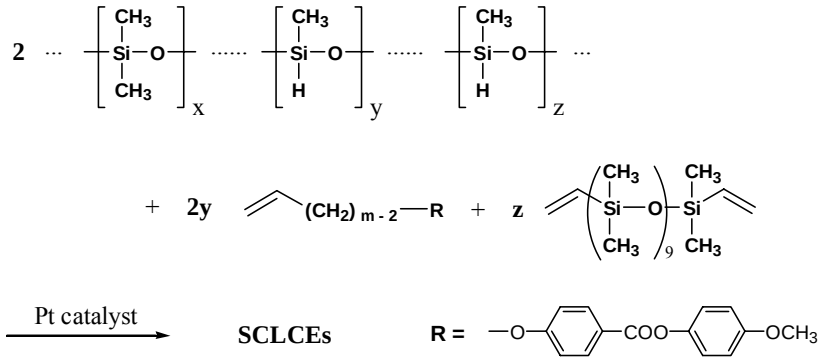

Figure 1-12 An example for synthesis of siloxane-based side-chain liquid crystalline elastomer in one step by Finkelmann *et. al*[19].

Another example for synthesizing siloxane-bases side-chain LC elastomer by Clarke *et al.* is shown in Figure 1-8 [35]. Polysiloxane backbones with Si-H functional group were substituted by mesogenic monomer containing a vinyl group via an addition reaction in the presence of platinum catalyst. After that, a trifunctional crosslinking agent was added to connect the preformed polymer backbone via the reaction between the vinyl groups of the crosslinker and unreacted Si-H groups on the backbone.

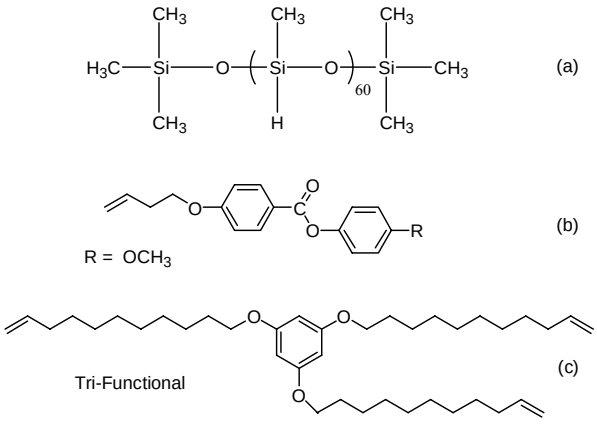

Figure 1-13 An example for crosslinking preformed polysiloxane side-chain LC elastomer with a trifunctional crosslinker by Clarke *et. al*. (a) polysiloxane backbone; (b) monomer; (c) crosslinker [35].

In addition to polysiloxane type of backbone, polyacrylates were also used as backbone chains. For example, Zentel *et. al.* synthesized side chain LC polyacrylates or polymethacrylates via radical copolymerization [31]. The preformed LC polymer has a small amount of functional hydroxyl groups, which can react with hexamethylene diisocyanate or methylenebis-(1.4-phenylene) diisocyanate to form network structures as shown in Figure 1-14. The chemical variations of the comonomers (e.g. the ratio between the monomer with mesogenic groups and the one with hydroxyl groups, hydrocarbon spacer length and terminal groups on side chain) and crosslinkers are listed in the attached table.

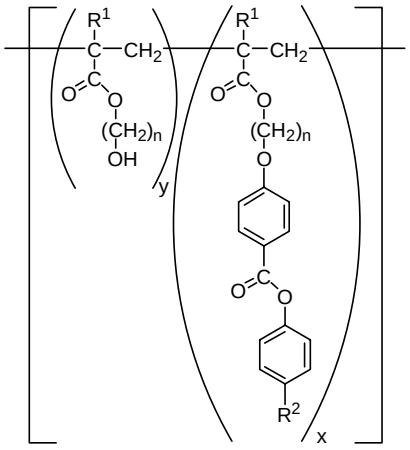

1-5

	R^1	R^2	*n*	*x : y*
1	CH_3	OCH_3	6	100:5
2	CH_3	$O(CH_2)_3CH_3$	6	100:5
3	H	OCH_3	6	100:5
4	H	OCH_3	2	100:5
5	H	CN	6	100:8

1a-5a: 1-5 crosslinked with OCN-$(CH_2)_6$-NCO

1b-5b: 1-5 crosslinked with

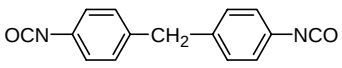

Figure 1-14 An example for synthesis of polyacrylate-based side-chain liquid crystalline elastomer by Zentel *et. al* [31] **.**

1.4.1.2 Synthesis of Main-chain Liquid Crystalline Elastomers

Compared with side-chain liquid crystalline elastomers, main-chain LC elastomers have been less investigated. The main reason is that the low solubility of the preformed linear LC polymers and the high transition temperature of the final main chain

LCEs reduced the interest of researchers in preparing them.

Zentel and Reckert prepared the MCLCEs with siloxane-based crosslinker in 1986 [31]. Figure 1-15 shows the chemical structures of precursor linear polymer and the crosslinker. The precursor linear main-chain liquid crystalline polymers were prepared via a solution polycondensation of the diol with allylmalonic acid or by a melt polycondensation of the diol and diethyl allylmalonate. A α,ω-bifunctionalized oligosiloxane reacted with the double bond on the polymer backbones as a crosslinking agent [31]. The mesophase of the precursor linear polymers were retained in the elastomers. Compared with the precursor linear polymer, lower phase transition temperatures were found in the elastomer because of the presence of flexible oligo(dimethylsiloxane) unit in the crosslinker.

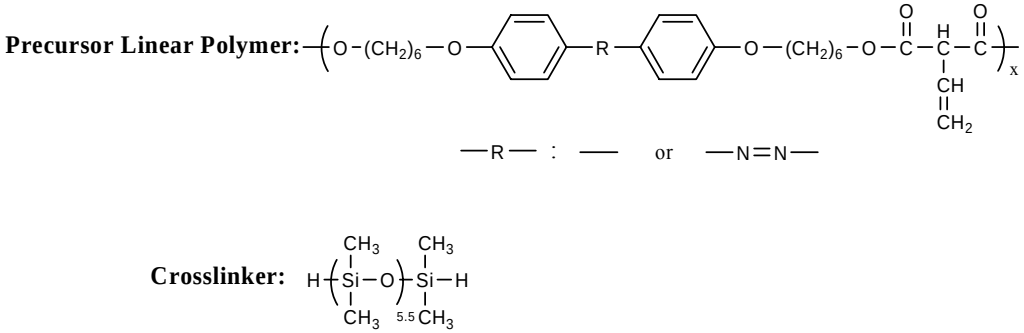

Figure 1-15 Chemical structures of precursor LC polymers and crosslinker by Zentel *et al.* [31].

In 1997, Bergmann *et al.* reported that they synthesized near room temperature nematic main-chain LCEs as shown in Figure 1-16 [36]. Semiflexible polyether chains were first prepared by phase-transfer catalyzed polyetherification of mesogens with a dibromoalkane. The polymers were then end-capped by an alkenyl-functionalized monomer.

Crosslinking preformed polyether :

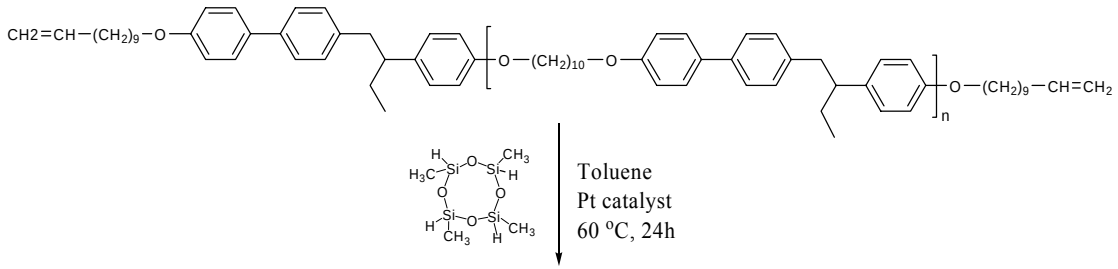

Figure 1-16 Synthesis of a main chain LCE by Bergmann *et al.* [36].

The linear polyethers were crosslinked by the hydrosilylation reaction between the terminal double bonds from the polyether and the Si-H groups of the tetrafunctional cyclosiloxane crosslinker. The synthesized LCEs have similar phase behaviors to their precursor linear polymers. No crystalline structures were found in the LCPs and LCEs. This was attributed to the long flexible alkyl chains in the polymer backbone and lateral ethyl groups on the mesogens preventing crystallization upon cooling [36].

In 2000, Finkelmann *et al.* reported a facile method to synthesize siloxane-based main-chain LCEs in one step [29] as shown in Figure 1-17.

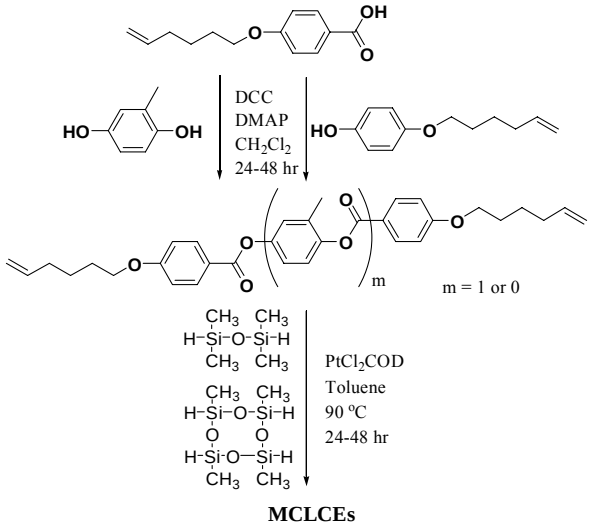

Figure 1-17 Synthesis of a main chain LCE by Finkelmann *et al.* [36].

In this method, no precursor linear polymers need to be synthesized in advance. Linear chain extension and crosslinking take place simultaneously. In this method, main-chain LCEs are obtained in one pot by platinum-catalyzed hydrosilylation of double bonds in mesogenic monomers with reactive equimolar Si-H groups in both the spacer and the crosslinker. Only dialkenyl mesogenic monomers are required to be synthesized. Both spacer (oligosiloxane) and crosslinker (cyclosiloxane) are commercially available. In addition, the crosslinking density can be better controlled by this method. Smectic C and nematic types of mesophase were observed in the synthesized MCLCEs.

1.4.2 Properties of Polydomain Liquid Crystalline Elastomers

The coupling of rubber elasticity of network structures and orientational order of mesogenic groups distinguishes the liquid crystalline elastomers from conventional elastomers. In this section, we will discuss the basic and typical properties of LCEs, mainly focusing on their thermal behavior and mechanical properties.

1.4.2.1 Thermal Behavior of Liquid Crystalline Elastomers

There are a number of chemical structure factors that affect the thermal behavior of LC elastomers, such as the overall flexibility of the polymer backbone, the nature of the mesogenic monomer, the type and length of spacer, the degree and type of crosslinking and so on.

The backbone flexibility greatly affects the glass transition temperature of LC elastomers. The glass transition temperature of siloxane-based elastomers is much lower than that of acrylate-based or methacrylated-based LC elastomers [19, 31]. This is because the rotation of Si-O bond is easier than that of a C-C bond. The Si-O bond is

longer than the C-C bond. The bond angle of Si-O is also larger than that of C-C. In addition, no additional substituents on the oxygen atom also make Si-O bond rotation easier than C-C bond rotation. Normally, if room temperature mesophases are required, siloxane-based LC elastomers are good materials of choice.

The glass transition of LCEs is also affected by the spacer length. Here, we use acrylate-based side-chain LC elastomers made by Zentel *et al.* as examples. The synthesis of these LCEs has been introduced in section 1.4.1.1. Increasing the number of methylene units on the side chain from two to six results in a 30 ºC decrease in the glass transition temperature of these materials [31].

Crosslinks usually induce a higher value of the glass transition temperature because of the additional constraints on segmental movement of polymer chains imparted by netpoints [34]. However, a low level of crosslinking does not make a significant change on transition temperatures as seen in Figure 1-18, so that the thermal behavior of those LC elastomers is similar to their LCP analogues [19, 31, 37].

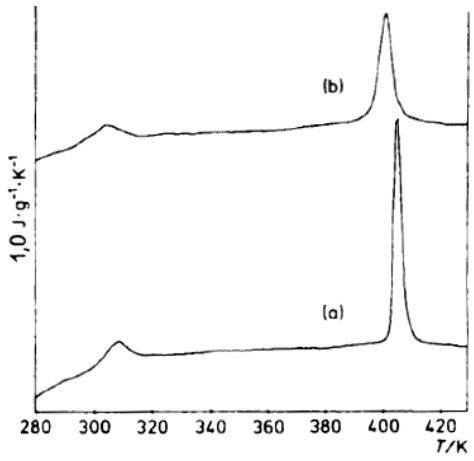

Figure 1-18 DSC measurement of a uncrosslinked main chain LC polymer (a) and the corresponding crosslinked LC elastomer (b), heating rate 20K/min [31]**.**

Compared with their LCP analogues, a low crosslinking density leads to a small decrease or increase (± 5K) in mesophase transition temperature by DSC measurement [31, 33, 38]. Decreasing or increasing mesophase transition temperature depends on the nature of employed crosslinking agents and the change in molecular weight before and after crosslinking. A decrease in transition temperature could result form non-mesogenic crosslinkers, which could disturb the LC order [16]. An increase in transition temperature occurs if an increase of the molecular weight accompanies the crosslinking process [16].

1.4.2.2 Mechanical Properties of Liquid Crystalline Elastomers

Normally, initially formed LC elastomers are in a polydomain state if no special measures were taken. A domain refers to a special area having its own preferred orientation. A polydomain LCE has many domains, whose local orientation misaligns with each other. Therefore, a polydomain LCE has no uniform global orientation in its mesophase [15, 35, 39-42]. Easy orientation of mesogenic groups in LC elastomers is a prominent feature [32, 43]. Hence, monodomain LCEs could be obtained by aligning the separate domains. It was found that a small elongation (~ 20% strain) is enough to form reversible monodomain structures in some SCLCEs [32, 44] but larger elongation is needed to pre-align polydomain MCLCEs [41, 45].

A typical nominal stress-versus-nominal strain curve of LC elastomers can be divided into three regions as shown in Figure 1-19 (a). The corresponding order parameter, *S*, of the material developed by extension as a function of applied stress is illustrated in Figure 1-19 (b).

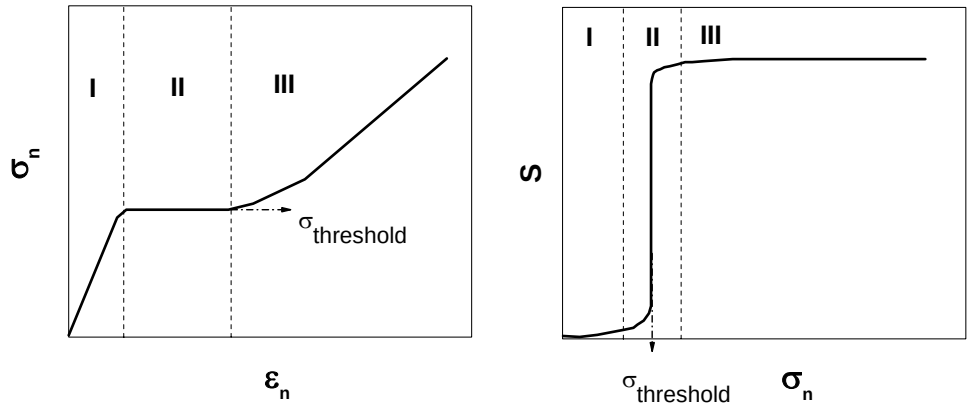

Figure 1-19 Schematic representation of a typical stress-strain curve of a LC elastomer and corresponding order parameter as a function of stress [42].

The three-region non-linear stress-strain behavior had been universally observed for LCEs [22, 26, 31, 33, 46-48]. In the first region, a linear stress-strain relationship is seen at small strains accompanied by a non-linear increase in the order parameter. The material behaves like a conventional rubber. In the second region, a stress plateau corresponding to a polydomain-to-monodomain (*P-M*) transition appears at medium strains.

The *P-M* transition is one of the unique features of LC elastomers. Optically, the originally opaque (polydomain) sample becomes transparent (monodomain) with extension as illustrated in Figure 1-20.

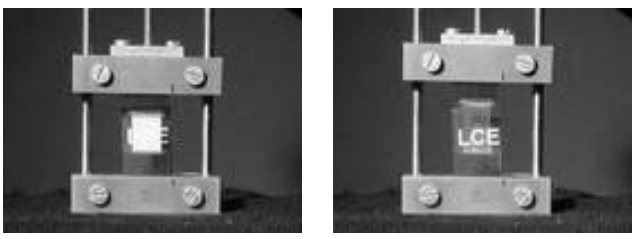

Figure 1-20 An originally opaque polydomain LCE (left) becomes transparent monodomain LCE (right) after P-M transition [15].

A dramatic increase in order parameter occurs within this region at a critical stress. In the third region, the *P-M* transition is finished and the stress starts to increase with applied strain again. But only a small amount of further orientation can be achieved in this region. The unique *P-M* transition has been observed experimentally in a variety of LCEs [35, 39-42, 49, 50].

One of the popular conjectures for *P-M* transition is that the transition takes place through the reorientation of individual domains rather than through domain growth [50-53]. Terentjev schematically illustrated this *P-M* transition in Figure 1-22. Under a uniaxial tension, the overall orientation of mesogens in a polydomain LC elastomer can be easily changed by the rotation of individual domains [54].

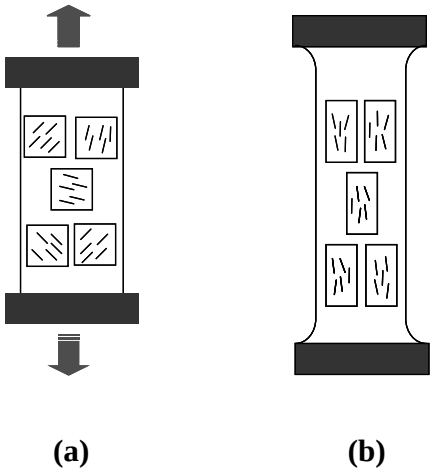

Figure 1-21 Schematic representation of a stretched a polydomain nematic elastomer undergoing a polydomain-to-monodomain transition by Terentjev [54].

In a polydomain LC elastomer, the polymer backbones within individual domains orient along the local director. Throughout the overall network, the director of each domain misaligns so that there is no ordering on a large-scale. The average domain size is about a few microns [35]. Since the domain size in a polydomain sample is close to

the wavelength of visible light and with the misalignment of the refractive index of individual domains, the local director field strongly scatters the light. Therefore, a polydomain sample is usually opaque. Applying uniaxial extension to a polydomain elastomer forces individual domains to rotate and local directors align along the stretching direction. Optically, the sample gradually becomes transparent upon stretching. Polydomain-to-monodomain transition plateau on the stress-strain curve is a macroscopic reflection of the microscopic reorientation of LC domains.

According to theoretical studies by Warner and Terentjev, the polydomain-to-monodomain transition plateau is also called the soft elastic region [55, 56]. The elongation of a polydomain LC elastomer network accompanies rotation of domains, which can be achieved without a large stress response. The plateau region is attributed to the relaxation of internal stress caused by the reorientation of local nematic directors via domain rotation along the stretching direction. Theoretically, ideal soft elasticity refers to a behavior of a material that can be uniaxially deformed without resistance [15]. In practice, this unusual soft elasticity effect of LCEs makes themselves potential candidates as efficient damping materials and artificial muscles [15].

Weakly crosslinked LC elastomers show elastic behavior in both isotropic and LC phases. This elastic behavior has been observed in side-chain LC elastomers [19, 32, 44, 57, 58] and main-chain and combined main-chain/side-chain LC elastomers [16, 34, 41]. Above the mesophase to isotropic phase transition temperature, $T_{lc\text{-}i}$, LC elastomers are isotropic rubbers, similar to conventional elastomers. Below $T_{lc\text{-}i}$, LC elastomers are anisotropic rubbers showing highly temperature-dependent and time-dependent behavior [58, 59]. Figure1-22 shows the stress-strain curves of a side-chain LC polyacrylate

measured by Terentjev *et al.* at different temperatures at a constant strain rate [58].

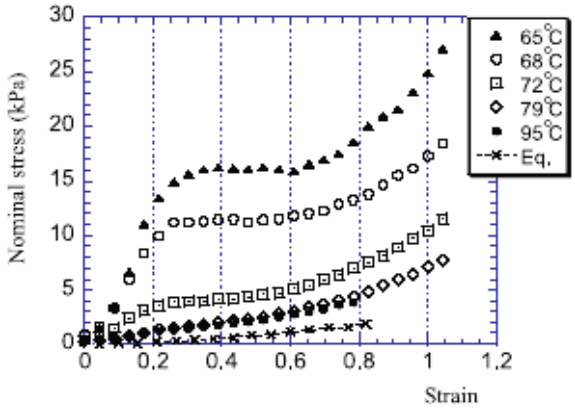

Figure 1-22 Stress-strain curves of a side chain LCE at different temperatures at a fixed strain rate [58].

The nematic-isotropic transition temperature of this LCE is ~90 ºC. During the experiment, the specimen state varied from the mesophase to the isotropic phase at elevated temperatures. The soft plateau region corresponding to *P-M* transition is seen between the strains of 0.2-0.6. The modulus and the length of soft plateau decrease with temperature. At a temperature above its clearing temperature, the stress-strain curve of the LCE is very similar to that of a conventional rubber.

The stress-strain behaviors of this LCE were also studied at different strain rates at a constant temperature (T) well below nematic transition (T_{ni}) as shown in Figure 1-23. At each strain rate, the data points on the stress-strain curve were obtained by this way, in which the specimen was extended in a small instant step and relaxed for a certain fixed time before the next step. Lower modulus and longer plateau region were observed by decreasing the strain rate [58].

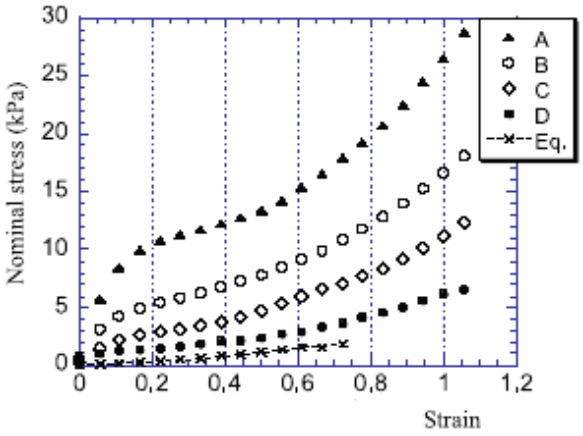

Figure 1-23 Stress-strain curves of a side chain LCE at different strain rates (A > B > C > D > Eq.) at a fixed temperature ($T/T_{ni} = 0.94$) [58].

1.4.3 Monodomain Liquid Crystalline Elastomers

Under certain circumstances, monodomain LC elastomers prepared through a mechanical extension can keep the chain orientation and strain temporarily without secondary crosslinking [41, 60]. Since these mechanically induced monodomain samples are not thermodynamically stable, their polydomain texture will recover if they are heated up to the isotropic state and then cooled below their clearing temperature.

Crosslinking the pre-aligned LCEs is an effective way to obtain stable monodomain LCEs. Two approaches have been sucessfuly used to produce monodomain LCEs. The first method is to pre-align parent LCPs in a magnetic field and then crosslink them. After heating this monodomain LCE to its isotropic phase and then cooling it back to its nematic phase, the originally macroscopic orientation of the nematic director is completely recovered [61, 62]. The second approach is first to mechanically pre-align a weak crosslinked LCE in its mesophase. A secondary crosslinking was then given to the pre-aligned elastomer. Therefore, a uniform director alignment is locked-in by the additional chemical links [22, 49].

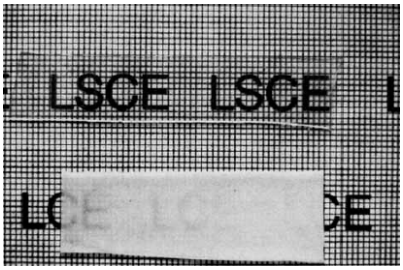

Figure 1-24 A monodomain LCE (above) prepared by two-stage crosslinking and its corresponding polydomain LCE (below) [22].

These monodomain LCEs are also called liquid single crystal elastomers (LSCE) [49]. Figure 1-24 shows a monodomain LCE produced by the latter method and its corresponding polydomain LCE. Both nematic LSCE [22, 24, 63, 64] and smectic LSCE [65-70] have been prepared by following the second approach. Highly anisotropic physical properties were found by Clarke in these monodomain LC elastomers, especially the reorientation process when the material was stretched in the direction perpendicular to the director [64]. Figure 1-25 gives examples to illustrate this interesting phenomenon.

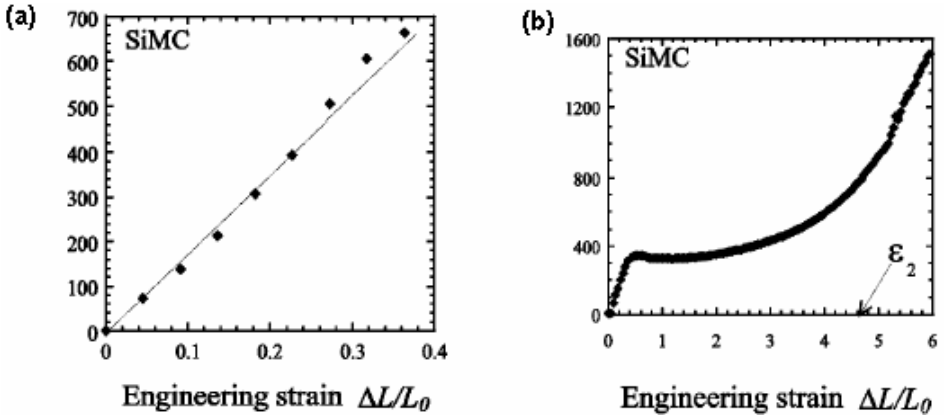

Figure 1-25 Stress-strain curves obtained by stretching a polysiloxane side chain monodomain LCE parallel to nematic director (a) and perpendicular to nematic order (b) [64].

It was found that the parallel modulus is much higher than the perpendicular modulus. The monodomain LCE being stretched perpendicular to its nematic director showed a plateau region in the stress-strain curve, which is similar to the polydomain-to-

monodomain transition of a polydomain LCE. According to the soft elasticity theory by Warner *et. al*, this plateau region corresponds to the rotation of nematic director, which follows a low energy deformation soft pathway as illustrated by Figure 1-26 [15].

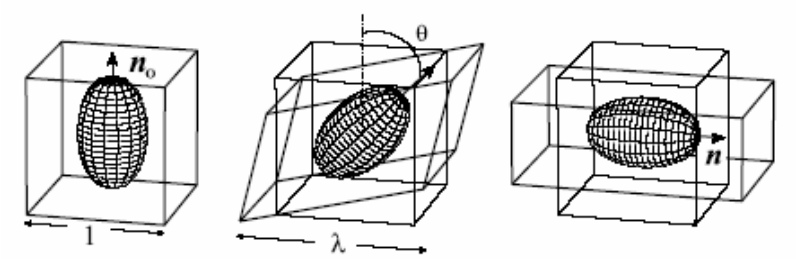

Figure 1-26 Soft deformation of a nematic elastomer through the director rotation [15].

The coupling between orientational order of mesogenic units and polymer backbone is a critical factor influencing the properties of the monodomain LCEs. Main chain LCEs with mesogenic units incorporated directly in the backbone will present higher coupling than side chain LCEs. Therefore, more dramatic soft elastic response will be expected from main chain LCEs. It was observed that side chain LCEs can undergo 50-60% elongation without energy cost, while main chain LCEs can bear above 300% elongation [15].

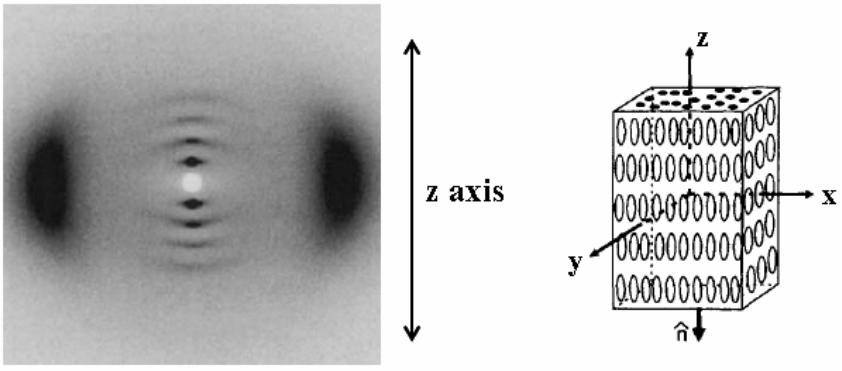

Figure 1-27 X-ray diffraction pattern and schematic sample geometry of a monodomain smectic A LCE by Finkelmann *et al.* [65]**.** The smectic layer normal is parallel to the z-axis.

Compared with nematic monodomain elastomers, smectic monodomain elastomers have been less studied. In 1997, Nishikawa *et. al* reported their investigations on side chain monodomain smectic LCEs. The X-ray diffraction study of the monodomain elastomers detected the macroscopically uniform alignment of molecules along the applied mechanical field (along z axis) while forming the monodomain structure and also identified smectic A mesophases in the monodomain LCEs as shown in Figure 1-27. All the mesogens have a preferred orientation along the z-axis. A layered structure forms in the x-y plane [65].

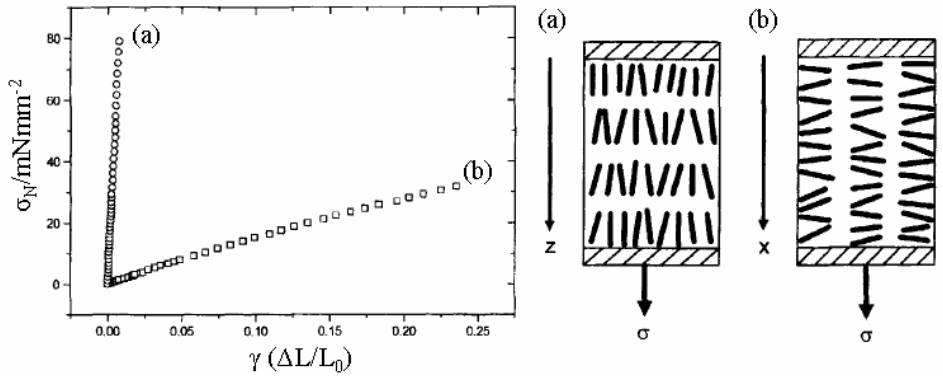

Figure 1-28 Stress-strain curve of a monodomain LCE being stretching parallel (a) and perpendicular (b) to the smectic layer normal (along the z-axis) [65].

A large modulus difference between the directions *parallel* and *perpendicular* to the layer normal was observed in the monodomain LCE as shown in Figure 1-28. The modulus parallel to the layer normal is much higher than the modulus perpendicular to the layer normal. The former is about 75 times larger than the latter. It was also found that, when the material was stretched and elongated in the direction *perpendicular* to the layer normal (along x-axis), there was no shrinkage in the film width (along z-axis) as shown in Figure 1-29.

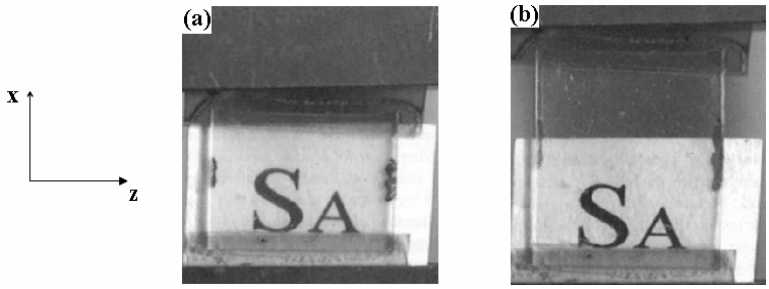

Figure 1-29 Photograph of a monodomain smectic A elastomer: (a) without strain; (b) under 80% extension [65].

The film thickness shrinks along the y-axis to keep the film volume approximately constant. The preserved film width in z-direction indicates a constant number of layers was kept during the film elongation along the x-axis, which indicates the molecules do not transfer across the layers along the z-axis. The film thickness shrinkages without a width change during the film deformation could come from the fluidity of mesogenic units in the x-y plane [65]. They found a completely different behavior in this monodomain elastomer when it was stretched in the direction *parallel* to the layer normal as shown in Figure 1-30.

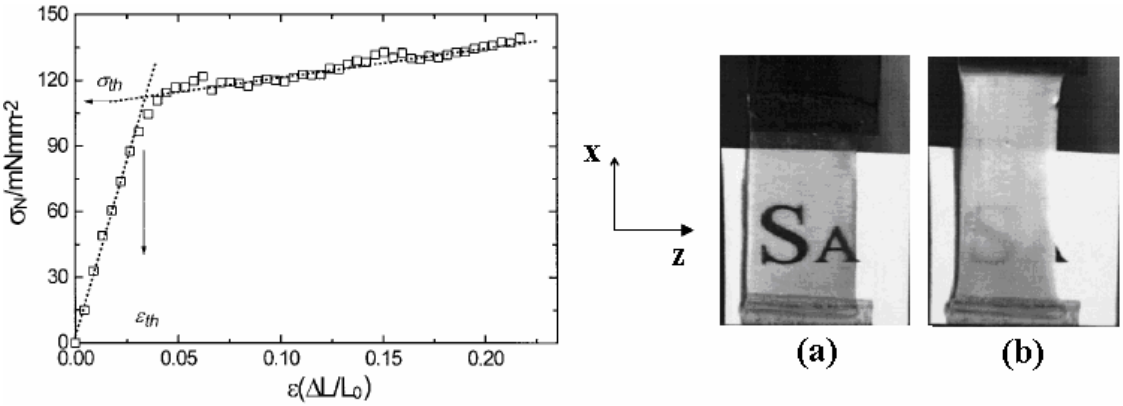

Figure 1-30 Stress-strain curve and photograph of a monodomain smectic elastomer being stretched in the direction parallel to the smectic layer normal: (a) without strain; (b) with 40% strain [66].

In the stress-strain curve, the modulus decreases remarkably at around 3% strain.

Optically, the smectic film remained translucent before the threshold strain (< 3%) but became opaque at larger strains (> 4%). X-ray studies found that an undulation of smectic layer occurs in the specimen before the threshold strain. At higher strains, the undulated smectic layers broke down and separated into small pieces [66]. Therefore, the film became opaque similar to the appearance of a polydomain LCE film.

1.5 Applications of Liquid Crystalline Elastomers

In this work, we are interested in the study of structure-property relationships in main chain liquid crystalline polymers and elastomers. They have potential applications as shape memory materials. And they are also useful as parent systems to explore molecular auxetic materials (negative Poisson's ratio materials). We will introduce these two types of materials and the applications.

1.5.1 Shape Memory Materials

Shape memory effect (SME) refers to a phenomenon in that the deformation in a material can be fixed temporarily by a process of programming (e.g. heating up, deformation and cooling down, etc.) and can later recover to its permanent shape via external stimuli, as shown in Figure 1-29.

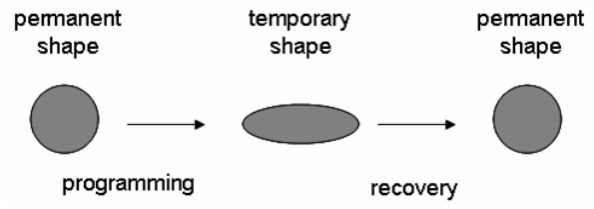

Figure 1-31 Schematic representation of shape memory effect [71].

The external stimulus could be temperature, light, electrical field, magnetic field, pH change, etc. If a shape change is caused by a temperature change, it is called a thermally induced shape memory effect [71].

The shape memory effect was first discovered in a gold-cadmium metallic alloy in 1951 [72]. Since then, many shape memory alloy (SMA) systems have shown shape memory effect, such as Ni-Ti, Cu-Zn-Al, Fe-Ni-C, Fe-Mn-Si alloys and others [71, 73]. SMAs have many advantages, such as biocompatibility, reversible shape memory, superelasticity, thermal stability. Their disadvantages, however, like high cost, low strains (<8%), and processing difficulties encouraged researchers to develop new materials showing a shape memory effect. Polymeric materials appeared to be attractive and appropriate candidates [71].

The development of polymer materials having a shape memory effect started in the 1960s, For example, polyethylene covalently crosslinked through ionizing irradiation, was broadly applied as heat shrinking film or tubing [74, 75]. Later on, a wide range of thermoplastic polymers and crosslinked polymers showing shape memory effect were developed, which has been thoroughly reviewed by Lendlein and Kelch [71]. Figure 1-32 gives an example of a shape memory copolymer transforming from a temporary spiral shape to the permanent rod shape at 46ºC.

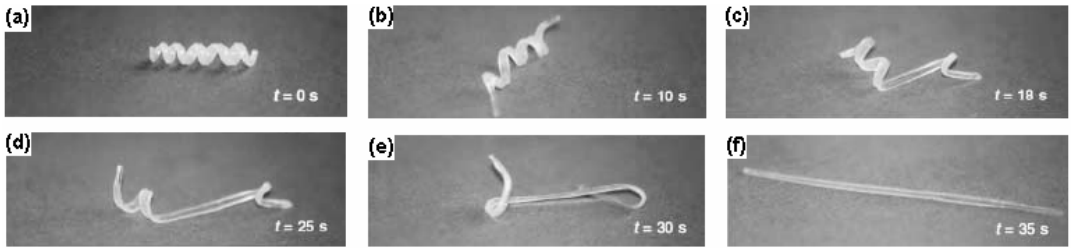

Figure 1-32 A shape memory polymeric rod changes from a temporary spiral shape to the permanent rod shape [71].

This material was synthesized from poly(ε-caprolatone)dimethacrylate and butylacrylate (comonomer) [71].

1.5.1.1 Molecular Mechanism of Thermally Induced Shape Memory Polymers

Shape memory polymers often contain network structures, which can arise through a physical or chemical crosslinking. Network structures allow large deformations above a certain transition temperature, like the glass transition temperature (T_g) or the melting temperature (T_m). Both of them can be the switching temperature between a temporary shape and a permanent shape. Below the switching temperature, the switching segment is much less flexible and the temporary shape can be fixed after removal of the external force. Above the switching temperature, the switching segment is flexible and the permanent shape can be recovered.

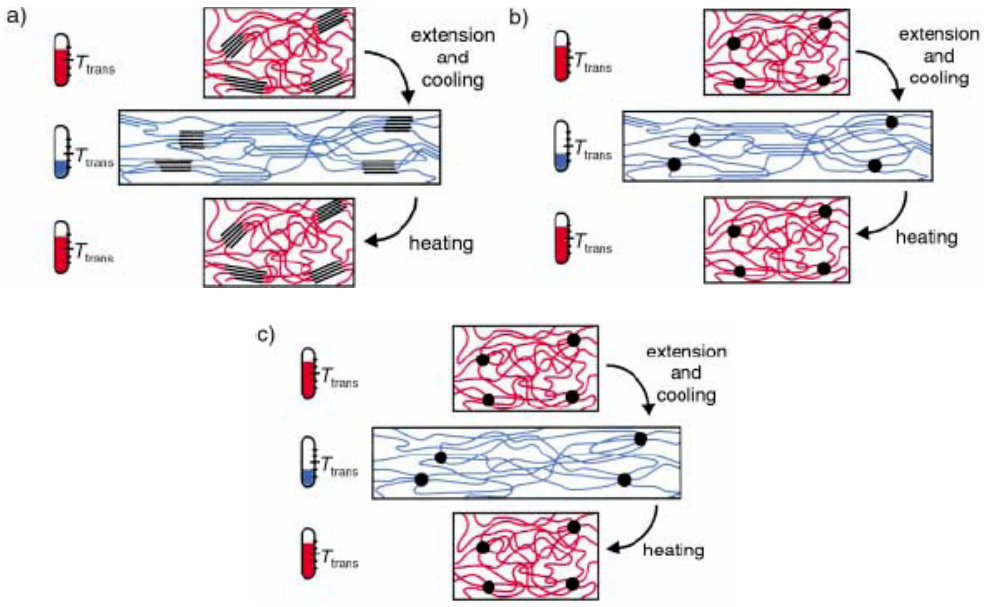

Figure 1-33 Schematic illustration of the molecular mechanism of thermally induced shape memory effect for (a) physically crosslinked multiblock copolymer ($T_{trans} = T_m$); (b) chemically crosslinked polymer ($T_{trans} = T_m$); (c) chemically crosslinked polymer ($T_{trans} = T_g$) [71]

The molecular mechanism of programming the temporary shape and recovering the permanent shape is schematically illustrated in Figure 1-33 [71]. In Figure 1-33 (a) and (b), the melting temperature of the switching segment is the switching temperature. The temporary shape of the material is fixed by deforming it above the switching temperature and then cooling it below the switching temperature. The difference between (a) and (b) is that the former has the physical crosslinks and the latter contains the chemical crosslinks. Their permanent shape is stabilized by the crystallites (the physical netpoints) formed by the segments with higher melting point in the case of (a) or covalent netpoints in the case of (b). In these two cases, the switching segments can form stress-induced crystallites initiated by cooling the material after being stretched above the switching temperature. The induced crystallites prevent the polymer chains from immediately going back the coiled structure after removal of the load. By heating these materials up to their melting temperatures, the stress-induced crystallites melt and the materials recover to their permanent shape. Figure 1-33 (c) shows another chemically crosslinked polymer, the glass transition temperature acts as the switching temperature in the shape memory process. The permanent shape in this case is stabilized by the covalent netpoints. The movements of the switching segments are frozen below the glass transition temperature, which stabilizes the temporary shape after removal of the external force. The permanent shape can be recovered by heating above the glass transition temperature [71].

Shape memory materials obtain their temporary shapes through the programming process. After heating up to the switching temperature, the material recovers its permanent shape and looses its temporary shape at the same time. After cooling down

the material below the switching temperature again, no temporary shape recovery could be achieved. This is called an one-way shape memory material [71]. For example, a one-way shape memory effect was observed in polydomain LCEs [60]. If the permanent shape and temporary shape can be repeatedly formed back and forth by heating or cooling through the switching temperature [73], it has two-way shape memory.

1.5.1.2 Liquid Crystalline Polymers and Elastomers with Shape Memory Effect

The shape memory effect of liquid crystalline polymers and elastomers are known [60, 70, 76-79]. These materials have attracted much attention recently because of their potential applications as artificial muscles [80, 81].

In 2003, Ratna *et al.* prepared a side chain LC elastomer fiber having a shape memory effect [78]. The components of the material are shown in Figure 1-34.

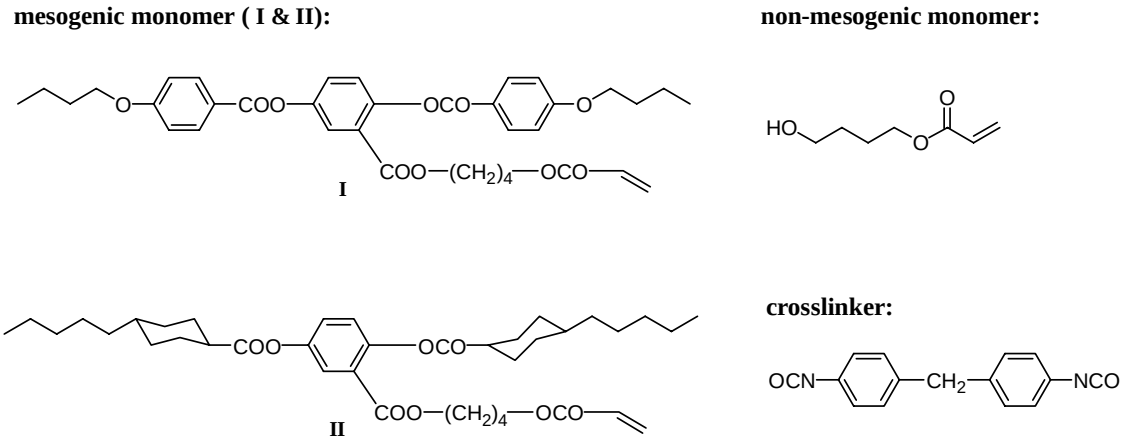

Figure 1-34 Components of a shape memory LC elastomer fiber synthesized by Ratna *et. al* [78]

Their side-chain liquid crystalline polymer containing two types of laterally attached mesogenic units and a small amount of non-mesogenic monomer as crosslinking sites was synthesized by radical polymerization. Further crosslinking was achieved by using a

diisocyanate unit. The crosslinked fiber exhibited a glass transition at 33 ºC and a reversible nematic-isotropic transition at 79.6 ºC. Fibers were drawn from the materials when the crosslinking started so that the sample was mechanically stretched into a monodomain state before the crosslinking was complete. These fibers presented a sharp decrease in length of ~ 30-35% at the mesophase to isotropic transition temperature. During the cooling cycle, this process is reversed with a sharp increase in length at the isotropic to mesophase transition temperature.

In 2003, Mather *et al.* reported that one-way shape memory effect was found in their siloxane-based main-chain LCEs shown in Figure 1-35 [60].

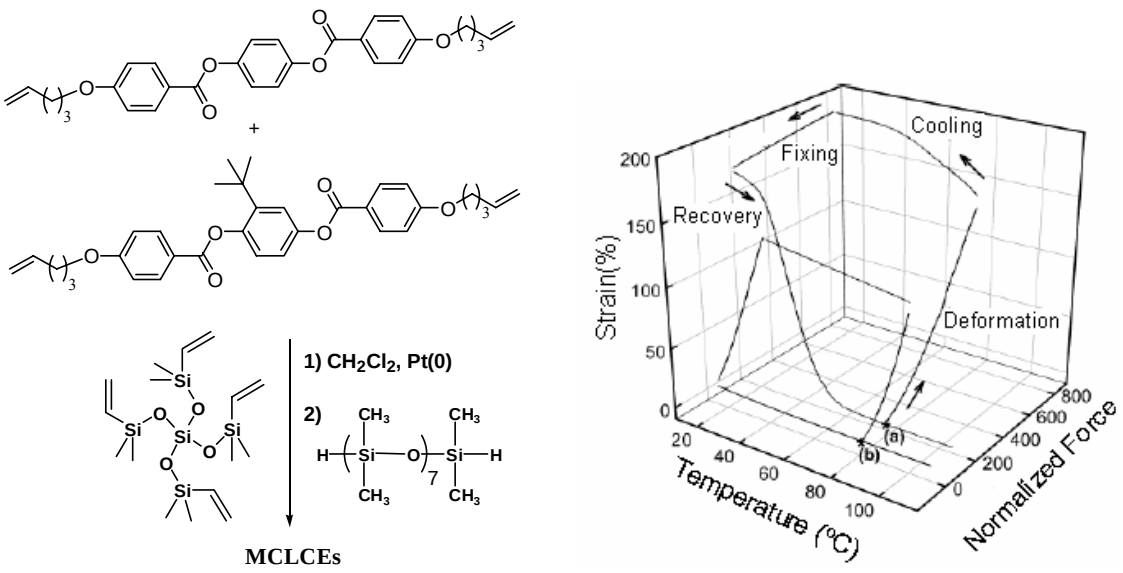

Figure 1-35 Synthesis of shape memory main-chain liquid crystalline elastomers and the thermodynamic analysis of shape fixing and shape recovery process by Mather *et. al* [60].

Two types of mesogenic monomers were incorporated into the polymer main-chain through a hydrosilylation reaction by employing polydimethylsiloxane as spacer

and tetrafunctional siloxane as crosslinker. The clearing temperature of the materials was tailored by varying the ratio of the comonomers. A smectic C type of mesophase was found in this material and was thought to be the key to fix the temporary shape of this material. The shape memory cycle in the Figure 1-35 starts with heating a specimen above its clearing temperature. In the isotropic state, the specimen is highly deformable without smectic structure. Then specimen is stretched and cooled down far below the clearing temperature into the smectic C phase. After removal of the load, the specimen shape can be fixed at about 83.6% of its maximally deformed shape. By comparison, a rubber recovers its original shape directly by removing the load. By heating the LCE specimen above the clearing temperature, the sample recovers about 99.1% of its permanent shape [60].

In 2005, Terentjev *et al.* reported self-assembled shape-memory fibers of triblock LC polymer [77].

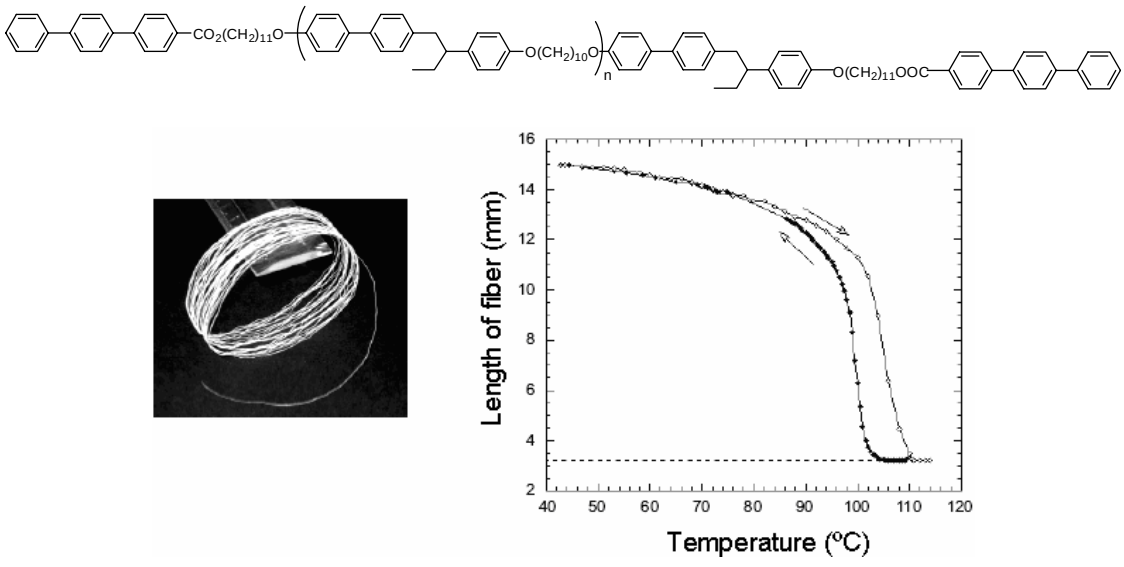

Figure 1-36 Chemical structure of the self-assembly shape memory fibers and its shape memory cycle by Terentjev *et. al* [77]

This polymer consists of a long main-chain LC polymer with terphenyl moieties at each end. The long central part provides large spontaneous elongation of the fiber along the nematic director in its nematic phase. The terphenyl moieties are thought to separate from the central polymer backbone and form semi-crystalline micelles acting as physical crosslinks of the network. Figure 1-36 shows the shape memory fibers which were drawn from the melt at a temperature above the nematic-isotropic transition temperature. In the full temperature range between the glass transition and nematic-isotropic transition, a large actuation strain (>500%) was found in these fibers.

1.5.2 Auxetic Materials

1.5.2.1 Poisson's Ratio and Materials with Negative Poisson's Ratio

The degree of deformation of a material under tensile or compression stress can be described by Poisson's ratio (ν) , which is defined as the ratio of the lateral strain ($\varepsilon_{lateral}$) to the longitudinal strain ($\varepsilon_{longitudinal}$) measured in a uniaxial tensile test as in Equation 1-1 [82].

$$\nu = -\frac{\varepsilon_{lateral}}{\varepsilon_{longitudinal}} \tag{1-1}$$

It is well known that conventional materials, like a rubber band, become thinner in cross-section while being stretched and expand in the cross-section while being compressed. Since most conventional materials become thinner in cross-section when they are under a uniaxial extension, the lateral strain of stretched materials is often negative. From the definition, the minus sign on the right-hand side of Equation 1-1 makes most conventional materials have positive values of Poisson's ratio. Table 1-1 lists Poisson's ratio of some solids, which ranges from 0 to about 0.5 [83-85].

Table 1-1 Poisson's ratio of some conventional materials

materials	**ν**	**materials**	**ν**
rubbers	0.5	common steel	0.27
soft biological tissues	0.5	polymer foams	0.1 ~ 0.4
polyethylene	0.46	glass	0.25
Nylon 6	0.39	concrete	0.2
PET	0.37-0.44	cork	0

However, there is a unique class of materials which behaves in a completely opposite way to conventional materials. These are called negative Poisson's ratio materials [84].

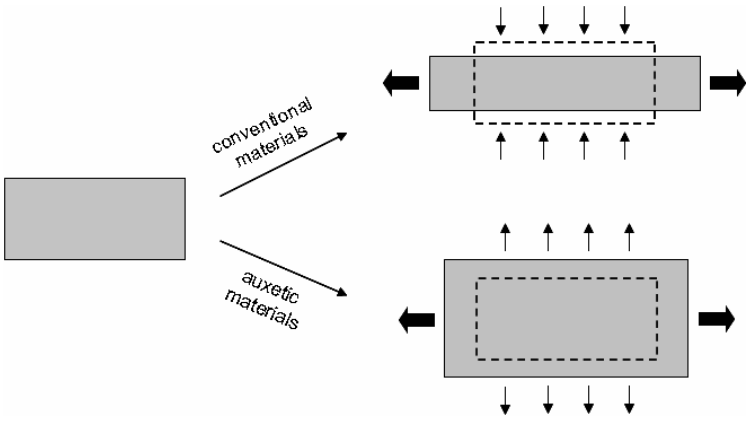

Figure 1-37 Under a uniaxial tensile stress, a conventional material becomes thinner in the cross-section, while an auxetic material expands in the cross-section. The thick arrow represents the stretching direction. The thin arrow represents the contraction in cross-section (conventional materials) or expansion in cross-section (auxetic materials) [83].

These materials expand laterally when stretched longitudinally and contract when compressed, which gives them a negative Poisson's ratio. In order to make the long phrase 'negative Poisson's ratio materials' short, Evans *et. al.* gave them another name - 'auxetic materials' or 'auxetics' [86] - derived from Greek *auxetos*, which means something that can expand. The physical response of the non-auxetic and auxetic materials to a uniaxial tensile force is compared in Figure 1-37 [83].

According to classical elasticity theory, the theoretical limit of Poisson's ratio of isotropic materials ranges from -1.0 to +0.5 [85]. There is no limitation of Poisson's ratio for an anisotropic material [87]. Although the idea that it is possible for materials to have a negative Poisson's ratio had been accepted over 150 years [88], only a small number of natural auxetic materials and man-made auxetic materials have been discovered or fabricated to date. Those auxetic materials at a different scale level have been reviewed by Evans *et al.* [89] and Yang *et al.* [90].

1.5.2.2 Natural Auxetic Materials

Auxetic behavior was first discovered in iron pyrites in the 1940's [88]. After that, the number of natural auxetic materials discovered increased gradually. It was found that most of the cubic elemental metals, some face-centered cubic rare gas solids, and some polycrystalline aggregated materials show negative Poisson's ratio effects [87, 91-93].

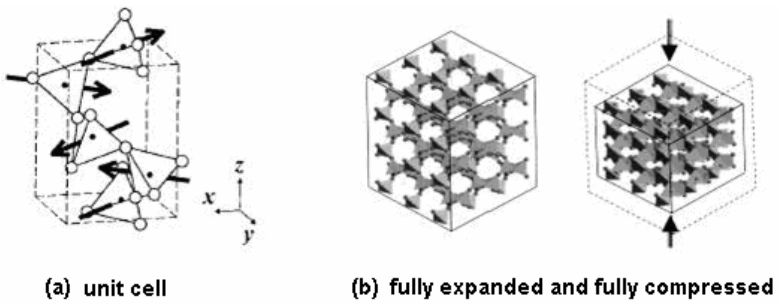

Figure 1-38 Schematic representation of α-cristobalite a) Unit cell, in which open circles represent oxygen atoms and solid circles represent silicon atoms; b) fully expanded and fully compressed α-cristobalite [94].

For instance, α-cristobalite is a typical auxetic material. It consists of a SiO_4 tetrahedral "building block" having an oxygen atom at each corner surrounding a central silicon atom. A mechanism for the auxetic effect was proposed by Yeganeh-Haeri *et al.*

[94]. They claimed the auxetic behavior comes from the cooperative rotation of SiO_4 tetrahedral units about an axis passing through the mid-points of two opposing edges of each tetrahedron as shown in Figure 1-36.

Most of the man-made auxetic materials are designed based on their framework geometry and deformation mechanism. Since auxetic behavior is scale-independent according to the theory of elasticity, auxetic behavior can be expected not only at the macroscopic and microscopic level, but also at the molecular level.

1.5.2.3 Man-made Auxetic Materials

1.5.2.3.1 Auxetic Structures

As shown in Figure 1-21, a conventional honeycomb shrinks in cross-section when stretched axially, which leads to a positive value in Poisson's ratio.

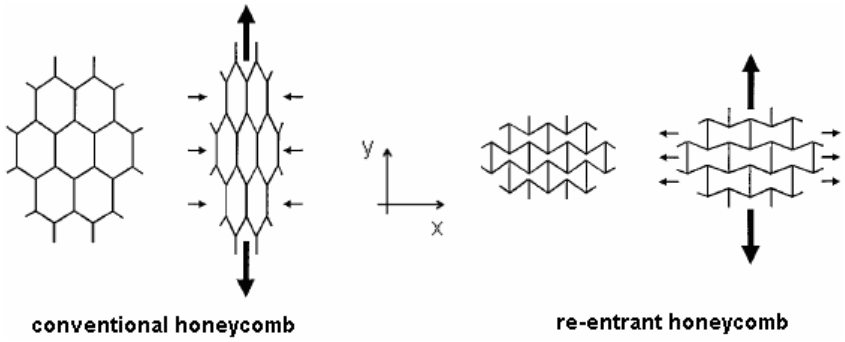

Figure 1-39 Schematic representation of different response of conventional honeycomb and re-entrant honeycomb to a uniaxial extension [95].

Negative Poisson's ratio can be obtained by modifying this architecture into a so-called re-entrant honeycomb [95]. Hinging ribs in re-entrant hexagonal cells will open up under an extension resulting in expansion in both *y*-direction and *x*-direction.

In 2000, Grima and Evans proposed a "rotating squares" and "rotating triangles"

geometry (Figure 1-40) to achieve auxetic behavior [96].

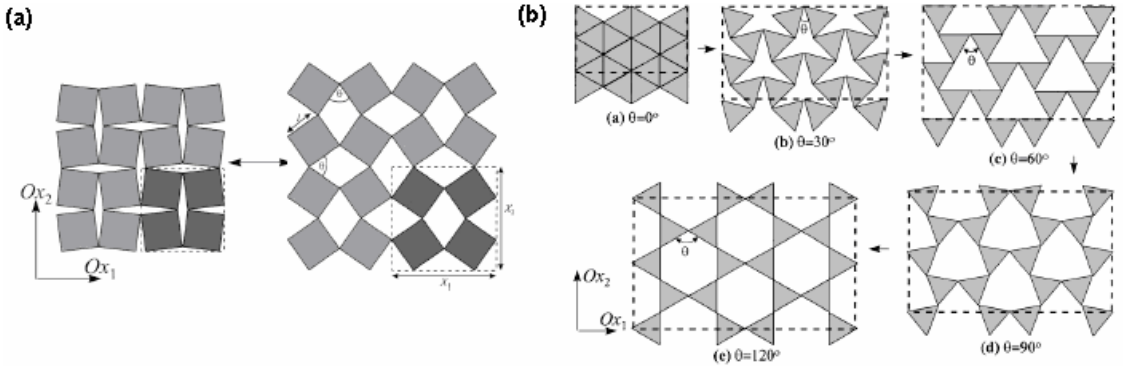

Figure 1-40 Response to the uniaxial extension of (a) "rotating squares" and (b) "rotating triangles" structure by Grima [96].

In these models, a number of rigid squares or triangles are connected at their vertices by hinges. The squares or triangles are assumed to be perfectly rigid and cannot deform upon loading. These structures can expand in 2-D direction resulting from the change in the angle θ between squares or triangles under tension. Being isotropic, these idealized structures have a constant Poisson's ratio of -1 regardless of the loading direction.

1.5.2.3.2 Macroscopic Auxetic Materials

Based on the above-mentioned 2-D re-entrant honeycombs (Figure 1-39), Evans *et. al.* fabricated macroscopic auxetic polymeric membranes as shown in Figure 1-41 using a laser ablation technique [97]. The re-entrant membrane possesses Poisson's ratio: ν_{xy} = -1.82 ± 0.05 and ν_{yx} = -0.51 ± 0.01). In contrast, a conventional membrane possesses positive Poisson's ratios: ν_{xy} = +0.86 ± 0.06 and ν_{yx} = +0.6 ± 0.1. Compared with conventional honeycombs, the polymeric membrane in the form of re-entrant honeycombs shows improved particulate size selectivity capabilities and membrane filter cleaning.

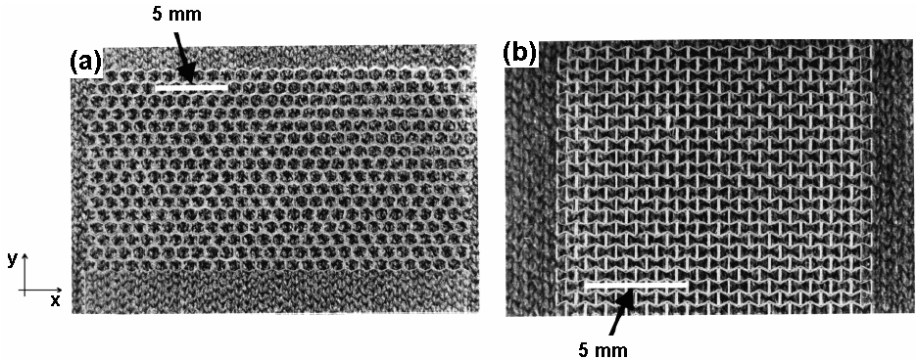

Figure 1-41 Polymeric membrane (a) conventional honeycombs; (b) re-entrant honeycombs [97].

The auxetic responses are considered to arise from the rib flexure and the rib hinging of reentrant honeycombs under uniaxial loading. The flexure of the honeycomb ribs was considered as the dominant deformation mechanism after comparing with the honeycomb theory. Filters made from this auxetic membrane can improve filtration process efficiency and reduce the number and frequency of the filter replacements [97].

Inspired by the deformation mechanism of re-entrant honeycomb to achieve an auxetic effect, three-dimensional polymer foams with negative Poisson's ratio were first made by Lakes in 1987 [84].

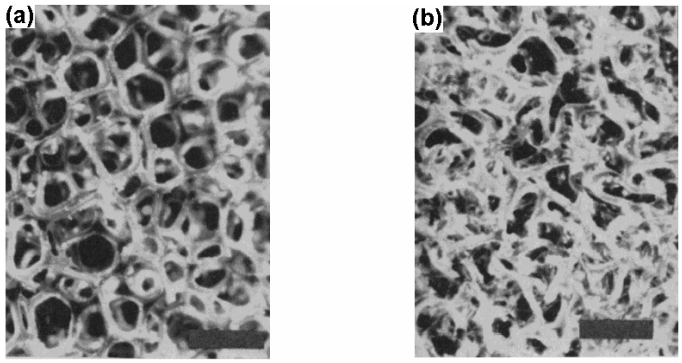

Figure 1-42 photograph of polymeric foams: (a) conventional open-cell foams; (b) re-entrant forms. The scale bar is 2 mm [84].

Low density open-cell conventional polymer foams in Figure 1-42 (a) were compressed

triaxially in a mold at a temperature above the softening temperature of the foam and then cooled to room temperature still under compression. After this processing, the ribs of the originally open-cells were pushed inward as shown in Figure 1-42 (b). The Poisson's ratio of these re-entrant foams was found to be around -0.7 [84]. Their experiments showed that the foams having a permanent volumetric compression factor of 1.4 - 4.0 exhibit negative Poisson's ratios. The cell size of the foams is 1 – 2 mm.

1.5.2.3.3 *Microscopic Auxetic Materials*

In 1989, Evans *et. al.* reported their discovery of a large negative Poisson's ratio (up to -12) exhibited by a microporous, anisotropic form of expanded polytetrafluoroethylene (PTFE) [98].

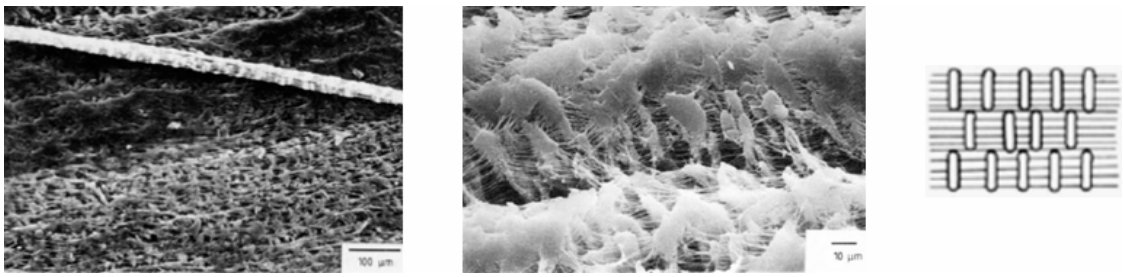

(a) **(b)** **(c)**

Figure 1-43 Microstructure of expanded PTFE showing a highly oriented axially aligned fibrous network with nodules: (a) low-magnification SEM photograph; (b) high-magnification SEM photograph; (c) schematic diagram.

The microporous fibrillar network structures of the material were produced by rapidly heating and drawing the sintered PTFE. The size of the pores depends on the initial draw condition. The nodes at the junctions of the fibrillar network are highly anisotropic particles of PTFE, which are the clusters of the original dispersion particles formed during the polymerization clearly shown in Figure 1-43 (a) and (b). In these pictures, fibrils of the network are oriented axially and the anisotropic nodes lie in the different

orientations. Figure 1-43 (c) above shows the extreme case, in which nodules lie perpendicular to the fibrils.

The structural changes in microporous PTFE under uniaxial extension are illustrated schematically in Figure 1-44. Initially, the fibrils and nodes aggregate together in a densified structure. While under uniaxial extension, fibrils are oriented along the stretching direction. The tension in the fibrils causes attached nodes to displace transversely and then they rotate under further extension. The translation and rotation of the nodules results in lateral expansion of the overall material with axial extension, therefore, a negative Poisson's ratio is achieved.

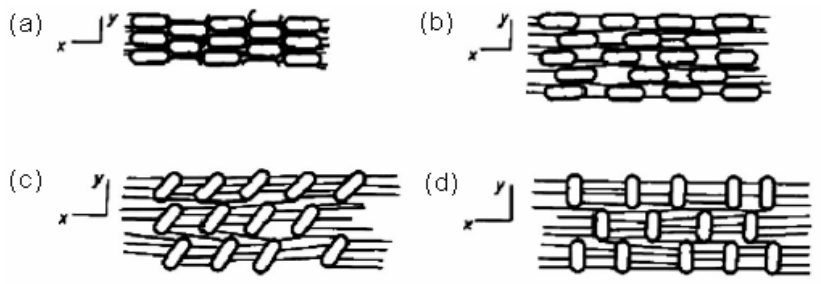

Figure 1-44 Schematic diagram of deformation mechanism of microporous PTFE showing lateral expansion under uniaxial extension: (a) initial densified microstructure; (b) transverse displacement of modes and lateral expansion; (c) further expansion produced by rotation of nodules; (d) fully expanded state [98].

Later on, several microscopic auxetic polymer materials having fibril-node microstructure similar to expanded PTFE were fabricated by Evans *et. al*, such as auxetic ultra-high molecular weight polyethylene (UHMWPE) rod ($\nu \approx$ -1.2) [99], polypropylene rod ($\nu \approx$ -0.22) [100], nylon rod [101], polypropylene rod ($\nu \approx$ -0.6) [102] and polyester fiber (ν = -0.65 ~ -0.75) [103].

1.5.2.3.4 *Molecular Auxetic Materials*

It is known that a negative Poisson's ratio can be achieved in man-made materials at both the macroscopic level (e.g. re-entrant polymer honeycomb) and the microscopic level (e.g. expanded PTFE). However, the low densities of foam or the formation of microscopic pores under deformation give these materials relatively weak mechanical properties. Materials used to make those auxetic materials are intrinsically not auxetic materials themselves. Design and synthesis of negative Poisson's ratio materials at the molecular level can possibly avoid the issue of decreased density and weak mechanical properties [86].

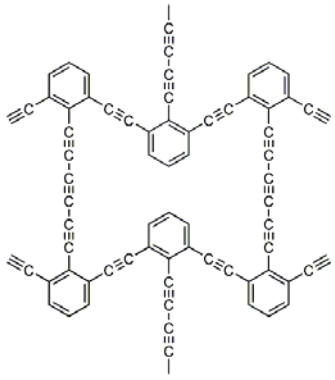

Figure 1-45 A proposed planar two-dimensional molecular auxetic structure consisting of benzene rings and acetylenes [86].

The first proposed molecular auxetic structure seen in Figure 1-45 was by Evans[86] who adopted Ashby's re-entrant honeycomb geometric unit. The repeat unit of the network consists of benzene rings as the cell junctions and acetylenes as diagonal and vertical branches. Although negative values of Poisson's ratio were calculated theoretically, no synthesis route was proposed.

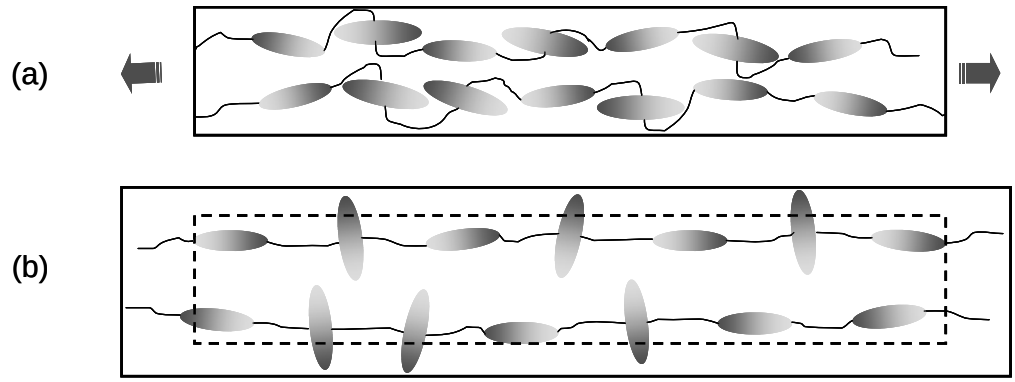

Figure 1-46 Schematic mechanism of auxetic effect achieved by incorporating laterally attached rods with terminally attached rods in MCLCP: (a) before stretching; (b) upon stretching [104].

Inspired by the auxetic behavior of expanded PTFE, main-chain liquid crystalline polymer (MCLCPs) based molecular auxetic materials were proposed and synthesized by Griffin *et al* in 1998. This idea is based on the mechanism of site-connectivity driven rod re-orientation [104]. In Figure 1-46, a series of rigid rods (some are terminally attached and some are laterally attached), are connected by flexible spacers. Initially, laterally attached rods (also called transverse rods) prefer to pre-align along the polymer main-chain because of the nematic liquid crystalline field or packing efficiency. Due to their chemical connectivity, upon stretching, lateral rods are expected to rotate in the direction normal to polymer backbone and push the neighboring chains further away. For this potential molecular auxetic material, the auxetic effect is expected to come from the increase in interchain packing distance when the material is under tension.

Two model polymers were prepared to examine the above-mentioned mechanism - 'site-connectivity transverse rod driven reorientation'- as shown in Figure 1-47.

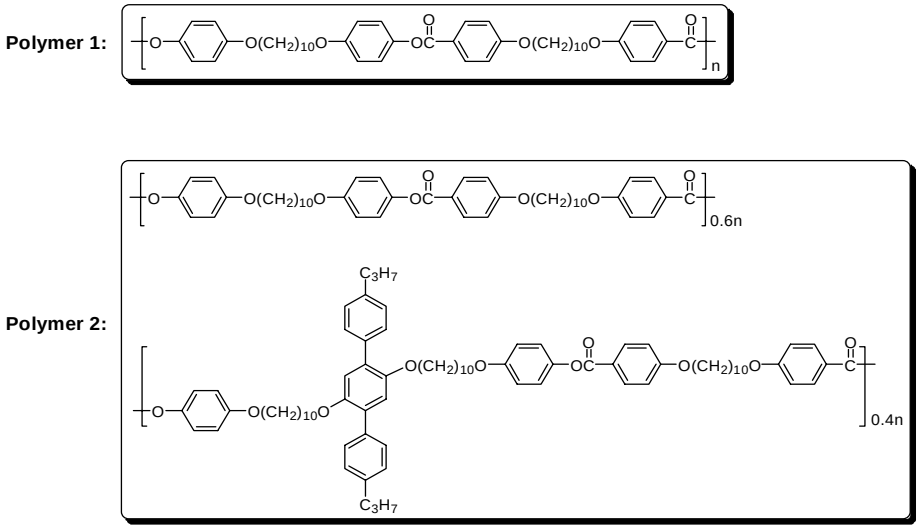

Figure 1-47 Chemical structures of two polymers: (1) only contains terminally attached rods; (2) contains both terminally and laterally attached rods [104].

Polymer **1** contains terminally attached rods alone and polymer **2** contains both terminally and attached rods. Both polymers are liquid crystalline polymers and show nematic-to-isotropic transition temperature at 215 °C (polymer 1) and 155 °C (polymer 2), respectively.

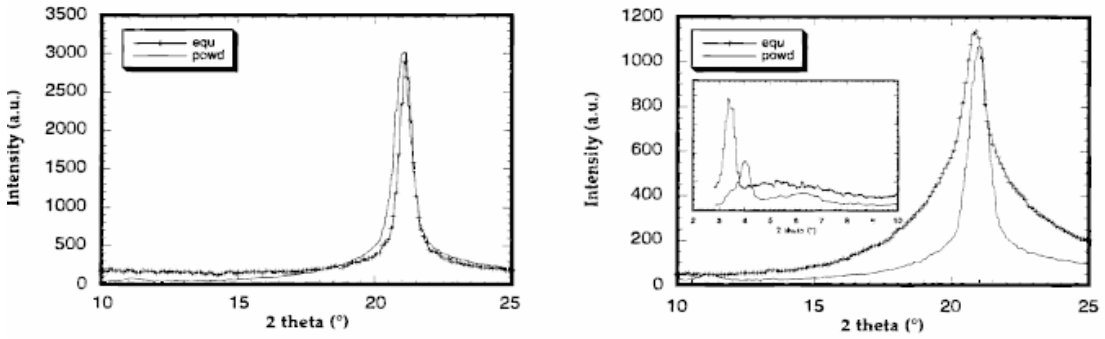

Figure 1-48 WAXD of LC polymers (a) without incorporation of laterally attached rods; (b) with incorporation of laterally attached rods [104].

X-ray diffraction is effective method to examine the potential for the auxetic effect by measuring interchain packing distance (*d*). Bragg's law ($n\lambda = 2d\sin\theta$) relates

the interchain packing distance with the diffraction angle (2θ), which can be detected directly by x-ray diffraction. For the x-ray incident source with a given wavelength (λ), the smaller the detected diffraction angle means the larger the interchain packing distance. Figure 1-48 shows equatorial x-ray scattering profiles for these two materials with comparable chemical structures. It was found that, for the polymer without laterally attached rods, the diffraction angle increases or interchain packing distance decreases upon stretching. This is a typical behavior of conventional polymer materials, because a more ordered and densified structure is obtained by stretching. For the polymer with laterally attached rods, an obvious decrease in the diffraction angle or increase in interchain packing distance was detected. This result likely indicates the rotation of laterally attached rods toward the chain normal under tension. Moratti [105] has shown through dynamic simulations that auxetic behavior should be seen with these swivelling mesogens of seven phenyl rings in the transverse rod. Cao et al. also synthesized liquid crystalline polymers with horizontal and lateral rods in main chain based on the site-connectivity transverse rod reorientation concept [106, 107].

1.6 Motivations and Objectives

It has proven difficult, due to the low solubility and the high transition temperature of main chain LCPs, to produce main chain LCEs by further crosslinking of LCPs. Therefore, main chain LCEs are still less studied than side chain LCEs. Siloxane chemistry introduced into the preparation of main chain LCEs by Finkelmann *et. al* provides researchers a facile route to produce and study the properties of main chain LCEs. The ultimate goal of this work is to establish structure-property relations in siloxane-based main chain liquid crystalline polymers and elastomers.

Mather *et al.* recently reported a one-way shape memory effect observed in their main chain LCEs [60]. The switching temperature of their LCEs is the smectic to isotopic transition temperature, which was tailored by varying the ratio of two mesogenic monomers with different lateral substituents. One-way shape memory effect was also found in our main chain LCEs. Comparing with the shape memory materials studied by Mather *et al.*, this work will cover a wider range of chemical variations, such as siloxane spacer length, crosslinker content, the terminal chain length and lateral substitutes of mesogenic unit. Specifically, the strain retention of LCEs as a function of chemical variations (e.g. crosslinker content, spacer length, terminal hydrocarbon chain and lateral substituents of mesogenic units, terphenyl transverse rods, etc.) and experimental parameters (e.g. initial strain, strain rate, temperature, etc.) will be examined.

Terphenyl transverse rods and pentaphenyl transverse rods were incorporated into siloxane-based MCLCPs and MCLCEs individually to explore the potential molecular auxetic effect. An experimental set-up was designed to measure Poisson's ratio of LCEs at large strains. Terphenyl transverse rod loading as well as crosslinker content in parent LCEs will be the chemical variations for the Poisson's ratio study. Elastomers are studied because of the molecular cooperativity of mechanical deformation in crosslinked materials.

In addition to the MCLCEs with rod-like mesogenic units, the MCLCEs with flat-shaped anthraquinone-based (AQ) mesogens will be investigated. The detection of characteristic π-π stacking diffractions in most of the AQ LCEs indicates the possibility to form columnar or even higher ordered columnar main chain LCEs. The effect of terminal chain length of AQ mesogens and siloxane spacer length on the columnar

mesophase formation as well as the thermal behaviors and mechanical properties will be discussed.

1.7 References

[1] H. Kelker, R. Hatz, and C. Schumann, *Handbook of liquid crystals*. Weinheim ; Deerfield Beach, Fla.: Verlag Chemie, 1980.

[2] F. Reinitzer, *Monatsh. Chem.*, vol. 9, pp. 421, 1888.

[3] O. Lehmann, *Z. Krist*, vol. *18*, pp. 464, 1890.

[4] D. Vorlander, *Ber. Dt. Jem. Gesell.*, vol. 43, pp. 3120-3135, 1910.

[5] P. J. Collings and M. Hird, *Introduction to liquid crystals : chemistry and physics*. London ; Bristol, PA: Taylor & Francis, 1997.

[6] G. W. Gray, *Thermotropic liquid crystals*. Chichester [East Sussex] ; New York: Published on behalf of the Society of Chemical Industry by Wiley, 1987.

[7] P. J. Collings, *Liquid crystals : nature's delicate phase of matter*, 2nd ed. Princeton, N.J.: Princeton University Press, 2002.

[8] G. W. Gray, "Low-molar-mass thermotropic liquid crystals [and discussion]," vol. 330, pp. 73-94, 1990.

[9] G. W. Gray, "The chemistry of liquid crystals," *Phil. Trans. R. Soc. Lond. A*, vol. 309, pp. 77-92, 1983.

[10] L. E. Alexander, *X-ray diffraction methods in polymer science* New York, Wileyinterscience 1969.

[11] L. Onsager, "The effects of shape on the interaction of colloidal particles," *Annals of the New York Academy of Sciences*, vol. 51, pp. 627-659, 1949.

[12] P. J. Flory, "Statistical thermodynamics of semi-flexible chain molecules," *Proceedings of the Royal Society of London Series A - Mathematical and Physical Sciences*, vol. 234, pp. 60-73, 1956.

[13] G. G. Odian, *Principles of polymerization*, 3rd ed. New York: Wiley, 1991.

[14] A. M. Donald and A. H. Windle, *Liquid crystalline polymers*. Cambridge [England] ; New York: Cambridge University Press, 1992.

[15] M. Warner and E. M. Terentjev, *Liquid crystal elastomers*. Oxford ; New York: Clarendon Press ; Oxford University Press, 2003.

[16] R. Zentel, "Liquid-crystalline elastomers," *Angewandte Chemie-International Edition in English*, vol. 28, pp. 1407-1415, 1989.

[17] E. M. Terentjev, "Liquid crystalline networks," *Current Opinion in Colloid & Interface Science*, vol. 4, pp. 101-107, 1999.

[18] S. Mayer and R. Zentel, "Liquid crystalline polymers and elastomers," *Current Opinion in Solid State & Materials Science*, vol. 6, pp. 545-551, 2002.

[19] H. Finkelmann, H. J. Kock, and G. Rehage, "Investigations on liquid-crystalline polysiloxanes. 3. Liquid-crystalline elastomers - a new type of liquid-crystalline material," *Makromolekulare Chemie-Rapid Communications*, vol. 2, pp. 317-322, 1981.

[20] K. D. Singer, M. G. Kuzyk, and J. E. Sohn, "2nd-order nonlinear-optical processes in orientationally ordered materials - Relationship between molecular and macroscopic properties," *Journal of the Optical Society of America B-Optical Physics*, vol. 4, pp. 968-976, 1987.

[21] M. J. Whitcombe, A. Gilbert, and G. R. Mitchell, "Synthesis and photochemistry of side-chain liquid-crystal polymers based on cinnamate esters," *Journal of Polymer Science Part A - Polymer Chemistry*, vol. 30, pp. 1681-1691, 1992.

[22] J. Kupfer and H. Finkelmann, "Nematic liquid single-cystal eastomers," *Makromolekulare Chemie-Rapid Communications*, vol. 12, pp. 717-726, 1991.

[23] H. Finkelmann, S. T. Kim, A. Munoz, P. Palffy-Muhoray, and B. Taheri, "Tunable mirrorless lasing in cholesteric liquid crystalline elastomers," *Advanced Materials*, vol. 13, pp. 1069-1072, 2001.

[24] H. Finkelmann, E. Nishikawa, G. G. Pereira, and M. Warner, "A new opto-mechanical effect in solids," *Physical Review Letters*, vol. 87, pp. 015501 (1-4), 2001.

[25] J. Cviklinski, A. R. Tajbakhsh, and E. M. Terentjev, "UV isomerisation in nematic elastomers as a route to photo-mechanical transducer," *European Physical Journal E*, vol. 9, pp. 427-434, 2002.

[26] K. Hammerschmidt and H. Finkelmann, "Stress-optical and thermomechanical measurements on liquid-crystalline elastomers," *Makromolekulare Chemie-Macromolecular Chemistry and Physics*, vol. 190, pp. 1089-1101, 1989.

[27] Y. L. Yu and T. Ikeda, "Soft actuators based on liquid-crystalline elastomers," *Angewandte Chemie-International Edition*, vol. 45, pp. 5416-5418, 2006.

[28] P. G. de Gennes, *C. R. Acad. Sci. Ser. B*, vol. 281, pp. 101-105, 1975.

[29] B. Donnio, H. Wermter, and H. Finkelmann, "Simple and versatile synthetic route for the preparation of main-chain, liquid-crystalline elastomers," *Macromolecules*, vol. 33, pp. 7724-7729, 2000.

[30] F. J. Davis, "Liquid-crystalline elastomers," *Journal of Materials Chemistry*, vol. 3, pp. 551-562, 1993.

[31] R. Zentel and G. Reckert, "Liquid-crystalline elastomers based on liquid-crystalline side group, main chain and combined polymers," *Makromolekulare Chemie-Macromolecular Chemistry and Physics*, vol. 187, pp. 1915-1926, 1986.

[32] W. Gleim and H. Finkelmann, "Thermoelastic and photoelastic properties of cross-linked liquid-crystalline side-chain polymers," *Makromolekulare Chemie-Macromolecular Chemistry and Physics*, vol. 188, pp. 1489-1500, 1987.

[33] R. Zentel and M. Benalia, "Stress-induced orientation in lightly cross-linked liquid-crystalline side-group polymers," *Makromolekulare Chemie-Macromolecular Chemistry and Physics*, vol. 188, pp. 665-674, 1987.

[34] F. J. Davis, A. Gilbert, J. Mann, and G. R. Mitchell, "The synthesis and properties of liquid-crystal elastomers," *Journal of the Chemical Society-Chemical Communications*, pp. 1333-1334, 1986.

[35] S. M. Clarke, E. M. Terentjev, I. Kundler, and H. Finkelmann, "Texture evolution during the polydomain-monodomain transition in nematic elastomers," *Macromolecules*, vol. 31, pp. 4862-4872, 1998.

[36] G. H. F. Bergmann, H. Finkelmann, V. Percec, and M. Y. Zhao, "Liquid-crystalline main-chain elastomers," *Macromolecular Rapid Communications*, vol. 18, pp. 353-360, 1997.

[37] R. Zentel, "Shape variation of cross-linked liquid-crystalline polymers by electric-fields," *Liquid Crystals*, vol. 1, pp. 589-592, 1986.

[38] S. Bualek and R. Zentel, "Crosslinkable liquid-crystalline combined main-chain side-group polymers with low glass-transition temperatures," *Makromolekulare Chemie-Macromolecular Chemistry and Physics*, vol. 189, pp. 791-796, 1988.

[39] E. R. Zubarev, R. V. Talroze, T. I. Yuranova, N. A. Plate, and H. Finkelmann, "Influence of network topology on polydomain-monodomain transition in side chain liquid crystalline elastomers with cyanobiphenyl mesogens," *Macromolecules*, vol. 31, pp. 3566-3570, 1998.

[40] J. Schatzle, W. Kaufhold, and H. Finkelmann, "Nematic elastomers - the influence of external mechanical-stress on the liquid-crystalline phase-behavior," *Makromolekulare Chemie-Macromolecular Chemistry and Physics*, vol. 190, pp. 3269-3284, 1989.

[41] C. Ortiz, M. Wagner, N. Bhargava, C. K. Ober, and E. J. Kramer, "Deformation of a polydomain, smectic liquid crystalline elastomer," *Macromolecules*, vol. 31, pp. 8531-8539, 1998.

[42] C. Ortiz, C. K. Ober, and E. J. Kramer, "Stress relaxation of a main-chain, smectic, polydomain liquid crystalline elastomer," *Polymer*, vol. 39, pp. 3713-3718, 1998.

[43] H. Finkelmann, H. J. Kock, W. Gleim, and G. Rehage, "Investigations on liquid-crystalline polysiloxanes. 5. Orientation of LC-elastomers by mechanical forces," *Makromolekulare Chemie-Rapid Communications*, vol. 5, pp. 287-293, 1984.

[44] W. Oppermann, K. Braatz, H. Finkelmann, W. Gleim, H. J. Kock, and G. Rehage, "Viscoelastic properties of silicone polymers with liquid-crystalline behavior," *Rheologica Acta*, vol. 21, pp. 423-426, 1982.

[45] M. Giamberini, P. Cerruti, V. Ambrogi, C. Vestito, F. Covino, and C. Carfagna, "Liquid crystalline elastomers based on diglycidyl terminated rigid monomers and aliphatic acids. Part 2. Mechanical characterization," *Polymer*, vol. 46, pp. 9113-9125, 2005.

[46] W. Kaufhold, H. Finkelmann, and H. R. Brand, "Nematic elastomers. 1. Effect of the spacer length on the mechanical coupling between network anisotropy and nematic order," *Makromolekulare Chemie-Macromolecular Chemistry and Physics*, vol. 192, pp. 2555-2579, 1991.

[47] M. Giamberini, E. Amendola, and C. Carfagna, "Curing of a rigid-rod epoxy-resin with an aliphatic diacid - an example of a lightly cross-linked liquid-crystalline thermoset," *Macromolecular Rapid Communications*, vol. 16, pp. 97-105, 1995.

[48] G. G. Barclay, S. G. Mcnamee, C. K. Ober, K. I. Papathomas, and D. W. Wang, "The mechanical and magnetic alignment of liquid-crystalline epoxy thermosets," *Journal of Polymer Science Part A - Polymer Chemistry*, vol. 30, pp. 1845-1853, 1992.

[49] J. Kupfer and H. Finkelmann, "Liquid-crystal elastomers - Influence of the orientational distribution of the cross-links on the phase-behavior and reorientation processes," *Macromolecular Chemistry and Physics*, vol. 195, pp. 1353-1367, 1994.

[50] S. M. Clarke, E. Nishikawa, H. Finkelmann, and E. M. Terentjev, "Light-scattering study of random disorder in liquid crystalline elastomers," *Macromolecular Chemistry and Physics*, vol. 198, pp. 3485-3498, 1997.

[51] S. V. Fridrikh and E. M. Terentjev, "Order-disorder transition in an external field in random ferromagnets and nematic elastomers," *Physical Review Letters*, vol. 79, pp. 4661-4664, 1997.

[52] Y. Zhao, "Some reflections on the direction of the stress-induced macroscopic orientation of the mesogenic groups in side-chain liquid-crystalline polymers - a new mechanism," *Polymer*, vol. 36, pp. 2717-2724, 1995.

[53] E. M. Terentjev, M. Warner, and G. C. Verwey, "Non-uniform deformations in liquid crystalline elastomers," *Journal De Physique II*, vol. 6, pp. 1049-1060, 1996.

[54] S. V. Fridrikh and E. M. Terentjev, "Polydomain-monodomain transition in nematic elastomers," *Physical Review E*, vol. 60, pp. 1847-1857, 1999.

[55] M. Warner, P. Bladon, and E. M. Terentjev, "Soft elasticity - Deformation without resistance in liquid-crystal elastomers," *Journal De Physique II*, vol. 4, pp.

93-102, 1994.

[56] A. Hotta and E. M. Terentjev, "Dynamic soft elasticity in monodomain nematic elastomers," *European Physical Journal E*, vol. 10, pp. 291-301, 2003.

[57] K. H. Hanus, W. Pechhold, F. Soergel, B. Stoll, and R. Zentel, "Phase-behavior and elastic properties of a slightly cross-linked liquid-crystalline main-chain polymer," *Colloid and Polymer Science*, vol. 268, pp. 222-229, 1990.

[58] A. Hotta and E. M. Terentjev, "Long-time stress relaxation in polyacrylate nematic liquid crystalline elastomers," *Journal of Physics-Condensed Matter*, vol. 13, pp. 11453-11464, 2001.

[59] S. M. Clarke and E. M. Terentjev, "Slow stress relaxation in liquid crystal elastomers and gels," *Faraday Discussions*, pp. 325-333, 1999.

[60] I. A. Rousseau and P. T. Mather, "Shape memory effect exhibited by smectic-C liquid crystalline elastomers," *Journal of the American Chemical Society*, vol. 125, pp. 15300-15301, 2003.

[61] C. H. Legge, F. J. Davis, and G. R. Mitchell, "Memory effects in liquid-crystal elastomers," *Journal De Physique II*, vol. 1, pp. 1253-1261, 1991.

[62] G. R. Mitchell, F. J. Davis, W. Guo, and R. Cywinski, "Coupling between mesogenic units and polymer backbone in side-chain liquid-crystal polymers and elastomers," *Polymer*, vol. 32, pp. 1347-1353, 1991.

[63] H. Finkelmann, A. Greve, and M. Warner, "The elastic anisotropy of nematic elastomers," *European Physical Journal E*, vol. 5, pp. 281-293, 2001.

[64] S. M. Clarke, A. Hotta, A. R. Tajbakhsh, and E. M. Terentjev, "Effect of cross-linker geometry on equilibrium thermal and mechanical properties of nematic elastomers," *Physical Review E*, vol. 64, pp. 061702 (1-8), 2001.

[65] E. Nishikawa, H. Finkelmann, and H. R. Brand, "Smectic A liquid single crystal elastomers showing macroscopic in-plane fluidity," *Macromolecular Rapid Communications*, vol. 18, pp. 65-71, 1997.

[66] E. Nishikawa and H. Finkelmann, "Smectic-A liquid single crystal elastomers - strain induced break-down of smectic layers," *Macromolecular Chemistry and Physics*, vol. 200, pp. 312-322, 1999.

[67] N. Assfalg and H. Finkelmann, "A smectic A liquid single crystal elastomer (LSCE): Phase behavior and mechanical anisotropy," *Macromolecular Chemistry and Physics*, vol. 202, pp. 794-800, 2001.

[68] K. Hiraoka and H. Finkelmann, "Uniform alignment of chiral smectic C elastomers induced by mechanical shear field," *Macromolecular Rapid Communications*, vol. 22, pp. 456-460, 2001.

[69] K. Hiraoka, Y. Uematsu, P. Stein, and H. Finkelmann, "X-ray diffraction studies on the phase-transformational behavior of a smectic liquid-crystalline elastomer composed of chiral mesogens," *Macromolecular Chemistry and Physics*, vol. 203, pp. 2205-2210, 2002.

[70] K. Hiraoka, W. Sagano, T. Nose, and H. Finkelmann, "Biaxial shape memory effect exhibited by monodomain chiral smectic C elastomers," *Macromolecules*, vol. 38, pp. 7352-7357, 2005.

[71] A. Lendlein and S. Kelch, "Shape-memory polymers," *Angewandte Chemie-International Edition*, vol. 41, pp. 2034-2057, 2002.

[72] L. C. Chang and T. A. Read, "Plastic deformation and diffusionless phase changes in metals - The gold-cadmium beta-phase," *Transactions of the American Institute of Mining and Metallurgical Engineers*, vol. 191, pp. 47-52, 1951.

[73] J. Van Humbeeck, "Shape memory alloys: A material and a technology," *Advanced Engineering Materials*, vol. 3, pp. 837-850, 2001.

[74] W. Chen, K. Xing, and L. Sun, "The heat shrinking mechanism of polyethylene film," *Radiation Physics and Chemistry*, vol. 22, pp. 593-601, 1983.

[75] S. Machi, "New trends of radiation processing applications," *Radiation Physics and Chemistry*, vol. 47, pp. 333-336, 1996.

[76] D. L. Thomsen, P. Keller, J. Naciri, R. Pink, H. Jeon, D. Shenoy, and B. R. Ratna, "Liquid crystal elastomers with mechanical properties of a muscle,"

Macromolecules, vol. 34, pp. 5868-5875, 2001.

[77] S. V. Ahir, A. R. Tajbakhsh, and E. M. Terentjev, "Self-assembled shape-memory fibers of triblock liquid-crystal polymers," *Advanced Functional Materials*, vol. 16, pp. 556-560, 2006.

[78] J. Naciri, A. Srinivasan, H. Jeon, N. Nikolov, P. Keller, and B. R. Ratna, "Nematic elastomer fiber actuator," *Macromolecules*, vol. 36, pp. 8499-8505, 2003.

[79] Y. P. Liu, K. Gall, M. L. Dunn, and P. McCluskey, "Thermomechanics of shape memory polymer nanocomposites," *Mechanics of Materials*, vol. 36, pp. 929-940, 2004.

[80] P. E. Cladis, "Phase transitions in liquid crystalline elastomers - A findamental aspect of LCEs as artificial muscles," *Proc. EuroMech408*, pp. 123-131, 2001.

[81] H. Wermter and H. Finkelmann, "Liquid crystalline elastomers as artificial muscles," *E-Polymers*, vol. 013, pp. 1-13, 2001.

[82] R. J. Young, *Introduction to polymers*. London ; New York: Chapman and Hall, 1983.

[83] A. Alderson, "A triumph of lateral thought," *Chemistry & Industry*, pp. 384, 1999.

[84] R. Lakes, "Foam structures with a negative Poisson's ratio," *Science*, vol. 235, pp. 1038-1040, 1987.

[85] Y. C. Fung, *Foundations of solid mechanics*. Englewood Cliffs, N.J.,: Prentice-Hall, 1965.

[86] K. E. Evans, M. A. Nkansah, I. J. Hutchinson, and S. C. Rogers, "Molecular network design," *Nature*, vol. 353, pp. 124-124, 1991.

[87] R. H. Baughman, J. M. Shacklette, A. A. Zakhidov, and S. Stafstrom, "Negative Poisson's ratios as a common feature of cubic metals," *Nature*, vol. 392, pp. 362-365, 1998.

[88] A. E. H. Love, *A treatise on the mathematical theory of elasticity*, 4th ed. New York,: Dover, 1944.

[89] K. E. Evans and A. Alderson, "Auxetic materials: functional materials and structures from a lateral thinking!," *Advanced Materials*, vol. 12, pp. 617-628, 2000.

[90] W. Yang, Z. M. Li, W. Shi, B. H. Xie, and M. B. Yang, "Review on auxetic materials," *Journal of Materials Science*, vol. 39, pp. 3269-3279, 2004.

[91] D. J. Gunton and G. A. Saunders, "Young's modulus and Poisson's ratio of arsenic, antimony and bismuth," *Journal of Materials Science*, vol. 7, pp. 1061-&, 1972.

[92] Y. Li, "Anisotropic behavior of Poisson's ratio, Young's modulus, and shear modulus in hexagonal materials," *Physica Status Solidi a-Applied Research*, vol. 38, pp. 171-175, 1976.

[93] F. Milstein and K. Huang, "Existence of a negative Poisson's ratio in FCC crystals," *Physical Review B*, vol. 19, pp. 2030-2033, 1979.

[94] A. Yeganehhaeri, D. J. Weidner, and J. B. Parise, "Elasticity of alpha-Cristobalite - A silicon aioxide with a negative Poisson's ratio," *Science*, vol. 257, pp. 650-652, 1992.

[95] L. J. Gibson, M. F. Ashby, G. S. Schajer, and C. I. Robertson, "The mechanics of two-dimensional cellular materials," *Proceedings of the Royal Society of London Series A - Mathematical Physical and Engineering Sciences*, vol. 382, pp. 25-42, 1982.

[96] J. N. Grima and K. E. Evans, "Auxetic behavior from rotating squares," *Journal of Materials Science Letters*, vol. 19, pp. 1563-1565, 2000.

[97] A. Alderson, J. Rasburn, S. Ameer-Beg, P. G. Mullarkey, W. Perrie, and K. E. Evans, "An auxetic filter: A tuneable filter displaying enhanced size selectivity or defouling properties," *Industrial & Engineering Chemistry Research*, vol. 39, pp. 654-665, 2000.

[98] B. D. Caddock and K. E. Evans, "Microporous materials with negative Poisson's ratios. 1. Microstructure and mechanical-properties," *Journal of Physics D-*

Applied Physics, vol. 22, pp. 1877-1882, 1989.

[99] K. L. Alderson and K. E. Evans, "The fabrication of microporous polyethylene having a negative poisson ratio," *Polymer*, vol. 33, pp. 4435-4438, 1992.

[100] A. P. Pickles, K. L. Alderson, and K. E. Evans, "The effects of powder morphology on the processing of auxetic polypropylene (PP of negative Poisson's ratio)," *Polymer Engineering and Science*, vol. 36, pp. 636-642, 1996.

[101] K. L. Alderson, A. Alderson, R. S. Webber, and K. E. Evans, "Evidence for uniaxial drawing in the fibrillated microstructure of auxetic microporous polymers," *Journal of Materials Science Letters*, vol. 17, pp. 1415-1419, 1998.

[102] K. L. Alderson, A. Alderson, G. Smart, V. R. Simkins, and P. J. Davies, "Auxetic polypropylene fibres Part 1 - Manufacture and characterisation," *Plastics Rubber and Composites*, vol. 31, pp. 344-349, 2002.

[103] N. Ravirala, K. L. Alderson, P. J. Davies, V. R. Simkins, and A. Alderson, "Negative Poisson's ratio polyester fibers," *Textile Research Journal*, vol. 76, pp. 540-546, 2006.

[104] C. B. He, P. W. Liu, and A. C. Griffin, "Toward negative Poisson's ratio polymers through molecular design," *Macromolecules*, vol. 31, pp. 3145-3147, 1998.

[105] P. Aldred and S. C. Moratti, "Dynamic simulations of potentially auxetic liquid-crystalline polymers incorporating swivelling mesogens," *Molecular Simulation*, vol. 31, pp. 883-887, 2005.

[106] C. Li, X. Xie, and S. Cao, "Synthesis and characterization of liquid crystalline copolymers containing horizontal and lateral rods in main chain," *Polymers for Advanced Technologies*, vol. 13, pp. 178-187, 2002.

[107] Y. liu, L. Zhang, J. Shi, and S. Cao, "Synthesis and characterization of liquid crystalline copolyesters containing horizontal and lateral rods in main chain (II)," *Reactive & Functional Polymers*, vol. 64, pp. 35-46, 2005.

CHAPTER 2

Experimental

2.1 Synthesis of LC Monomers, MCLC Polymers and MCLC Elastomers

2.1.1 Synthesis Strategies

In this work, all the main-chain LC polymers and LC elastomers were synthesized by a modified procedure based on standard LCP and LCE hydrosilylation reactions[1-3]. It is basically an addition of the Si-H bond of siloxane spacer or crosslinker across the vinyl double bond of the mesogens. In our method, this step-growth polymerization is carried out at room temperature and is catalyzed by platinum(0) complexes called Karstedt catalyst.

For linear LC polymers, there are two building blocks, a divinyl mesogenic monomer and a flexible siloxane spacer unit (Figure 2-1). Both of them have the functionality of two. Linear polymers form via the connection of **X**-**X** and **Y**-**Y** units in sequence. In order to obtain a linear polymer with appropriate high molecular weight, a exatct 1:1 stoichiometry of '**X**' group and '**Y**' group is required in the reaction system[4].

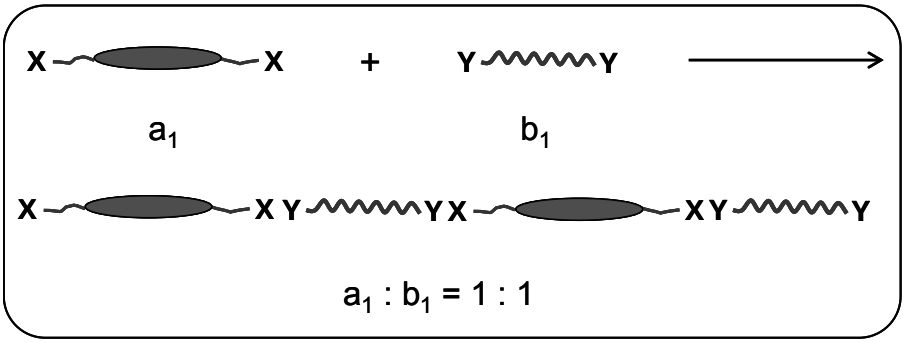

Figure 2-1 Schematic representation of linear LC polymer synthesis. '**X**' represents a double bond in divinyl mesogenic monomer. '**Y**' represents a Si-H bond in siloxane spacer.

By incorporating the a second siloxane (Figure 2-2) with different chain length or a second divinyl non-mesogenic monomer, like a transverse rod (Figure 2-3), a series of linear LC copolymers was obtained. By varying the ratio of two different spacers or two different divinyl monomers, the phase behavior of LC copolymers can be tailored.

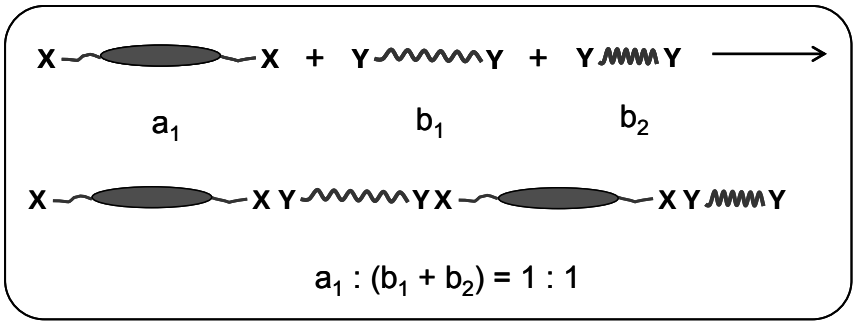

Figure 2-2 Schematic representation of linear LC copolymer synthesis. '**X**' represents a double bond in divinyl mesogenic monomer. '**Y**' represents a Si-H bond in both siloxane spacers with different chain length.

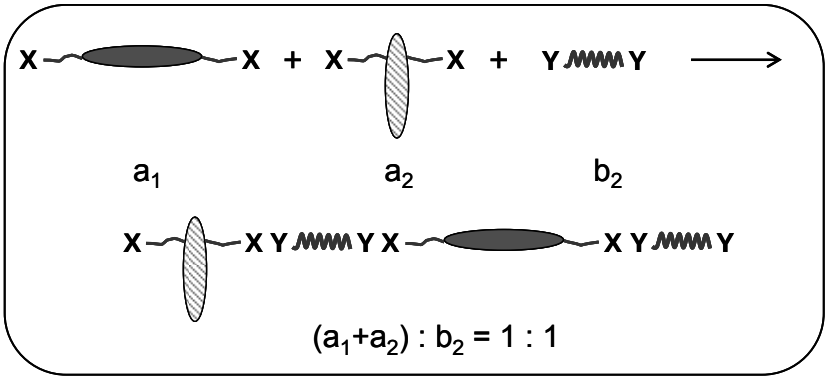

Figure 2-3 Schematic representation of linear LC copolymer synthesis. '**X**' represents a double bond in both divinyl mesogenic and non-mesogenic monomer. '**Y**' represents a Si-H bond in siloxane spacer.

For LC elastomers, one more building block, a siloxane crosslinker, is needed apart from **X**-**X** and **Y**-**Y** (Figure 2-4). A four functionality crosslinker is used in this work. To get a network structure, a 1:1 stoichiometry of **X** group and **Y** group is also needed. The crosslinking density of the elastomer can be tailored by varying the ratio of

spacer and crosslinker.

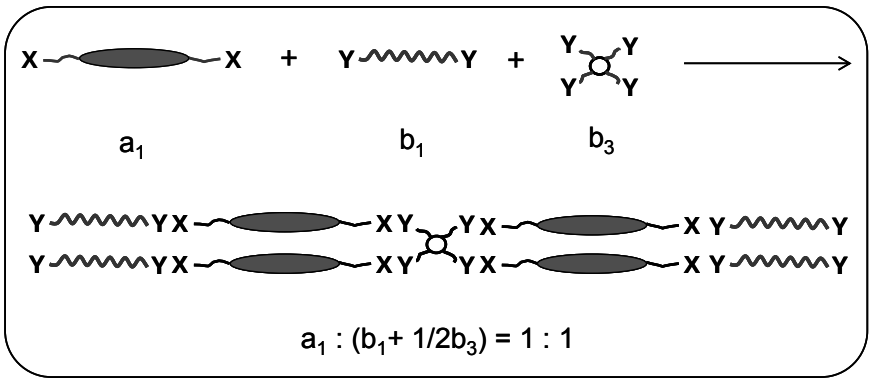

Figure 2-4 Schematic representation of LC elastomer synthesis. '**X**' represents a double bond in LC monomer. '**Y'** represents a Si-H bond in both siloxane spacer and siloxane crosslinker.

Similar to the synthesis of a linear copolymer, the composition of LC elastomers can also be varied by introducing a second divinyl monomer. For example, transverse rods can be introduced into LC elastomers as shown in Figure 2-5. The effect of transverse rods on the LC elastomers can be studied by varying the ratio of LC monomer and transverse rod.

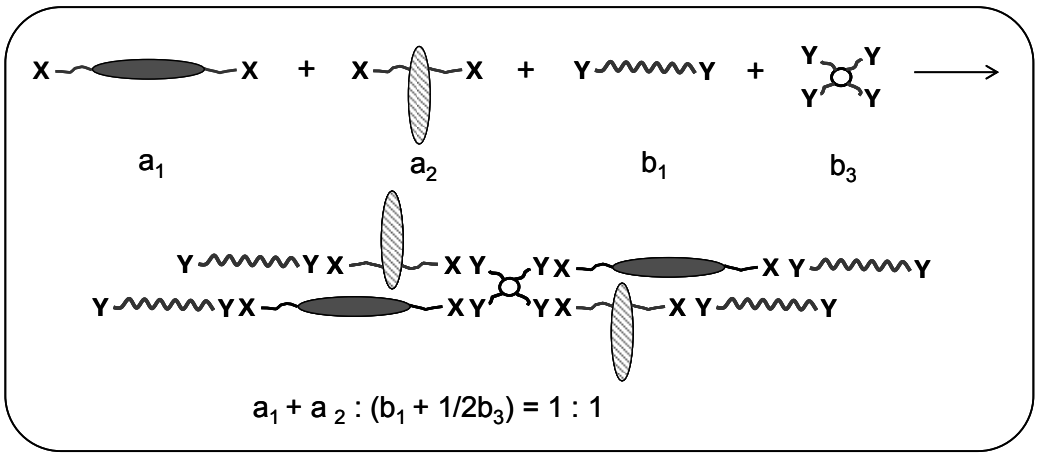

Figure 2-5 Schematic representation of LC elastomer synthesis. '**X**' represents a double bond both in mesogenic and non-mesogenic monomer. '**Y**' represents a Si-H bond both in siloxane spacer and siloxane crosslinker.

2.1.2 Materials

Three types of siloxane spacer, polydimethylsiloxane (DP = 8) (Si8) and 1,1,3,3,5,5-hexamethyl-trisiloxane (Si3), 1,4-bis(dimethylsilyl)benzene were used in this work. Polydimethylsiloxane and bis(dimethylsilyl)benzene were purchased from Aldrich and trisiloxane was obtained from Huls Petrarch Systems. One type of crosslinker reagent, 2,4,6,8-tetramethylcylcotetrasiloxane, was used and was obtained from Aldrich. The coupling reagent, Dimethylaminopyridiniumtoluenesulphonate (DPTS), was synthesized in our lab. All the other reagents, such as ethyl 4-hydroxybenzoate, 11-bromo-1-undecene, 6-bromo-1-hexene, 5-bromo-1-pentene, allyl bromide, methylhydroquinone, tetrafluorohydroquinone, hydroquinone, 4,4'-biphenol, platinum (0)-1,2-divinyl-1,1,3,3-tetramethyldisiloxane (3 wt% complex in xylenes), 1,3-Diisopropylcarbodiimide (DiPC), potassium carbonate, sodium hydroxide, sulfuric acid, were purchased from Aldrich. All the solvents used were obtained from Aldrich, such as acetonitrile (>99.5%), dichloromethane (>99.5%), ethanol (denatured), anhydrous dichloromethane (99.8%), pyridine (99.8%). They were used without further treatment.

2.1.3 Synthesis and Structure Identification of Calamitic LC Monomers

In this work, several calamitic LC monomers with similar general structure but with variations in terminal chain length, lateral substituent and rigid core length were synthesized and listed in Table 2-1. The general synthetic route for these monomers is shown in Figure 2-3. This route consists of three steps: alkylation of phenyl ester [5], hydrolysis of alkylated ester and room temperature esterification [6] of hydroquinone or hydroquinone derivatives, respectively.

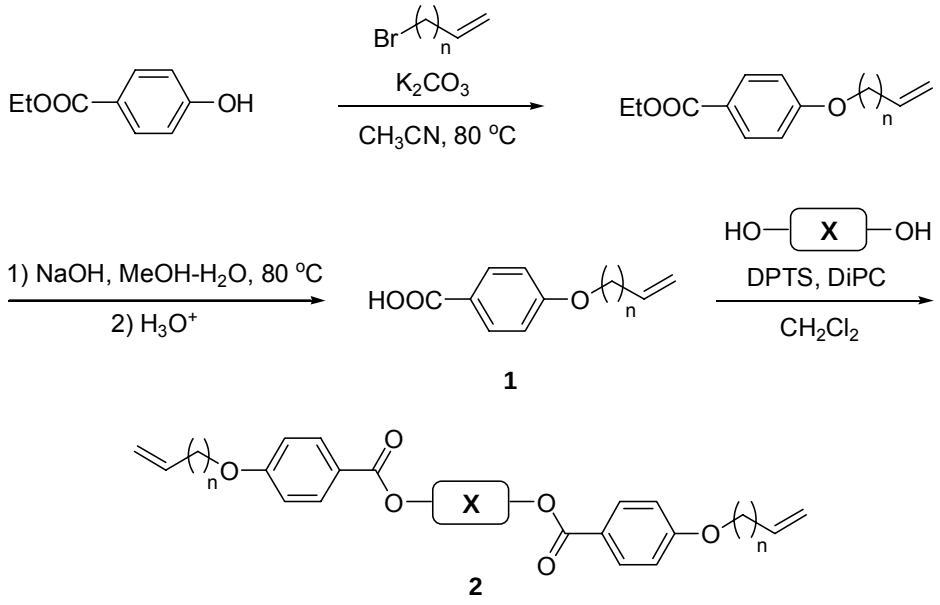

Figure 2-6 General synthetic route of calamitic LC monomers

Table 2-1 Synthesized benzoic acids and LC monomers

	n		**n**	**X**		**n**	**X**
1a	1	**2a**	1	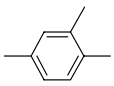	**2d**	9	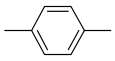
1b	3	**2b**	3	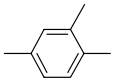	**2e**	9	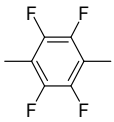
1c	9	**2c**	9	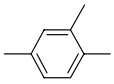	**2f**	9	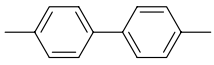

The synthesis of benzoic acid **1c** and LC monomer **2c** is described in detail as an example. For the rest of synthesized monomers, only quantities of reactants and yield of final products are reported. For all the benzoic acids and LC monomers, chemical structure identification by ^{1}H NMR and transition temperatures by DSC are listed as well.

Synthesis of benzoic acid ***1c***

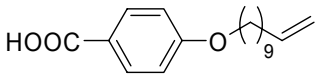

1c

A round-bottomed flask was equipped with a magnetic stirbar and charged with ethyl 4-hydroxybenzoate (16.8 g, 100 mmol), 11-bromo-1-undecene (27.0 g, 110 mmol), and 200 mL acetonitrile. Potassium carbonate (20.9 g, 150 mmol) was added until all the solids in the flask dissolved. The mixture was heated to reflux for 48 hours and then cooled to room temperature. After removing potassium carbonate by filtration, the filtrates were concentrated by removal of acetonitrile under reduced pressure. The residue in a yellow oil-state was transferred to a flask containing methanol (400 mL) and 10 N sodium hydroxide solution (100 mL). The mixture was heated to reflux for 12 hours and poured into 2 L water then acidified with sulfuric acid (pH≈1). White precipitates were filtered and washed by large amount of distilled water. The material was then air dried for 12 hours and recrystallized from acetonitrile to afford 11.7 g (66%) of white crystals.

^{1}H NMR ($CDCl_3$): δ 1.31 (m, 12H, O-$CH_2CH_2(\underline{CH_2})_6CH_2CH{=}CH_2$), 1.81 (m, 2H, O-$CH_2\underline{CH_2}(CH_2)_6CH_2CH{=}CH_2$), 2.03 (m, 2H, O-$CH_2CH_2(CH_2)_6\underline{CH_2}CH{=}CH_2$), 4.04(t, 2H, O-$\underline{CH_2}$), 4.96 (m, 2H, CH=$\underline{CH_2}$), 5.80 (m, 1H, $\underline{CH}{=}CH_2$), 7.26 (t, 2H, Ar), 8.07 (t, 2H, Ar), 11.00 (s, 1H, COO$\underline{H}$).

DSC: Cr · 85.8 · LC_1 · 124.1 · LC_2 · 138.4· I.

*Synthesis of benzoic acid **1a***

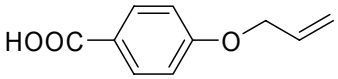

1a

Quantities: ethyl 4-hydroxybenzoate (16.8 g, 100 mmol), allyl bromide (26.9 g, 220 mmol), acetonitrile (200 mL), potassium carbonate (33.5 g, 240 mmol), methanol (400 mL), and 10 N sodium hydroxide solution (100 mL), dilute sulfuric acid (2000 mL). 11.7 g (66%) product was obtained.

^{1}H NMR ($CDCl_3$): δ 4.61 (d, 2H, O-$\underline{CH_2}$), 5.24 (m, 2H, CH=$\underline{CH_2}$), 5.89 (m, 1H, $\underline{CH}$=CH_2), 7.00 (m, 2H, O-$\underline{Ar}$-CO_2), 8.00 (t, 2H, O-$\underline{Ar}$-CO_2), 11.00 (s, 1H, COO$\underline{H}$).

Mp: 165 - 166 ºC.

*Synthesis of benzoic acid **1b***

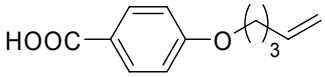

1b

Quantities: ethyl 4-hydroxybenzoate (16.8 g, 100 mmol), 5-bromo-1-pentene (17.3 g, 110 mmol), acetonitrile (200 mL), potassium carbonate (20.9 g, 150 mmol), methanol (400 mL), and 10 N sodium hydroxide solution (100 mL), dilute sulfuric acid (2000 mL). 18.7 g (91%) product was obtained.

^{1}H NMR ($CDCl_3$): δ 1.75 (m, 2H, O-$CH_2\underline{CH_2}CH_2CH$=$CH_2$), 1.96 (m, 2H, $\underline{CH_2}CH$=CH_2), 3.94 (t, 2H, O-$\underline{CH_2}$), 5.00 (m, 2H, CH=$\underline{CH_2}$), 5.70 (m, 1H, $\underline{CH}$=CH_2), 6.98 (m, 2H, O-$\underline{Ar}$-CO_2), 8.02 (t, 2H, O-$\underline{Ar}$-CO_2), 11.00 (s, 1H, COO$\underline{H}$).

DSC: Cr · 100.7 · LC · 185.9 · I.

*Synthesis of LC monomer **2c***

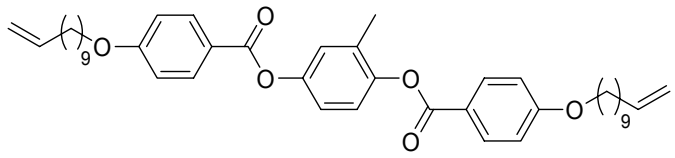

2c

A round-bottomed flask equipped with a magnetic stirbar was charged with compound **1c** (13.04 g, 44 mmol), methylhydroquinone (2.51 g, 20 mmol), DPTS (1.80 g, 6 mmol) and 100 mL dichloromethane. DiPC (11.22 g, 88 mmol) was added *via* syringe after all the solids dissolved. The mixture reaction was stirred at room temperature for 24 hours and then poured to 500 mL methanol. White precipitates were filtered and air dried for 12 hours. The resulting solid was recrystallized from ethanol to afford a white solid of 12.22 g (91%).

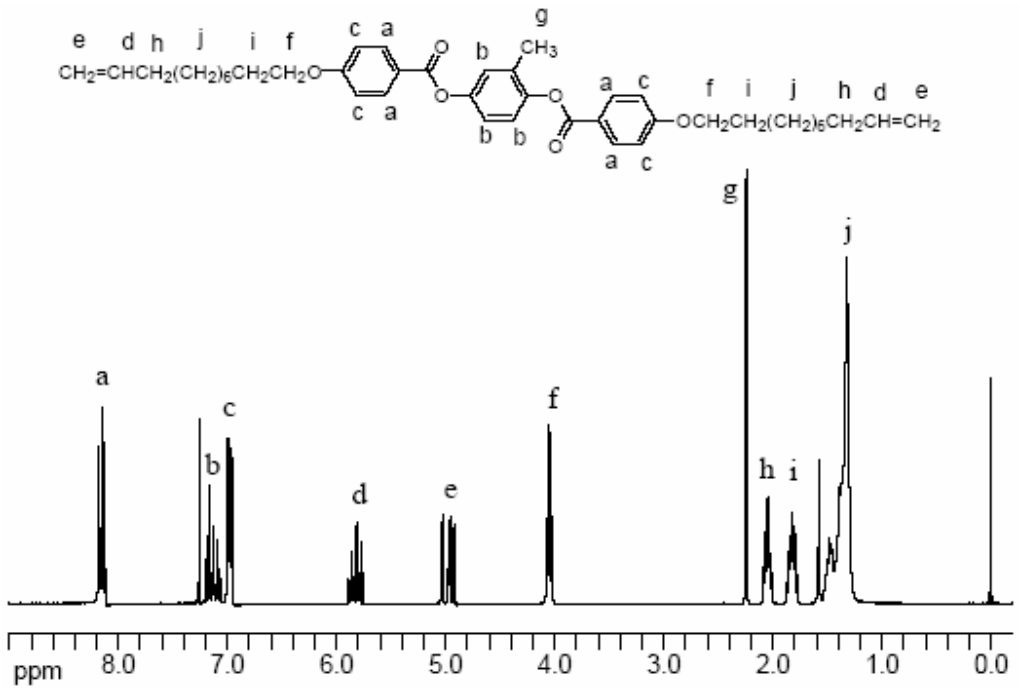

Figure 2-7 ^{1}H NMR spectrum of C11(MeHQ) LC monomer ***2c***

^{1}H NMR ($CDCl_3$): δ 1.38 (m, 24H, O-CH_2CH_2($\underline{CH_2}$)$_6$$CH_2CH$=$CH_2$), 1. 82 (m, 4H, O-$CH_2\underline{CH_2}$($CH_2$)$_6$$CH_2CH$=$CH_2$), 2.04 (m, O-$CH_2CH_2$($CH_2$)$_6$$\underline{CH_2}$CH=CH2), 2.24 (s, 3H, Ar$\underline{CH_3}$), 4.06 (t, 4H, O-$\underline{CH_2}$), 5.43 (m, 4H, CH=$\underline{CH_2}$), 6.07 (m, 2H, $\underline{CH}$=CH_2), 7.00 (m, 4H, O-$\underline{Ar}$-CO_2), 7.16 (m, 3H, $\underline{Ar}CH_3$), 8.16 (t, 4H, O-$\underline{Ar}$-CO_2).

DSC: Cr · 76 · LC · 137 · I

*Synthesis of LC monomer **2a***

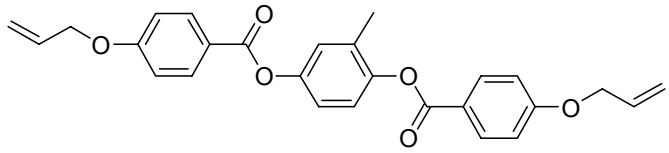

2a

Quantities: compound **1a** (8.00 g, 44 mmol), methylhydroquinone (2.51 g, 20 mmol), DPTS (1.80 g, 6 mmol), DiPC (11.22 g, 88 mmol), dichloromethane (100 mL), methanol (500 mL). The crude material was recrystallized from hot isopropanol to afford 8.25 g (93%) of white solid.

^{1}H NMR ($CDCl_3$): δ 2.25(s, 3H, Ar$\underline{CH_3}$), 4.65 (d, 4H, O-$\underline{CH_2}$), 5.43 (m, 4H, CH=$\underline{CH_2}$), 6.07 (m, 2H, $\underline{CH}$=CH_2), 7.00 (m, 4H, O-$\underline{Ar}$-CO_2), 7.16 (m, 3H, $\underline{Ar}CH_3$), 8.16 (t, 4H, O-$\underline{Ar}$-CO_2).

DSC: Cr · 141 · LC · 216 · I

*Synthesis of LC monomer **2b***

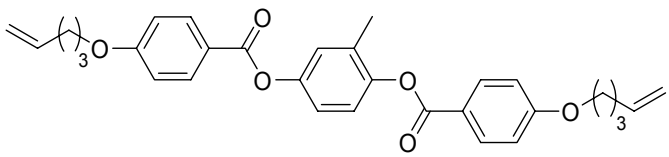

2b

Quantities: compound **1b** (9.27 g, 44 mmol), methylhydroquinone (2.51 g, 20 mmol), DPTS (1.80 g, 6 mmol), DiPC (11.22g, 88 mmol), dichloromethane (100 mL), methanol (500 mL). The crude material was recrystallized from hot ethanol to afford 8.14 g (81%) of white solid.

^{1}H NMR ($CDCl_3$): δ 1.94 (m, 4H, O-$CH_2\underline{CH_2}CH_2CH{=}CH_2$), 2.24(s, 3H, Ar$\underline{CH_3}$), 2.28 (m, 4H, $\underline{CH_2}CH{=}CH_2$), 4.07 (t, 4H, O-$\underline{CH_2}$), 5.10 (m, 4H, CH=$\underline{CH_2}$), 5.84 (m, 2H, $\underline{CH}{=}CH_2$), 6.98 (m, 4H, O-$\underline{Ar}$-CO_2), 7.16 (m, 3H, $\underline{Ar}CH_3$), 8.15 (t, 4H, O-$\underline{Ar}$-CO_2).

DSC: Cr · 100.6 · LC · 185.9 · I. (Lit [7]: Cr · 100.4 · N · 185.8 · I).

*Synthesis of LC monomer **2d***

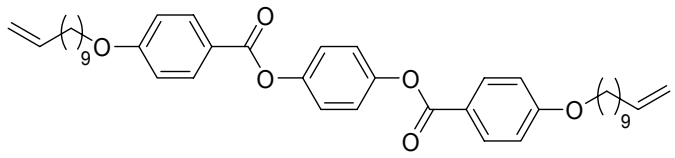

2d

Quantities: **1c** (13.04 g, 44 mmol), hydroquinone (2.22 g, 20 mmol), DPTS (1.80 g, 6 mmol), DiPC (11.22 g, 88 mmol), dichloromethane (100 mL), methanol (500 mL). The crude material was recrystallized from hot ethanol to afford 12.30 g (94%) of white solid.

^{1}H NMR ($CDCl_3$): δ 1.36 (m, 24H, O-$CH_2CH_2(\underline{CH_2})_6CH_2CH{=}CH_2$), 1.83 (m, 4H, O-$CH_2\underline{CH_2}(CH_2)_6CH_2CH{=}CH_2$), 2.04 (m, O-$CH_2CH_2(CH_2)_6\underline{CH_2}$CH=CH2), 4.05 (t, 4H, O-$\underline{CH_2}$), 4.97 (m, 4H, CH=$\underline{CH_2}$), 5.83 (m, 2H, $\underline{CH}{=}CH_2$), 6.98 (d, 4H, O-$\underline{Ar}$-CO_2), 7.26 (s, 4H, O-$\underline{Ar}$-O), 8.15 (d, 4H, O-$\underline{Ar}$-CO_2).

DSC: Cr · 111 · LC_1 · 138 · LC_2 · 174 · I. (Lit [1]: Cr · 103 · S_A · 130 · N · 168 · I).

*Synthesis of LC monomer **2e***

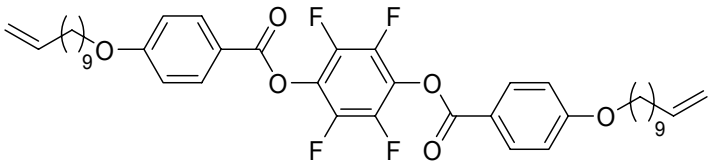

2e

Quantities: **1c** (43.6 g, 147 mmol), tetrafluorohydroquinone (13.0 g, 0.070 mol), DPTS (4.51 g, 0.015 mol), DiPC (37.48 g, 0.294 mol), pyridine (30 mL), dichloromethane (560 mL), methanol (2000 mL). The crude material was recrystallized from hot ethanol to afford 43.9 g (86%) of white solid.

^{1}H NMR ($CDCl_3$): δ 1.36 (m, 24H, O-CH_2CH_2($\underline{CH_2}$)$_6$$CH_2CH$=$CH_2$), 1.83 (m, 4H, O-$CH_2\underline{CH_2}$($CH_2$)$_6$$CH_2CH$=$CH_2$), 2.04 (m, O-$CH_2CH_2$($CH_2$)$_6$$\underline{CH_2}$CH=CH2), 4.06 (t, 4H, O-$\underline{CH_2}$), 4.96 (m, 4H, CH=$\underline{CH_2}$), 5.80 (m, 2H, $\underline{CH}$=CH_2), 7.00 (d, 4H, O-$\underline{Ar}$-CO_2), 8.15 (d, 4H, O-$\underline{Ar}$-CO_2).

DSC: Cr · 91 · LC · 129 · I.

*Synthesis of monomer **2f***

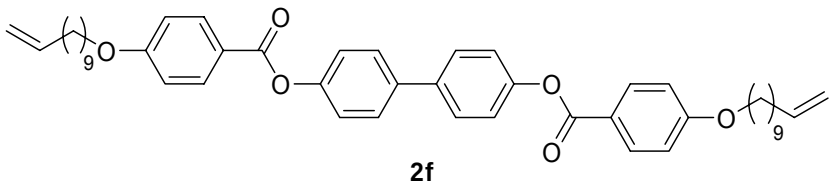

2f

Quantities: **1c** (19.56 g, 66 mmol), 4,4'-biphenol (5.76 g, 30 mmol), DPTS (3.96 g, 1. 2 mmol), DiPC (11.22g, 88 mmol), pyridine (30 mL), dichloromethane (250 mL),

methanol (800 mL). The crude material was recrystallized from hot ethanol to afford 21.6 g (98%) of white solid.

^{1}H NMR ($CDCl_3$): δ 1.36 (m, 24H, O-CH_2CH_2($\underline{CH_2}$)$_6$$CH_2CH$=$CH_2$), 1.83 (m, 4H, O-$CH_2\underline{CH_2}$($CH_2$)$_6$$CH_2CH$=$CH_2$), 2.04 (m, O-$CH_2CH_2$($CH_2$)$_6$$\underline{CH_2}$CH=CH2), 4.06 (t, 4H, O-$\underline{CH_2}$), 4.96 (m, 4H, CH=$\underline{CH_2}$), 5.80 (m, 2H, $\underline{CH}$=CH_2), 6.92 (d, 4H, O-$\underline{Ar}$-CO_2), 7.21 (d, 4H, O-$\underline{Ar}$-$\underline{Ar}$-O),7.55 (m, 4H, O-$\underline{Ar}$-$\underline{Ar}$-O), 8.03 (d, 4H, O-$\underline{Ar}$-CO_2).

DSC: Cr_1 · 98 · Cr_2 · 133 · LC_1 · 224 · LC_2 · 264 · I.

2.1.4 Synthesis of Main-chain LC Polymers

Standard hydrosilylation was adapted in our research to prepare the linear polymer. In the polymerization, the double bonds of the mesogenic monomers and the Si-H group of the siloxane spacer react to form a linear polymer main chain in the presence of the platinum catalyst.

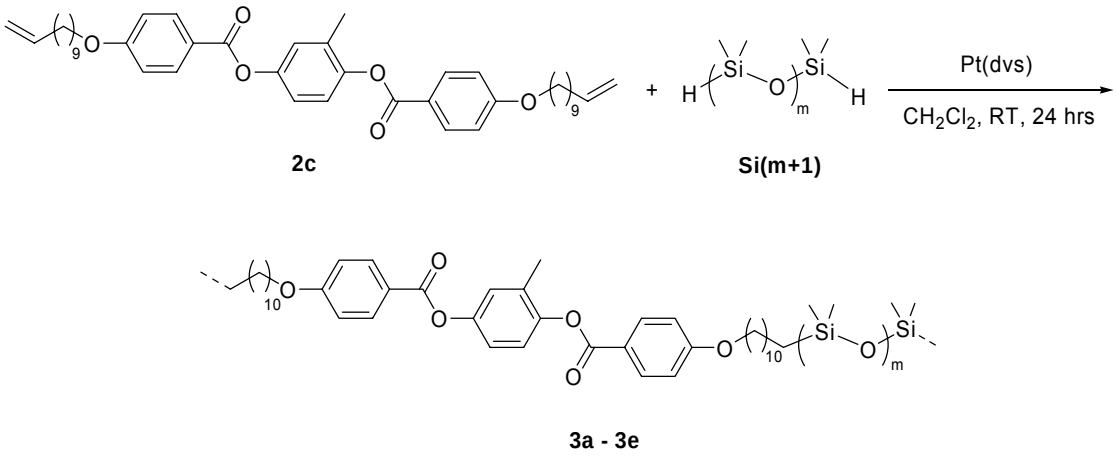

Figure 2-8 Synthetic route of LC polymer by varying the ratio of short spacer (**Si3**) and long spacer (**Si8**)

Synthesis of polymer ***3a - Si3/Si8(0/100)***

An oven-dried two-necked round-bottomed flask equipped with a magnetic stirbar and two rubber stoppers was cooled to room temperature under an argon purge. The flask was charged with monomer **2c** (1.706 g, 2.50 mmol) and octasiloxane (1.478 g, 2.50 mmol). Anhydrous dichloromethane (8 mL) was transferred to the flask via a syringe. After solids in the flask dissolved completely, 50 μL platinum (0)-1,3-divinyl-1,1,3,3-tetramethyldisiloxane catalyst solution (2.5-3.0%) was added *via* an Eppendorf pipette. The polymerization was carried out under the protection of argon for 24 hrs. The resulting viscous polymer was diluted with 8mL of dichloromethane and filtered by a 0.2 μm Millipore® filter, and poured into a PTFE coated flat-bottomed pan. After the solvent evaporated completely, a film-like polymer sample formed in the pan. Fibers can be hand-drawn from the LCP melts in the mesophase.

Since the preparation of the other polymers in this family is the same as that for polymer **3a**, only the quantities of reactants involved in the preparation are shown here.

Synthesis of polymer ***3b - Si3/Si8(25/75)***

Quantities: monomer **2c** (1.638 g, 2.40 mmol), 1,1,3,3,5,5-hexamethyl-trisiloxane (0.128 g, 0.60 mmol), octasiloxane (0.940 g, 1.80 mmol), platinum (0)-1,3-divinyl-1,1,3,3-tetramethyldisiloxane (50 μL), anhydrous dichloromethane (8 mL).

Synthesis of polymer ***3c - Si3/Si8(50/50)***

Quantities: monomer **2c** (1.638 g, 2.40 mmol), 1,1,3,3,5,5-hexamethyl-trisiloxane (0.255 g, 1.20 mmol), octasiloxane (0.709 g, 1.20 mmol), platinum (0)-1,3-divinyl-

1,1,3,3-tetramethyldisiloxane (50 μL), anhydrous dichloromethane (8 mL).

Synthesis of polymer ***3d - Si3/Si8(75/25)***

Quantities: monomer **2c** (1.638 g, 2.40 mmol), 1,1,3,3,5,5-hexamethyl-trisiloxane (0.383 g, 1.800 mmol), octasiloxane (0.355 g, 0.60 mmol), platinum (0)-1,3-divinyl-1,1,3,3-tetramethyldisiloxane (50 μL), anhydrous dichloromethane (8 mL).

Synthesis of polymer ***3e - Si3/Si8(100/0)***

Quantities: monomer **2c** (1.706 g, 2.50 mmol), 1,1,3,3,5,5-hexamethyl-trisiloxane (0.532 g, 2.50 mmol), platinum (0)-1,3-divinyl-1,1,3,3-tetramethyldisiloxane (50 μL), anhydrous dichloromethane (8 mL).

The number average molecular weight ($\overline{Mn}$) and the weight average molecular weight ($\overline{Mw}$) of synthesized polymers were determined by gel permeation chromatography (GPC). For these five polymers, ($\overline{Mn}$) ranges from 14000 to 25000 and ($\overline{Mw}$) ranges from 36000 to 63000.

Normally, the final product of a polymerization is a mixture of molecules of different molecular weight. The breadth of molecular weight distribution in a product is described by the polydispersity index (PDI), which can be calculated from Equation 2-1.

$$PDI = \frac{\overline{Mw}}{\overline{Mn}} \qquad (2\text{-}1)$$

The closer the value of PDI is to one, the narrower is the distribution of a polymer. From GPC experiments, the PDI of our polymers ranges from 2 to 3, which is a reasonable

range of PDI as found in many step polymerizations [4].

Table 2-2 Molecular weight and polydispersity of linear polymer **3a-3e**

Polymer	$\overline{Mn}$	$\overline{Mw}$ (g/mol)	PDI
3a-Si3/Si8(0/100)	24601	52327	2.13
3b-Si3/Si8(25/75)	13983	36311	2.60
3c-Si3/Si8(50/50)	19757	60859	3.08
3d-Si3/Si8(75/25)	21753	63218	2.90
3e-Si3/Si8(100/0)	21396	43550	2.04

2.1.5 Synthesis of Main-chain LC Polymers with Terphenyl Transverse Rod

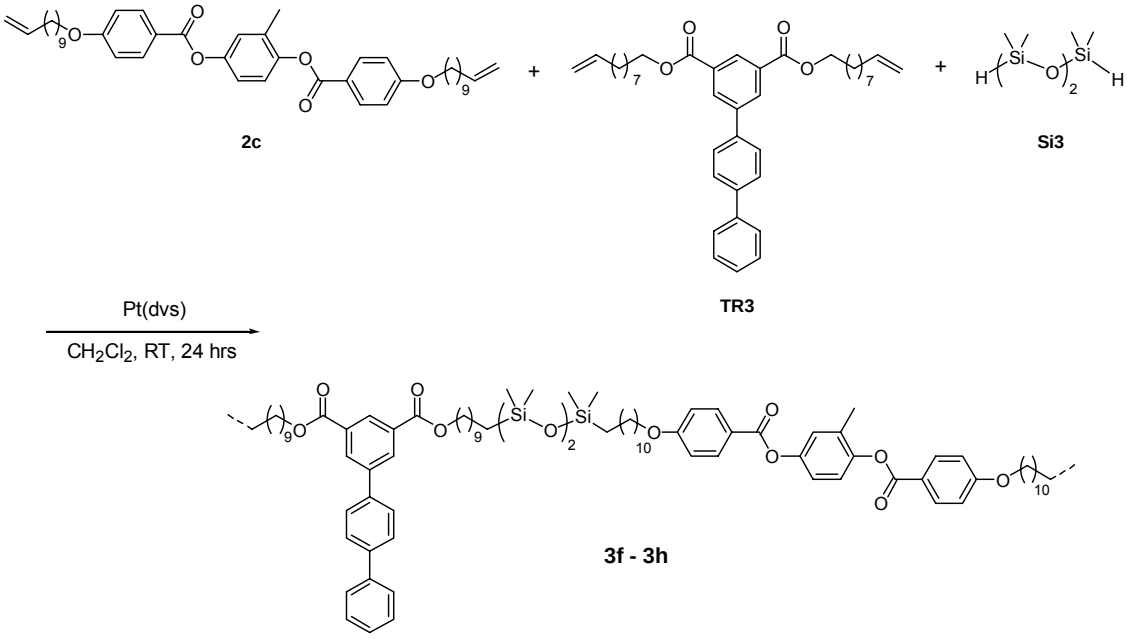

Figure 2-9 Synthetic route to C11(MeHQ)Si3 LC polymer by varying the amount of terphenyl transverse rod (TR3)

Synthesis of polymer ***3f – C11(MeHQ)/TR3(75/25)Si3***

An oven-dried two-necked round-bottomed flask equipped with a magnetic stirbar

and two rubber stoppers was cooled to room temperature under an argon purge. The flask was charged with monomer **2c** (1.229 g, 1.800 mmol), terphenyl transverse rod (0.364 g, 0.600mmol), and 1,1,3,3,5,5-hexamethyl-trisiloxane (0.511 g, 2.400 mmol). Anhydrous dichloromethane (8 mL) was transferred to the flask via a syringe. After solids in the flask dissolved completely, 50 μL platinum (0)-1,3-divinyl-1,1,3,3-tetramethyldisiloxane catalyst solution (2.5-3.0%) was added via an Eppendorf pipette. The polymerization was carried out under the protection of argon for 24 hrs. The resulting viscous polymer was diluted with 8mL of dichloromethane and filtered by a 0.2 μm Millipore® filter, and poured into a PTFE coated flat-bottomed pan. After the solvent evaporate completely, a film-like polymer sample can be collected.

Synthesis of polymer ***3g – C11(MeHQ)/TR3(50/50)Si3***

Quantities: monomer **2c** (0.819 g, 1.200 mmol), terphenyl transverse rod (0.728 g, 1.200 mmol), 1,1,3,3,5,5-hexamethyl-trisiloxane (0.511 g, 2.400 mmol), platinum (0)-1,3-divinyl-1,1,3,3-tetramethyldisiloxane (50 μL), anhydrous dichloromethane (8mL).

Synthesis of polymer ***3h – C11(MeHQ)/TR3(25/75)Si3***

Quantities: monomer **2c** (0.410 g, 0.600mmol), terphenyl transverse rod (1.092 g, 1.800 mmol), 1,1,3,3,5,5-hexamethyl-trisiloxane (0.511 g, 2.400 mmol), platinum (0)-1,3-divinyl-1,1,3,3-tetramethyldisiloxane (50 μL), anhydrous dichloromethane (8mL).

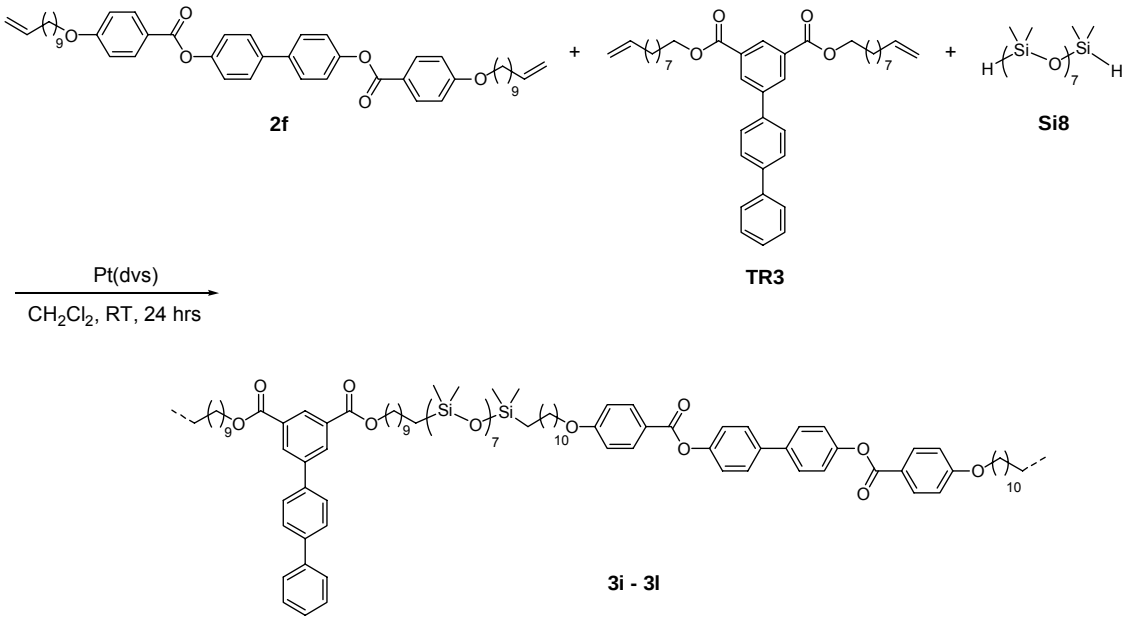

Figure 2-10 Synthetic route to C11(Biph)Si8 LC polymer by varying the amount of terphenyl transverse rod (**TR3**)

Synthesis of polymer ***3i – C11(Biph)/TR3(100/0)Si8***

An oven-dried two-necked round-bottomed flask equipped with a magnetic stirbar and two rubber stoppers was cooled to room temperature under an argon purge. The flask was charged with monomer **2f** (1.790 g, 2.400 mmol) and octasiloxane (1.419 g, 2.400 mmol). Anhydrous dichloromethane (8 mL) was transferred to the flask via a syringe. After solids in the flask dissolved completely, 50 μL platinum (0)-1,3-divinyl-1,1,3,3-tetramethyldisiloxane solution (2.5-3.0%) was added via an eppendorf pipette. The polymerization was carried out under the protection of argon for 24 hrs. The resulting viscous polymer was diluted with 8mL of dichloromethane and filtered by a 0.2 μm Millipore® filter, and poured into a PTFE coated flat-bottomed pan. After the solvent evaporate completely, a film-like polymer sample can be collected.

Synthesis of polymer ***3j – C11(Biph)/TR3(75/25)Si8***

Quantities: monomer **2f** (1.343 g, 1.800 mmol), terphenyl transverse rod (0.364 g, 0.600 mmol), octasiloxane (1.419 g, 2.400 mmol), platinum (0)-1,3-divinyl-1,1,3,3-tetramethyldisiloxane (50 μL), anhydrous dichloromethane (8 mL).

Synthesis of polymer ***3k – C11(Biph)/TR3(50/50)Si8***

Quantities: monomer **2f** (0.895 g, 1.200 mmol), terphenyl transverse rod (0.728 g, 1.200 mmol), octasiloxane (1.419 g, 2.400 mmol), platinum (0)-1,3-divinyl-1,1,3,3-tetramethyldisiloxane (50 μL), anhydrous dichloromethane (8 mL).

Synthesis of polymer ***3l – C11(Biph)/TR3(25/75)Si8***

Quantities: monomer **2f** (0.448 g, 0.600 mmol), terphenyl transverse rod (1.093 g, 1.800 mmol), octasiloxane (1.419 g, 2.400 mmol), platinum (0)-1,3-divinyl-1,1,3,3-tetramethyldisiloxane (50 μL), anhydrous dichloromethane (8 mL).

2.1.6 Synthesis of Main-chain LC Elastomers

In Chapter 1, we introduced Finkelmann's one step method to synthesize main-chain LC elastomers [2] and Mather's approach to main-chain LC elastomers as shape memory materials [3]. Both of them adopted the standard hydrosilylation reaction, but their film fabrication methods were different. Finkelmann's reaction was carried out in a concentrated toluene solution and under centrifugation at 90 °C for 24-48 hrs. A swollen gel was then removed from the reaction cell and hung at one end to keep it straight. A polydomain LCE film was obtained after the solvent evaporated slowly. A monodomain LCE film was obtained by aligning a swollen gel under load and secondary crosslinking

at 30 °C under high vaccum. Mather's synthesis was carried out initially in an ice bath and then the reaction solution was injected into an aligned cell to cure the film. Compared with their approaches, our fabrication method is relatively facile. Our hydrosilylation reaction is carried out in a concentrated dichloromethane solution at room temperature. It was observed that gelation occurs around 5 minutes after the addition of platinum(0) catalyst. Therefore, filtration of reaction solution and film casting must be accomplished before gelation happens. In our work, after adding the catalyst, the reaction was normally given 3-4 minutes before the next step in which the reaction solution was filtered through a 0.5 μm millipore filter. After that, the filtrate was poured into a Teflon-coated flat-bottomed pan with a covered lid. A slow evaporation of solvent was found to be important and necessary to form a smooth and integral film. After 12 hours, the cured film can be easily peeled from the pan by spraying a small amount of ethanol between film and pan. The film was dried in air for 24 hours before characterization.

In order to investigate the effect of crosslinking density, spacer length and structures of mesogenic groups on the integrity and physical properties of the LCE films, a family of LC elastomers were synthesized and fabricated by the method described above. The synthesis generally route is as shown in Figure 2-11. Since a same reactivity of Si-H group in both spacer and crosslinker was assumed, a random distribution of crosslinking sites was expected in the prepared LCEs [8].

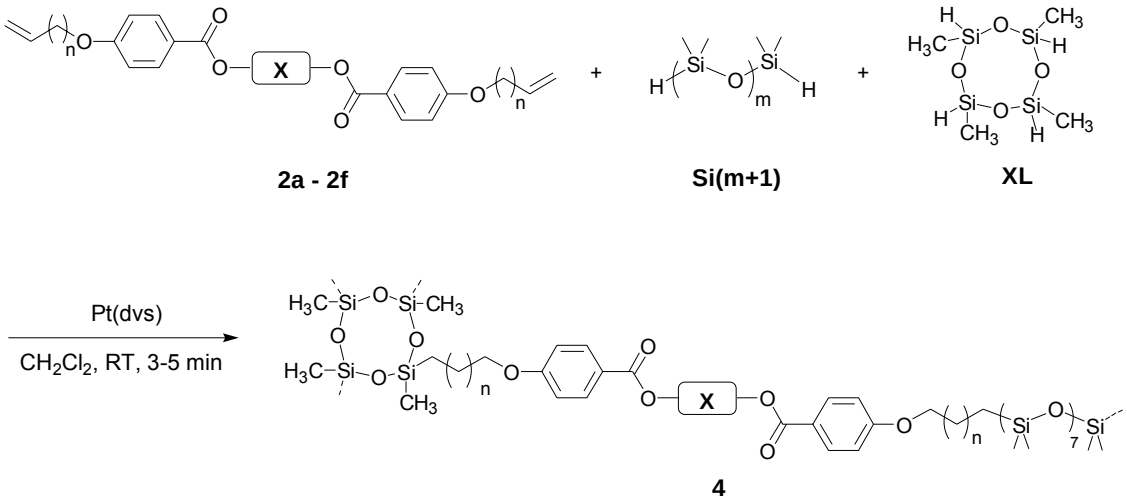

Figure 2-11 General synthetic route of LCEs by varying crosslinker content, spacer length and mesogenic groups

The compositions, e.g. crosslinker content, siloxane spacer and mesogenic monomer, of each LCE are listed in Table 2-3.

Table 2-3 Components and compositions of synthesized LCEs

Elastomer	Monomer	Si3 (m = 2) mol%	Si8 (m = 7) mol %	XL mol %
4a	**2c**	0	90	5
4b	**2c**	0	80	10
4c	**2c**	0	70	15
4d	**2c**	0	60	20
4e	**2c**	0	50	25
4f	**2a**	0	80	10
4g	**2b**	0	80	10
4h	**2a**	80	0	10
4i	**2b**	80	0	10
4j	**2c**	80	0	10
4k	**2d**	0	80	10
4l	**2e**	0	80	10

Note:

2a: X = 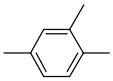 and n = 1; **2b**: X = 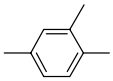 and n = 3;

2c: X = 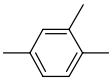 and n = 9; **2d**: X = 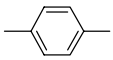 and n = 9; **2e**: X = 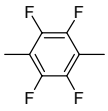 and n = 9.

Here, the synthesis of LCE **4b** is described as an example. For the other LCEs, only quantities of reactants are reported. The crosslinker content was calculated based on the molar fraction of crosslinker to the total molar amount of spacer and crosslinker in the final material.

Synthesis of LCE ***4b - C11(MeHO)Si8XL10***

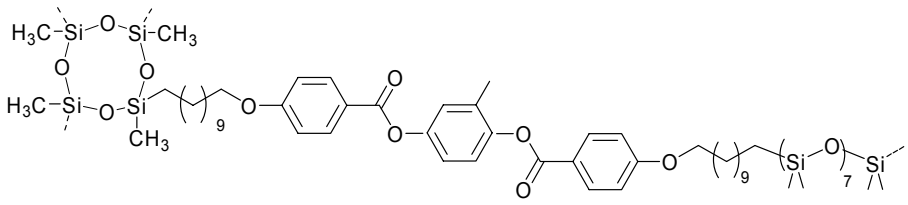

4b

An oven-dried two-necked round-bottomed flask equipped with a magnetic stirbar and two rubber stoppers was cooled to room temperature under an argon purge. The flask was charged with monomer **2c** (1.706 g, 2.50 mmol), octasiloxane spacer (1.182 g, 2.00 mmol), crosslinker 2,4,6,8-tetramethylcylcotetrasiloxane (0.060 g, 0.25 mmol). Anhydrous dichloromethane (8 mL) was transferred to the flask via a syringe. After solids in the flask dissolved completely, 50 µL platinum (0)-1,3-divinyl-1,1,3,3-tetramethyldisiloxane solution (2.5-3.0%) was added via an Eppendorf pipette. The

reaction was carried out at room temperature. The reaction solution was filtered by 0.2 μm Millipore® filter after having reacted for 3-5 minutes and then was quickly poured into a PTFE coated flat-bottomed pan. The pan was covered by a plastic lid in order to let the solvent evaporate slowly. A thin film formed in the pan after the solvent evaporated, which could be easily peeled from the pan sometimes with the aid of ethanol.

Synthesis of LCE ***4a*** **-** ***C11(MeHQ)Si8XL5***

Quantities: monomer **2c** (1.706 g, 2.50 mmol), octasiloxane (1.330 g, 2.25 mmol), 2,4,6,8-tetramethylcylcotetrasiloxane (0.030 g, 0.125 mmol), platinum (0)-1,3-divinyl-1,1,3,3-tetramethyldisiloxane (50 μL), anhydrous dichloromethane (8 mL).

Synthesis of LCE ***4c*** **-** ***C11(MeHQ)Si8XL15***

Quantities: monomer **2c** (1.706 g, 2.50 mmol), octasiloxane (1.034 g, 1.75 mmol), 2,4,6,8-tetramethylcylcotetrasiloxane (0.091 g, 0.375 mmol), platinum (0)-1,3-divinyl-1,1,3,3-tetramethyldisiloxane (50 μL), anhydrous dichloromethane (8 mL).

Synthesis of LCE ***4d*** **-** ***C11(MeHQ)Si8XL20***

Quantities: monomer **2c** (1.706 g, 2.500 mmol), octasiloxane (0.887 g, 1.500 mmol), 2,4,6,8-tetramethylcylcotetrasiloxane (0.121 g, 0.500 mmol), platinum (0)-1,3-divinyl-1,1,3,3-tetramethyldisiloxane (50 μL), anhydrous dichloromethane (8 mL).

Synthesis of LCE ***4e*** **-** ***C11(MeHQ)Si8XL25***

Quantities: monomer **2c** (1.638 g, 2.40 mmol), octasiloxane (0.710 g, 1.20 mmol), 2,4,6,8-tetramethylcylcotetrasiloxane (0.145 g, 0.60 mmol), platinum (0)-1,3-divinyl-1,1,3,3-tetramethyldisiloxane (50 μL), anhydrous dichloromethane (8 mL).

Synthesis of LCE ***4f – C3(MeHQ)Si8XL10***

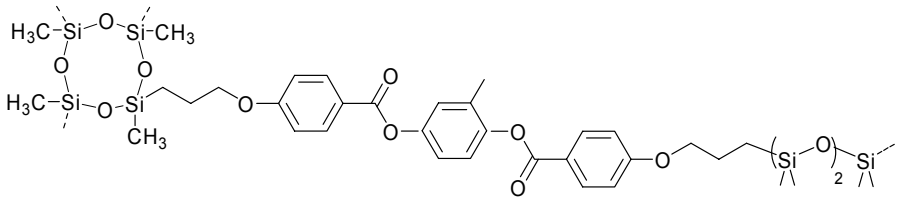

4f

Quantities: monomer **2a** (1.134 g, 2.50 mmol), octasiloxane (1.182 g, 2.00 mmol), 2,4,6,8-tetramethylcylcotetrasiloxane (0.060 g, 0.25 mmol), platinum (0)-1,3-divinyl-1,1,3,3-tetramethyldisiloxane (50 μL), anhydrous dichloromethane (8 mL).

Synthesis of LCE ***4g – C5(MeHQ)Si8XL10***

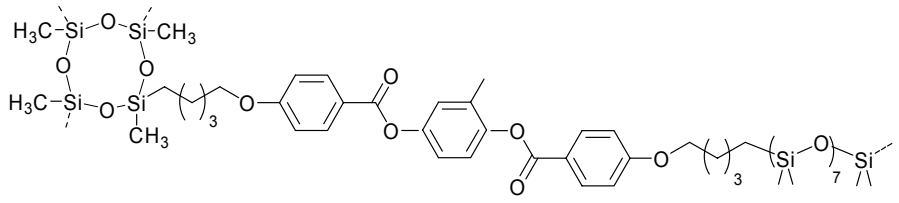

4g

Quantities: monomer **2b** (1.277 g, 2.50 mmol), octasiloxane (1.182 g, 2.00 mmol), 2,4,6,8-tetramethylcylcotetrasiloxane (0.060 g, 0.25 mmol), platinum (0)-1,3-divinyl-1,1,3,3-tetramethyldisiloxane (50 μL), anhydrous dichloromethane (8 mL).

Synthesis of LCE ***4h – C3(MeHQ)Si3XL10***

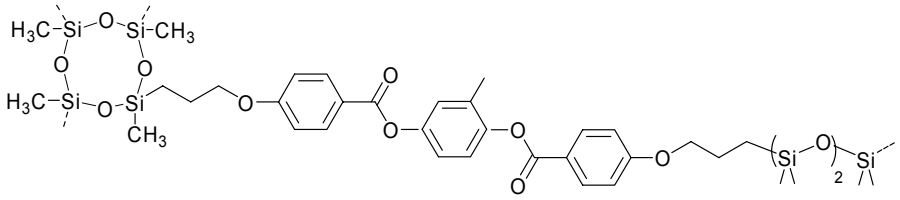

4h

Quantities: monomer **2a** (1.134 g, 2.50 mmol), 1,1,3,3,5,5-hexamenthyl-trisiloxane (0.426 g, 2.00 mmol), 2,4,6,8-tetramethylcylcotetrasiloxane (0.060 g, 0.25 mmol), platinum (0)-1,3-divinyl-1,1,3,3-tetramethyldisiloxane (50 μL), anhydrous dichloromethane (8 mL).

Synthesis of LCE ***4i – C5(MeHQ)Si3XL10***

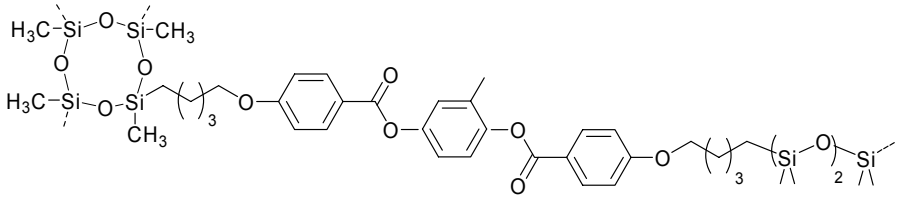

4i

Quantities: monomer **2b** (1.277 g, 2.50 mmol), 1,1,3,3,5,5-hexamenthyl-trisiloxane (0.426 g, 2.00 mmol), 2,4,6,8-tetramethylcylcotetrasiloxane (0.060 g, 0.25 mmol), platinum (0)-1,3-divinyl-1,1,3,3-tetramethyldisiloxane (50 μL), anhydrous dichloromethane (8 mL).

Synthesis of LCE ***4j – C11(MeHQ)Si3XL10***

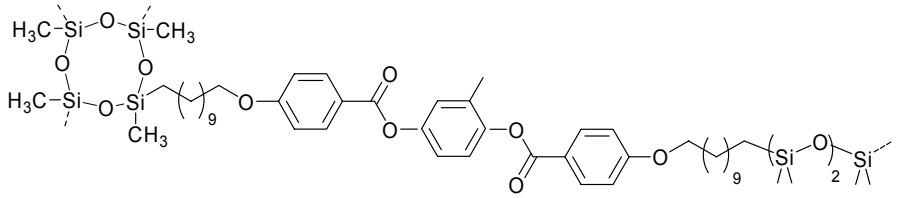

4j

Quantities: monomer **2c** (1.706 g, 2.50 mmol), 1,1,3,3,5,5-hexamenthyl-trisiloxane (0.426 g, 2.00 mmol), 2,4,6,8-tetramethylcylcotetrasiloxane (0.060 g, 0.25 mmol), platinum (0)-1,3-divinyl-1,1,3,3-tetramethyldisiloxane (50 μL), anhydrous dichloromethane (8 mL).

As so far described, all the synthesized LCEs contain only a single type of mesogen, which has three benzene rings linked by ester group with a methyl group on the central benzene ring. In order to investigate the influence of lateral substituents on physical properties of the LC elastomers, we prepared another two types of mesogens by changing the lateral substituents on the central aromatic ring.

Synthesis of LCE ***4k - C11(4H)Si8XL10***

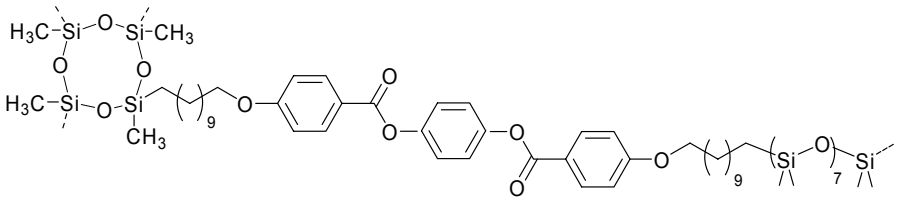

4k

Quantities: monomer **2d** (1.671 g, 2.50 mmol), octasiloxane (1.182 g, 2.00 mmol),

2,4,6,8-tetramethylcylcotetrasiloxane (0.060 g, 0.25 mmol), platinum (0)-1,3-divinyl-1,1,3,3-tetramethyldisiloxane (50 μL), anhydrous dichloromethane (8 mL).

Synthesis of LCE ***4l - C11(4F)Si8XL10***

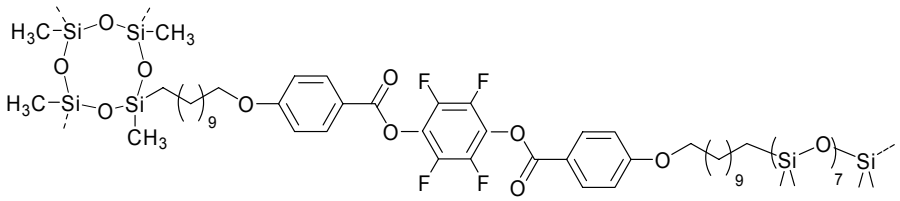

4l

Quantities: monomer **2e** (1.862 g, 2.50 mmol), octasiloxane (1.182 g, 2.00 mmol), 2,4,6,8-tetramethylcylcotetrasiloxane (0.060 g, 0.25 mmol), platinum (0)-1,3-divinyl-1,1,3,3-tetramethyldisiloxane (50 μL), anhydrous dichloromethane (8 mL).

In addition to trisiloxane and octasiloxane, a more rigid siloxane spacer 1,4-bis(dimethylsilyl)benzene (**Siph**) was also used to prepare LC elastomers ***4m, 4n*** and ***4o*** to investigate the effect of spacer flexibility on the properties of LC elastomers.

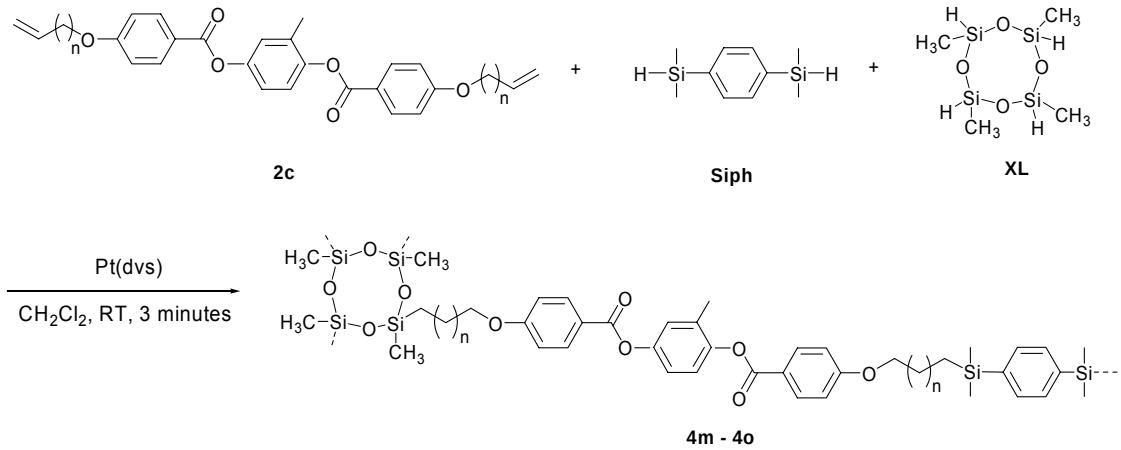

2c **Siph** **XL**

4m - 4o

Figure 2-12 Synthetic route to LC elastomer with **Siph** spacer by varying hydrocarbon terminal chain of mesogenic unit

Synthesis of LCE ***4m – C3(MeHQ)SiphXL10***

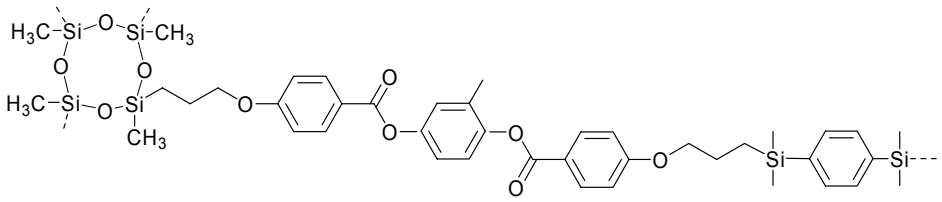

4m

Quantities: monomer **2a** (1.134 g, 2.50 mmol), 1,4-bis(dimethylsilyl)benzene (0.397 g, 2.00 mmol), 2,4,6,8-tetramethylcylcotetrasiloxane (0.060 g, 0.25 mmol), platinum (0)-1,3-divinyl-1,1,3,3-tetramethyldisiloxane (50 µL), anhydrous dichloromethane (8 mL).

Synthesis of LCE ***4n – C5(MeHQ)SiphXL10***

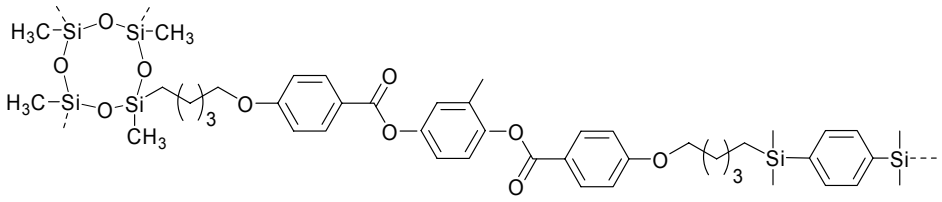

4n

Quantities: monomer **2b** (1.277 g, 2.50 mmol), 1,4-bis(dimethylsilyl)benzene (0.397 g, 2.00 mmol), 2,4,6,8-tetramethylcylcotetrasiloxane (0.060 g, 0.25 mmol), platinum (0)-1,3-divinyl-1,1,3,3-tetramethyldisiloxane (50 µL), anhydrous dichloromethane (8 mL).

Synthesis of LCE ***4o - C11(MeHQ)SiphXL10***

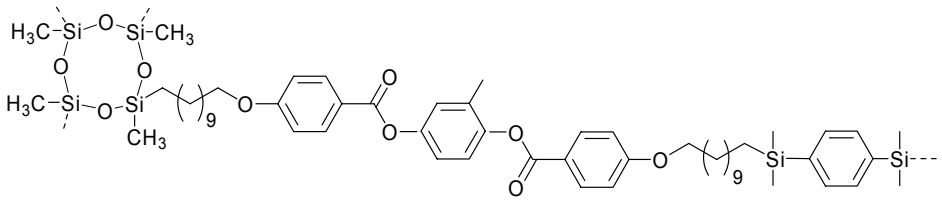

4o

Quantities: monomer **2c** (1.706 g, 2.50 mmol), 1,4-bis(dimethylsilyl)benzene (0.397 g, 2.00 mmol), 2,4,6,8-tetramethylcylcotetrasiloxane (0.060 g, 0.25 mmol), platinum (0)-1,3-divinyl-1,1,3,3-tetramethyldisiloxane (50 μL), anhydrous dichloromethane (8 mL).

2.1.7 Synthesis of Main-chain LC Elastomers with Terphenyl Transverse Rod

A series of LC elastomers with terphenyl transverse rod (**TR3**) ranging from 10 mol% to 40 mol% were synthesized to investigate the effect of a transversely attached rod on properties of LC elastomers and their potential as auxetic materials.

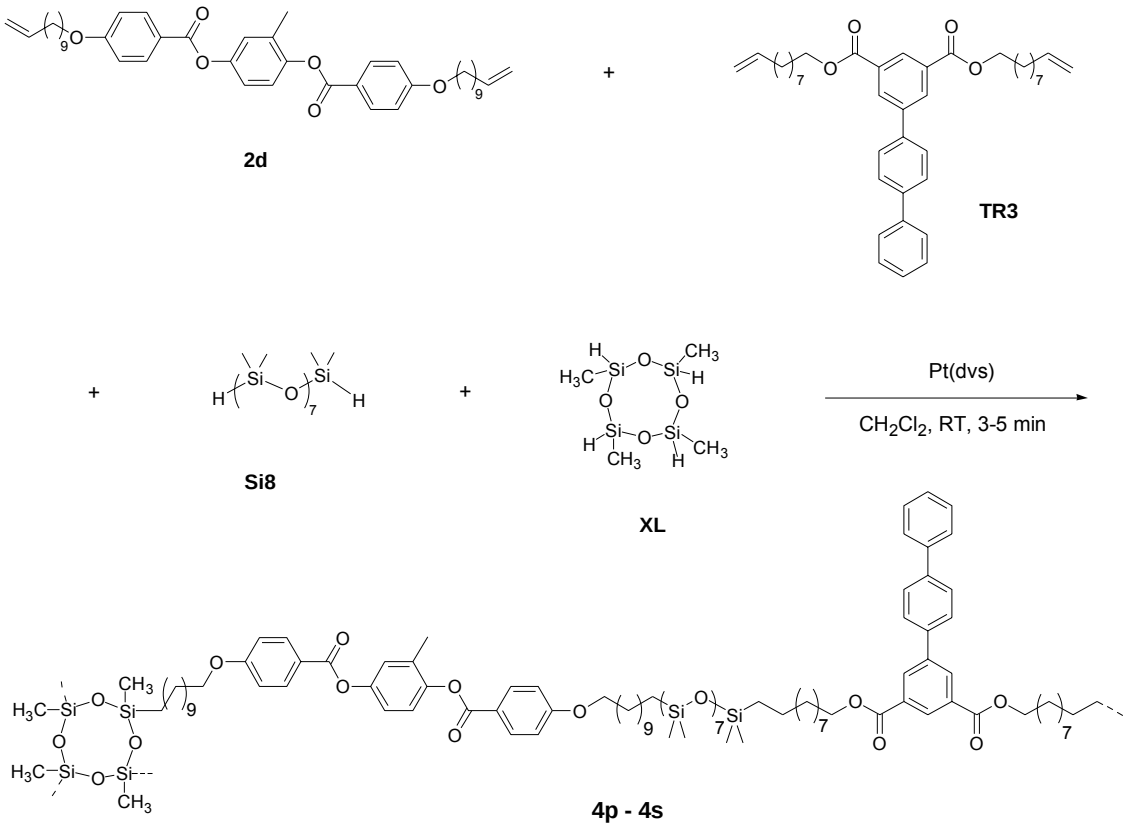

Figure 2-13 Synthesis route of C11(MeHQ)Si8XL10 with various amount of transverse rod

Synthesis of LCE ***4p - C11(MeHQ)/TR3 (90/10)***

An oven-dried two-necked round-bottomed flask equipped with a magnetic stirbar and two rubber stoppers was cooled to room temperature under an argon purge. The flask was charged with monomer **2c** (1.536 g, 2.250 mmol), terphenyl transverse rod

(0.152 g, 0.250 mmol), octasiloxane (1.182 g, 2.000 mmol), 2,4,6,8-tetramethylcylcotetrasiloxane (0.060 g, 0.250 mmol). Anhydrous dichloromethane (8 mL) was transferred to the flask via a syringe. After solids in the flask dissolved completely, 50 μL platinum (0)-1,3-divinyl-1,1,3,3-tetramethyldisiloxane solution (2.5-3%) was added *via* an eppendorf pipette. The reaction was carried out at room temperature for 3-5 minutes and then filtered by 0.2 μm Millipore® filter, and poured into a PTFE coated flat-bottomed pan. The pan was covered by a plastic cover in order to let the solvent evaporate slowly. A thin film formed in the pan after the solvent evaporated completely and could be easily peeled from the pan with the aid of some ethanol.

Synthesis of LCE ***4q - C11(MeHQ)/TR3 (80/20)***

Quantities: monomer **2c** (1.365 g, 2.000 mmol), terphenyl transverse rod (0.303 g, 0.500 mmol), octasiloxane (1.182 g, 2.000 mmol), 2,4,6,8-tetramethylcylcotetrasiloxane (0.060 g, 0.250 mmol), platinum (0)-1,3-divinyl-1,1,3,3-tetramethyldisiloxane (50 μL), anhydrous dichloromethane (8 mL).

Synthesis of LCE ***4r - C11(MeHQ)/TR3 (70/30)***

Quantities: monomer **2c** (1.194 g, 1.750 mmol), terphenyl transverse rod (0.455g, 0.750 mmol), octasiloxane (1.182 g, 2.000 mmol), 2,4,6,8-tetramethylcylcotetrasiloxane (0.060 g, 0.250 mmol), platinum (0)-1,3-divinyl-1,1,3,3-tetramethyldisiloxane (50 μL), anhydrous dichloromethane (8 mL).

Synthesis of LCE ***4s - C11(MeHQ)/TR3 (60/40)***

Quantities: monomer **2c** (1.024 g, 1.500 mmol), terphenyl transverse rod (0.607g,

1.000 mmol), octasiloxane (1.182 g, 2.000 mmol), 2,4,6,8-tetramethylcylcotetrasiloxane (0.060 g, 0.250 mmol), platinum (0)-1,3-divinyl-1,1,3,3-tetramethyldisiloxane (50 μL), anhydrous dichloromethane (8 mL).

2.2 General Characterization Methods and Instrumentations

Thin layer chromatography (TLC) plates (silica gel on aluminum) from Aldrich were used to examine the extent of reaction during the synthesis of LC monomers and intermediates. Several TLC solvents, such as mixture of hexane and ethyl acetate (2:1 or 1:2) and a mixture of methanol and chloroform, were used depending on the polarities of the molecules under examination.

The LC monomer composition was identified by Mercury Vx 300 MHz ^{1}H nuclear magnetic resonance (NMR) spectrometer. Deuterated chloroform (CDCl3) and tetramethylsilane (TMS) were used as solvent and internal standard, respectively.

The LC elastomer preparation involved the reaction between Si-H groups (from siloxane spacer and siloxane crosslinker) and vinyl groups (from LC monomers). The conversion of Si-H bond to Si-C bond was examined by Fourier transform infrared spectroscopy (FT-IR) following the disappearance of the Si-H absorption band at about 2130 cm^{-1} and the C=C absorption at 1648-1640. The spectrum was collected using 32 scans at 4 cm^{-1} resolution in the 450 - 4000 cm^{-1} region by a Perkin Elmer FT-IR.

The extent of crosslinking of LC elastomers was examined by swelling experiments. In this experiment, LC elastomers samples were placed in toluene at room temperature for 24 hours. During this process, the swelling reagent, toluene, was replaced with fresh toluene three times in order to remove soluble molecules as much as possible. The sol-fraction (*sol%)* of elastomers was calculated by equation (2-1), which

is the weight ratio of soluble moieties after swelling ($\Delta W=W_0-W_1$) to the weight of the initial specimen before swelling (W_0). The residual solid weight of the specimen after swelling is W_1.

$$Sol\% = \frac{W_0 - W_1}{W_0} \tag{2-1}$$

It has been reported that the sol- fraction of some siloxane-based LCEs ranges from 5% to 25% [2, 9].

2.3 Characterization of Liquid Crystal Phases

There are three main techniques to identify liquid crystal phases, which are differential scanning calorimetry, X-ray diffraction and polarized optical microscopy.

2.3.1 Differential Scanning Calorimetry

Differential scanning calorimetry (DSC) is a technique to measure the energy difference required to keep a nearly identical temperature between a substance and an inert reference material at a controlled heating or cooling rate as shown in Figure 2-14 [10].

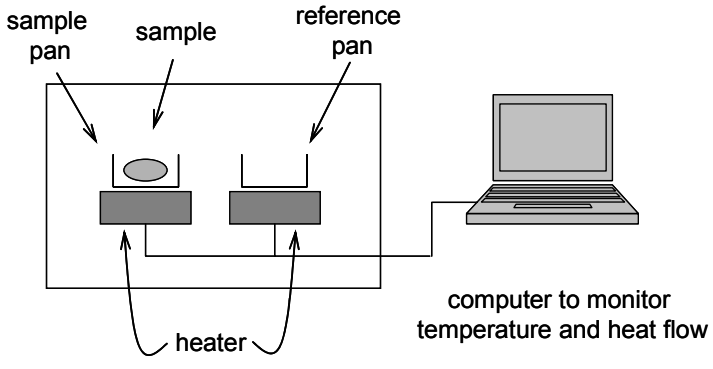

Figure 2-14 Schematic representation of a differential scanning calorimeter.

From DSC, the enthalpy and heat capacity changes associated with phase transitions can be determined. Figure 2-15 gives an example of thermal analysis of a low molar mass liquid crystal prepared in our lab by DSC.

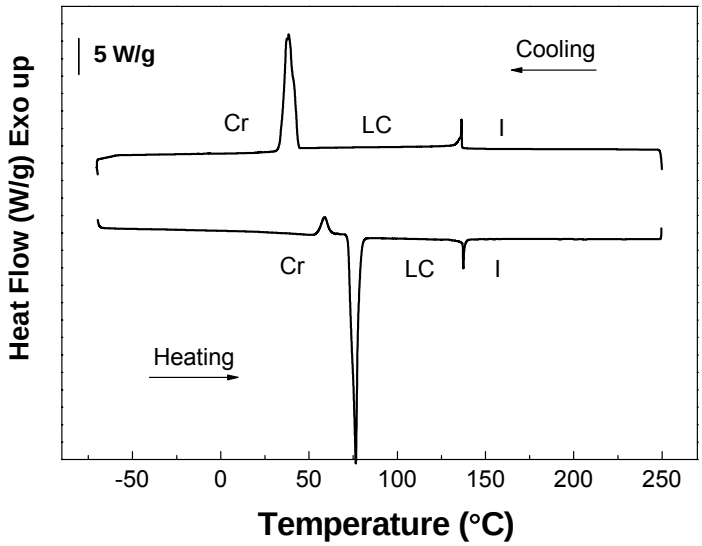

Figure 2-15 An example of DSC traces of a low molar mass liquid crystal.

In a DSC trace of a crystalline or liquid crystalline material, there is normally a temperature displacement in the formation of a crystalline phase or a mesophase in the cooling cycle as compared with a heating cycle. This displacement is also called the extent of supercooling. Compared with a crystalline material, the supercooling of a liquid crystal-liquid crystal or a liquid crystal-isotropic transition is typically small. This is a fast and facile way to judge the likely presence of a liquid crystalline material by DSC.

In this work, the phase transition temperature and corresponding latent heat of LC monomers, polymers, and elastomers was determined by a TA Q100 differential scanning

calorimeter. The measurement was performed on a specimen of about 15 mg at a heating and cooling rate of 10°C/min under a nitrogen flow of 50 mL/min. The instrument was calibrated by using indium as a standard. The collected data was analyzed by the TA Universal Analysis software.

2.3.2 X-ray Diffraction

X-ray diffraction is a powerful technique to identify microscopic structures. Diffraction occurs when X-rays scattered from a material constructively interfere as illustrated in Figure 2-16 (a). The wavelength of X-ray is of a few angstroms in many commercial instruments, which is of the same order as that of interatomic distances in a crystalline or liquid crystalline substance. Therefore, X-rays can be diffracted from a material having regularly repeating structures.

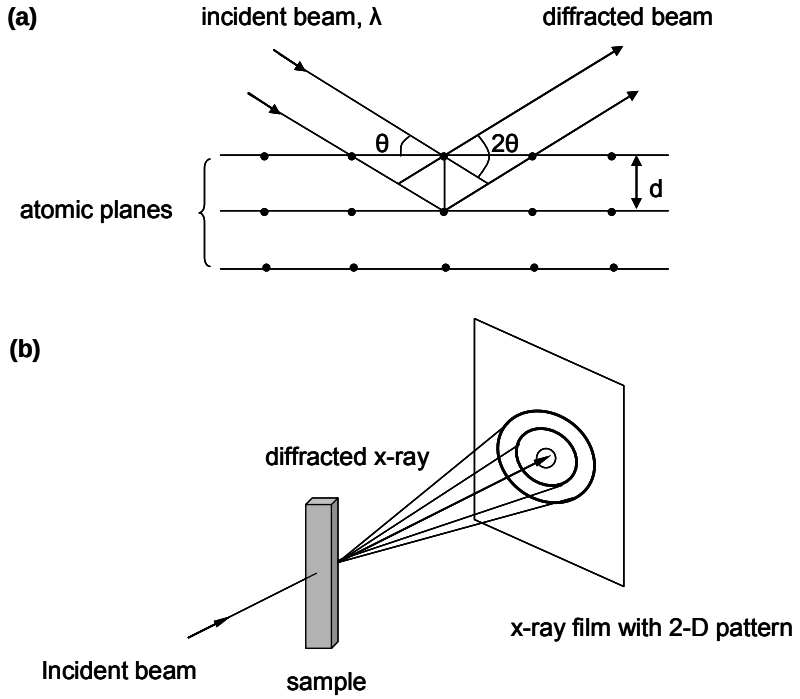

Figure 2-16 Schematic illustration of (a) definition of λ, 2θ and d in Bragg equation; (b) 2-D x-ray diffraction pattern of an unoriented sample.

The collected diffraction data provide information about the structure of the materials seen in Figure 2-16 (b). Bragg's law, expressed in equation (2-2), describes the relations between the wavelength of an incident x-ray beam, distance between diffracting atomic planes (or *d*-spacing) and the angle of diffraction as shown in Figure 2-16 (a) [11, 12].

$$n\lambda = 2d \sin\theta \tag{2-2}$$

where

λ - wavelength of incident x-ray beam;

d - distance between diffracting atomic planes;

2θ - angle of diffraction;

n - an integer.

The mesophase type of LC materials can be preliminarily identified by a 2-D X-ray diffraction pattern of oriented samples.

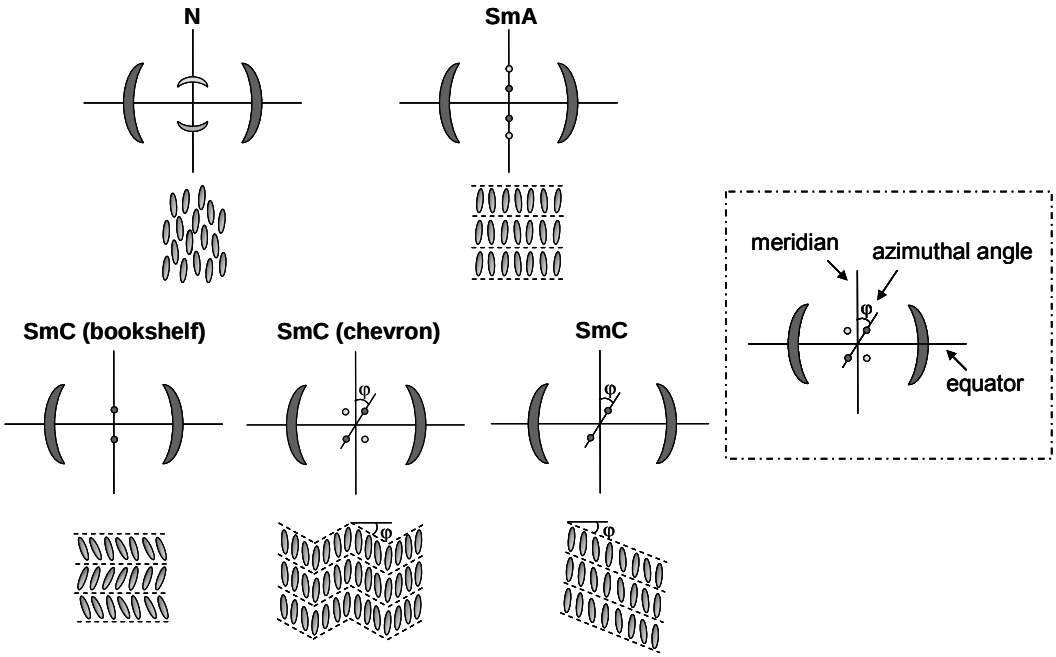

Figure 2-17 Schematic representation of X-ray diffraction pattern of nematic, smectic A and smectic C phases [13]

As shown in Figure 2-17, diffuse arcs along the meridian at small angles are often observed in nematic phases. Smectic phases are characterized by sharp Bragg spots due to the ordered layer structure or layer periodicity. In smectic A phases, the director is normal to the smectic layer, which results in the Bragg reflections being located along the meridian. For smectic C phases, several possible patterns can be observed. Depending on how the phases are formed, mesogen and layer can adopt different mutual orientations. If a smectic C phase forms from a smectic A phase, the layer orientation can be retained and the mesogens tilt like being put in a *bookshelf*. As a result, the Bragg reflection remains along the meridian. If the orientation of mesogens is retained by an external force like a magnetic or mechanical field, the layers tilt and arrange themselves in the shape of *chevron*. Therefore, the Bragg reflections tilt with respect to the director. Figure 2-17 also shows another possible arrangement of smectic structure, in which the director is oriented along the meridian and layers tilt toward a single direction. Diffraction arcs along the equator shown at the wide angle region are related to the intermolecular packing distance[13].

In this work, both wide angle x-ray diffraction (WAXD) and small angle x-ray scattering (SAXS) measurements of polymer and elastomer specimens were performed at room temperature with a Rigaku Micromax-002 (Cu, λ=1.5418Å) diffractometer and a Rigaku R-aixs IV++ 2-D detection system. The X-ray source was operated at 45 KV and 0.66 mA. The incident x-ray beam was perpendicular to the surface of specimens. For WAXD, the distance between sample and detector is 100 mm, which allows the diffraction data to be collected from $2^\circ < 2\theta < 50^\circ$. For SAXS, the distance between sample and detector is 750 mm, which allows the diffraction data to be collected from 1º

< 2θ < 10º. All the data were calibrated for background scattering before analysis. The analysis of diffraction patterns was carried out by Area Max V. 100 and MDI Jade 6.1 software.

2.3.3 Polarized Optical Microscopy

Polarized Optical Microscopy is based on the birefringence of anisotropic materials, such as liquid crystals. Anisotropic materials demonstrate two different refractive indices $n_{//}$ and $n_{\perp}$ in two orthogonal directions. Birefringence (Δn) is used to describe the difference and its magnitude is defined by equation (2-3).

$$\Delta n = n_{//} - n_{\perp} \tag{2-3}$$

When light passes through a birefringent material, it is decomposed into an ordinary ray and an extraordinary ray. These two rays travel at different speeds which make them out of phase. When the rays out of phase emit from the birefringent material, they generate interference patterns.

Figure 2-18 schematically illustrates the principle of a polarized optical microscope with two polarizers crossed with each other.

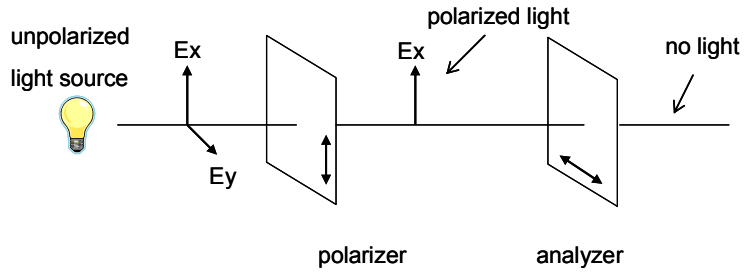

Figure 2-18 Schematic illustration of the effect of a crossed polarizer and analyzer [14].

When light goes through the polarizer, it becomes linearly polarized along the x-axis. If

there is nothing or an isotropic material between the polarizer and the analyzer, no light polarized along a-axis can go through the analyzer. Therefore, a dark view shows under the microscope. If anisotropic materials, like liquid crystals, are put between the polarizer and the analyzer, interference patterns or textures will be observed. Viewed under POM, different types of liquid crystals show their characteristic textures, which is often used to identify liquid crystal phases. For instance, nematic phase show thread-like texture and smectic A shows fan-like texture as shown in Figure 2-19 [13, 15].

(a) (b) (c)

Figure 2-19 Textures of liquid crystal phases observed under POM: (a) nematic; (b) smectic A; (c) smectic C [15].

In addition, birefringence is temperature dependent. The optical anisotropy disappears when the liquid crystal is at a time temperature above its mesophase to isotropic transition temperature. Therefore, the clearing temperature can be determined by following the appearance of dark field under POM with a hot stage.

Birefringence was observed in our LCEs under POM by cooling the samples from their isotropic state. For LCEs, the length scales of textures are often too small for reliable interpretation by POM [16]. In addition, our LCE samples are relatively thick (~ 150 – 200 microns), which make it even more difficult to distinguish their mesophase by this technique.

2.3.4 Order Parameter of Oriented Liquid Crystalline Polymers and Elastomers

The order parameter (S) is often used to represent the average degree of orientation of an LC domain. The order parameter of an LC domain in LCP fibers and stretched LCEs can be calculated by Hermann's equation (2-4) [17].

$$S = \frac{3\langle Cos^2\varphi \rangle - 1}{2} \tag{2-4}$$

where φ is the angle between the director of an individual domain and the stretching direction, and < > represents the average value of $Cos^2\varphi$ over the whole LC domains. The raw data of intensity and azimuthal angle were collected by azimuthal scans passing through the wide-angle interchain scattering region. The average cosine square of $\boldsymbol{\alpha}$ can be calculated by equation (2-5).

$$\langle Cos^2\alpha \rangle = \frac{\int_0^{\pi/2} I(\alpha)\, Sin\alpha\, Cos^2\alpha\, d\alpha}{\int_0^{\pi/2} I(\alpha)\, Sin\alpha\, d\alpha} \tag{2-5}$$

where α is the angle between the scattering planes normal and the director of individual LC domain and $I(\alpha)$ is the scattering intensity.

By assuming an orthogonal structure for a unit cell, the summation of average cosine square of angles between x, y, z axes is equal to 1. If a symmetric molecular long axis is also assumed, the value of $Cos^2\varphi$ can be obtained by equation (2-6). Then the order parameter can be calculated by equation (2-4) [17].

$$\langle Cos^2\varphi \rangle = 1 - 2\langle Cos^2\alpha \rangle \tag{2-6}$$

2.4 Characterization of Mechanical Properties of Liquid Crystalline Elastomers

2.4.1 Stress-strain Measurement

Tensile testing of elastomer samples was performed by a RSA-III type solids analyzer with a 3500 g transducer at room temperature. For LCEs, all the samples were cut into rectangular specimens (L×W×T = 20 mm × ~ 3 mm × ~ 0.2 mm). The narrow elongated sample geometry is adopted to minimize the edge effects during the extensional deformation [18]. The initial cross-section (A_0) and initial length of sample (L_0) were used to calculate the nominal stress (σ_N) and strain (ε), respectively.

$$\sigma_N = \frac{f}{A_0} \tag{2-7}$$

$$\varepsilon = \frac{L}{L - L_0} \tag{2-8}$$

True stress (σ_T) is calculated based on the actual cross-section (A) by assuming no volume change during extension.

$$\sigma_T = \frac{f}{A} \tag{2-9}$$

In most cases, yielding corresponds to the maximum load in the load-elongation curve. Therefore, yield stress can be simply regarded as the true stress at the maximum observed load. Since yield stress is often achieved at a relatively low strain, the engineering definition of yield stress is almost equal to the true stress definition of yield stress.

For a material having no observed yield point, another definition of yield stress is required. In this work, the Considere criterion [18] was taken to evaluate the yield stress and strain.

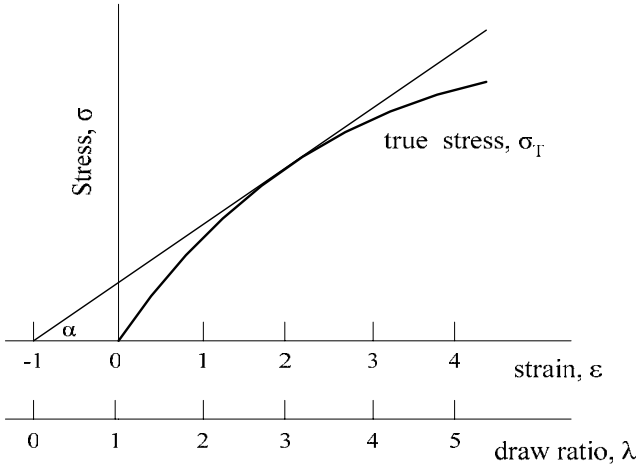

Figure 2-20 The Considere construction to evaluate the yield stress and strain

According to this criterion, the true stress versus strain or true stress versus draw ratio curve should be plotted first as shown in Figure 2-37. The yield stress is given by the tangent α of a line drawn from the point -1 on the strain axis or the point zero on the draw ratio axis to the true stress-strain curve.

In this work, three different strain rates, 5×10^{-2} s^{-1}, 5×10^{-3} s^{-1} and 5×10^{-4} s^{-1} were used. Among them, 5×10^{-3} s^{-1} is the standard strain rate used to report the mechanical properties of our materials and the other two are used to investigate the influence of strain rate on mechanical properties. The initial extension of specimens for strain relaxation experiment was also obtained from Rheometrics RSA-III type solids analyzer. This analyzer is equipped with an oven to enclose the sample. The environment temperature inside the oven is monitored by a temperature controller. Monodomain samples were obtained by stretching the corresponding polydomain sample through the polydomain-to-monodomain transition region by an Instron 5567.

2.4.2 Hysteresis and Strain Recovery Measurement

Hysteresis of LC elastomer specimens was detected by loading-unloading cycles performed by an RSA-III solids analyzer at room temperature. Three maximum strains, respectively located in regions before, during and after the polydomain-to-monodomain (P-M) transition, were selected as the ending point of loading and the starting point of unloading. Choices of these three maximum strains varied with material types. Both loading and unloading strain rates were set as 5×10^{-3} s^{-1}.

For strain recovery measurement, two line marks were drawn on the surface of specimens. The length between marks was measured with an accuracy of 0.5 mm. During the experiment, the sample was first stretched at the strain of 5×10^{-3} s^{-1} to a target strain value. Then, the sample was quickly taken from the clamp and laid on a flat surface in order to avoid any load. The instantaneous length (L) was read as a function of time. The residual strain (ε_{res}) was calculated according to the instantaneous and initial length.

$$\varepsilon_{res} = \frac{L - L_0}{L_0} \tag{2-10}$$

Strain recovery experiments of deformed specimens at elevated temperature were performed in a beaker with hot water. The heat was provided by a hot plate and the temperature was monitored by a thermometer. At a predetermined temperature, the deformed specimen remained in hot water for at least 10 minutes and then was taken for immediate length measurements.

2.4.3 Stress Relaxation

Stress relaxation of LC elastomer specimens was investigated by an RSA-III

solids analyzer at room temperature. In this experiment, a rectangular specimen was under uniaxial extension at a target strain and then the instrument recorded the instantaneous stress of the sample as a function of time with the target strain as a constant. The stress relaxation behavior of our LC elastomers was studied by fitting the curves to a single stretched exponential function as expressed by a modification of the Kohlrausch-Williams-Watt (KWW) equation [19], which was also adopted by Ortiz [20] and Carfagna [21] to analyze the stress relaxation behaviors of their LC elastomers.

$$\sigma_n(t) = (\sigma_{\max} - \sigma_{\min}) \exp(-t/\tau)^{\beta} + \sigma_{\min} \tag{2-11}$$

where t is the experimental time, σ_{max} is the instantaneous (unrelaxed) nominal stress at $t = 0$, σ_{min} is the long-time (relaxed) nominal stress at $t = \infty$, and τ is the characteristic relaxation time. The parameter β is a measure of the narrowness of the distribution and is approximately 0.5 for flexible and isotropic polymers [20].

Since the initial strain (ε_0) is kept as a constant in the stress relaxation process, the KWW equation can be given in another form in terms of time-dependent relaxation modulus $E_R(t)$.

$$E_R(t) = \sigma_n(t) / \varepsilon_0 \tag{2-12}$$

$$E_R(t) = (E_0 - E_f) \exp(-t/\tau)^{\beta} + E_f \tag{2-13}$$

where $E_0 = E_R\ (t = 0)$ is the instantaneous (unrelaxed) modulus, $E_f = E_R\ (t = t_f)$ is the long-tine (relaxed) modulus and t_f is the final time recorded in the stress relaxation experiment. The value of β and τ can be estimated from experimental data by rearranging equation (2-13) into equation (2-14):

$$\ln\ln[1/R(t)] = -\beta \ln(\tau) + \beta \ln(t) \tag{2-14}$$

where R(t) is the 'relaxation function' which is equal to $[E(t) - E_f]/(E_0 - E_f)$. Plotting

lnln[1/$R(t)$] versus ln(t) give a linear curve with a slope equals to β and a y-intercept equals to $-\beta \ln\tau$.

2.4.4 Poisson's Ratio Measurement

The simultaneous dimension change in longitudinal and lateral direction under a uniaxial extension or compression can be described by Poisson's ratio, which is defined by equation (2-15) [22].

$$\nu = -\frac{\varepsilon_{lateral}}{\varepsilon_{longitidinal}} \tag{2-15}$$

A Poisson's ratio measurement was set up based on the definition. As illustrated in Figure 2-21, a rectangular specimen (25 mm × 8 mm × 0.2 mm) was marked with 4 spots, (a, b, c and d), in the middle region of the specimen in order to measure the change in length and width upon stretching.

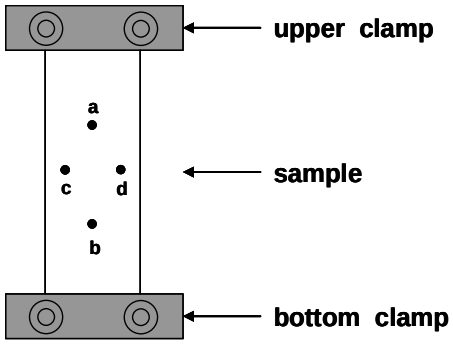

Figure 2-21 Schematic representation of a specimen for Poisson's ratio measurement

The distance between *a* and *b,* and the distance between *c* and *d* represent the instantaneous width (W) and length (L), respectively. If we use W_0 and L_0 represent the original width and length, equation (2-15) can be rewritten as

$$\nu = -\frac{\frac{W - W_0}{W_0}}{\frac{L - L_0}{L_0}} \tag{2-16}$$

The experiment was carried out by stretching specimens (RAS-III solids analyzer) at the strain rate of 5×10^{-3} s^{-1} and recording the images (Canon 4300 camera, 1 image/15 seconds) instantaneously. Image-Pro Plus 5.0 software was used to measure the distance between spots with the unit of pixel. The distance between marks on the sample was measured by counting the number of pixels between them on the images.

It was known that Poisson's ratio of an isotropic material is an elastic constant at small strains [18]. In our work for the auxetic effect investigation, we followed the dimensional change of LCE samples in a large strain region (including elastic and anelastic deformation). We will use *strains ratio* instead of *Poisson's ratio* to describe the dimensional change at large strains.

2.5 References

[1] G. Kossmehl, B. Gerecke, N. Harmsen, F. Schroder, and H. M. Vieth, "Liquid crystalline main chain polysiloxane esters and their monomers. 1. Synthesis of some di(omega-unsaturated esters) and their thermal behaviour," *Molecular Crystals and Liquid Crystals Science* vol. 269, pp. 39-53, 1995.

[2] B. Donnio, H. Wermter, and H. Finkelmann, "Simple and versatile synthetic route for the preparation of main-chain, liquid-crystalline elastomers," *Macromolecules*, vol. 33, pp. 7724-7729, 2000.

[3] I. A. Rousseau and P. T. Mather, "Shape memory effect exhibited by smectic-C liquid crystalline elastomers," *Journal of the American Chemical Society*, vol. 125, pp. 15300-15301, 2003.

[4] G. G. Odian, *Principles of polymerization*, 3rd ed. New York: Wiley, 1991.

[5] T. W. G. Solomons and C. B. Fryhle, *Organic chemistry*, 7th ed. New York: Wiley, 2000.

[6] J. S. Moore and S. I. Stupp, "Room-temperature polyesterification," *Macromolecules*, vol. 23, pp. 65-70, 1990.

[7] I. A. Rousseau, "Development of soft polymeric networks showing actuation behavior: from hydorgels to liquid crystalline elastomers," *PhD Thesis, University of Connecticut*, 2004.

[8] F. J. Davis, "Liquid-crystalline elastomers," *Journal of Materials Chemistry*, vol. 3, pp. 551-562, 1993.

[9] M. A. A. Cortes, "Synthesis and physical properties of unsymmetric main-chain liquid crystal elastomers," *PhD Thesis, University of Exeter*, 2006.

[10] D. Campbell, R. A. Pethrick, and J. R. White, *Polymer characterization : Physical techniques*, 2nd ed. Cheltenham, U.K.: Stanley Thornes, 2000.

[11] K. Hiraoka, Y. Uematsu, P. Stein, and H. Finkelmann, "X-ray diffraction studies on the phase-transformational behavior of a smectic liquid-crystalline elastomer composed of chiral mesogens," *Macromolecular Chemistry and Physics*, vol. 203, pp. 2205-2210, 2002.

[12] N. Kasai and M. Kakudo, *X-ray diffraction by macromolecules*. Tokyo Berlin ; New York: Kodansha ; Springer, 2005.

[13] I. W. Hamley, *Introduction to soft matter : polymers, colloids amphiphiles, and liquid crystals*. Chichester New York: Wiley, 2000.

[14] P. J. Collings, *Liquid crystals : nature's delicate phase of matter*, 2nd ed. Princeton, N.J.: Princeton University Press, 2002.

[15] I. Dierking, *Textures of liquid crystals*. Weinheim: Wiley-VCH, 2003.

[16] S. M. Clarke, E. M. Terentjev, I. Kundler, and H. Finkelmann, "Texture evolution during the polydomain-monodomain transition in nematic elastomers," *Macromolecules*, vol. 31, pp. 4862-4872, 1998.

[17] L. E. Alexander, *X-ray diffraction methods in polymer science* New York, Wileyinterscience 1969.

[18] I. M. Ward and D. W. Hadley, *An introduction to the mechanical properties of solid polymers*. Chichester ; New York: J. Wiley & Sons, 1993.

[19] G. Williams, D. C. Watts, S. B. Dev, and A. M. North, "Further considerations of non symmetrical dielectric relaxation behaviour arising from a simple empirical decay function," *Transactions of the Faraday Society*, vol. 67, pp. 1323-&, 1971.

[20] C. Ortiz, C. K. Ober, and E. J. Kramer, "Stress relaxation of a main-chain, smectic, polydomain liquid crystalline elastomer," *Polymer*, vol. 39, pp. 3713-3718, 1998.

[21] M. Giamberini, P. Cerruti, V. Ambrogi, C. Vestito, F. Covino, and C. Carfagna, "Liquid crystalline elastomers based on diglycidyl terminated rigid monomers and aliphatic acids. Part 2. Mechanical characterization," *Polymer*, vol. 46, pp. 9113-9125, 2005.

[22] F. Rodriguez, *Principles of polymer systems*, 4th ed. Washington, DC: Taylor & Francis, 1996.

CHAPTER 3

Thermal and X-ray Analysis of MCLC Polymers and Elastomers

3.1 Thermal and X-ray Analysis of MCLCPs

It is known that alkyl and siloxane spacers have a significant effect on the LC behaviors of MCLCPs and MCLCEs [1-4]. In order to study the effect of mixing two flexible siloxane chain extender (spacer) units on the phase behavior of our LC polymers, five linear polymers (**3a-3e**) were synthesized by varying the ratio of short spacer Si3 (m=2) to long spacer Si8 (m=7) including the end numbers. Thermal properties of these five polymers were studied by DSC as shown in Figure 3-1 with heating and cooling rate of 10 °C/min.

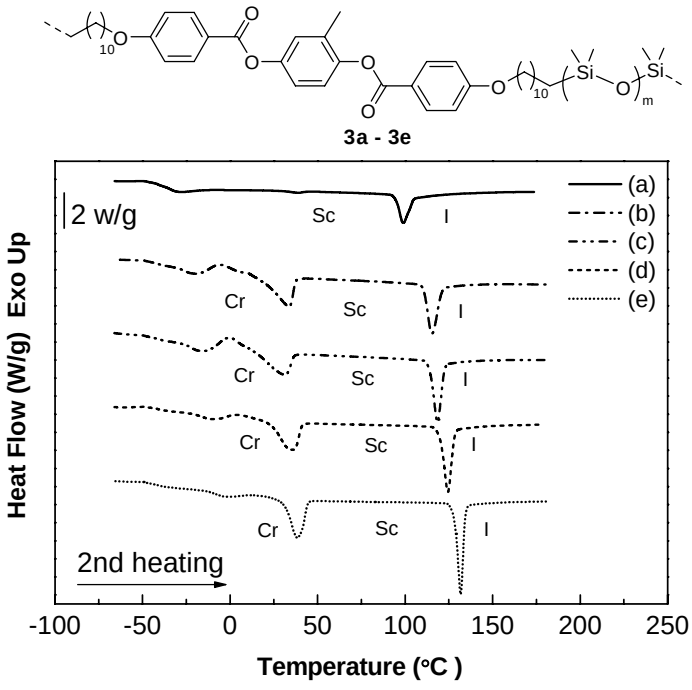

Figure 3-1 DSC traces (2nd heating) of linear polymers **3a - 3e**: (a) **Si3/Si8** (0/100); (b) **Si3/Si8** (25/75); (c) **Si3/Si8** (50/50); (d) **Si3/Si8** (75/25); (e) **Si3/Si8** (100/0)**.**

The transition temperatures of these polymers are reported in Table 3-1.

Table 3-1 Transition temperature from DSC of linear polymer **3a - 3e**

	Tg (°C)	Clearing temperature (Sc-I) (°C)	
		1st cooling	2nd heating
Polymer **3a**-Si3/Si8(0/100)	-36	95	99
Polymer **3b**-Si3/Si8(25/75)	-25	112	115
Polymer **3c**-Si3/Si8(50/50)	-23	114	118
Polymer **3d**-Si3/Si8(75/25)	-16	120	124
Polymer **3e**-Si3/Si8(100/0)	-13	127	132

It was found that the glass transition temperature (T_g) of these LCPs increases gradually from -36 ˚C to -13 ˚C with increasing the fraction of short spacer **Si3**. The low Tg of the materials is due to the incorporation of flexible siloxane spacers into the polymer main chains. Pure polydimethylsiloxane has a very low T_g (around -127 °C) [5] reflecting the large flexibility of siloxane chains. A mesophase to isotropic phase transition shows in both heating and cooling cycles. With the increase of the fraction of short spacer (**Si3**), the mesophase to isotropic transition (clearing temperature, T_{cl}) also shifts to higher temperature. It was also found that the existence of short spacer (**Si3**) in the LC polymers results in partially crystalline structures with the melting temperature (T_m) around 40 °C.

The gradual increase in both T_g and T_{cl} with increasing the fraction of short spacer (**Si3**) likely comes from the flexibility of the polymer chains. Increasing the fraction of shorter siloxane spacer (**Si3**) reduces the flexibility of polymer chains, which results in an increase in T_g and T_{cl}. In addition, a single value of T_g and T_{cl} as well as a continuous variation in T_g and T_{cl} indicate a homogeneous distribution of these two siloxane spacers at the molecular level in the polymers. This result also indicated that T_g and T_{cl} of these

MCLCPs could be tailored by varying siloxane spacer length and composition.

Room temperature WAXD of C11(MeHQ)Si8 LCP ***3a*** oriented fiber (hand drawn from the melt) detected four crossed diffraction arcs in the small angle region, which indicate the presence of a smectic C type of mesophase at room temperature. It is thought that the smectic behavior is driven by microphase segregation of the rigid mesogenic units, the alkyl and the siloxane spacer segments [6].

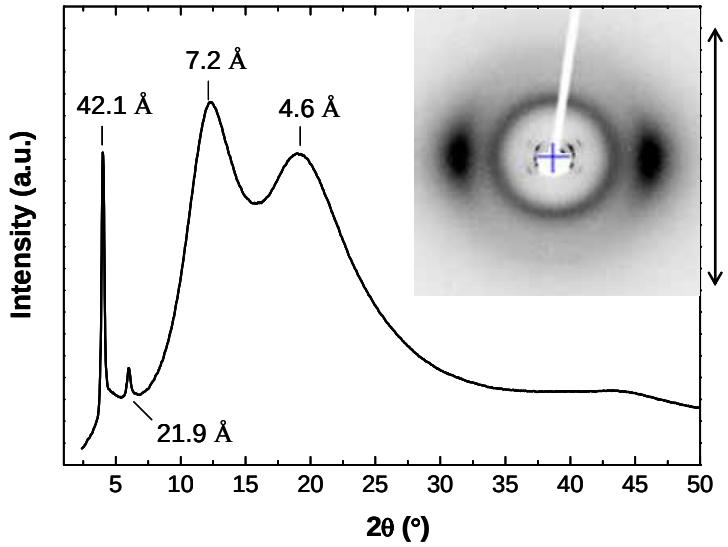

Figure 3-2 WAXD profile and 2D pattern of oriented C11(MeHQ)**Si8** LC polymer (S = 0.68) at room temperature.

According to Bragg's equation, the average smectic C layer spacing is about 44 Å (from the second order diffraction). Since the primary diffraction from the smectic layers shows at a region (~ 4º) out of the effective WAXD detection region (> 5º), the value of smectic layer distance is best calculated based on the second order diffraction. The interchain packing distance of siloxane spacer and that of hydrocarbon spacer was 7.2 Å and 4.6 Å, respectively. The diffraction intensity maxima at wide angles located at the

equator means the polymer main chains were macroscopically oriented along the fiber axis (arrow direction in Figure 3-2). The order parameter of this LCP is about 0.68 from this diffraction by azimuthal scan. WAXD and SAXS profiles and patterns of C11(MeHQ)Si3 LCP are shown in Figure 3-3.

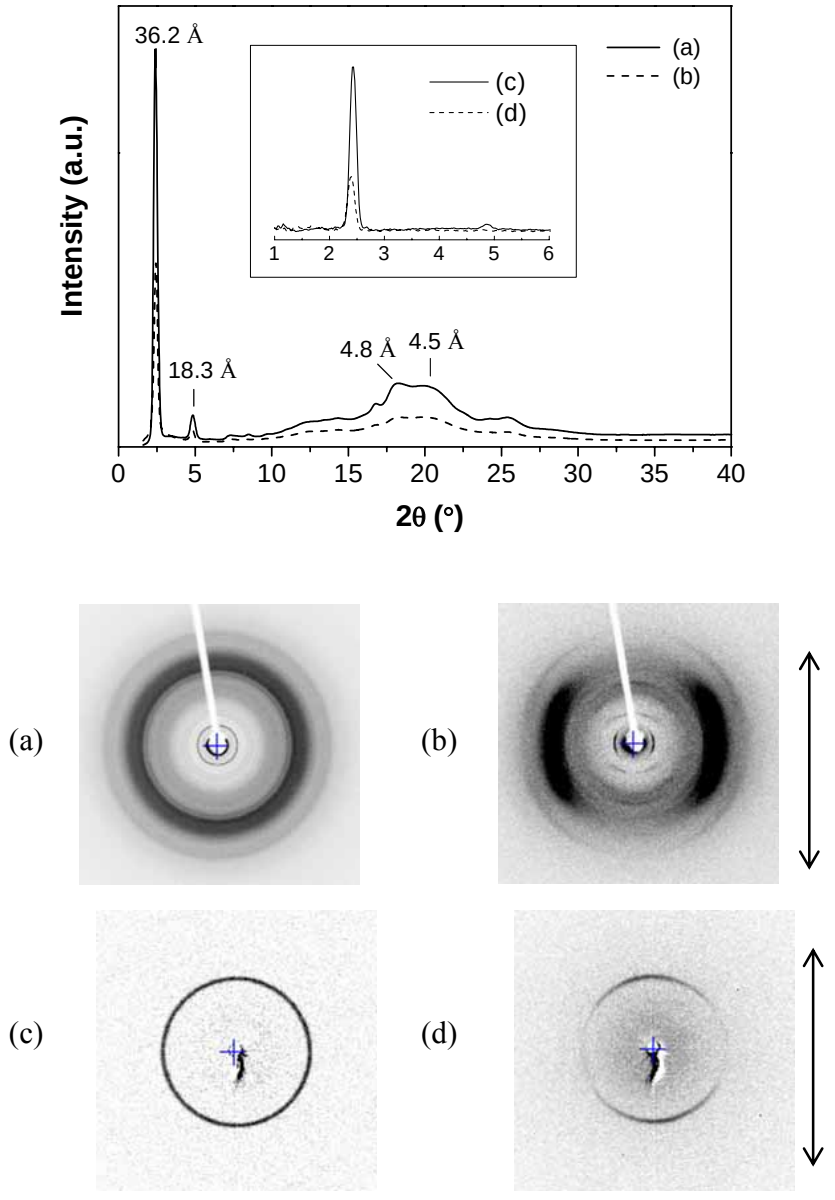

Figure 3-3 X-ray studies of C11(MeHQ)**Si3** LC polymer: WAXD (a) unoriented; (b) oriented fiber (S = 0.44) ; SAXS (c) unoriented; (d) oriented (fiber). The arrow direction is along the fiber axis at room temperature.

From its WAXD pattern, the primary diffraction at small angles appears partially hidden by the beam stop. Its second diffraction intensity maximum is located at the equator which is not consistent with the observation from SAXS (diffraction intensity maxima located on the meridian). The mesophase can not be identified from this information. Further X-ray analysis is needed to identify the mesophase. The strong diffraction at small angles indicates the presence of a smectic layered structure with the layer spacing of about 36 Å (from the second order of diffraction). The more complicated diffraction detected at middle angles may be related to crystalline structures, which have been observed by DSC. The order parameter is around 0.44 for this polymer which indicates the polymer chains are poorly oriented along the stretching direction.

3.2 Thermal and X-ray Analysis of MCLCPs with Terphenyl Transverse Rods

As mentioned in chapter 1, we synthesized potential molecular auxetic materials by introducing laterally attached transverse rods into a liquid crystalline polymer system. Terphenyl transverse rod (**TR3**) capable of 90 ° rotation was one of the transverse rods synthesized in our lab. The 1,3-disubstitution in the isophthalates allows for a perpendicular orientation of the transverse rod upon extension of the spacer groups [7].

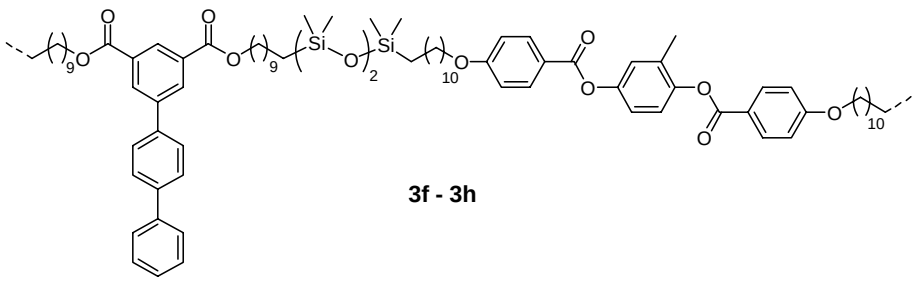

3f - 3h

It is an isophthalate-based terphenyl transverse rod with flexible arms containing ten methylene units. Our goal is to create a stable and accessible fiber-forming mesophase

with transverse rod incorporation. Transverse rod incorporation might pose a problem in this regard. In Figure 3-4, it is seen that the addition of 25 mol% **TR3** into C11(MeHQ)Si3 LC polymer began to broaden the LC phase transition peak significantly.

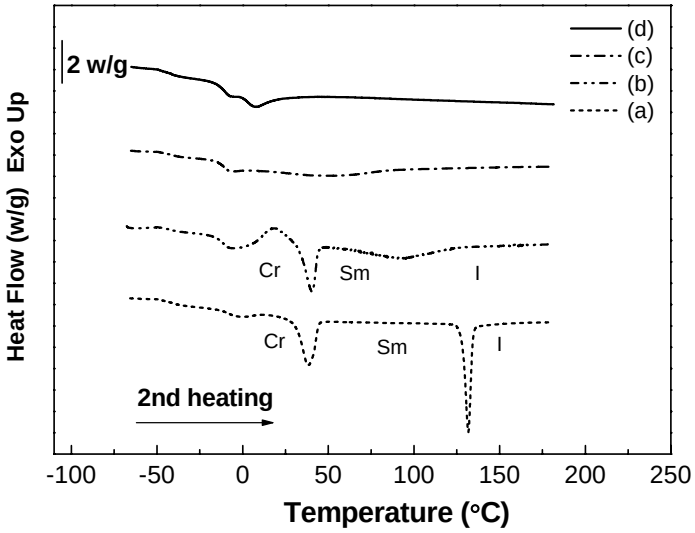

Figure 3-4 DSC traces (2nd heating) of C11(MeHQ)Si3 LC polymers (***3e*** and ***3g-3h***) with various amount of **TR3** (a) 0 mol%; (b) 25 mol%; (c) 50 mol%; (d) 75 mol%.

The peak of the mesophase to isotropic phase transition broadened and the peak maximum moved to lower temperature with increasing the loading of **TR3** from 0% to 75%. This is reasonable because the transverse rod itself, although anisotropic in structure, is not mesogenic and the overall rod orientation of the mesophase is likely disrupted by the transverse rod. The reduced orientation directly results in the decrease of its clearing temperature. As for the polymer ***3g*** with 50 mol% and polymer ***3h*** with 75 mol% **TR3**, it is difficult to establish the presence of a mesophase by DSC.

After incorporating 50 mol% **TR3** into the C11(MeHQ)Si3 LC polymer, a smectic C type of mesophase was detected from WAXD (2nd order diffraction) in Figure 3-5 (b) and SAXS (1st order diffraction) in Figure 3-5 (d) since the presence of four

Bragg arcs at small angles arranged in a crossed pattern was observed. The slight decrease in layer spacing of this polymer (35.6Å) compared with its parent polymer (36.6 Å) is possibly due to the tilted smectic C layer structure.

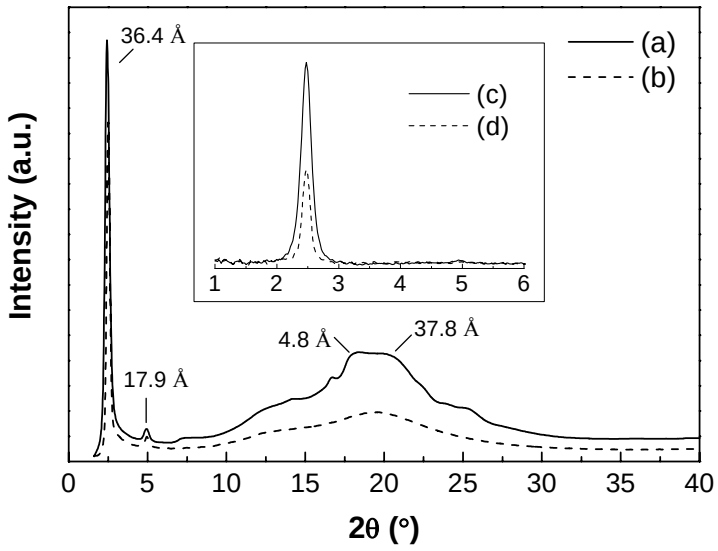

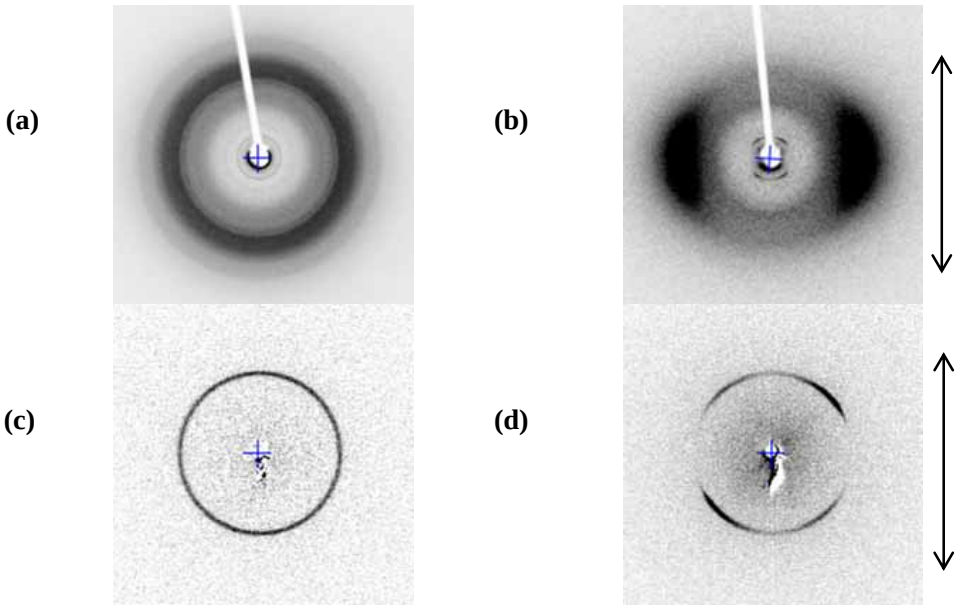

Figure 3-5 X-ray study of C11(MeHQ)**Si3** LC polymer with 50 mol% **TR3**: WAXD (a) unoriented; (b) oriented fiber (S = 0.63); SAXS (c) unoriented; (d) oriented fiber at room temperature.

Compared with the C11(MeHQ)Si3 LC polymer, a C11(Biph)Si8 LC polymer ***3i*** with an longer mesogenic core was synthesized. A series of LC polymers ***3j – 3l*** based on this parent system were also synthesized by varying the amount of TR3.

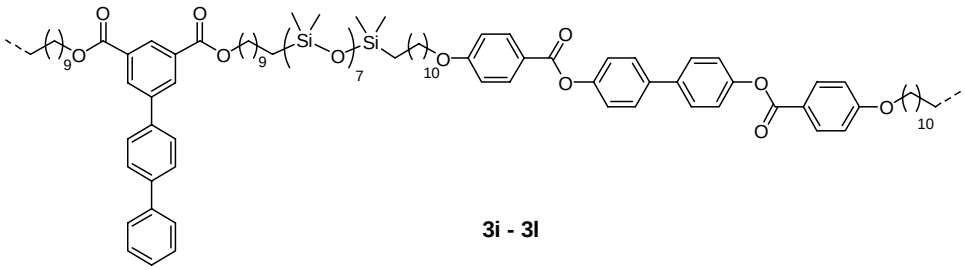

3i - 3l

A higher mesophase to isotropic transition temperature and a wider mesophase range coupled with likely a better pre-alignment of transverse rods are expected from the C11(Biph)Si3 parent polymer. DSC analysis found that C11(BiPh) LC with the longer mesogen core was more effective in retaining the mesophase stability when **TR3** were added as shown in Figure 3-6.

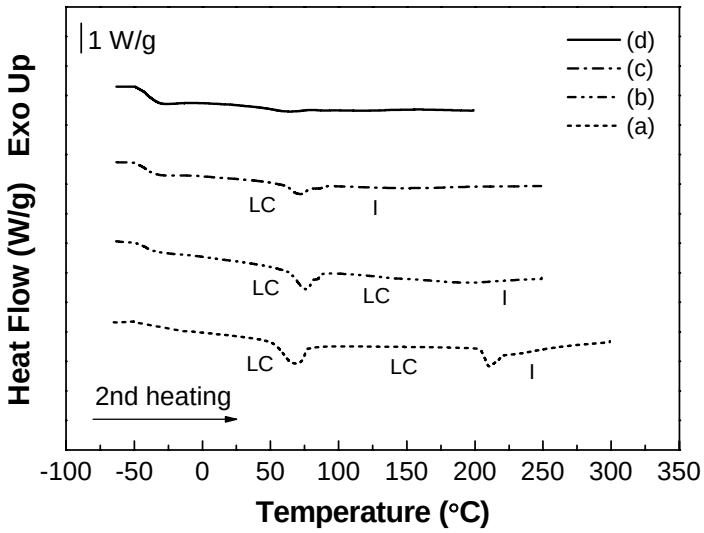

Figure 3-6 DSC traces of C11(Biph)Si8 LC polymer (***3i-3l***) with various amount of **TR3**: (a) 0 mol%; (b) 25 mol%; (c) 50 mol%; (d) 75 mol%.

Although the higher temperature mesophase to isotropic phase transition peak disminishes rapidly by increasing the fraction of **TR3**, the lower temperature mesophase to isotropic phase transition peak can still be distinguished even with 75 mol% loading of **TR3**.

A mesophase of smectic A type was found in the parent polymer by WAXD indicated by the diffraction intensity maxima located on the meridian at small angles as shown in Figure 3-7 (b).

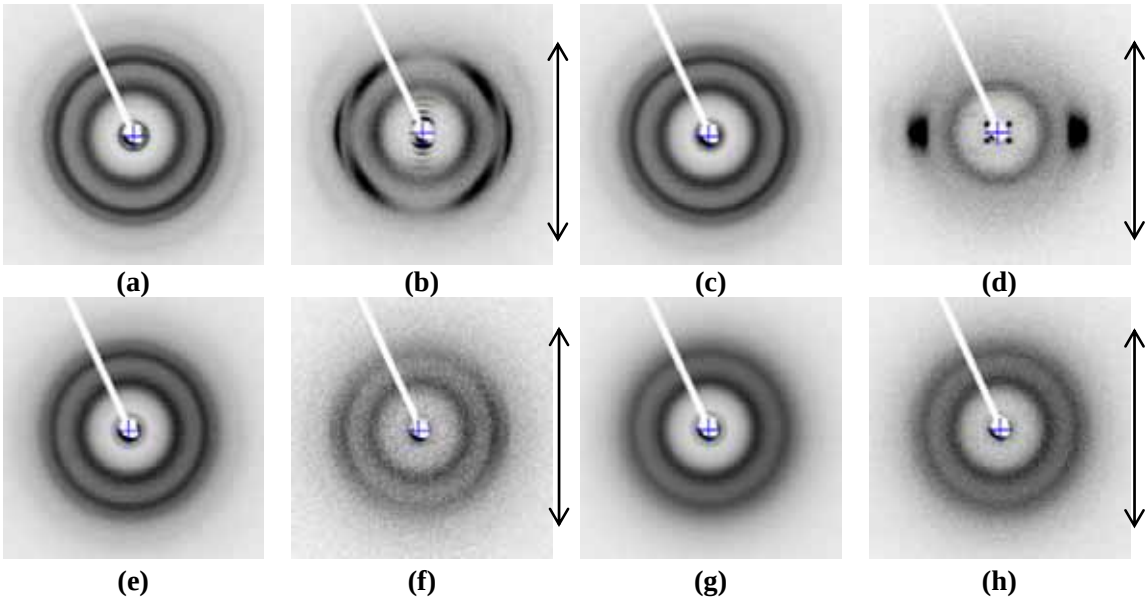

Figure 3-7 X-ray patterns of C11(**Biph**)Si8 LC polymers with **TR3**: (a) 0 mol% unoriented; (b) 0 mol% oriented; (c) 25 mol% unoriented; (d) 25 mol% oriented (S=0.84); (e) 50 mol% unoriented; (f) 50 mol% oriented(S=0.57); (g) 75 mol% unoriented; (h) 75 mol% oriented(S=0.18) at room temperature.

A diffraction pattern typical of a smectic C mesophase was detected in the C11(BiPh)Si8 polymer with 25 mol% **TR3** as seen in Figure 3-7 (d). For the polymer with even higher **TR3** loading (50 mol% and 75 mol% **TR3**), diffractions from layer structures could be detected in Figure 3-7 (f) and (h) at small angles, although they were less sharp than the LCPs with lower **TR3** loading. For all the polymers, their primary diffractions were

partially hidden by the X-ray beam. Among them, only the parent polymers and polymers with 25mol% **TR3** clearly showed the second order diffractions. The S_A layer distance of the parent polymer C11(BiPh)Si8 is around 47.4 Å. The S_C layer distance of the polymer with 25 mol% TR3 is around 46.6 Å. For the parent polymer C11(MeHQ)Si8, the characteristic diffraction from the hydrocarbon chains at wide angles is split into four arcs, which indicates a tilted arrangement of hydrocarbon chains. The reason for this is not clear. A characteristic π-π stacking diffraction (d = 3.5 Å) was found which is likely due to the close packing of the biphenyl mesogenic cores.

3.3 Thermal and X-ray Analysis of MCLCEs

In addition to the effect of alkyl spacer, siloxane spacer and terphenyl transverse rod on the mesophase behaviors as discussed in MCLCPs, additional chemical variations, such as crosslinker content and lateral substituents, were examined to establish the structure-property relationships of our MCLCEs as potential shape memory materials and potential auxetic materials.

3.3.1 Effect of Crosslinking

A family of LCEs ***4a*** - ***4e*** with the same C11(MeHQ) mesogen, the same long siloxane spacer Si8 but the various fraction of crosslinker was chosen to investigate the effect of crosslinking on the thermal properties and mesophases of LCEs.

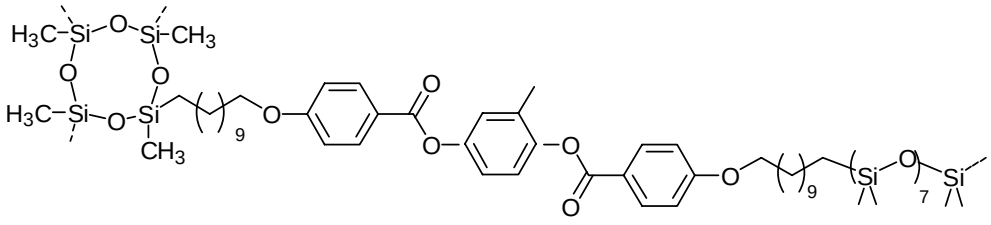

4a - 4e

The thermal properties of this group of LCEs were analyzed by DSC. Their glass transition temperatures and clearing temperatures are reported in Table 3-2.

Table 3-2 Transition Temperatures of LCEs by Varying Crosslinker Content

Elastomer	**Tg (°C)**	**Clearing temperature (Sc-I) (°C)**	
		1st cooling cycle	**2nd heating cycle**
3a – C11(MeHQ)Si8XL0	-33	94	98
4a - C11(MeHQ)Si8XL5	-28	96	101
4b - C11(MeHQ)Si8XL10	-25	101	104
4c - C11(MeHQ)Si8XL15	-23	102	110
4d - C11(MeHQ)Si8XL20	-18	108	119
4e - C11(MeHQ)Si8XL25	-12	123	133

The comparison of linear LC polymer ***3a*** with lightly crosslinked LC elastomer ***4a*** illustrates that a low level of crosslinking (5 mol%) does not markedly affect the phase behavior of the materials. With further increasing the extent of crosslinking, the effect becomes more and more dramatic. Both their glass transition temperature and clearing temperature shift upwards continuously with an increase in crosslinker content. For lightly crosslinked samples, like with 5 and 10 mol% crosslinkers, the constraints on the segmental motion of polymer chains are not significant. Polymer chains still have high mobility in the mesophase. After increasing crosslinker beyond a certain amount, hindrance due to crosslinking becomes problematic. The reduced mobility of polymer segments and main chains inevitably leads to an increase in glass transition temperature and clearing temperature [8]. In addition, when the crosslinker content reaches 15 mol% (film ***4c***), its DSC trace begins to show a broadened mesophase to isotropic phase

transition peak. So do the films ***4d*** and ***4c*** with 20 mol% and 25 mol% crosslinker, respectively. Broadening of the transition peak indicates that the high crosslinking density makes the mesophase formation difficult. But it is still out of our expectation that our elastomers with such a high crosslinker content (up to 25 mol%) can still retain liquid crystalline order. The observed increase in phase transition temperature with increase of crosslinker content agrees with Zentel's observation [9]. He claimed the increase of phase transition temperatures might come from the increase of molecular weight during the crosslinking reaction.

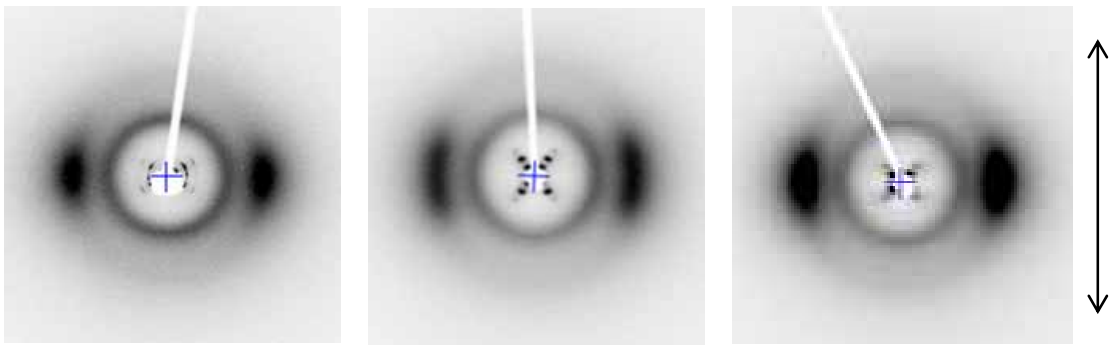

(a) (b) (c)

Figure 3-8 X-ray patterns of C11(MeHQ)Si8 LC polymer and elastomer analogous with various crosslinker content: (a) 0 mol% (oriented fiber); (b) 10 mol% (stretched); (c)) 25 mol% (stretched) at room temperature.

WAXD studies found a smectic C type of mesophase in C11(MeHQ)Si8 LC polymer and elastomers no matter the amount of crosslinker in the network as illustrated in Figure 3-8. For C11(MeHQ)Si8 fiber, the smectic layer spacing is about 44 Å. For the stretched elastomer with 10 mol% crosslinker, the smectic layer spacing is around 42 Å. With increasing the crosslinker content up to 25 mol%, a small decrease in layer spacing, 39 Å, was found.

3.3.2 Effect of Hydrocarbon Spacer and Siloxane Spacer

The combined effects of the hydrocarbon spacer and the siloxane spacer on the thermal properties of MCLCEs are summarized in Table 2-6.

Table 3-3 Thermal Properties of LCEs with various Terminal Chains and Spacers

Elastomers	T_g (°C)	$T_{LC1-LC2}$ (°C)	T_{cl} (°C)
4f-C3(MeHQ)Si8XL10	-	-	-
4h-C3(MeHQ)Si3XL10	4.3	33.7	80.1
4m-C3(MeHQ)SiphXL10	-	-	68.8
4g-C5(MeHQ)Si8XL10	-13.1	58.5	75.6
4i-C5(MeHQ)Si3XL10	18.3	99.0	123.5
4n-C5(MeHQ)SiphXL10	47.4	-	85.3
4b-C11(MeHQ)Si8XL10	-22.9	-	104.2
4j-C11(MeHQ)Si3XL10	-5.7	-	131.4
4o-C11(MeHQ)SiphXL10	12.7	-	109.3

DSC traces of LCEs with C11(MeHQ) mesogen with different types of siloxane spacer were plotted together for comparison in Figure 3-9.

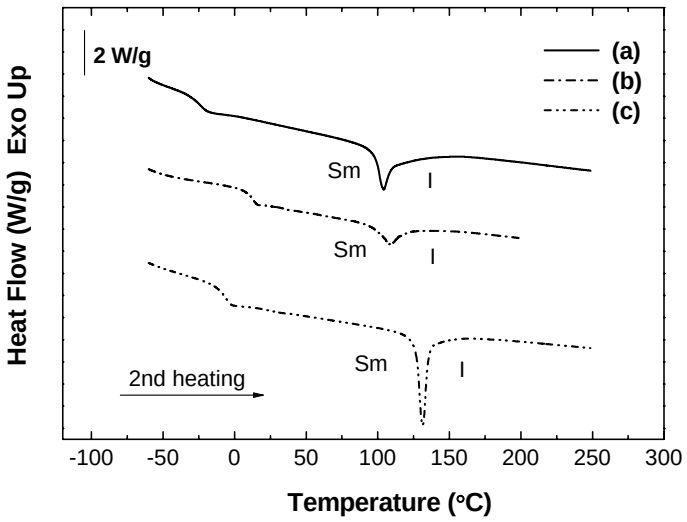

Figure 3-9 DSC traces (2nd heating) of elastomers with different siloxane spacers (a) ***4b*** - C11(MeHQ)Si8XL10; (b) ***4k*** - C11(MeHQ)SiphXL10; (c) ***4f*** - C11(MeHQ)Si3XL10.

Elastomer ***4b*** has flexible and longer siloxane spacers – **Si8**. Elastomer ***4k*** contains less soft and shorter siloxane spacers - **Siph**. Elastomer ***4f*** has flexible and shorter siloxane spacers - **Si3**. Compared with the elastomer with **Si8**, the increase in glass transition temperature by replacing **Si8** with **Siph** is higher than that with **Si3**. But the increase in clearing temperature by replacing **Si8** with **Siph** is lower than that with **Si3**. As a result, the effect of siloxane spacer on T_g follows **Siph** > **Si3** > **Si8** but the influence of siloxane spacer on T_{cl} follows the sequence of **Si3** > **Siph** > **Si8**.

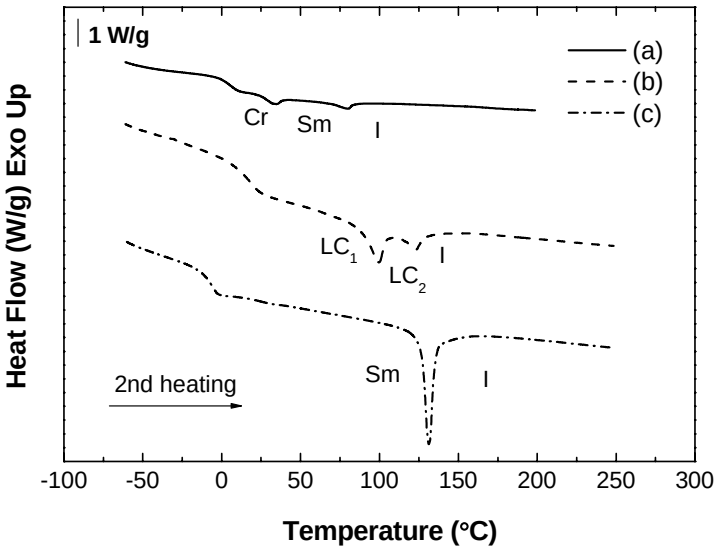

Figure 3-10 DSC traces (2nd heating) of elastomers with different hydrocarbon spacers (a) ***4h*** – C3(MeHQ)Si3XL10; (b) ***4i*** - C5(MeHQ)Si3XL10; (c) ***4f*** - C11(MeHQ)Si3XL10.

The hydrocarbon spacers may have two opposite effects on the glass transition temperature of LC elastomers. Long hydrocarbon spacers could increase the free volume, which lead to the decrease in T_g. On the other hand, the steric hindered effect of the long hydrocarbon chains could increase T_g. Similarly, the long hydrocarbon chains may reduce T_{cl} by acting as plasticizing agents or increase T_{cl} due to their steric hindered

effect. Increasing or decreasing the transition temperature depends on which effect is dominant[10]. For our LC elastomers, we found that the longer hydrocarbon chain resulted in higher clearing temperature as shown in Figure 3-10, which means the steric hindered effect dominates. Increasing the length of hydrocarbon spacer length from three methylene units to five methylene units results in increasing T_g from 4.3 ºC to 18.3 ºC, which means the steric effect dominates. However, increasing the hydrocarbon spacer length up to eleven methylene units leads to an apparent decrease in T_g (-5.7 ºC), which indicates the free volume increase due to the long hydrocarbon spacer overwhelms the steric effect from this long hydrocarbon spacer.

X-ray analysis indicated a smectic C phase in C11(MeHQ)Si8XL10 at room temperature. The same mesophase was found in C11(MeHQ)Si3XL10 with short siloxane spacer Si3 as shown in Figure 3-11.

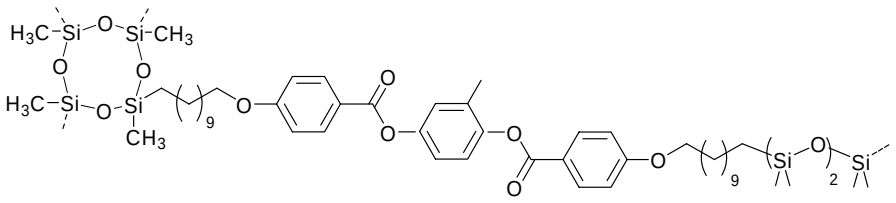

4j

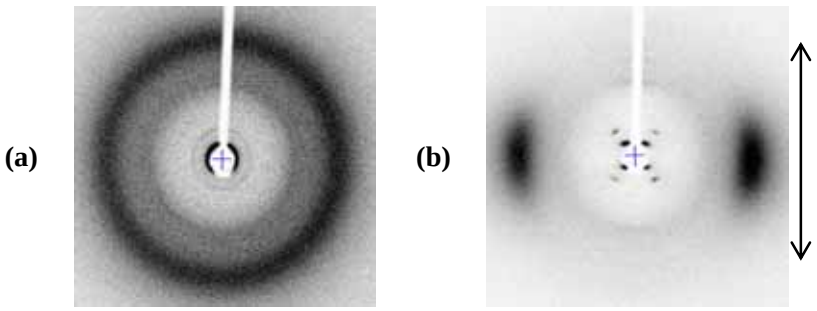

Figure 3-11 X-ray pattern of C11(MeHQ)Si3XL10 (a) as-cast (35.6 Å); (b) stretched (35.1 Å) at room temperature.

The estimated layer spacings of as-cast and stretched specimen are 35.6 Å and 35.1 Å, respectively.

A smectic C mesophase was also found in C3(MeHQ)Si3XL10 with short hydrocarbon spacer (C3) and short siloxane spacer (Si3) as seen in Figure 3-12. The layer spacing of this material is around 22.8 Å.

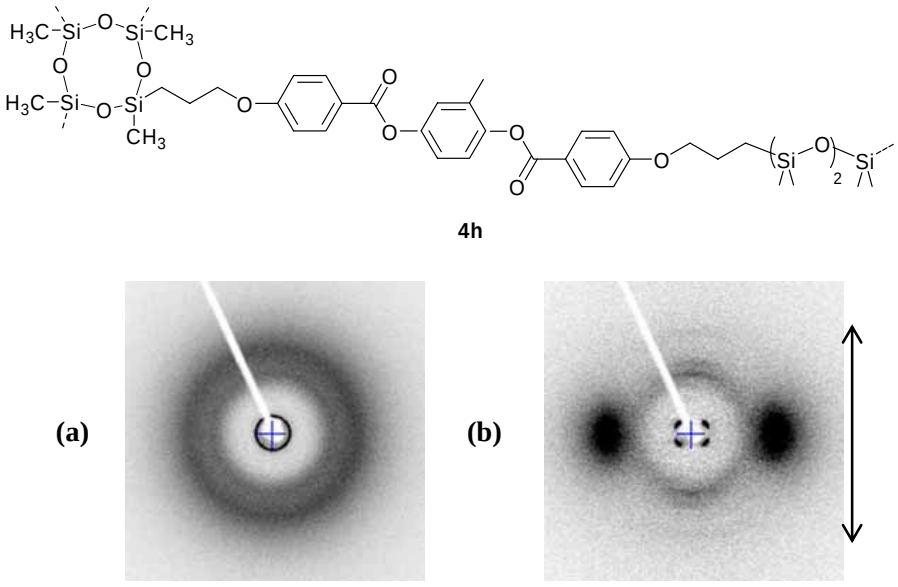

Figure 3-12 X-ray patterns of C3(MeHQ)Si3XL10 (a) as-cast (22.8 Å); (b) stretched (22.8 Å) at room temperature.

3.3.3 Effect of Lateral Substituents

It was known that the modification of lateral substituents could greatly effect of the mesophase behavior of low molar mass liquid crystals[11, 12]. In this work, we slightly changed the lateral substituents on the central benzene ring of the mesogenic core to study their effect on the physical properties of LCEs.

In addition to the mesogens with methylene substituents, another two LCEs were synthesized, C11(4H)Si8XL10 and C11(4F)Si8XL10. C11(4H)Si8XL10 LCE has no

substituents on the central benzene ring of its mesogenic rod.

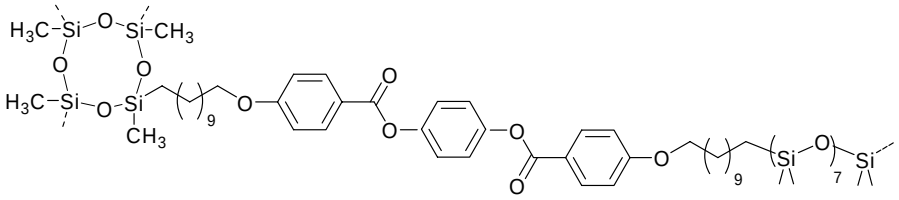

4k

A glass transition temperature was undetectable by DSC. Two pairs of reversible transition peaks showed in heating and cooling cycles in Figure 3-13.

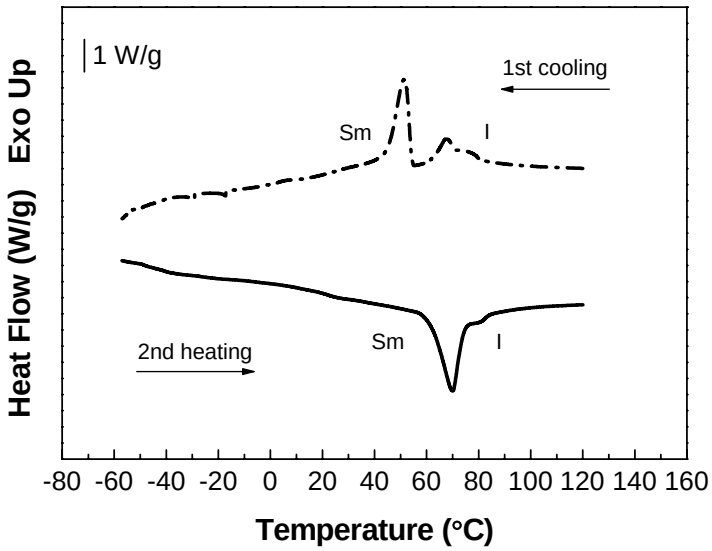

Figure 3-13 DSC traces (1st cooling and 2nd heating) of LC elastomer ***4k*** – C11(4H)Si8XL10

The small thermal hysteresis between heating and cooling cycle for each pair of peaks indicates that both of them are likely mesophase transitions. The symmetrical structure of the mesogen results in the higher mesophase to isotropic transition temperature (139 ºC) of this material compared with C11(MeHQ)Si8XL10 with less symmetry in the

mesogens.

WAXD study found a smectic C mesophase with layer spacing of 42.6Å for the as-cast specimen and 41.2 Å for a stretched specimen at room temperature. Further X-ray study at elevated temperature is needed to identify the second mesophase. The peak intensity maximum is located on the equator at the wide angle region. This indicates the hydrocarbon chains are macroscopically oriented along the stretching direction. The peak intensity maxima located on the meridian in the middle angle region indicate the presence of layer structures with the layer normal parallel to the stretching direction formed. According to the diffraction peak position, layer structures were likely formed by the segregation of siloxane spacers. In addition, a weak characteristic π-π stacking diffraction was detected in this material. Without the steric intervention from the methyl substituent on the central aromatic ring, lamellar packing of the polymer backbones is easier for C11(4H)Si8XL10.

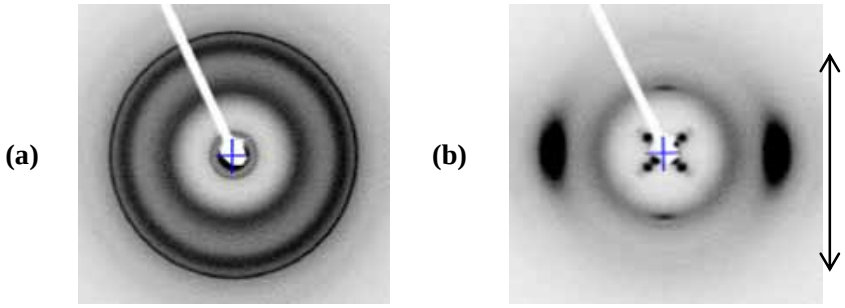

Figure 3-14 X-ray patterns of C11(4H)Si8XL10 (a) as-cast (42.6Å); (b) stretched (41.2 Å) at room temperature.

LCE ***4l***, C11(4F)Si8XL10, has its central benzene ring fully substituted by fluorine atoms.

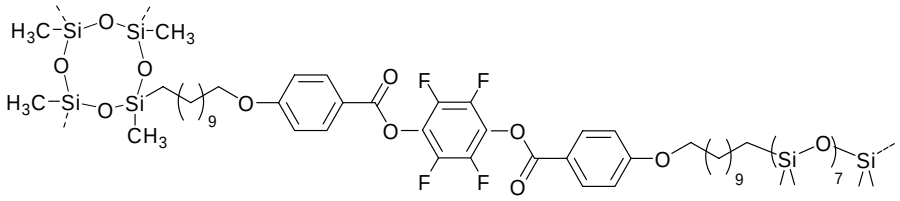

4l

Although C11(4F)Si8XL10 has a symmetrical structure of the mesogenic rod, the small steric effect of fluorine substituents on the packing and the polarity of the C-F bonds overwhelms the symmetry of mesogens. Therefore, this material has a lower mesophase to isotropic transition temperature (~70 ºC) than either C11(MeHQ)Si8XL10 and C11(4H)Si8XL10.

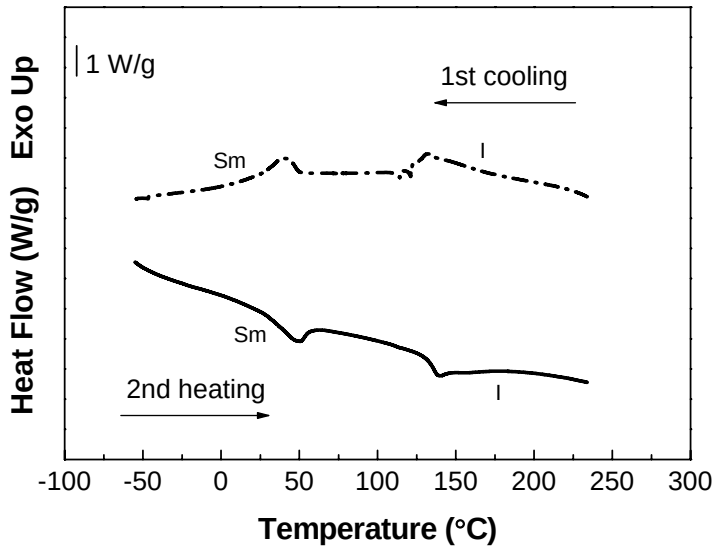

Figure 3-15 DSC traces (1st cooling and 2nd heating) of LC elastomer ***4j*** – C11(4F)Si8XL10.

WAXD detected very strong but less sharp diffraction patterns arranged in a crossed shape at the small angle region indicating a titled smectic mesophase in the material at room temperature. The peak intensity located on the equator illustrates the hydrocarbon

chains orient along the stretching direction. The layer structure formed by the segregation of siloxane spacer also exhibits diffractions on the meridian. Compared with C11(4H)Si8XL10, characteristic π-π stacking diffraction of this material is apparently stronger. The possible reason could be the strong segregation of fluorine substituents on the central benzene ring force the neighboring closer to each other, which strengthens the π-orbital overlapping.

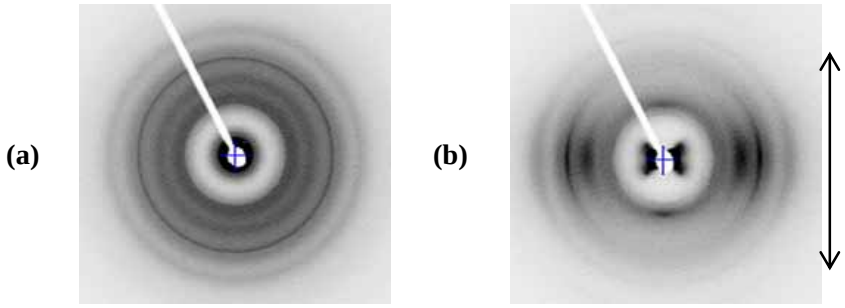

Figure 3-16 X-ray pattern of C11(4F)Si8XL10 (a) as-cast (34.8Å); (b) stretched (34.8 Å) at room temperature.

3.3.4 Effect of Non-mesogenic Terphenyl Transverse Rod

Terphenyl transverse rods were incorporated into C11(MeHQ)Si8XL10 to explore the potential for an auxetic effect at room temperature. A series of these LCEs ***4p - 4s*** with different loading of TR3 were synthesized and their transition temperatures are reported in Table 3-4.

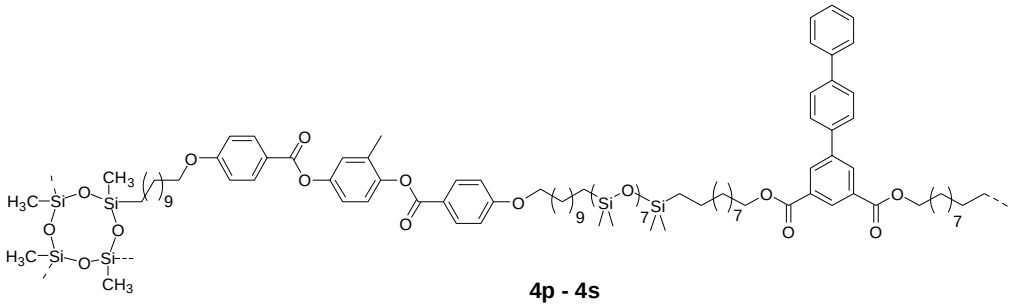

4p - 4s

Table 3-4 Transition temperatures from DSC of LC elastomers incorporating TR3

Elastomers	Tg (°C)	Clearing temperature (°C)	
		1st cooling	2nd heating
4b - (0 mol% **TR3**)	-25	101	105
4p - (10 mol% **TR3**)	-25	81	85
4q- (20 mol% **TR3**)	-23	73	80
4r - (30 mol% **TR3**)*	-24	55	64
4s - (40 mol% **TR3**)*	-25	34	50

* This material has a broad phase transition peak and the clearing temperature is taken at the peak maximum.

No apparent influence on Tg was found by introducing **TR3** into the parent LC elastomer. However, **TR3** has a great effect on clearing temperature. It was found that increasing the loading of **TR3** leads to a broader transition peak and a decrease in clearing temperature as illustrated in Figure 3-17.

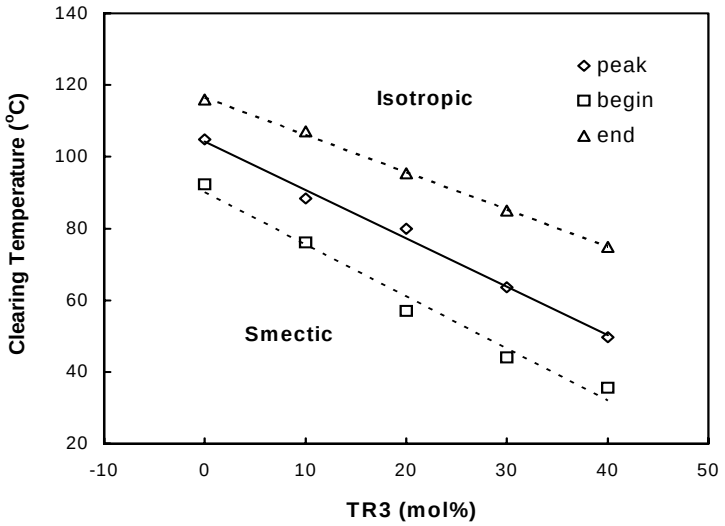

Figure 3-17 Effect of **TR3** on the thermal behavior of parent elastomer ***4b*** - C11(MeHQ)Si8XL10

It was found that 10 mol% loading of **TR3** began to decrease the clearing

temperature and broaden the LC transition peak. Since **TR3** is a rigid monomer but not a liquid crystal itself, introducing non-mesogenic monomers into the LC elastomer system inevitably disrupts the liquid crystalline stability. The more **TR3** in the system, the less the liquid crystallinity the system can bear.

Although DSC analysis showed the mesophase disrupting nature of **TR3,** WAXD studies detected a similar smectic-C type of mesophase in all the stretched elastomers with **TR3** in their parent elastomer C11(MeHQ)Si8XL10 as seen in Figure 3-18. It was also found that the amount of **TR3** loading does not greatly influence the overall chain orientation of the stretched materials.

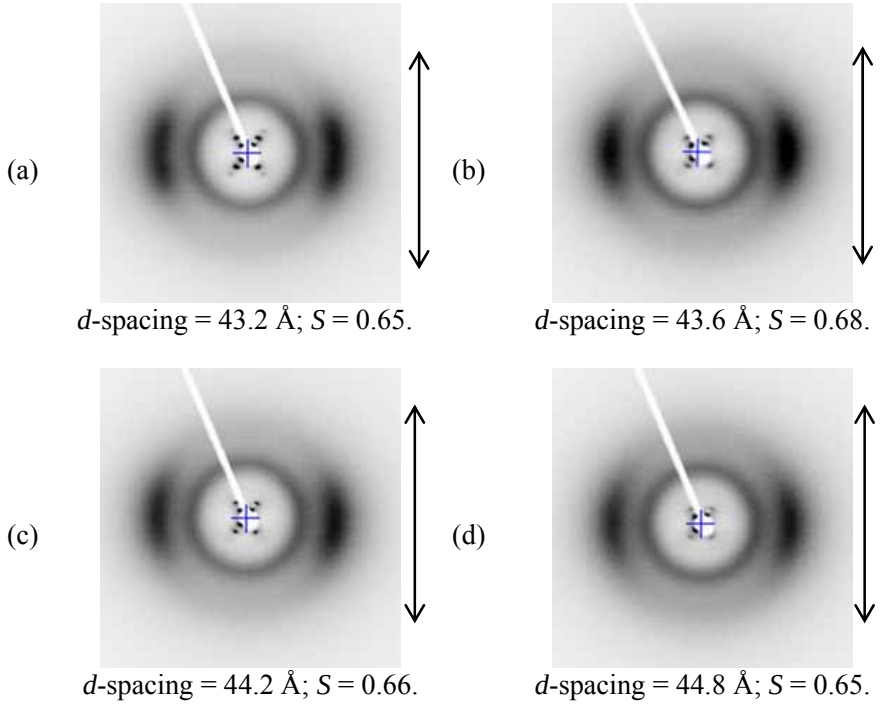

d-spacing = 43.2 Å; *S* = 0.65. *d*-spacing = 43.6 Å; *S* = 0.68.

d-spacing = 44.2 Å; *S* = 0.66. *d*-spacing = 44.8 Å; *S* = 0.65.

Figure 3-18 X-ray pattern of stretched C11(MeHQ)Si8 LC elastomers with various amount of TR3: (a) 10 mol% ; (b) 20 mol%; (c)) 30 mol%; (d) 40 mol% at room temperature.

All the specimens with about 200% initial strain have an order parameter ranging from 0.65 to 0.68. The disrupting nature may also be seen by the gradually decreased value of

the layer spacing with **TR3** loading as noted in Figure 3-18. The rigid part of transverse rod **TR3** is shorter than that of C11(MeHQ) monomer. It is reasonable that the average layer spacing gets smaller by increasing the fraction of TR3.

3.4 Results and Discussions

In this chapter, we investigated the effect of chemical variations, e.g. siloxane spacer, hydrocarbon spacer, crosslinker content, terphenyl transverse rod and lateral substituents of mesogenic units, on the mesophase behavior of MCLCPs and MCLCEs by thermal and X-ray analysis.

For a given LC monomer, C11(MeHQ), it was found that the clearing temperature of the LC polymer can be tailored by varying the ratio of long siloxane spacer **Si8** to short siloxane spacer **Si3**. The clearing temperature shifts to a higher value with an increase of the amount of short spacer **Si3**. The continuous change in clearing temperature indicates a homogeneous distribution of these two different spacers at the molecular level in the polymers. Meanwhile, incorporating spacer **Si3** also induces the formation of partially crystalline structures in LC polymers. The glass transition temperature shows a gradual change as the ratio of these two spacers is varied.

Terphenyl transverse rod (**TR3**) was introduced in the C11(MeHQ)Si3 LC polymers. Due to the non-mesogenic nature of **TR3**, mesophase stability of the parent polymer is diminished. From DSC, the clearing transition peak of the polymer with 50 mol% **TR3** loading was almost undetectable. WAXD and SAXS studies found smectic A-like and smectic C-like mesophase in the parent polymer and polymer with 50 mol% **TR3** loading, respectively. Because tilted smectic layer structure induced by **TR3** components, the layer spacing of the fiber specimen with 50 mol% **TR3** decreased to

35.6 Å from its original value of 36.2 Å.

TR3 was introduced in C11(Biph)Si8 LC polymers with the longer mesogen core and siloxane spacer. For this LC polymer, a larger amount of **TR3** (up to 75%) can be accommodated without loss of the mesophase. Smectic A type of mesophase was found in the parent LC polymer. And again, it was changed into smectic C type of mesophase by introducing **TR3**.

The thermal properties of C11(MeHQ)Si8 elastomers were studied first by varying the crosslinker content. It was found that both the glass transition and clearing temperature are dependent on the crosslinking density. Both of temperatures shift to higher values with increasing of the crosslinker content. Increase in the amount of crosslinker can apparently broaden the mesophase to isotropic transition because of the the increasing restriction effect of crosslinking on the mesogen mobility. Among these LC elastomers, the ones with 5% and 10% crosslinker show a sharp and reversible mesophase to isotropic transition. A wide mesophase window covering over 130 ºC was found in both of these elastomers.

In addition to spacers **Si3** and **Si8**, the spacer 1,4-bis(dimethylsilyl)benzene (**Siph**) was introduced into our LC elastomers especially for investigating the effect of siloxane spacer on the transition temperatures. The effect of spacer on the glass transition temperature follows **Siph** > **Si3** > **Si8** but the influence of spacer on clearing temperature follows the sequence of **Si3** > **Siph** > **Si8**.

The effect of terminal hydrocarbon chain of the transition temperature was studied by varying methylene units from three to eleven. It was found that the glass transition temperature decreases with increasing hydrocarbon chain length, which may be

contributed by the plasticizing effect of the long chain. The longer hydrocarbon chain resulted in higher clearing temperature, which likely means the steric hinderance effect dominates.

Two elastomers C11(4H)Si8XL10 and C11(4F)Si8XL10 were synthesized to study the effect of lateral substituents of mesogens on the transition temperatures. Compared with C11(MeHQ)Si8XL10, these two exhibit more complicated thermal behaviors by DSC. Two pairs of mesophase transition peaks were found in C11(4H)Si8XL10 having no substituent on the central ring. Compared with this elastomer, C11(MeHQ)Si8XL10 and C11(4F)Si8XL10 show lower transition temperatures. A possible reason could be the steric effect of the methyl substituent and four fluorine substituents on the central benzene ring of the mesogen.

Introducing **TR3** into the elastomer C11(MeHQ)Si8XL10 has no apparent effect on the glass transition temperature but has a large effect on the clearing temperature. Since **TR3** is a non-mesogenic monomer, it disrupts the mesophase stability and broadens the mesophase to isotropic phase transition peak and decreases the clearing temperature as well.

From DSC analysis, we determined the mesophase windows of our MCLCPs and MCLCEs. Room temperature is located within those temperature windows. Therefore, we can study mesophase behavior of the synthesized polymers and elastomer by room temperature WAXD and SAXS. A smectic A type of mesophase was found in both C11(MeHQ)Si3 and C11(Biph)Si8 linear LC polymers. The mesophase in both elastomers changes into a smectic C type after introducing **TR3**, which indicates **TR3** has the ability to induce the formation of a smectic C mesophase. A smectic C type of

mesophase pattern was found in C11(MeHQ)Si8 LC polymer with longer silioxane spacer compared with C11(MeHQ)Si3 LC polymer. The analogous elastomers of these linear LC polymers are always in smectic C mesophase instead of smectic A.

Smectic C mesophase was found in all the elastomers studied in this work. The reason that the tilted layer structure is favored by the elastomers could possibly relate to the incompatibility of components and spacing filling efficiency. The aromatic rigid cores and hydrocarbon terminal chains of mesogens are highly incompatible with a siloxane spacer and with themselves. In order to achieve the most stable state, the segregation of these segments occurs at a nanoscale level which is consistent with the smectic layer spacing of about 40 Å detected by WAXD at small angle region. Similar nanophase segregations have been found in both low molar mass liquid crystals [13-16] and liquid crystalline polymers [6, 17-19].

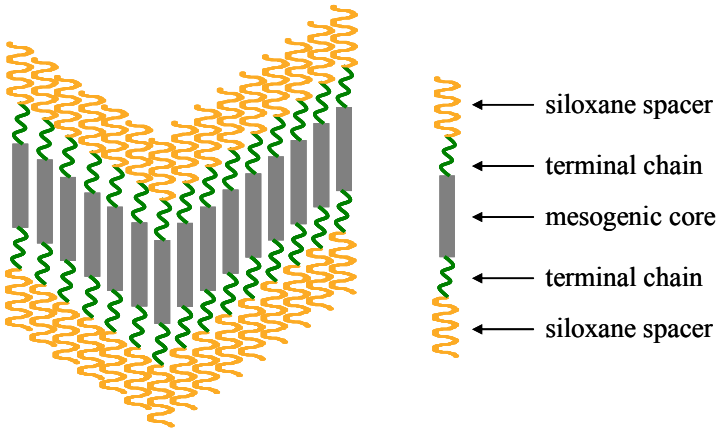

Figure 3-19 Schematic illustration of the arrangement of polymer backbone to form smectic C type of mesophase (chevron)

The flexible siloxane spacer tends to coil up and forms a bulky section on the backbone. Siloxane components naturally have a tendency to segregate from hydrocarbons. They are normally in a highly coiled state, which gives them a wider cross-section area

compared with that of a fully extended chain configuration [16]. The mesogenic core is rigid and fully extended. Terminal hydrocarbon chains of mesogens tend to coil in a fluid phase to minimize energy but to a smaller extent compared with a siloxane spacer. All the three components are connected together to form the polymer backbone. Therefore, the cross-section area varies along the backbone. The bulky siloxane spacer section occupies around its neighborhood. This creates void space nearby which has to be filled to minimize energy. Therefore, the neighboring polymer chains offset each other to some extent and arrange themselves into a 'chevron' shape as shown in Figure 3-19. In the 'chevron' arrangement, the polymer backbone is parallel to the orientation direction. The layer normal points to at an angle to the polymer backbone.

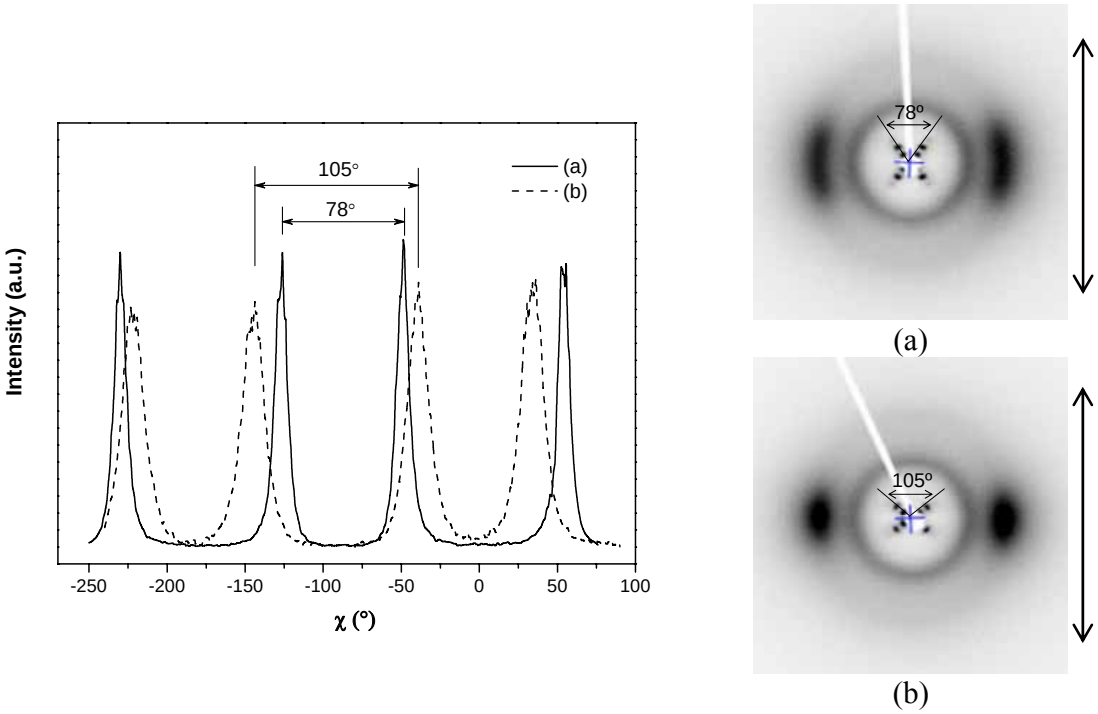

Figure 3-20 X-ray pattern and azimuthal scan of stretched C11(MeHQ)Si8XL10 with more than 200% initial strain: (a) with strain recovery; (b) without strain recovery at room temperature.

It was found that the smectic layer tilt angle could be changed by stretching as shown in

Figure 3-20 for C11(MeHQ)Si8XL10. Stretching makes the neighboring backbones offset further from each other, which leads to an increase in the tilt angle. Azimuthal scanning of the two x-ray patterns at the small angle region clearly illustrates the tilt angle increase from ~36º to ~53º by stretching. The same phenomenon was also observed in C11(MeHQ)Si8XL10 with 20 mol% **TR3** as illustrated in Figure 2-31.

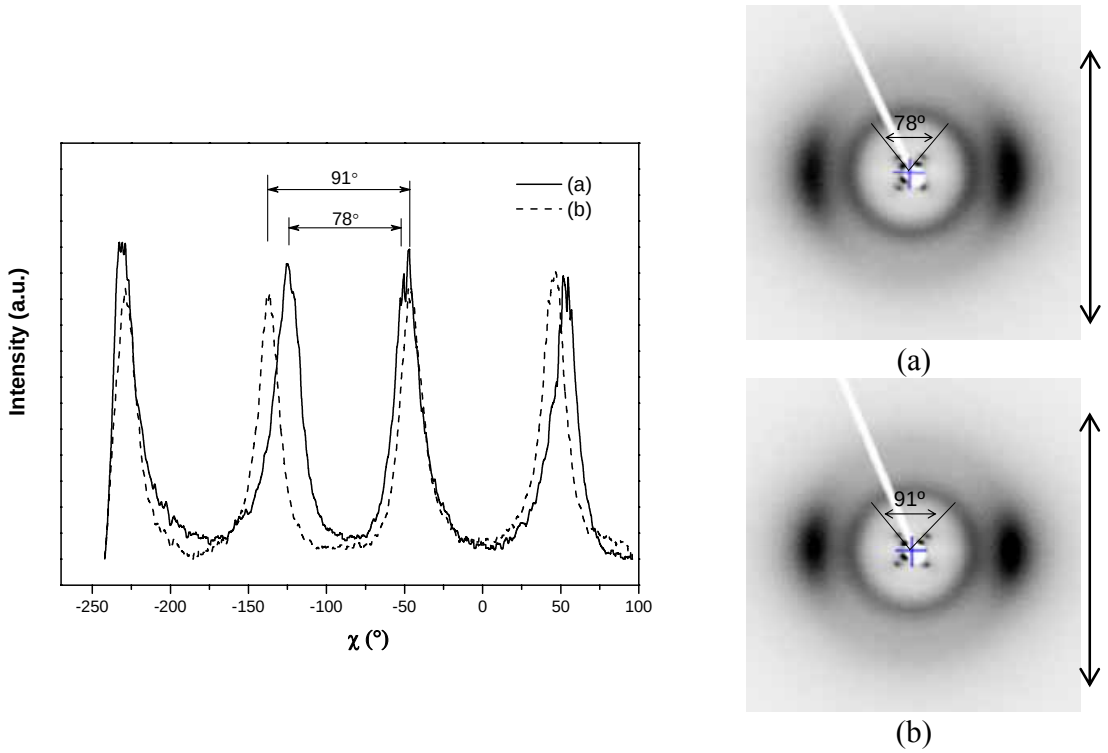

Figure 3-21 X-ray pattern and azimuthal scan of stretched C11(MeHQ)Si8XL10 containing 20 mol% TR3 with more than 200% initial strain: (a) with strain recovery; (b) without strain recovery.

The smaller increase in smectic layer tilt angle of C11(MeHQ)Si8XL10 with 20 mol% TR3 than that of it parent LCE by further stretching may also be an indication of the disruption of the mesophase by terphenyl transverse rod.

3.5 References

[1] G. Kossmehl, B. Gerecke, N. Harmsen, H. M. Vieth, and D. Wolff, "Liquid crystalline main chain polysiloxane esters and their monomers. II. Synthesis and thermal behaviour of polysiloxane esters with linear and tilted aromatic ester moieties," *Molecular Crystals and Liquid Crystals Science and Technology Section a-Molecular Crystals and Liquid Crystals*, vol. 317, pp. 1-21, 1998.

[2] B. Donnio, H. Wermter, and H. Finkelmann, "Simple and versatile synthetic route for the preparation of main-chain, liquid-crystalline elastomers," *Macromolecules*, vol. 33, pp. 7724-7729, 2000.

[3] I. A. Rousseau, "Development of soft polymeric networks showing actuation behavior: from hydorgels to liquid crystalline elastomers," *PhD Thesis, University of Connecticut*, 2004.

[4] M. A. A. Cortes, "Synthesis and physical properties of unsymmetric main-chain liquid crystal elastomers," *PhD Thesis, University of Exeter*, 2006.

[5] G. G. Odian, *Principles of polymerization*, 3rd ed. New York: Wiley, 1991.

[6] C. Pugh, J. Y. Bae, J. Dharia, J. J. Ge, and S. Z. D. Cheng, "Induction of smectic layering in nematic liquid crystals using immiscible components. 2. Laterally attached side-chain liquid-crystalline poly(norbornene)s and their low-molar-mass analogues with hydrocarbon/oligodimethylsiloxane substituents," *Macromolecules*, vol. 31, pp. 5188-5200, 1998.

[7] C. B. He, P. W. Liu, P. J. McMullan, and A. C. Griffin, "Toward molecular auxetics: Main chain liquid crystalline polymers consisting of laterally attached para-quaterphenyls," *Physica Status Solidi B-Basic Solid State Physics*, vol. 242, pp. 576-584, 2005.

[8] B. Wunderlich, *Thermal analysis of polymeric materials*. Berlin: Springer, 2005.

[9] R. Zentel and G. Reckert, "Liquid-crystalline elastomers based on liquid-crystalline side group, main chain and combined polymers," *Makromolekulare Chemie-Macromolecular Chemistry and Physics*, vol. 187, pp. 1915-1926, 1986.

[10] F. J. Davis, "Liquid-crystalline elastomers," *Journal of Materials Chemistry*, vol.

3, pp. 551-562, 1993.

[11] H. Kelker, R. Hatz, and C. Schumann, *Handbook of liquid crystals*. Weinheim ; Deerfield Beach, Fla.: Verlag Chemie, 1980.

[12] P. J. Collings, *Liquid crystals : nature's delicate phase of matter*, 2nd ed. Princeton, N.J.: Princeton University Press, 2002.

[13] C. A. Vieth, E. T. Samulski, and N. S. Murthy, "Multilayered crystalline-structures and liquid-crystalline phases in a mesogen with siloxane tails," *Liquid Crystals*, vol. 19, pp. 557-563, 1995.

[14] N. Olsson, B. Helgee, G. Andersson, and L. Komitov, "A new series of siloxane liquid crystalline dimers exhibiting the antiferroelectric phase," *Liquid Crystals*, vol. 32, pp. 1139-1150, 2005.

[15] G. Galli, M. Reihmann, A. Crudeli, E. Chiellini, Y. Panarin, J. Vij, C. Blanc, V. Lorman, and N. Olsson, "Design of siloxane liquid crystals forming a de Vries SmA* phase," *Molecular Crystals and Liquid Crystals*, vol. 439, pp. 2111-2123, 2005.

[16] D. Guillon, M. A. Osipov, S. Mery, M. Siffert, J. F. Nicoud, C. Bourgogne, and P. Sebastiao, "Synclinic-anticlinic phase transition in tilted organosiloxane liquid crystals," *Journal of Materials Chemistry*, vol. 11, pp. 2700-2708, 2001.

[17] E. Nishikawa and E. T. Samulski, "New mesogens with cubic phases: hydrogen-bonded bipyridines and siloxane-containing benzoic acids - I. Preparation and phase behaviour," *Liquid Crystals*, vol. 27, pp. 1457-1462, 2000.

[18] M. Rossle, L. Braun, D. Schollmeyer, R. Zentel, J. P. F. Lagerwall, F. Giesselmann, and R. Stannarius, "Differences between smectic homo- and co-polysiloxanes as a consequence of microphase separation," *Liquid Crystals*, vol. 32, pp. 533-538, 2005.

[19] M. IbnElhaj, A. Skoulios, D. Guillon, J. Newton, P. Hodge, and H. J. Coles, "Structural characterization of new ferroelectric liquid-crystalline siloxanes," *Journal De Physique Ii*, vol. 6, pp. 271-279, 1996.

CHAPTER 4

Mechanical Characterization of MCLC Elastomers

In the previous chapter, we introduced the synthesis of linear LC polymers as well as LC elastomers. The number average molecular weight of the synthesized polymers ranges from 14000 to 25000. All the linear polymers are readily drawn into fibers. However, the glass transition temperatures of the LC polymers are much lower than room temperature due to the flexible siloxane spacers. These fibers are soft and even sticky at room temperature. It is difficult to do mechanical property measurements for these fiber samples under tension. Formation of network structures can permit formation of more mechanically robust samples, since crosslinking imposes additional constraints on the polymer chains. However, simply introducing a crosslinker into the system cannot guarantee integrity of the LCE films. In fact, in order to form non-sticky and smooth-surface solid films with low crosslinking density (<10 mol%), there is an optimum combination of terminal chain length of the mesogen and length of the siloxane spacer. The mechanical properties of LCEs in this work mainly focus on the stress-strain behavior, strain recovery, mechanical hysteresis and Poisson's ratio. For each property, we will discuss the controlling influences from the perspective of crosslinking density, flexible siloxane spacer length, terminal hydrocarbon chain length and the specific chemical structure of the LC monomer. The dependence of mechanical behavior on temperature, strain rate and, for relaxation studies, on initial imposed strain is also discussed.

4.1 Shape of Polymer Chains in Liquid Crystalline Elastomers

A liquid crystalline elastomer and a conventional rubber are quite different, mainly because they differ in chain anisotropy. Anisotropy of the constituent chains plays a vital role in the physical properties of the liquid crystalline elastomers. Therefore, the average shape of polymer backbone in liquid crystalline elastomer is very important [1]. At a molecular level, the polymer chain in a conventional rubber is in a coiled form or a sphere. The dimension can be estimated by the average radius of gyration, ***R***, as illustrated in Figure 4-1. One dimension is sufficient to characterize their properties [1].

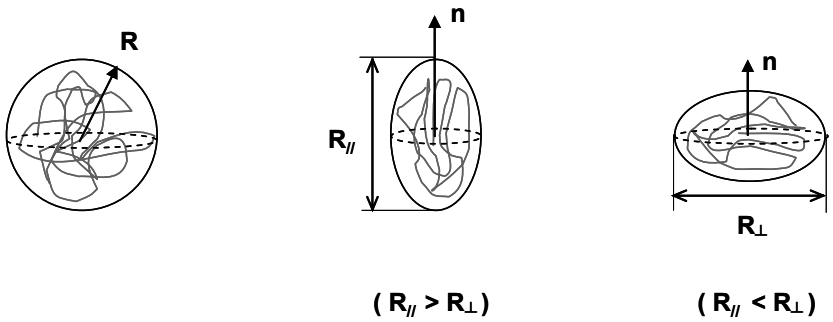

Figure 4-1 A spherical shape of polymer chain in conventional rubber (left) and a prolate (middle) and an oblate (right) shape of polymer chain in liquid crystalline elastomers.

However, the shape of polymer chains in LC elastomers is distorted due to the liquid crystalline order [1, 2]. At least one more dimension is needed to characterize the anisotropic polymer chains. Here, $R_{//}$ and $R_{\perp}$ are additionally designated to the radius of gyration in the direction parallel and perpendicular to the director *n*, respectively, as shown in Figure 4-1. The polymer could adopt a prolate shape if the aligned mesogenic units elongate the shape of polymer backbone along the principle axis of the director ($R_{//} > R_{\perp}$) or an oblate shape if the elongated polymer backbone is perpendicular to the orientation of the director ($R_{//} < R_{\perp}$).

The arrangement of mesogenic groups and the polymer backbone in nematic polymers is clearly illustrated by Warner and Terentjev as in Figure 4-2. A main-chain nematic polymer in a prolate shape shows the highest chain anisotropic due to the direct chemical connectivity of the mesogenic units within the backbone. The side-on side-chain nematic polymer also in a prolate shape exhibits a relatively weaker anisotropy but still a substantial backbone alignment. The two end-on side-chain nematic polymers could be in prolate (backbone elongated along the director) or oblate (backbone elongated normal to the director) shapes depending on the selection of spacer [3]. Their mesogenic units are weakly coupled to the backbone compared with the first two cases.

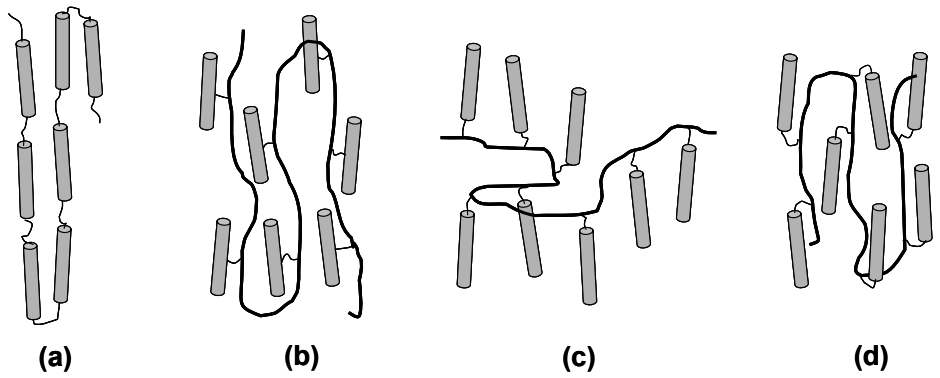

Figure 4-2 Shapes of nematic polymers: (a) main-chain (prolate) ; (b) side-on side-chain(prolate); (c) end-on side-chain (oblate); (d) end-on side-chain (prolate) [1].

The chain anisotropy, r, can be defined by equation (4-1),

$$r = \frac{R_{//}}{R_{\perp}} = \frac{1+2Q}{1-Q} \tag{4-1}$$

where Q refers to the nematic order parameter [1]. The order parameter is also represented by S in previous chapters. For isotropic materials, such as conventional

rubber or liquid crystalline elastomers in the isotropic state, polymer chains are randomly oriented ($Q = 0$), so that the r equals to 1. When liquid crystalline elastomers are in their mesophase, Q has a value less than 1, which results in r having a value greater than 1 if the polymer chain is in a prolate shape or less than 1 if the polymer chain takes an oblate shape.

4.2 Classical Rubber Elasticity

Large and reversible deformation is the most noticeable feature making natural rubber and other elastomers distinguished from other substances [4]. A typical stress-strain curve of a natural rubber is shown in Figure 4-3.

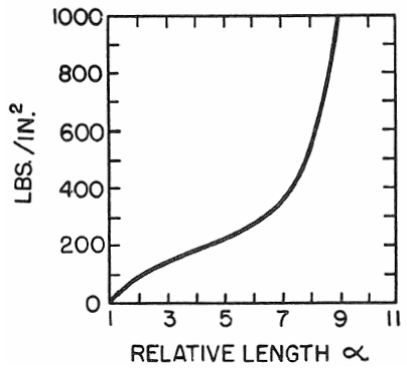

Figure 4-3 A typical stress-strain curve for a natural rubber by Flory [4].

In this curve, the stress increases slowly up to ~ 500% elongation (relative length $\alpha = \sim 6$ in the figure) then follows a sharp rise in stress until the rubber breaks at 3000 lbs/in^2 (out of the plot). The slope increase between 4 and 6 relative length is associated with crystallization induced by stretching [4].

In classical rubber elasticity theory, there are several assumptions for an "ideal" rubber [4-6]. First of all, an affine deformation assumption is often applied to an ideal rubber, in which a network deformation can be reflected by the macroscopic shape

change in the material macroscopically. Secondly, no volume change is assumed to occur during stretching. Thirdly, entropy change or uncoiling is the only response of an ideal rubber to external extension. Once the deforming force being removed, a restoring force makes the polymer chain return to its unstretched state. The relations between the external force and the corresponding strain response can be established from thermodynamic considerations and is given by equation (4-2).

$$\sigma = \rho \frac{RT}{Mc}(\lambda - \frac{1}{\lambda^2}) \tag{4-2}$$

where ρ is the density of rubber, Mc is the number average molar mass between netpoints, R is the universal gas constant, T is the temperature in Kelvin, λ is the ratio of extended length (L) to the original length (L_0). The extension ratio and strain (ε) are connected by $\lambda = 1 + \varepsilon$. At very small strain, $\lambda - 1/\lambda^2$ equals to 3ε. Therefore, equation (4-2) can be rewritten as

$$\sigma = 3\rho \frac{RT}{Mc}\varepsilon \tag{4-3}$$

since

$$\sigma = E\varepsilon \tag{4-4}$$

where E is Young's modulus. Combining equation (4-3) and (4-4) gives an expression for the average molecular weight between netpoints [5].

$$Mc = \frac{3\rho RT}{E} \tag{4-5}$$

At a temperature above the glass transition temperature but below the clearing temperature, polymer chains of LC elastomers are highly anisotropic. However, when the temperature is above the clearing temperature, the anisotropy of polymer chains is disrupted completely so that the materials become isotropic conventional elastomers.

Therefore, the average molecular weight of LC elastomers can be evaluated by equation 4-5 if all the related parameters are measured at a temperature above the materials' clearing temperature.

4.3 Stress-strain Behavior of Polydomain MCLC Elastomers

It has been found that liquid crystalline elastomers inevitably form very fine polydomain structures if no special processing was performed during preparation [3, 7, 8]. Terentjev *et. al.* has claimed that a polydomain structure is a thermodynamic equilibrium state for liquid crystalline elastomers because of the "quenched disorder" in the system, which might come from synthesis defects, chain entanglements, netpoints, etc. [9, 10]. In our work, we use solution casting as our film fabrication method, which has been described in detail in chapter 2. All the components, the LC monomer, spacer and crosslinker, were thoroughly mixed together before chain extension and crosslinking reactions started. The same reactivity of Si-H groups, both in the difunctional siloxane spacer and the tetrafunctional crosslinker was assumed. The distribution of each component in the system was random, which led to polydomain structures for all the as-cast films.

4.3.1 Effect of Crosslinking Density

Five LC elastomers (***4a*** - ***4e***), C11(MeHQ)Si8XL5 - C11(MeHQ)Si8XL25, were synthesized by varying the crosslinker content (XL), which ranges from 5 mol% to 25 mol%, to study the effect of crosslinker density on the mechanical properties.

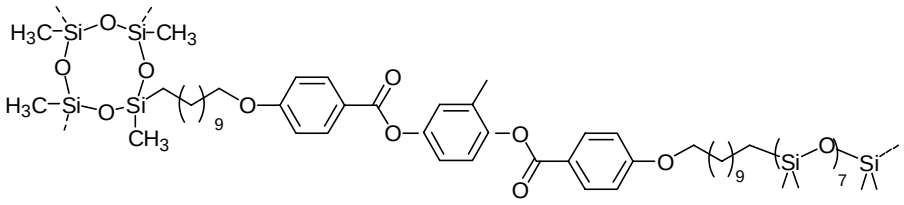

4a - 4e

Thermal and X-ray analysis revealed a smectic C mesophase structure for this series of LCEs. Strain-stress curves obtained at room temperature are plotted in Figure 4-3.

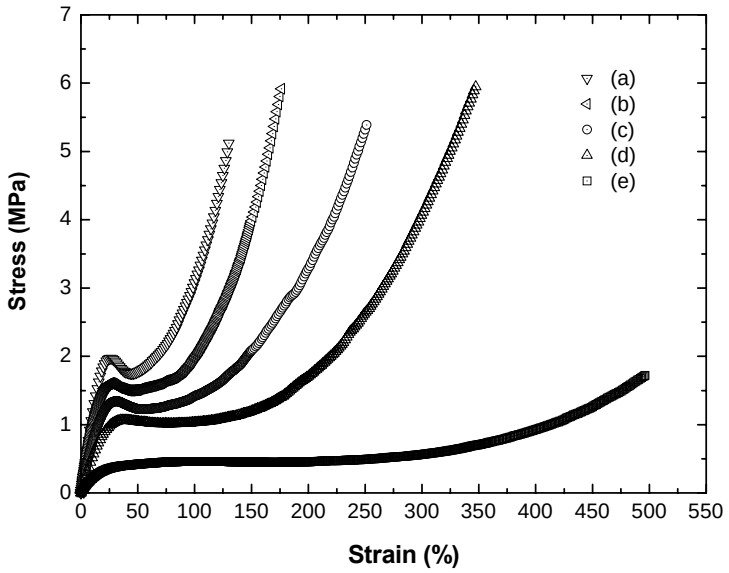

Figure 4-4 Effect of crosslinker (XL) content on the mechanical properties of C11(MeHQ)Si8 elastomers: (a) ***4e*** – 25 mol% XL; (b) ***4d*** - 20 mol% XL (c) ***4c*** - 15 mol% XL; (d) ***4b*** - 10 mol% XL; (e) ***4a*** – 5 mol% XL.

A general trend was found in these elastomers: the higher the crosslinker content the higher the Young's modulus and the higher the threshold stress to begin the polydomain-to-monodomain (*P-M*) transition (when no apparent yield point appears) or the yield stress (when a yield point is observable). Increasing the amount of crosslinker also leads to a shorter *P-M* transition plateau region and to a lower elongation at break.

An obvious yield point (further elongation results in a decrease in load) appears in the stress-strain curve when the crosslinker content reaches 15 mol% or higher value. The detailed results from these strain-stress measurements are summarized in Table 4-1.

Table 4-1 Mechanical Properties of LC Elastomers 4a-4f

	Young's Modulus (MPa)	Threshold Stress/ Yield Stress (MPa)	Elongation at break (%)
4a – 5 mol% XL	2.9	0.4	592
4b – 10 mol% XL	6.3	1.2	347
4c – 15 mol% XL	8.7	1.4	250
4d – 20 mol% XL	11.5	1.7	176
4e – 25 mol% XL	12.2	2.0	130

As was discussed in section 4.2, LCEs can be considered as ordinary rubbers at temperatures above their clearing temperature due to the anisotropy of polymer chains being disrupted completely. Therefore, the average molecular weight of LC elastomers can be experimentally evaluated by obtaining the Young's modulus in their isotropic state and applying equation 4-5. Before discussing the experimental results, the relation between the average molecular weight (between netpoints) and the crosslinker content is calculated numerically for comparison.

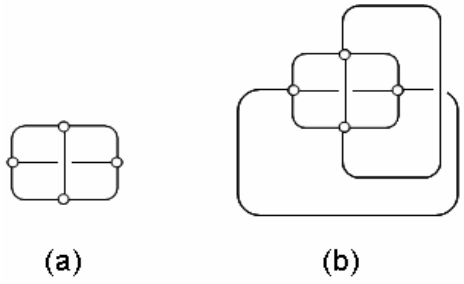

Figure 4-5 A perfect network structure (a) φ = 3; (b) φ = 4. *φ* refers to functionality [11].

For this calculation, a perfect LC network is assumed as illustrated in Figure 4-5. A perfect network means that no free end exists in the system. This determines a fixed relation between crosslinker content and the number of mesogens between netpoints. For the networks, no matter the crosslinker functionality, the overall number of polymer chains (N) in the network can always be related to the number of crosslinkers or to the number of netpoints (μ) and the functionality (φ) of crosslinker by equation (4-6) [11].

$$\varphi \mu = 2N \tag{4-6}$$

In order to calculate the average number (n) of mesogens between netpoints in our LC elastomer, it is necessary to define other quantities as follows:

N' – overall number of mesogenic monomers in the network, therefore, $n = \frac{N'}{N}$;

φ' – functionality of mesogen;

γ – molar fraction of crosslinker in the network.

In our reaction system for LC elastomer synthesis, there are two types of reactive functional groups. One is the vinyl group (carbon-carbon double bond) belonging to divinyl LC monomer; the other is the Si-H group belonging to both the chain-extending siloxane spacer and the cyclic crosslinker. The assumption of a perfect network requires perfect stoichiometry in the system. In other words, the overall number of vinyl double bond must be identical to the overall number of Si-H groups since these react in a 1:1 ratio. Therefore, the overall number of netpoints can also be expressed by equation (4-7).

$$\mu = N'\gamma \tag{4-7}$$

By combining equation (4-6) and (4-7), we have

$$\varphi N'\gamma = 2N \tag{4-8}$$

$$\frac{N'}{N} = \frac{2}{\varphi\gamma} \tag{4-9}$$

Since the functionality of crosslinker in our LCEs is always 4, we have

$$n = \frac{N'}{N} = \frac{1}{2\gamma} \tag{4-10}$$

With this derived equation, it is possible to calculate the average number of mesogens or number of repeat units (DP) between netpoints. These are listed in Table 4-2.

Table 4-2 Calculated number of mesogens between netpoints

γ	0.05	0.10	0.15	0.20	0.25	0.30	0.35	0.40	0.45	0.50
γ (mol%)	5	10	15	20	25	30	35	40	45	50
n	10	5	3.3	2.5	2	1.7	1.4	1.25	1.1	1

With low crosslinker content, for instance, 5 mol%, there are 10 mesogens between netpoints on average. In this case, the mesogens are expected to move freely and easily gather together to form an ordered structure. The perturbation of netpoints to the liquid crystalline order is expected to be relatively weak. However, with higher crosslinker content, the number of mesogens between netpoints quickly becomes smaller. At 25mol%, there are only 2 mesogens between every two netpoints on average. The perturbation of netpoints to the liquid crystalline order becomes significant. The mesogens are more confined in the tight network structure. This reduction in liquid crystalline order is reflected in the broaden mesophase to isotropic phase transition peaks in DSC traces with increasing crosslinker. The polydomain-to-monodomain transition plateau shown in stress-strain curves is a characteristic feature of LC elastomers. Under a uniaxial stress, polydomains with local but not global orientational order rotate to align

themselves along the stretching direction and gradually transform into a monodomain. Increasing crosslinker content not only affects the global orientational order but also the local LC order. Eventually, with the increase of crosslinker, the disruption effect becomes severe enough to preclude the formation of LC order. Correspondingly, a gradually shortening of *P-M* transition plateaus with an increase of crosslinker was observed. For instance, a much longer *P-M* transition plateau region was found in elastomer with 5 mol% crosslinker than that in elastomer with 25 mol% crosslinker as seen in Figure 4-4.

The longer elongation at break with decreasing crosslinker can also be explained by the number of mesogens between netpoints. More mesogens between netpoints also means more flexible groups (both hydrocarbon spacer and siloxane spacer) between netpoints. This increased flexibility makes the elastomers with low crosslinker content more extensible than those with high crosslinker content. In addition, higher crosslinker content (fewer mesogens between netpoints) indicates a material of tighter network structure, which results in higher Young's modulus in these elastomers.

Experimentally, the average molecular weight between netpoints of LCEs can be calculated by Equation 4-5 after obtaining the Young's modulus above the clearing temperature of each LCE samples. The experimental results were listed in Table 4-3.

Table 4-3 Experimental results of the average number of mesogens between netpoints

	T_{cl} (ºC)	$T_{exp.}$ (ºC)	*E(MPa)*	M_{repeat}	*Mc*	$n_{exp.}$
XL5	101	117.7	0.21	1248.2	46403	37
XL10	104	113.0	0.26	1248.2	37029	30
XL15	110	132.7	0.59	1248.2	17150	14
XL20	119	149.9	1.04	1248.2	10142	8
XL25	133	164.8	1.12	1248.2	9750	8

A smooth but non-linear relation was found between the number of mesogens between netpoints and the crosslinker content was found both in numerical calculations and experiments as shown in Figure 4-6.

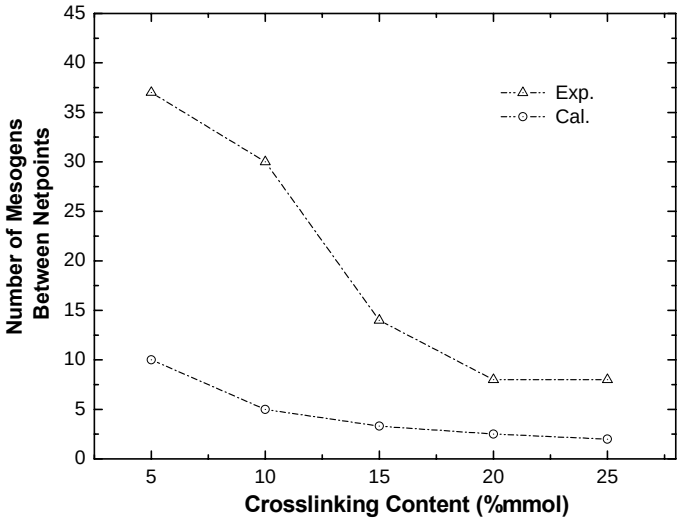

Figure 4-6 Comparison of the average number of mesogenic groups between netpoints as a function of crosslinker content from the experiments and the numerical calculations.

Both curves illustrate that the average number of mesogens between netpoints decreases quickly when the crosslinker content is small (~ less than 15%). After that point, an increase in the amount of crosslinker leads to a slow decrease in the average number of mesogens between netpoints. Experimental results indicate more mesogens are between netpoints than that from numerical calculation, which may mean less perfect crosslinking occurs during reaction. The sol-fraction is a parameter to evaluate the soluble components after the crosslinking. The sol-fraction of these LCEs ranges from 3% to 15%, which is close to the sol-fraction (21% -22%) reported for a similar elastomer with 5 mol% and 20 mol% crosslinker by Finkelmann *et al.* [12]

LCEss **4a** and **4b** with 5 mol% and 10mol% crosslinker, respectively, show

characteristic stress-strain response of an LC elastomer to external force. LCE **4b** is chosen as an example to discuss mechanical properties of main-chain LCEs. This elastomer consists of a calamitic mesogenic unit *C11(MeHQ)*, a long siloxane spacer *Si8* and 10 mol% of a cyclic-siloxane crosslinker *XL*. Figure 4-7 shows the stress-strain curve of this sample at room temperature in which it behaves as a typical liquid crystalline elastomer [8]. The curve consists of three regions which have typically been observed both in side-chain polydomain LCEs[8, 13] and main-chain polydomain LCEs[7, 14] under uniaxial stress.

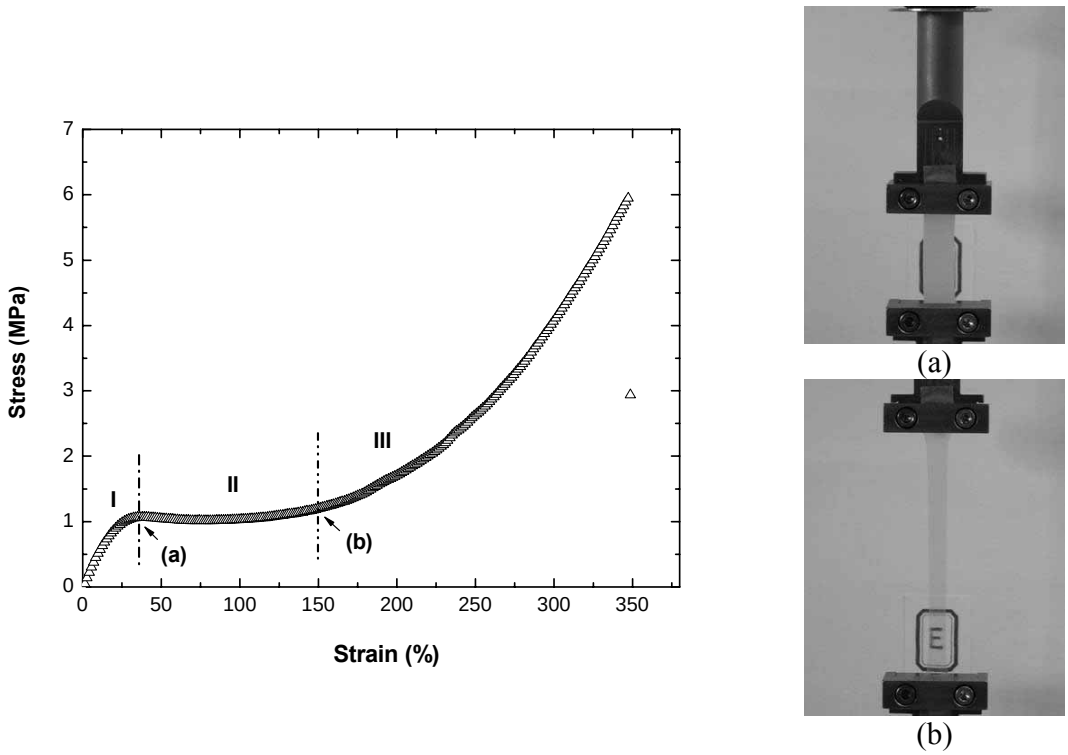

Figure 4-7 Nominal stress-strain curves of main-chain liquid crystalline elastomer **4b** C11(MeHQ)Si8XL10 at room temperature (left) and pictures of as-cast and stretched specimens (right): (a) the beginning of the stress-strain plateau; (b) the end of the stress-strain plateau.

Region I represents elastic response and covers a short range of strain. At the end of this region, the threshold stress is reached. Deformation occurring in this region can recover

completely and quickly. Individual domains are ready to rotate toward the stretching direction. Region II is a plateau, in which a mainly reversible polydomain-to-monodomain (*P-M*) transition takes place. At the beginning of the plateau, the LC elastomer is a macroscopically unoriented opaque polydomain sample, seen in Figure 4-7 (a). Mesogens in a given polydomain have a local orientation within the domain but no global orientation within the whole sample, since microscopic anisotropy of chain conformation is averaged out on the macroscopic scale. Upon stretching, the external force causes the rotation of individual domains and results in a macroscopically ordered elastomer. Since the average shape of main-chain LCEs is prolate along the local director[1], the alignment of local director along the tension direction leads to extension of the whole specimen. Therefore, a soft stress plateau is seen in the stress-strain curve over a large interval of elongation. Optically, the specimen undergoes an opaque to transparent transformation at the same time as shown in Figure 4-7, from (a) to (b). At the microscopic level, local directors reorient themselves along the stretching direction resulting in a monodomain sample. After the polydomain to monodomain transition is complete, the modulus begins to increase again and the stress-strain curve enters region III. It was found that the deformation that occurred in region II and region III cannot be recovered completely at room temperature but can be recovered by heating or by immersion in an appropriate solvent.

During the *P-M* transition, each domain with its local director in a different orientation rotates toward the extension direction in order to follow the low energy soft deformation path. However, each domain rotates from a different initial state so that the resulting shape changes could be incompatible [1]. The observed threshold stress has

been attributed to the additional mechanical energy induced by this elastic incompatibility between different domains. Theoretically, the threshold stress can be estimated as ~ μQ_{ch} with μ being the elastic modulus and Q_{ch} being the parameter of chain anisotropy [15]. Therefore, for materials with a similar elastic modulus, higher anisotropy of the network results in a higher threshold stress. This has been demonstrated by experimental reports. For instance, a main-chain LC elastomer made by Otiz *et al.* [7] has a threshold stress of 3.5 MPa. Clarke *et al.* [13] reported that their polysiloxane side-chain LC elastomer has a threshold stress of 11 KPa. A polyacrylate side-chain LC elastomer prepared by Finkelmann *et al.* [8] shows a threshold stress of 12 KPa. It is apparent that main-chain LC elastomers have a much higher threshold stress than that of side-chain LC elastomers because of their high chain anisotropy. The threshold stress of our C11(MeHQ)Si8XL10 main-chain LC elastomer is 1.2 MPa, which is of the same order of magnitude as that of Otiz's main-chain LC elastomer. Due to the soft spacer, polydimethylsiloxane which was introduced onto the C11(MeHQ)Si8XL10 polymer backbone and results in a low modulus, its threshold stress is smaller than, but comparable to, that of Otiz's material.

The width of the P-M transition plateau is also related to the anisotropy of the network. For instance, the plateau of less anisotropic side-chain LC elastomers only ranges from 20% to 30% [13]. A main-chain smectic-A elastomer can have a plateau from 10% to 100% [7]. Our C11(MeHQ)Si8XL10 is a main-chain smectic-C type elastomer. Its plateau develops from 40% to 120%. This is because main-chain LC elastomers have much higher chain anisotropy than side-chain LC elastomers.

4.3.2 Effect of Temperature

The mechanical properties of polymeric materials are known for temperature- and time-dependence due to their viscoelastic natures[5, 6]. The stress-strain behavior of C11(MeHQ)Si8XL10 LCE was measured at elevated temperatures as seen in Figure 4-8.

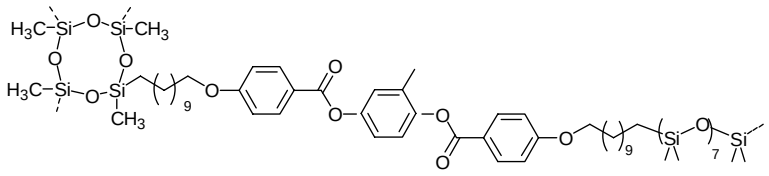

4b

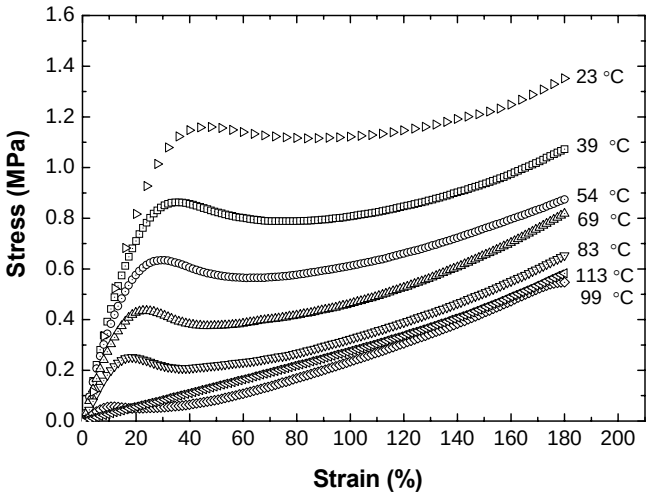

Figure 4-8 Nominal stress-strain curves of C11(MeHQ)Si8XL10 LCE ***4b*** (T_{cl} = 104 °C) at elevated temperatures .

In this series of curves, all the other curves except for the 113 ºC curve were obtained in its mesophase. At room temperature, the elastomer shows a typical three region stress-strain response to the loading. With the increase of temperature, a dramatic decrease in Young's modulus, plateau threshold stress and length of plateau were observed. Above the clearing temperature, the material behaves the same as a conventional elastomer.

Similar temperature dependence of the stress-strain response has also been observed in nematic side-chain elastomers [16-18] and smectic main-chain elastomers [7, 14].

Table 4-4 and Figure 4-9 shows Young's modulus of C11(MeHQ)Si8XL10 decreases from 5.46 MPa at room temperature to 0.33 MPa at 113 ºC.

Table 4-4 Threshold stress and Young's modulus of C11(MeHQ)Si8 at elevated temperatures

Temperature (ºC)	23	39	54	69	83	99	113
Young's modulus (MPa)	5.46	4.87	4.52	3.63	2.43	0.84	0.33
Threshold stress (MPa)	1.16	0.86	0.63	0.43	0.25	0.06	-

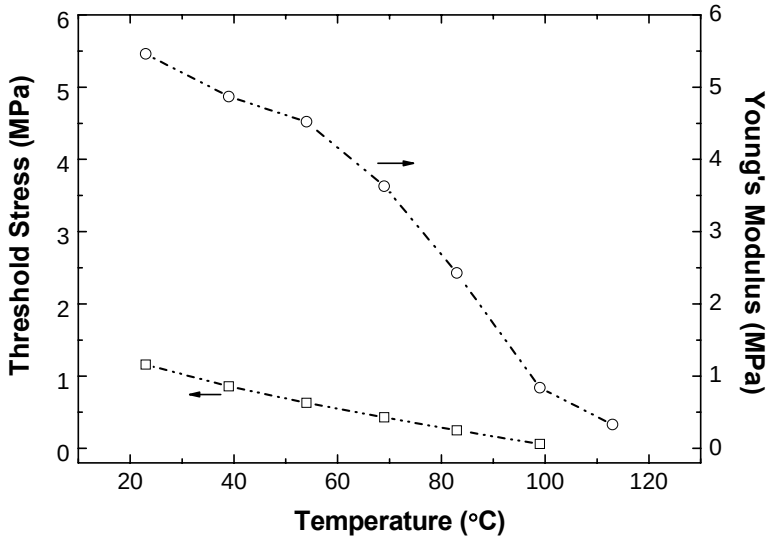

Figure 4-9 Dependence of threshold stress (□) and Young's modulus (○) of C11(MeHQ)Si8XL10 on the temperature.

Meanwhile, an almost linear decrease occurs in the threshold stress from 1.2 MPa at room temperature to 0.06 MPa at 99 °C (the on-set of mesophase to isotropic phase transition). For LC elastomers, the anisotropic network becomes more disordered with temperature until it eventually becomes isotropic above its clearing temperature. The chain anisotropy decreases drastically during this process. The decrease in the threshold

stress with temperature demonstrates its dependence on the chain anisotropy. Similar observations were also reported in some SCLC elastomers[16, 17, 19] and MCLC elastomers[7, 14] previously.It is apparent that the length of the *P-M* transition plateau narrows with temperature as shown in Figure 4-8. The chain anisotropy is thought to contribute to this behavior. The clearing temperature of C11(MeHQ)Si8XL10 is around 104 ºC. At room temperature (~ 23ºC), the polymer chain is highly anisotropic. At the same strain rate, it takes longer time to finish the rotation of all individual domains with higher chain anisotropy along the stretching direction. Therefore, it has the longest plateau region. With the increase of temperature, from 39 ºC to 99 ºC, the polymer chains become more and more isotropic, so that the plateau becomes shorter and shorter. At 113 ºC, well above its clearing temperature, the material shows stress-strain response like a conventional rubber since it is in an isotropic state at this temperature.

4.3.3 Effect of Strain Rate

The dependence of mechanical behavior on time can be experimentally evaluated by varying the strain rate. The strain rate is related to the relaxation time of the chain during the extension. When the strain rate is lower, the chains have longer time to relax before the next extension step. The ideal case occurs when the chains have long enough time to completely relax between each extension step. This state represents a thermodynamic equilibrium, in which no stress plateau will show on the stress-strain curve. However, it is difficult to reach an equilibrium state in a real experiment [18, 20] due to the slow relaxation process of the polymer chains.

The dependence of stress-strain response of LCEs on strain rate was investigated at room temperature ($T_g < T < T_{cl}$) by varying the strain rate from 5×10^{-2} s^{-1} to 5×10^{-4} s^{-1}.

Figure 4-10 gives the stress-strain curves at various strain rates for both C11(MeHQ)Si8XL10 and C11(MeHQ)Si3XL10, respectively. The difference in these two elastomers lies in the length of the siloxane spacer.

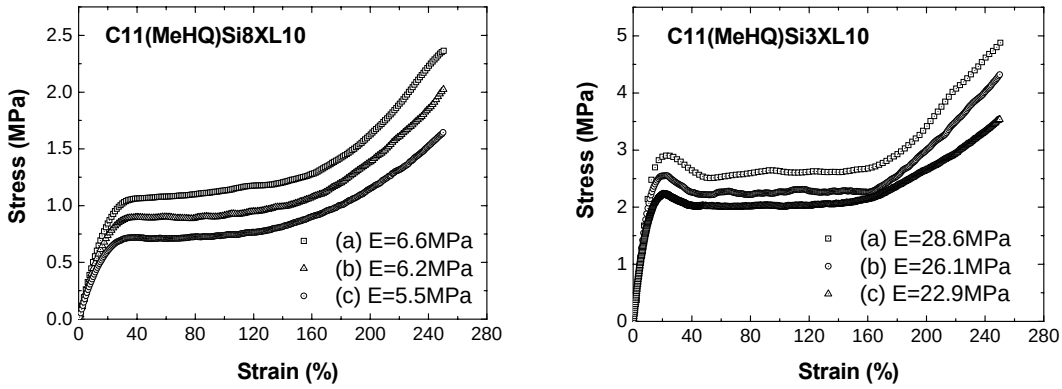

Figure 4-10 Nominal stress-strain curves of C11(MeHQ)Si8XL10 and C11(MeHQ)Si3XL10 at different strain rates: (a) 5×10^{-2} s^{-1}; (b) 5×10^{-3} s^{-1}; (c) 5×10^{-4} s^{-1}.

Both elastomers show the characteristic three regions in their stress-strain curves at all strain rates. The stress response at small strain region (< 1%) has less dependence on strain rate, but becomes more dependent on strain rate at higher strain. It is apparent that both materials show lower Young's modulus, lower threshold stress to the *P-M* transition and a flatter plateau region at lower strain rate compared with that at higher strain rate.

4.3.4 Effect of Spacer

The flexible siloxane spacer not only extends the polymer main chain but also effectively decreases the glass transition temperature of the materials [21, 22]. In this work, three siloxane spacers, polydimethylsiloxane (Si8), 1,1,3,3,5,5-hexamethyl-trisiloxane (Si3) and 1,4-bis(dimethylsilyl)benzene (Siph) were varied in a LC elastomer

with the same C11(MeHQ) mesogenic monomer and 10 mol% crosslinker to investigate the effect of spacer on LCE mechanical properties.

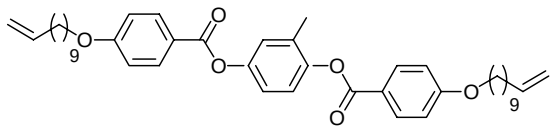

2c - C11(MeHQ)

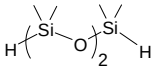

1,1,3,3,5,5-hexamethyl-trisiloxane

Si3

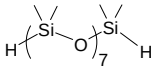

polydimethylsiloxane (DP=8)

Si8

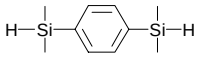

1,4-bis(dimethylsilyl)benzene

Siph

Room temperature stress-strain curves of these three LCEs were plotted in Figure 4-11. It was found that, compared with the longer spacer **Si8**, the relatively shorter spacers **Si3** and **Siph** give the elastomers a higher Young's modulus. DSC analysis shows that the glass transition temperature of LCE with **Si8** is around -23°C, while **Si3** and **Siph** give the glass transition temperature at -6°C and 13°C, respectively.

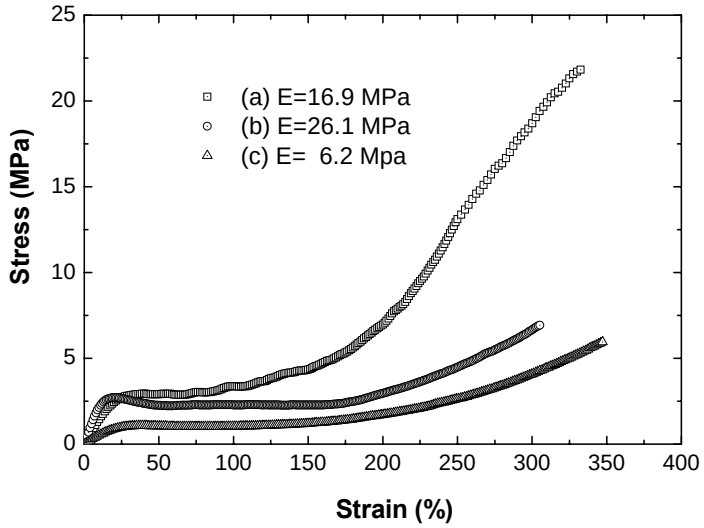

Figure 4-11 Nominal stress-strain curves at room temperature of (a) ***4j*** - C11(MeHQ)SiPhXL10; (b) ***4f*** - C11(MeHQ)Si3XL10; (c) ***4b*** - C11(MeHQ)Si8XL10.

The temperature difference between the glass transition temperature and room temperature is a determinant of the ability of a material to resist deformation under external force at room temperature. Because the LCE with **Si8** has a glass transition temperature far below room temperature, it is the softest material among these three LCEs. These stress-strain curves also show that C11(MeHQ)**SiPh**XL10 has a shorter P-M transition plateau compared with C11(MeHQ)**Si3**XL10 and C11(MeHQ)**Si8**XL10. All of the LCEs can be extended to more than three times of their original length. But C11(MeHQ)**SiPh**XL10 breaks at a much higher stress (~22 MPa) than C11(MeHQ)**Si3**XL10 (~7 MPa) and C11(MeHQ)**SiPh**XL10 (~ 6 MPa).

4.3.5 Effect of Hydrocarbon Spacer

During the process of making LCE films with siloxane spacers **Si3** and **Si8** and 10 mol% crosslinker, it was found that the length of the hydrocarbon spacer (the terminal hydrocarbon chains on mesogenic monomer) greatly affects the integrity of as-cast films.

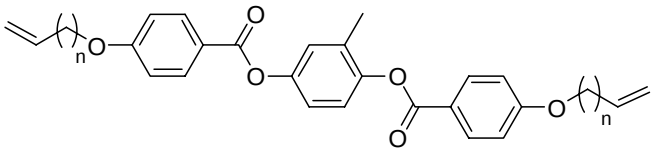

C3(MeHQ): n = 1
C5(MeHQ): n = 3
C11(MeHQ): n= 9

The mesogens with four and five methylene units were reported previously [12, 21]. Incorporating the mesogenic monomer with three methylene repeat units as terminal chains and with long spacer **Si8** always results in a tacky **C3**(MeHQ)Si8XL10 product. It is known that a highly ordered smectic LC polymer is less tacky (more rigid) that its non-LCP counterpart [23]. The LC monomer with five methylene repeat units, **C5**(MeHQ)Si8XL10, forms a non-sticky, free standing and integral film. The LCE film,

C11(MeHQ)Si8XL10, is always smooth and integral. As-cast **C3**(MeHQ)Si3XL10 is less tacky than **C3**(MeHQ)Si8XL10 but gets tacky gradually with time. **C5**(MeHQ)Si3XL10 and **C11**(MeHQ)Si3XL10 both form smooth and integral films. LC elastomers with long carbon spacer and short siloxane spacer tend to form a smooth and flexible film. The stress-strain curves of four of these four materials are plotted together in Figure 4-12.

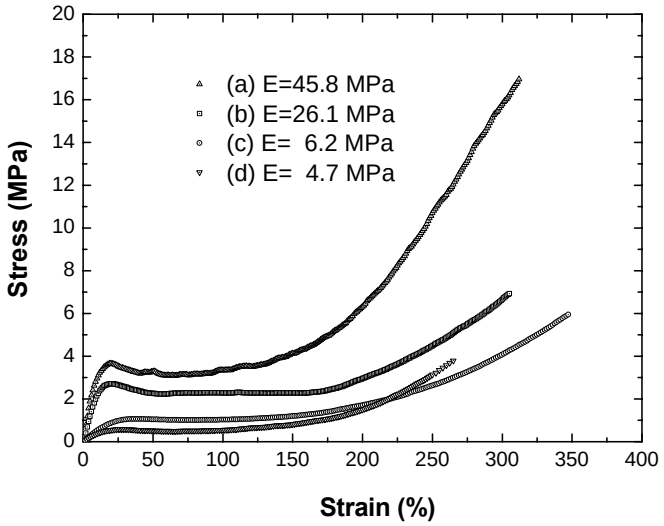

Figure 4-12 Nominal **s**tress-strain curves at room temperature of (a)C5(MeHQ)Si3XL10; (b)C11(MeHQ)Si3XL10; (c) C11(MeHQ)Si8XL10 (d) C5(MeHQ)Si8XL10.

It was found that, no matter the length of terminal chain of the mesogenic units, LC elastomers with shorter spacer **Si3** always have higher stress response than those with longer spacer **Si8** when undergoing uniaxial extension. However, the effect of terminal chain length on the stress-strain behavior of LC elastomers with **Si3** spacer is different from those with **Si8** spacer. **C5**(MeHQ)Si3XL10 has higher Young's modulus, higher yield stress, higher tensile strength but shorter P-M transition plateau than does

C11(MeHQ)Si3XL10. When **Si8** was used as spacer, an opposite effect was found by changing the length of terminal chain, although the difference is not great. In general, **C5**(MeHQ)Si8XL10 exhibits lower Young's modulus, threshold stress to *P-M* transition, elongation at break and tensile strength than **C11**(MeHQ)Si8XL10. Since the strain at the end of the stress plateau is directly related to the shape anisotropy of the polymer chain [20], the longer hydrocarbon spacer (C11) and the longer siloxane group (Si8) have greater chain anisotropy in these four LCEs.

4.3.6 Effect of Lateral Substituent on Mesogenic Unit

It is well known that chemical modification of lateral substituents can greatly change the phase behavior of low molar mass liquid crystals[24] and liquid crystalline polymers[25]. It was of interest to investigate how significant the effect will be on LCEs if we modify the lateral substituents on the LC monomer. Therefore, we synthesized another two LCEs, ***4k*** - C11(**4H**)Si8XL10 and ***4l***-C11(**4F**)Si8XL10 in addition to LCE ***4b***-C11(MeHQ)Si8XL10. In C11(**4H**)Si8XL10, the central benzene ring has no substituents only hydrogens. In C11(**4F**)Si8XL10, all the hydrogen atoms on the central benzene ring are substituted by fluorine atoms.

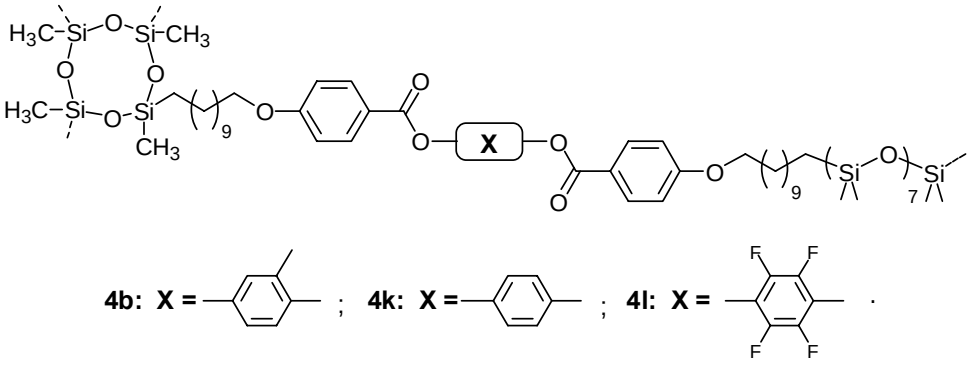

The lateral substituent methyl group in the C11(MeHQ) mesogen makes the molecule less symmetrical, which results in poor crystal packing. The symmetrical structure of C11(4H) and C11(4F) mesogens tend to induce more ordered packing in the network than C11(MeHQ). The more ordered structure is also consistent with DSC analysis in which the glass transition of C11(4H)Si8XL10 and C11(4F)Si8XL10 is almost undetectable. However, the glass transition temperature of C11(MeHQ)Si8XL10 is clearly shown in the DSC trace at about -25 ºC (from 2nd heating cycle). The assumption is that the 4H and 4F elastomers have little unorganized regions and therefore no T_g is observed.

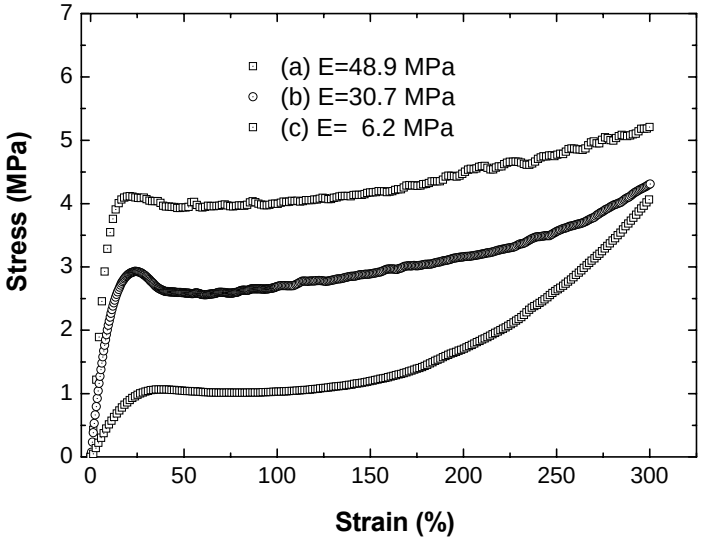

Figure 4-13 Nominal **s**tress-strain curves at room temperature of (a) ***4l*** - C11(4F)Si8XL10; (b) ***4k*** - C11(4H)Si8XL10; (c) ***4h*** - C11(MeHQ)Si8XL10.

In Figure 4-13, C11(MeHQ)Si8XL10 shows the lowest stress response to the external force among these three elastomers. C11(MeHQ)Si8XL10 has a Young's modulus of ~6 MPa. The Young's moduli of C11(4F)Si8XL10 and C11(4H)Si8XL10

are ~50 MPa and ~30 MPa, respectively. Different from C11(MeHQ)Si8XL10, both C11(4H)Si8XL10 and C11(4F)Si8XL10 exhibit an observable yield point, which is similar to the typical phenomenon for semicrystalline polymers [5, 6, 26]. After the yield point, their nominal stress drops and then climbs up gradually with strain. Visually, necking was clearly observed in C11(4H)Si8XL10 and C11(4F)Si8XL10 at the yield points. No apparent necking but rather a narrowing in width could be observed in C11(MeHQ)Si8XL10. The steric effect and polarizability of lateral substituents on the mesogen are considered to explain differences in mechanical behaviors of these elastomers. For C11(MeHQ)Si8XL10, the steric effect of the lateral methyl group on the central benzene ring results in a less efficient lamellar packing structure. No crystalline structure but a liquid crystalline structure could form in this elastomer. However, C11(4F)Si8XL10 and C11(4H)Si8XL10 contain mesogens with symmetrical structures. It is relatively easier for them to pack more orderly than C11(MeHQ)Si8XL10. The secondary interactions between neighboring mesogens are more effective in these two LCEs than that in C11(MeHQ)Si8XL10. X-ray scattering measurement detected π-π stacking in both C11(4H)Si8XL10 and C11(4F)Si8XL10. For C11(4F)Si8XL10, although the steric effect of fluoro substituents could disrupt the lamellar packing, the stronger polarity of fluoro substituents enhances the lamellar packing.

4.3.7 Effect of Non-mesogenic Rigid Unit with Special Molecular Architecture

For all the LC elastomers discussed so far, their rigid segments are always terminally extended first by a hydrocarbon chain and then by a more flexible siloxane chain. In this section, we will introduce terphenyl transverse rods (**TR3**) with a specially designed architecture into main-chain LC elastomers and discuss their effect on the

thermal properties, mesophase and mechanical properties.

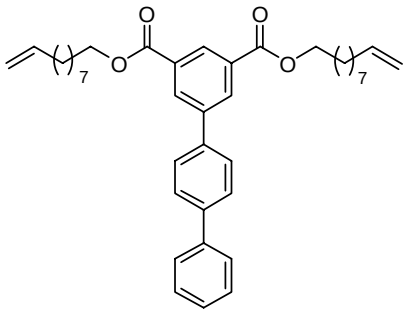

TR3

The possibility of incorporating this material into the parent system for examination of these as potential auxetic materials based on site-connectivity driven transverse rod reorientation mechanism was also investigated. The rods involved in this study are isophthalate-based terphenyl transverse rods with flexible arms containing ten methylene units. LC elastomers ***4p-4s*** were synthesized through copolymerization of monomer C11(MeHQ) LC with **TR3** by varying the ratio between them.

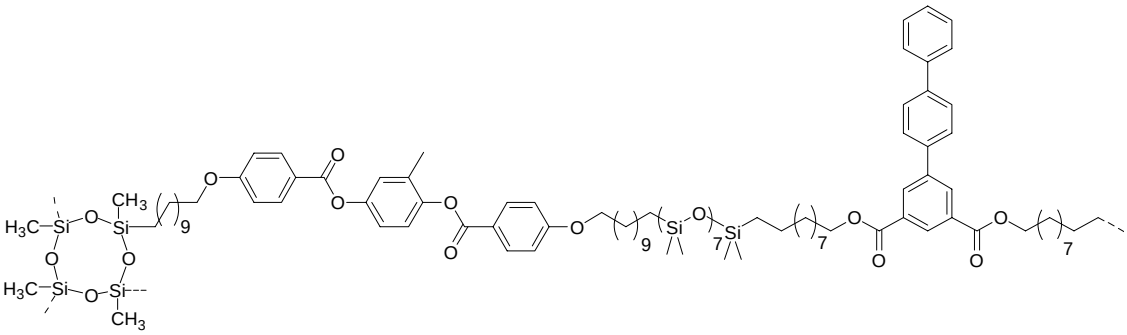

4p - 4s

The LC elastomer with 10 mol% crosslinker was selected as the parent elastomer to investigate if auxetic behavior could be found in this system. There are two reasons for choosing the C11(MeHQ)Si8XL10 system for this investigation. First of all, 10 mol% crosslinker is the optimum crosslinker content for the system to have a stable liquid crystal phase and mechanical robustness of the film. Of course, less crosslinker

content could give excellent liquid crystal order, but the intengity of the elastomer film is reduced at the same time. Secondly, the elastomer with 10 mol% crosslinker shows a typical liquid crystalline elastomer stress-strain response. The wide plateau region covers about 100% strain. In that region, the macroscopically disordered mesogens reorient themselves along the stretching direction. In order to achieve an auxetic effect based on the mechanism of site-connectivity driven transverse rod rotation, a pre-alignment of transverse rods with mesogens along the stretching direction is necessary. This is expected to be realized in the wide plateau region together with the reorientation of mesogens. After the pre-alignment, transverse rods are expected to rotate to the chain normal and push the neighboring chain away under further extension.

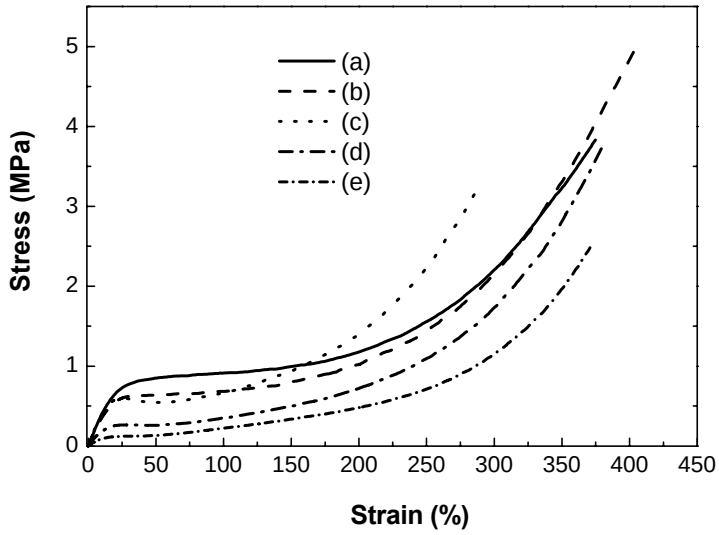

Figure 4-14 Effect of terphenyl transverse rod (TR3) on the mechanical properties of C11(MeHQ)Si8XL10 Elastomers ***4p-4s*** with various TR3 amount: (a) 0 mol%; (b) 10 mol%; (c) 20 mol%; (d) 30 mol%; (e) 40 mol%.

Figure 4-14 illustrates that the LC elastomer with 10 mol% **TR3** shows similar stress-strain response to that of the parent LC elastomer (0 mol% **TR3**). LC elastomers

with 30 mol% **TR3** and 40 mol% **TR3** behave much like ordinary elastomers with low Young's modulus and a very short plateau region. The LCE with 20 mol% **TR3** behaves differently from the others. It has a similar linear region to the parent LCE and LCE with 10 mol% **TR3**. However, after the linear region, it shows an observable yield point first and then enters a short plateau region. After that, the stress increases rapidly and then failure follows at a relatively lower elongation (< 300%). It was thought 20 mol% **TR3** loading might be a critical point for the auxetic effect. Below 20 mol% **TR3** loading, the number of transverse rods might be too low and the rotation of transverse rods to the chain normal might be surpressed. Above 20 mol% **TR3** loading, liquid crystalline order might not be retained properly (consistent with DSC analysis) so that it is difficult to obtain a good pre-alignment of transverse rods along the polymer backbone.

4.4 Strain Recovery of Polydomain MCLC Elastomers

The deformation of amorphous polymers in the glassy state is commonly distinguished into elastic, anelastic and plastic [27-32] deformations. Anelastic and plastic deformation together are called nonelastic deformation. Nonelastic deformation also has been investigated in semi-crystalline polymers [33-37]. Some researchers studying semi-crystalline polymers prefer "nonelastic reversible and nonelastic irreversible deformation" to "anelastic and plastic deformation" in order to avoid any confusion [34]. In this discussion, we use the short terms - "anelastic and plastic deformation" - for convenience. A strain recovery test is normally used to study these deformations. For amorphous materials, the elastic deformation of a sample recovers instantaneously after unloading. It takes a longer (often a very long time) to recover anelastic. However, this anelastic strain recovery process can be accelerated by

increasing temperature. It has been reported that the anelastic deformation can be erased by heating the material close to a temperature about 20 °C below its glass transition temperature [33]. For semi-crystalline polymers being deformed in a glassy state, anelastic deformation can be reversed by heating the material above its glass transition temperature and below the onset of melting. Plastic deformation cannot be removed even by heating very close to the onset of crystal melting [34]. A fast-relaxing component and a slow-relaxing component were also used to describe the kinetics of elastic and anelastic, respectively [33]. There are few literature reports discussing shape recovery phenomena in liquid crystalline elastomers [7, 14, 38, 39].

We are interested in the shape recovery phenomenon because it reflects the strain retention capability of the synthesized LC elastomers as shape memory materials. Therefore, we performed a series of shape recovery experiments by considering the influences coming from the length of hydrocarbon spacer, the lateral substituent on mesogenic core, flexibility of siloxane spacer and crosslinking density.

4.4.1 Typical Strain Recovery Behavior of LC Elastomers

All the specimens involved with the shape recovery experiments have a glass transition temperature below room temperature and a clearing temperature much higher than room temperature. Therefore, when the experiments were carried out at room temperature, all the materials were deformed in their mesophase. They are all soft and extendable. In this section, we choose C11(MeHQ)Si8XL10 LC elastomer as an example to describe the typical shape recovery phenomenon observed in our LCEs. C11(MeHQ)Si8XL10 has a glass transition temperature of -25 °C and a clearing temperature of 104 °C. X-ray analysis showed the LCE is in a smectic C phase at room

temperature.

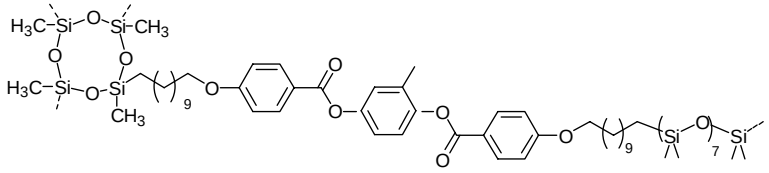

4b

4.1.1.1 Strain Recovery Behavior of C11(MeHQ)Si8XL10 LCE

In the room temperature strain recovery experiment, seven rectangular polydomain C11(MeHQ)Si8XL10 specimens were stretched to different strain levels ranging from 0.5 to 3.5. After reaching the target extension, the specimen was quickly removed from the clamps and placed flat on a smooth surface. The instantaneous length (L) of each sample was measured under zero loads over a wide time window (> 1200 minutes). The residual strains of these specimens were plotted as a function of time in Figure 4-15.

It was found that strain retention is a function of the initial strain (ε_0) - the larger the initial strain, the greater the final strain retention. The recovery behavior of each specimen, no matter with high or low initial strain, shows a fast decay followed by a plateau. Figure 4-15 (b) indicates that the majority of the strain recovery occurs within one minute. After that, the decay slows down quickly. From strain recovery experiments, we observed that only the specimen with an initial strain of 0.5 or 50% can recover to its original length completely under the experimental condition. From the stress-strain curve, it is known that 50% strain is at the very beginning of the polydomain to monodomain transition. Polydomain structure is still dominant in the specimen. However, for the rest of the deformed specimens, more and more monodomain structure forms within the specimen upon stretching.

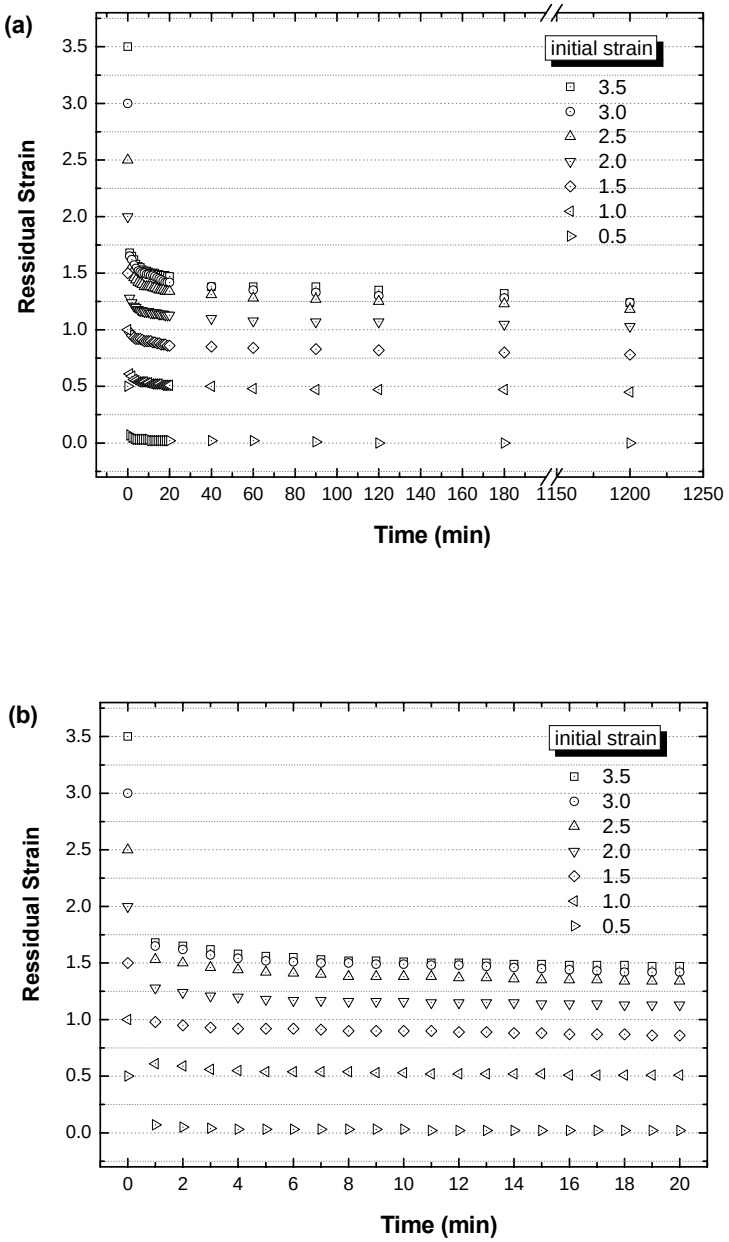

Figure 4-15 Room temperature strain recovery of C11(MeHQ)Si8XL10 films under zero loads after being deformed to various strain level: (a) 0-1200 minutes; (b) 0-20 minutes.

None of these specimens can recover to their original dimension at room temperature by itself, which indicates that the monodomain component plays an important role in "freezing" the deformation. The deformation locked by monodomain structure cannot be

fully recovered directly at room temperature. Under these conditions, the monodomain is a temporally stable state for the elastomers. It should be remembered that these elastomers were not crosslinked in a monodomain. This experiment indicates that the degree of macroscopic orientation of domains with their interdomain barrier walls greatly affects the strain recovery behavior of LC elastomers [20]. These barrier heights are easily accessible at temperatures near the clearing temperature of the LCE, but are not accessible at temperatures far below the clearing temperature. Therefore, in the LC phase at temperatures near the clearing temperature, the material is fully elastic. While far below the clearing temperature, anelastic behavior is seen results in slow recovery to the original polydomain state. The deformed domains cannot recover their original dimensions at low temperatures. Monodomain and polydomain structures act oppositely during the shape recovery process. The former restricts the strain recovery but the latter allows it.

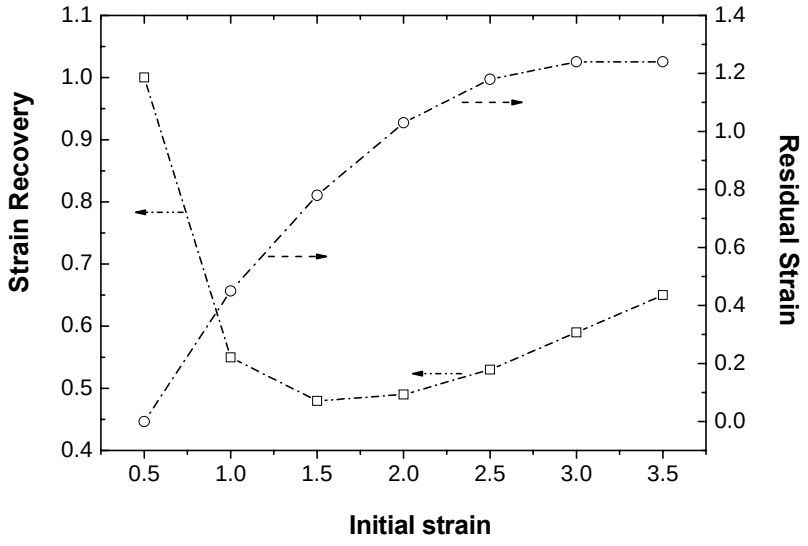

Figure 4-16 Residual strain and strain recovery of C11(MeHQ)Si8XL10 as a function of initial strains.

Another interesting observation is that the retained strain is not proportional to the initial strain. In Figure 4-15, it is apparent that the difference in residual strain between neighboring points gradually decreases with the same increment of initial strain. This non-linear relationship between the residual strain and the initial strain is clearly presented in Figure 4-16. In addition, the strain recovery (defined by equation 4-11) of this material experienced a decrease then an increase upon increasing the initial strain. The strain recovery is defined by equation 4-11.

$$\text{Strain recovery} = \frac{\varepsilon_0 - \varepsilon_{residual}}{\varepsilon_0} = 1 - \frac{\varepsilon_{residual}}{\varepsilon_0} \tag{4-11}$$

The specimen with 50% and 150% initial strain exhibit the highest and lowest strain recovery, respectively. The 50% initial strain point is located at the beginning of the *P-M* transition. A polydomain structure dominates in this material. Deformation cannot be retained by polydomain structure. Between 50% and 150% initial strains, the polydomain structure is transformed into a monodomain which increases the material's ability to retain deformation. The increase in residual strain was more pronounced than that in the initial strain. Therefore, strain recovery decreased gradually with the development of the *P-M* transition (with increase in strains). The stress-strain curve of this material showed that *P-M* transition is almost complete at 150% strain. After the *P-M* transition, further stretching brings the monodomain structure to a greater perfection but did not give as much change as that during the P-M transition. Further stretching likely contributed to extension of flexible hydrocarbon spacers and siloxane spacers instead of the reorientation of individual domains. Since the increase in residual strain is slower than that in initial strain after *P-M* transition, the strain recovery of the material

begins to increase again after 150% strain in Figure 4-16.

Very few strain recovery studies of MCLCEs had been reported. Ortiz's epoxide-based MCLCEs showed 17% strain recovery after being given 290% strain [7]. Carfagna *et al.* reported 33% and 65% strain recovery in their epoxide-based MCLCEs with 180% and 300% initial strain, respectively [14]. Mather et al. claimed about 17% strain recovery of their siloxane-based MCLCE with about 180% initial strain [39]. All those strain recovery experiments including ours were done under somewhat different experimental conditions from each other. Among these researchers, Mather first proposed that the smectic C structure was attributed to the temporary shape retention [39].

4.1.1.2 Effect of Strain Rate on Strain Recovery of C11(MeHQ)Si8XL10 LCE

Tensile testing of C11(MeHQ)Si8XL10 showed that the strain rate affects its stress-strain behavior as illustrated in Figure 4-17.

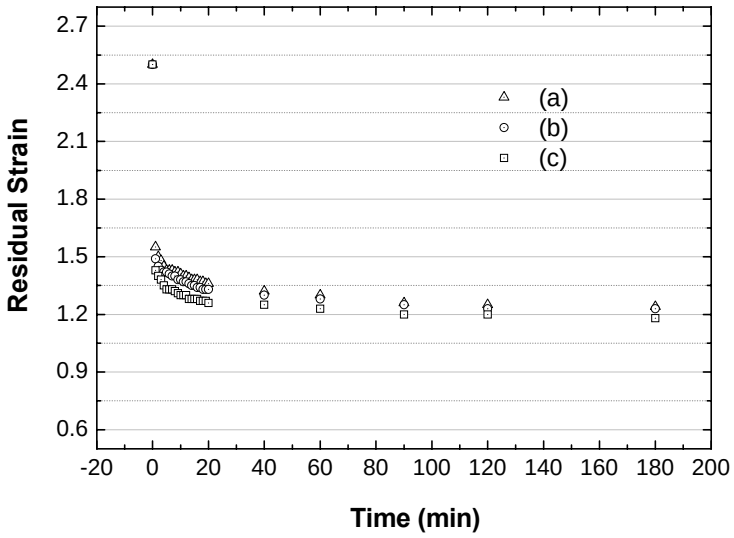

Figure 4-17 Room temperature strain recovery of C11(MeHQ)Si8XL10 with different initial strain rate: (a) 5×10^{-4} s^{-1}; (b) 5×10^{-3} s^{-1}; (c) 5×10^{-2} s^{-1}.

In the high strain region, stress-strain response showed apparent dependence on strain rate. Higher strain rate resulted in a higher value of stress at a give applied strain. The dependence of strain recovery on the strain rate was also investigated in this material. Three different strain rates, 5×10^{-4} s^{-1}, 5×10^{-3} s^{-1} and 5×10^{-2} s^{-1} were varied for the measurements. All the specimens extended to 250% strain at different strain rate relaxed to almost the same value of strain (~120%). An identical experiment on another LC elastomer with short siloxane spacer, C11(MeHQ)Si3XL10, also showed independence of strain recovery on strain rate.

4.1.1.3 Effect of Initial Strain on Thermal Properties of C11(MeHQ)Si8XL10 LCE

During the strain recovery study of C11(MeHQ)Si8XL10 LCE, it was found that strain retention after the removal of loading depended on the initial strain. The higher initial elongation results in a larger retained strain. It was thought that reorientation of LC domains fixed the residual deformation. Ortiz et. al. observed the elongation and reorientation of LC domains in their stretched MCLC elastomer under polarized optical microscope [7]. We used DSC analysis to study the monodomain structure evolution associated energy change with different initial strains. Seven C11(MeHQ)Si8XL10 LCE specimens with various initial strains were analyzed by DSC. The resulting DSC traces plus the DSC profile of unoriented C11(MeHQ)Si8XL10 as cast specimen were plotted together for comparison in Figure 4-18. Normally, the first cooling and the second heating cycle are used for analysis in order to guarantee all the specimens having the same history. The originally history (thermal, processing) of specimens can be removed by the first heating cycle. In this study, the DSC records information related to strain retention and orientation of the specimens. Therefore, DSC data of the first heating cycle

were collected. The energy released for the shape recovery can be evaluated by area of the exothermal transition peak.

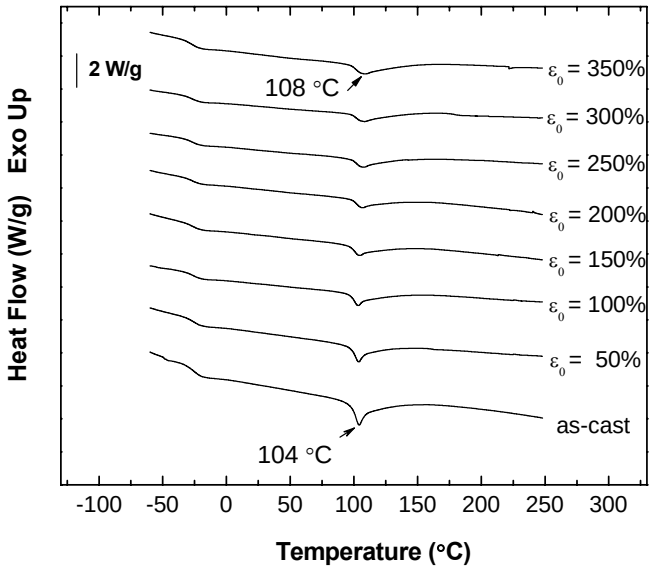

Figure 4-18 Comparison of 1st heating DSC (10 °C/min) traces of C11(MeHQ)Si8XL10 LCEs with different initial strain (from 350% to 50%) with as-cast polydomain LCE.

During the DSC scanning, a continuous upward shift in mesophase-isotropic transition temperature and a broadening in peak area with initial strain were observed. No obvious change in glass transition temperature was observed. By comparing the two extreme cases in this study, the one without any elongation and the one with the highest elongation, it was found that the specimen with 350% initial elongation had about 4 °C upward shifted in clearing temperature and the corresponding transition peak was much broaden and less sharp compared with the unstretched specimen.

This phenomenon can be explained in terms of the mesophase stability affected by the arrangement of polymer chains. In the mesophase, the initial elongation induces the orientation of polymer chains, which stabilizes the mesophase. Polymer chains in an

isotropic phase have no preferred orientation. The energy barrier between isotropic phase and oriented mesophase is proportional to the extent of orientation, which is in turn proportional to the initial strain. It was observed that more deformation could be retained by the material with higher initial strain. Consequently, more energy must be put into the system to deform the network and the mesophase to isotropic phase transition temperature rises with increasing the initial strain. This phenomenon is analogous to phase transition temperatures increased by crosslinking a sample in the nematic phase, which was predicted by Warner theoretically [40] and observed by Davis experimentally [41]. Because the crosslinking puts more constraints into the system, additional energy is needed to change the shape of the polymer chains from the oblate or prolate form to the isotropic form (without preferred orientation). In this case, the orientation of the polymer chains plays the same role in putting additional constraints into the system. The mechanical stretching induced small increase in the phase transition temperature LC elastomer was also observed by Zentel experimentally [42].

From the thermodynamic point of view, the mesophase to isotropic transition is the first order transition, which can be expressed by the Gibbs-Helmholtz equation (4-12).

$$\Delta G_{transition} = \Delta H_{transition} - T_{transition}\Delta S_{transition} \tag{4-12}$$

When a material undergoes a first order phase transition, a thermal equilibrium state is assumed, in which $\Delta G_{transtion} = 0$. Therefore, transition temperature can be calculated by equation 4-13 [43].

$$T_{transtiion} = \frac{\Delta H_{transition}}{\Delta S_{transtion}} \tag{4-13}$$

In the experiment, we observed an increase in transition temperature with initial strain.

The elongation of specimen orients polymer chains along the stretching direction, which results in decreasing the entropy of the whole system. The higher initial strain leads to the smaller initial entropy of the system. At the phase transition temperature, polymer chains gain energy to go back to the unoriented state, which increases the entropy of the system. Eventually, at the phase transition temperature, the system having the largest initial strain or the lowest entropy experiences the largest entropy change. Since we observed the increase in transition temperature with increase in initial strains experimentally, the increase in absolute value of enthalpy change should be greater than that in entropy change. However, the broadened peak and baseline shift make it difficult to calculate $\Delta H_{transition}$ (peak area) accurately.

4.1.1.4 Effect of Initial Strains on the Stress-strain Behavior of Relaxed C11(MeHQ)Si8XL10 LCE

According to DSC studies, it is known that the initial strain affects the thermal properties of C11(MeHQ)Si8XL10 by increasing the mesophase to isotropic transition temperature. It was interesting to find that the initial elongation also has a significant influence on subsequent mechanical properties. A further tensile test was given to a group of relaxed C11(MeHQ)Si8XL10 specimens (after strain recovery) with different initial strains as shown in Figure 4-19. The initial strain has a great effect on the mechanical properties of C11(MeHQ)Si8XL10 LC elastomer. It was found that, in general, larger initial strain leads to a higher Young's modulus, a shorter plateau region, a lower elongation at break, and a larger tensile strength.

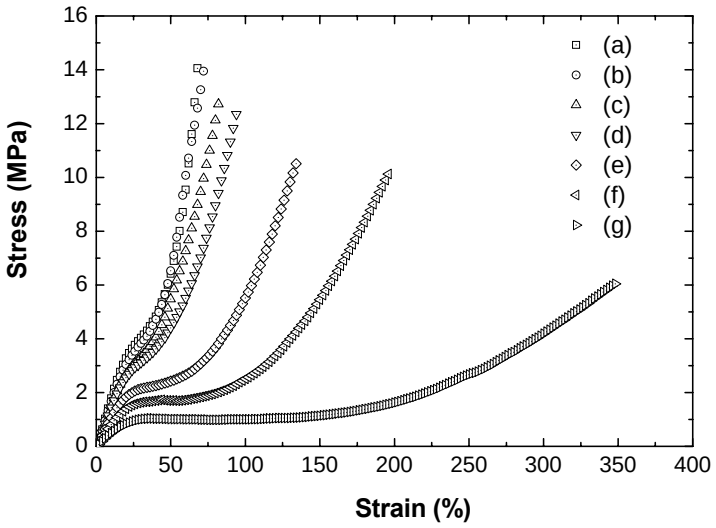

Figure 4-19 Stress-strain curves of relaxed C11(MeHQ)Si8XL10 LC elastomers with various initial strains: (a) 350%; (b) 300%; (c) 250%; (d) 200%; (e) 150%; (f) 100%; (g) 50%.

The changes in Young's modulus of C11(MeHQ)Si8XL10 LCE with increase of initial elongation were shown in Figure 4-20.

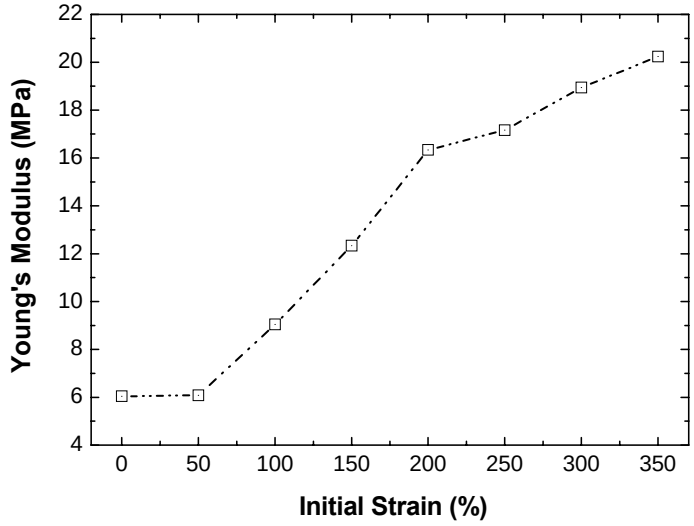

Figure 4-20 Young's modulus of C11(MeHQ)Si8XL10 as a function of initial elongation after relaxation.

Young's modulus of the material increases with initial strains but their relation is not linear. The Young's modulus of the specimens dominated by a polydomain state (with 50%, 100% and 150% initial elongation) increases slowly. After that point, a fast increase in Young's modulus of specimens with 200% initial elongation (more monodomain structure than polydomain structure) was found. After the initial strain reaches 250%, Young's modulus keeps increasing but at a slower pacer. There is another fast increase in Young's modulus shows in the specimen with 300% initial strain, which was thought to be related with the occurrence of strain-hardening in this sample upon stretching.

Among all the specimens, the specimen (g) with 50% initial strain exhibits the longest *P-M* transition plateau region on its stress-strain curve. In fact, this specimen behaves the same as the unstrained as-cast specimen because its initial 50% strain was not retained but returned completely to its original dimensions after the removal of the loading. For the specimen (a) with 350% initial strain, its stress-strain curve has an inflextion but no plateau region. This indicates that the monodomain state dominates in this pre-strained specimen. Furthermore, its stress goes up rapidly until the specimen fails at a relatively small elongation (~70%). Among these specimens, only three (e, f, and g with 150%, 100%, and 50% initial elongation, respectively) show an obvious plateau region. By comparing their retained strains with the stress-strain curve of an unstrained as-cast specimen (Figure 4-7, page 12), these specimens have residual strains comparable to the very beginning of the plateau, the linear elastic region, and the original position, respectively. Polydomain states are likely sifnificant in these specimens. Therefore, a polydomain to monodomain transition can still be optically observed by further stretching

these specimens. For specimens with 200%, 250%, 300% and 350% initial strain, their residual strains are comparable to points half way into the plateau region, at the end of plateau region and out of the plateau (strain hardening region), respectively. Monodomain structures gradually become dominant in these specimens with increasing initial strain. WAXD was performed on these pre-strained C11(MeHQ)Si8XL10 LCEs with different initial strains as shown in Figure 4-21. From WAXD, the LCE with 50% initial strain shows eccentially the same diffraction pattern as the unoriented film. With increasing the initial strain to 100%, not only is the orientation of polymer chain along the stretching direction obvious but also the orientation in the smectic mesophase can be distinguished.

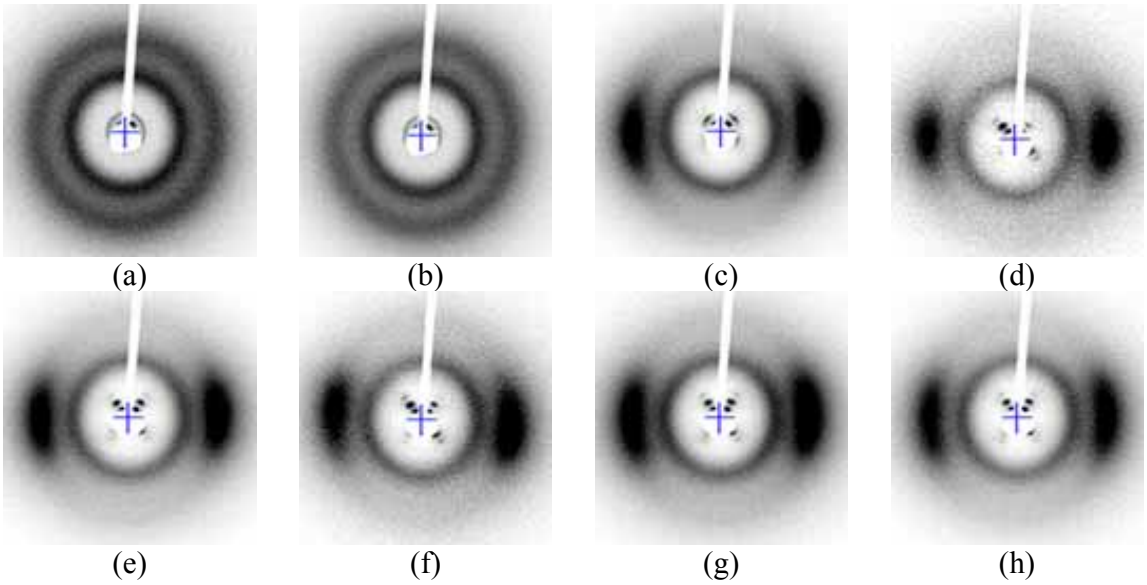

Figure 4-21 WAXD patterns of C11(MeHQ)Si8XL10 with different initial strains: (a) 0%; (b) 50%; (c) 100%; (d)150%; (e) 200%; (f)250%; (g) 300%; (h) 350%.

The higher order diffractions from the smectic layer were observed with further increasing the initial strains. There are no significant changes in the macroscopically orientation of domains. Order parameters of these LCEs were measured by azimuthal

scan of the interchain region of these patterns. Order parameter of the pre-strained specimen is plotted as a functional of initial strain in Figure 4-22.

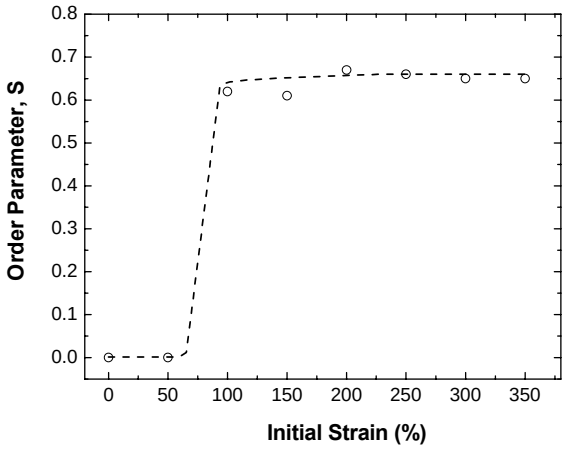

Figure 4-22 Effect of initial strain on the order parameter of C11(MeHQ)Si8XL10 LC elastomer

A "S" shape order parameter versus strain curve was obtained, which is analogous to the typical order parameter versus stress curve of LC elastomers [7, 13, 15]. It was found that there is an abrupt increase in order parameter when the material undergoes a strain between 50% and 100%. After that, further elongation can not significantly increase the order parameter further. The samples **c** - **h** can, even with no loading after the initial extension, retain orientational ordering through a locking in of the strain-induced monodomain structure.

4.1.1.5 Strain Recovery of C11(MeHQ)Si8XL10 LCE at Elevated Temperatures

The strain recovery in our LCEs at room temperature has been intensively studied. The effect of temperature on the strain recovery will be discussed in this section. It was found that temperature accelerates the strain recovery process as shown in Figure 4-23. The strain the material can retain after unloading is related to the difference between

recovery temperature and the clearing temperature. When the deformed material is at a temperature much lower than the clearing temperature of the sample, deformation cannot be recovered quickly.

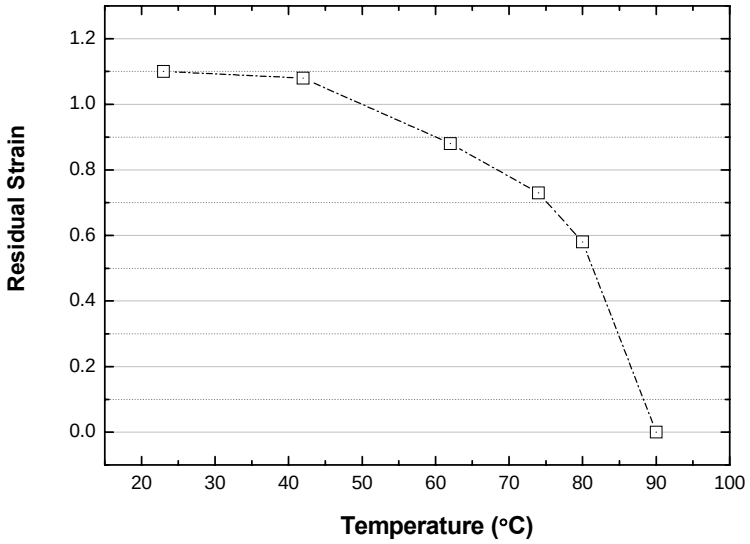

Figure 4-23 The residual strain of C11(MeHQ)Si8XL10 with 250% initial strain as a function of temperature.

With an increase of temperature, the sample begins to show observable shrinkage. When the temperature approaches the clearing temperature, strain recovery becomes faster. When the temperature reaches to the on-set temperature (90 °C) of the mesophase to isotropic phase transition (peak maximum at 104 °C), full shape recovery was observed. It is not necessary to heat a LC elastomer above its clearing temperature to achieve a full shape recovery. At 90 °C, C11(MeHQ)Si8XL10 has sufficient thermal energy to overcome the energy barrier between the monodomain and polydomain states and it recovered to its original dimension completely. This is similar to the thermomechanically activated nature of strain recovery found in fully amorphous glassy

polymers and other semicrystalline polymers [33, 34, 44].

The shape of a deformed C11(MeHQ)Si8XL10 can also be recovered by using an appropriate solvent (such as acetone) as shown in Figure 4-24 .

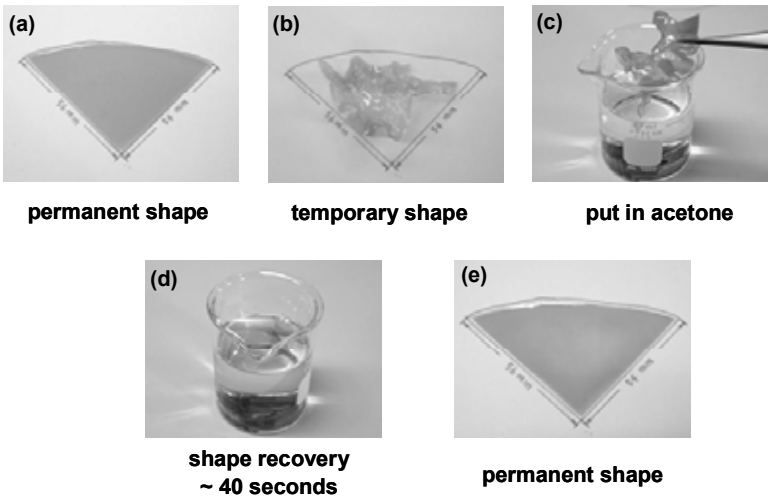

Figure 4-24 Solvent induced shape recovery process of C11(MeHQ)Si8XL10**.**

In this experiment, a polydomain C11(MeHQ) film (a) was randomly deformed into a temporary shape (b). The deformed film (b) was immersed in acetone (c). After staying in acetone for about 40 seconds, the film (d) recovered its original shape but swelled with acetone. The swollen film recovered to its permanent shape (e) after the solvent evaporated completely. The shape retention of C11(MeHQ)Si8XL10 was attributed to the monodomain organization formed during deformation. At room temperature, the monodomain to polydomain transition energy barrier can not be easily overcome, very slow kinetics. So, the temporary shape was essentially fixed. The small solvent molecules can enter network easily and act as plasticizers. The monodomain to polydomain barrier was reduced by the plasticizing effect from the solvent. Therefore, the polymer chain coiled back to the original polydomain state in solvent resulting in a

complete shape recovery of the LCE film after solvent evaporation.

In general, after initial strain followed by the removal of load, the strain recovery process of our parent LCE proceeds by a fast elastic recovery followed by a slow anelastic recovery. The oriented smectic arrangement of the monodomain structure played a critical role in the strain recovery process. At room temperature, the energy barrier associated with the P-M transition can not be overcome by the elastic restoring force of the LCE. Therefore, the strain was held by the monodomain structures. The extent of strain retention depended on the stability of the monodomain structure under the experimental conditions. The strain recovery, mainly the anelastic recovery, can be accelerated by increasing the temperature above room temperature. Increasing the temperature provided the more thermal energy so that the strain retention decreased. Monodomain structures were able to be completely converted to polydomain structures when sufficient energy was provided (close to the clearing temperature). Decreasing *P-M* transition energy barrier (such as swelling the deformed LCE in an appropriate solvent) can also facilitate the recovery.

4.4.2 Effect of Crosslinker Content

Room temperature strain recovery experiments were also performed on a series of C11(MeHQ)Si8 LC elastomers with various crosslinker content. From the stress-strain behavior studies in section 4.3.1, we know that the crosslinker content has a significant effect on mechanical properties, such as Young's modulus, threshold stress or yield stress and the plateau region. However, the influence of the amount of crosslinker on the residual strain that C11(MeHQ)Si8 LC elastomers retain is not as dramatic as is shown in Figure 4-25. It was found that LC elastomers with different crosslinking density show

the similar strain retention values. For instance, LC elastomers having 150% initial strain can retain 60% - 80% strain and those having 180% initial strain can retain 70% - 90% strain.

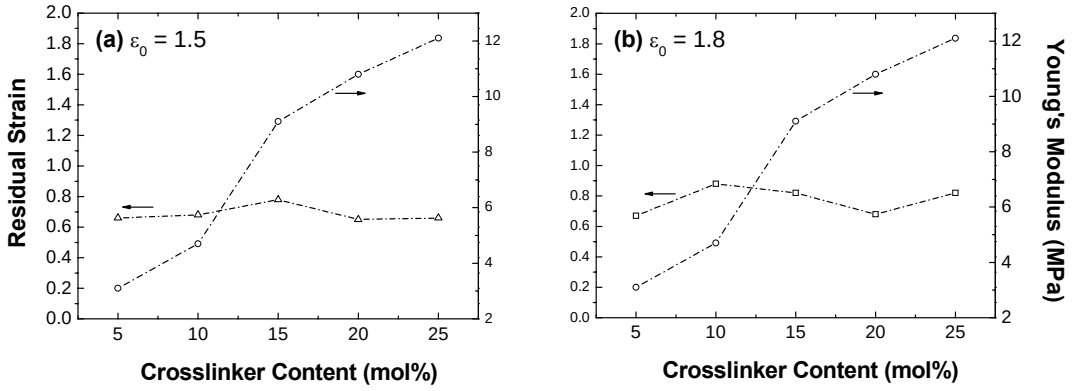

Figure 4-25 Residual strain and corresponding Young's modulus of C11(MeHQ)Si8 elastomers with various crosslinker content having (a)150% and (b) 180% initial strains.

This indicates that the extent of crosslinking point does not play an important role in shape fixing of the LC elastomers. The molecular mechanism of shape retention is likely different from that responsible for more typical mechanical properties, like the Young's modulus.

4.4.3 Effect of Siloxane Spacer

In this section, the shape recovery experiment was carried out with C11(MeHQ)XL10 elastomers with three different siloxane spacers as follows.

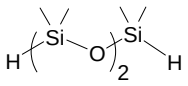

1,1,3,3,5,5-hexamethyl-trisiloxane

Si3

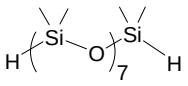

polydimethylsiloxane (DP=8)

Si8

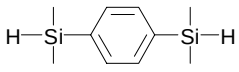

1,4-bis(dimethylsilyl)benzene

Siph

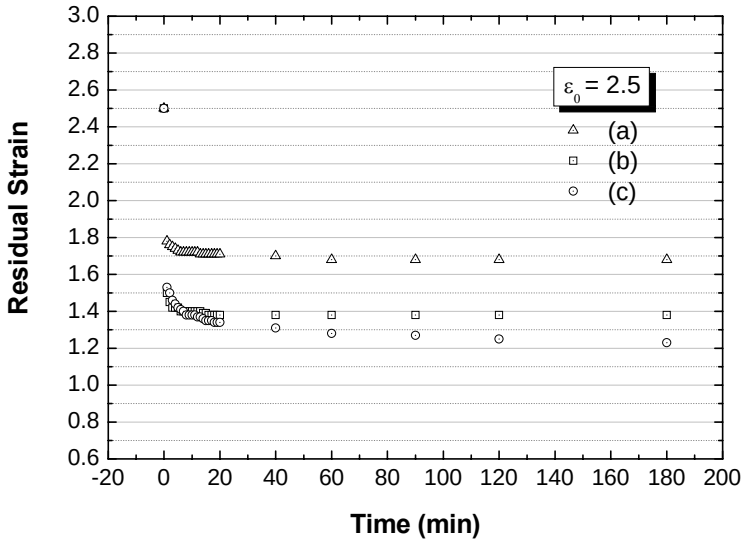

Figure 4-26 Room temperature strain recovery of C11(MeHQ)XL10 LCEs with various siloxane spacers having a 250% initial strain: (a) Si3; (b)Siph; (c) Si8.

In Figure 4-26, it is seen that C11(MeHQ)Si3XL10 has the greatest ability to retain strain at room temperature (the operating temperature), followed by C11(MeHQ)SiphXL10 and C11(MeHQ)Si8XL10. Table 4-5 compares the temperature difference (ΔT_1) between the glass transition temperature and room temperature as well as the difference between room temperature and the clearing temperature (ΔT_2) as well.

Table 4-5 Difference between transition temperature and room temperature of C11(MeHQ)XL10 with various siloxane spacers ($\varepsilon_0 = 2.5$)

	T_g (ºC)	$\Delta T_1 = r.t.^{(a)} - T_g$ (ºC)	*retained strain*	$\Delta T_2 = T_{cl} - r.t.$ (ºC)	T_{cl} (ºC)
C11(MeHQ)Si3XL10	-6	29	1.68	108	131
C11(MeHQ)SiphXL10	13	10	1.38	86	109
C11(MeHQ)Si8XL10	-23	46	1.23	81	104

(a): *r.t.* refers to room temperature (23 ºC).

The effect of spacer on ΔT_2 matches the effect on shape retention capability. The larger the value of ΔT_2 the higher value of residual strain. This indicates the relations between the clearing temperature is a better predictor of shape retention ability.

4.4.4 Effect of Terminal Hydrocarbon Chain on Mesogenic Unit

From the previous section, it is known that C11(MeHQ)Si3XL10 with a short siloxane spacer can keep higher residual strain than C11(MeHQ)Si8XL10 with a long siloxane spacer. In this section, the combined influences of hydrocarbon spacer length and siloxane spacer length will be discussed. It was found that replacing short hydrocarbon spacer **C5** with long hydrocarbon spacer **C11** always results in greater strain retention.

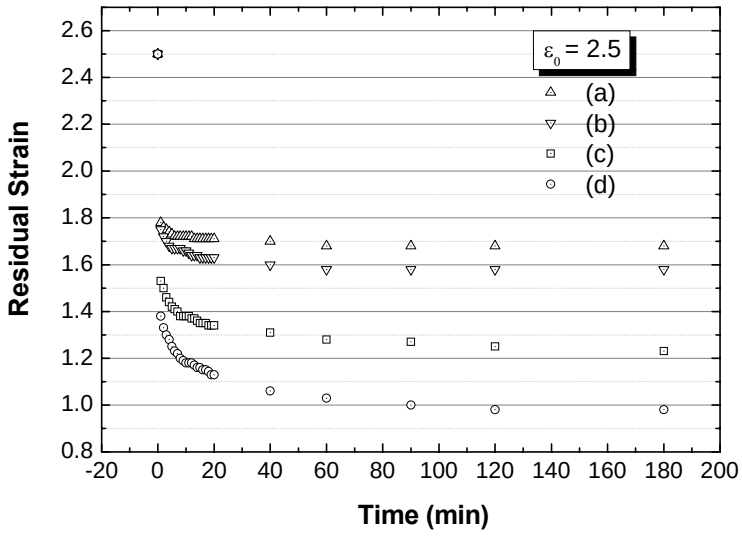

Figure 4-27 Effect on room temperature strain recovery of LC elastomers by varying length of terminal chain on mesogenic unit and length of spacer: (a) C11(MeHQ)Si3XL10; (b) C5(MeHQ)Si3XL10; (c) C11(MeHQ)Si8XL10; (d) C5(MeHQ)Si8XL10.

The transition temperatures of these four materials as well as the temperature differences from the room temperature are summarized in Table 4-6.

Table 4-6 Difference between transition temperatures and room temperature of LC elastomers with various hydrocarbon and siloxane spacers ($\varepsilon_0 = 2.5$)

	T_g (ºC)	$\Delta T_1 = r.t.^{(a)} - T_g$ (ºC)	*retained strain*	$\Delta T_2 = T_{cl} - r.t.$ (ºC)	T_{cl} (ºC)
C11(MeHQ)Si3XL10	-6	29	1.68	108	131
C5(MeHQ)Si3XL10	18	5	1.58	100	123
C11(MeHQ)Si8XL10	-23	46	1.23	81	104
C5(MeHQ)Si8XL10	-13	36	0.98	53	76

(a): *r.t.* refers to room temperature (23 ºC).

By combining the data from this Table 4-4 with the information from Figure 4-27, it is obvious that the LCEs having higher clearing temperature can retain more strain. It was found that C11(MeHQ)**Si3**XL10 and C5(MeHQ)**Si3**XL10 have higher clearing temperatures than C11(MeHQ)**Si8**XL10 and C5(MeHQ)**Si8**XL10, respectively. This indicates that shorter siloxane spacers induce higher clearing temperature. The **C11**(MeHQ)Si3XL10 and **C11**(MeHQ)Si8XL10 have higher clearing temperatures than **C5**(MeHQ)Si3XL10 and **C5**(MeHQ)Si8XL10 respectively which means longer hydrocarbon spacers induce higher clearing temperature. Therefore, a short siloxane spacer and a long hydrocarbon spacer facilitate shape retention. At room temperature, the LCEs with higher clearing temperature are also relatively stiff compared with those with lower clearing temperature.

4.4.5 Effect of Lateral Substituents of Mesogenic Unit

From stress-strain measurements, we found that modifying the lateral substituents of the mesogenic unit can greatly change the mechanical properties of MCLC elastomers. Room temperature strain recovery experiments were also performed on these three materials. In Figure 4-28, C11(4H)Si8XL10 shows the highest retained strain followed

by C11(4F)Si8XL10 and C11(MeHQ)Si8XL10.

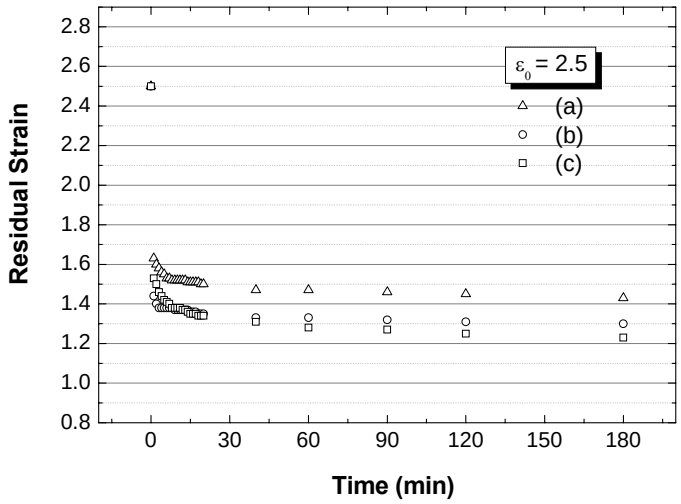

Figure 4-28 Effect of lateral substituents on mesogenic units on room temperature strain recovery: (a) C11(4H)Si8XL10; (b) C11(4F)Si8XL10; (c) C11(MeHQ)Si8XL10.

There are no great differences in their abilities to keep deformation. This result again indicates a different molecular mechanism of shape retention from that of typical mechanical properties of LCEs, although the specific reason is not yet clear.

4.4.6 Effect of Non-mesogenic Monomer

In addition to the crosslinker content, siloxane spacer, hydrocarbon spacer and lateral substituents on the mesogenic units, the mesophase stability can also be affected by other factors. For instance introducing a non-mesogenic monomer, terphenyl transverse rod (**TR3**), can directly modify mesophase stability. In this section, four C11(MeHQ)Si8XL10 elastomers with incremental loading of **TR3** (from 10 mol% to 40 mol%) will be discussed for shape recovery. DSC analysis of these materials detected an almost linear decrease in clearing temperature and a broadened mesophase-isotropic

transition with increasing loading of **TR3.**

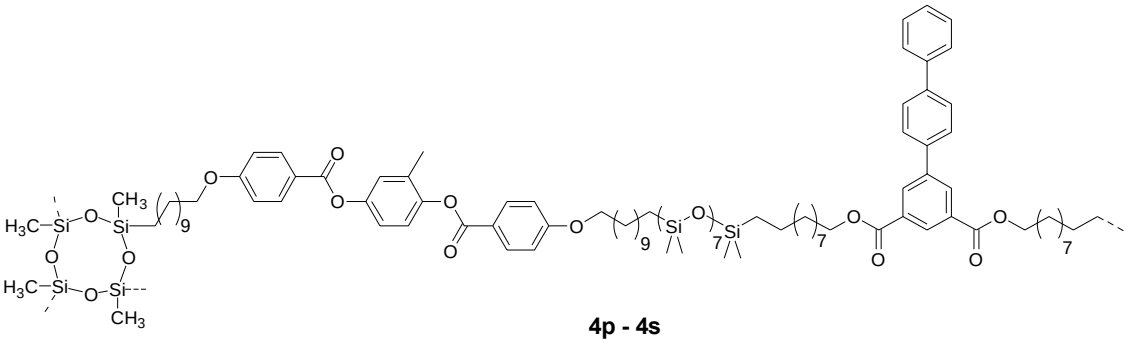

However, **TR3** did not show a significant influence on their glass transition temperatures. Therefore, any changes in shape recovery ability introduced by adding **TR3** can be related to mesophase stability.

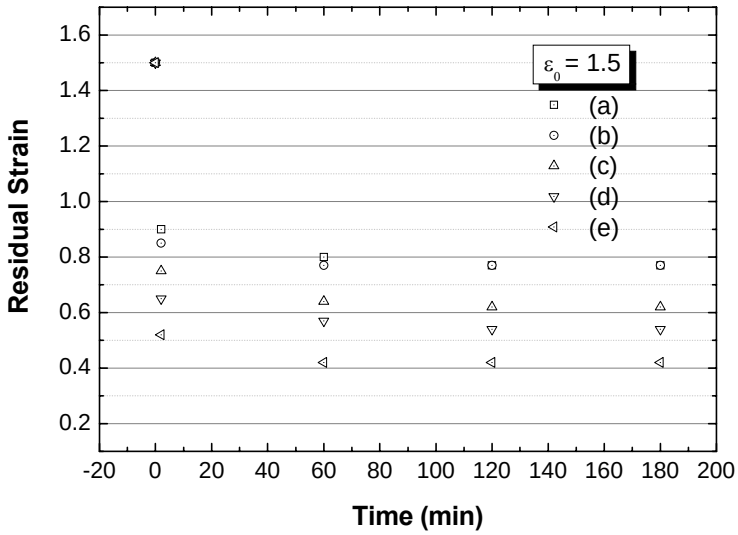

Figure 4-29 Room temperature shape recovery of C11(MeHQ)Si8XL10 with various amount of **TR3** loading under zero loads after 150% initial strain : (a) 0 mol% TR3; (b) 10 mol% TR3; (c) 20 mol% TR3; (d) 30 mol% TR3; (e) 40 mol% TR3.

In Figure 4-29, all the samples with **TR3** show a similar fast decay followed by a plateau in accord with their parent LCE. It was observed that 10 mol% **TR3** loading does not

obviously change the strain recovery behavior compared to that of the parent elastomer. With a further increase in the transverse rod loading, a larger strain recovery was seen over the same period of time. Due to the potential disrupting nature of transverse rod to the mesophase stability, the incorporation of transverse rod accelerates the room temperature shape recovery of its parent C11(MeHQ)Si8XL10 LCE. Varying the loading of TR3 can be generally used to tailor the shape retention and shape recovery ability of LC elastomers.

4.5 Stress Relaxation of MCLC Elastomers

It was observed that the deformation of our MCLCEs can be partially retained by the oriented smectic layer structures (monodomain structures) after the removal of stress.

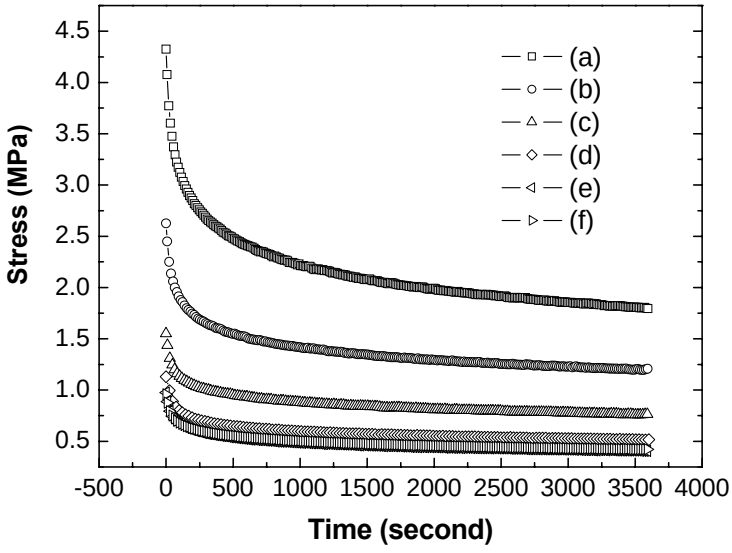

Figure 4-30 Stress relaxation curve of C11(MeHQ)Si8XL10 at strains: (a) 300%; (b) 250%; (c) 200%; (d) 150%; (e) 100%; (f) 50%.

The strain recovery indicates the presence of chain relaxation at zero stress. Stress relaxation experiments were performed on C11(MeHQ)Si8XL10 with various initial

strains (50% - 300%). For each strain, the values of stress were collected as a function of time.

The relaxation time *(τ)* of each specimen can be calculated by fitting the stress relaxation curves to the Kohlrausch-Williams-Watt (KWW) equation (4-14). The analysis procedure is analogous to that of Ortiz *et al.*[45]

$$\sigma_n(t) = (\sigma_{\max} - \sigma_{\min}) \exp(-t/\tau)^{\beta} + \sigma_{\min} \tag{4-14}$$

The detailed fitting procedure has been introduced in Chapter 2, section 2.2.5.3. After rearrangement of the original KWW equation, a new equation (4-15) was obtained.

$$\ln \ln[1/R(t)] = -\beta \ln(\tau) + \beta \ln(t) \tag{4-15}$$

A plot of $\ln \ln[1/R(t)]$ *versus* $\ln(t)$ is linear with a slope equal to β and an intercept equal to $-\beta \ln \tau$. β is a parameter to measure the narrowness of the distribution.

From the curve fittings shown in Figure 4-31, it was found that the stress relaxation time (τ) of C11(MeHQ)Si8XL10 with different initial strains ranges from 228 seconds to 306 seconds and the parameter (β) is in the range of 0.52 - 0.55. No apparent dependence of the stress relaxation time on the initial strain was observed. Ortiz et al. did stress relaxation experiments on a polyisoprene rubber at room temperature and a main chain LCE in its mesophase. Polyisoprene shows a longer relaxation time (τ = 415 s, β = 0.42) than the LCE ($\tau \approx 79$ s, $\beta \approx 0.39$) [45]. The relaxation time of our C11(MeHQ)Si8XL10 is between that of Ortiz's materials. It was thought that the chain flexibility is related to the relaxation behavior. The more flexible chain leads to the longer stress relaxation time. Among these three materials, polyisoprene rubber has the lowest Tg (-60 ºC). With the presence of siloxane spacer in C11(MeHQ)Si8XL10, it has lower Tg (around -25 ºC) than Ortiz's LCE.

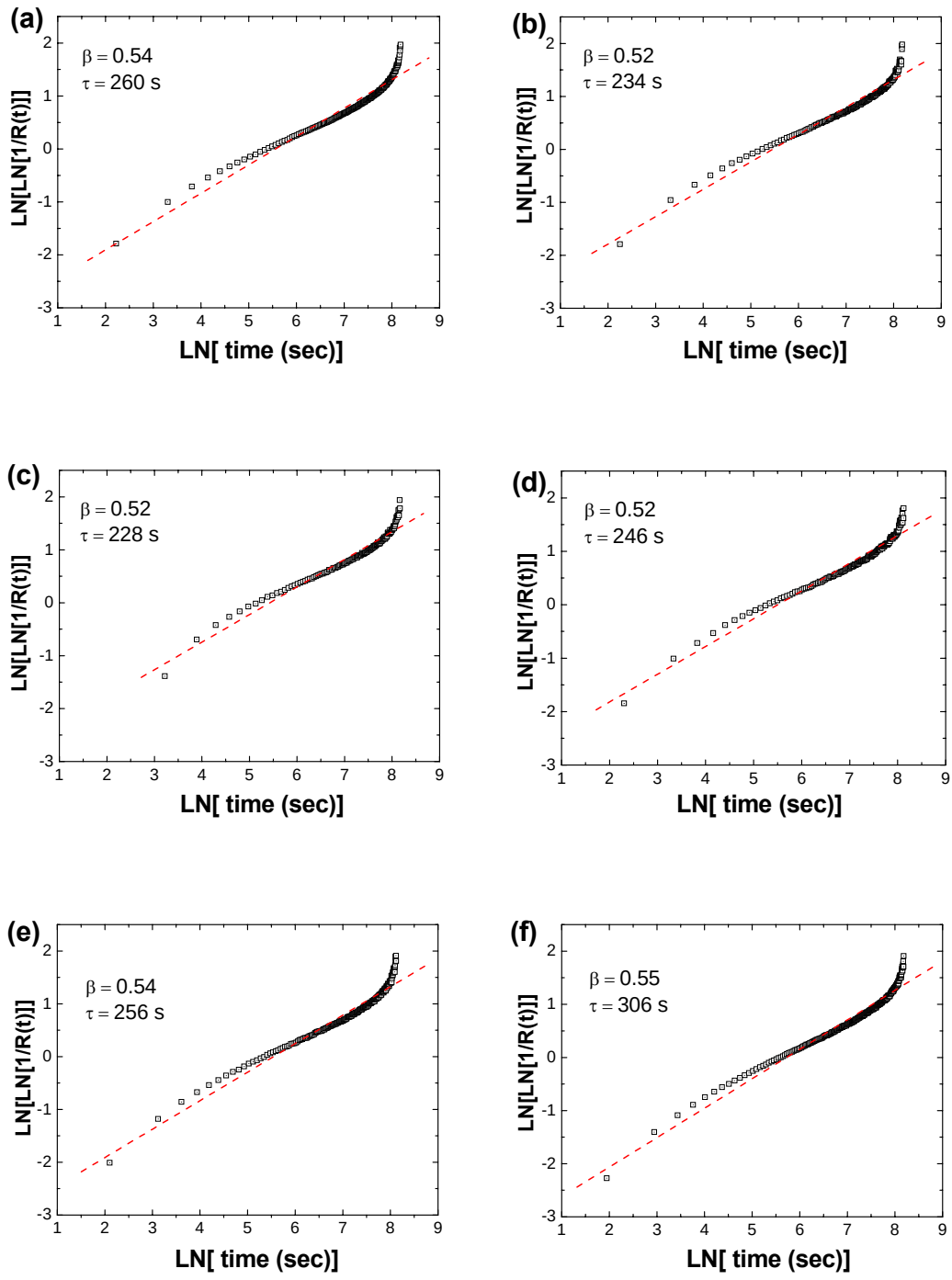

Figure 4-31 Stress relaxation curves fit to the KWW equation in the form of $\ln\ln[1/R(t)]$ *versus* $\ln(t)$ for the C11(MeHQ)Si8XL10 with different initial strain (ε_0): (a) ε_0 = 50%; (b) ε_0 = 100%; (c) ε_0 = 150%; (d) ε_0 = 200%; (e) ε_0 = 250%; (f) ε_0 = 300%.

In this work, another less flexible LCE (*p*-phenylene transverse rod with short siloxane

spacer **Si3**) was also found to have a shorter characteristic relaxation time ($\tau \approx 211$ s, $\beta \approx 0.52$) than C11(MeHQ) based LCEs.

4.6 Mechanical Hysteresis of MCLC Elastomers

Mechanical hysteresis reflects the energy dissipation during the deformation of a material. The area of the hysteresis loop is related to the dissipated energy [5]. All the LC elastomers we synthesized in this work exhibit mechanical hysteresis to some extent. The factors influencing the hysteresis behavior could be loading history and the chemical structures among others.

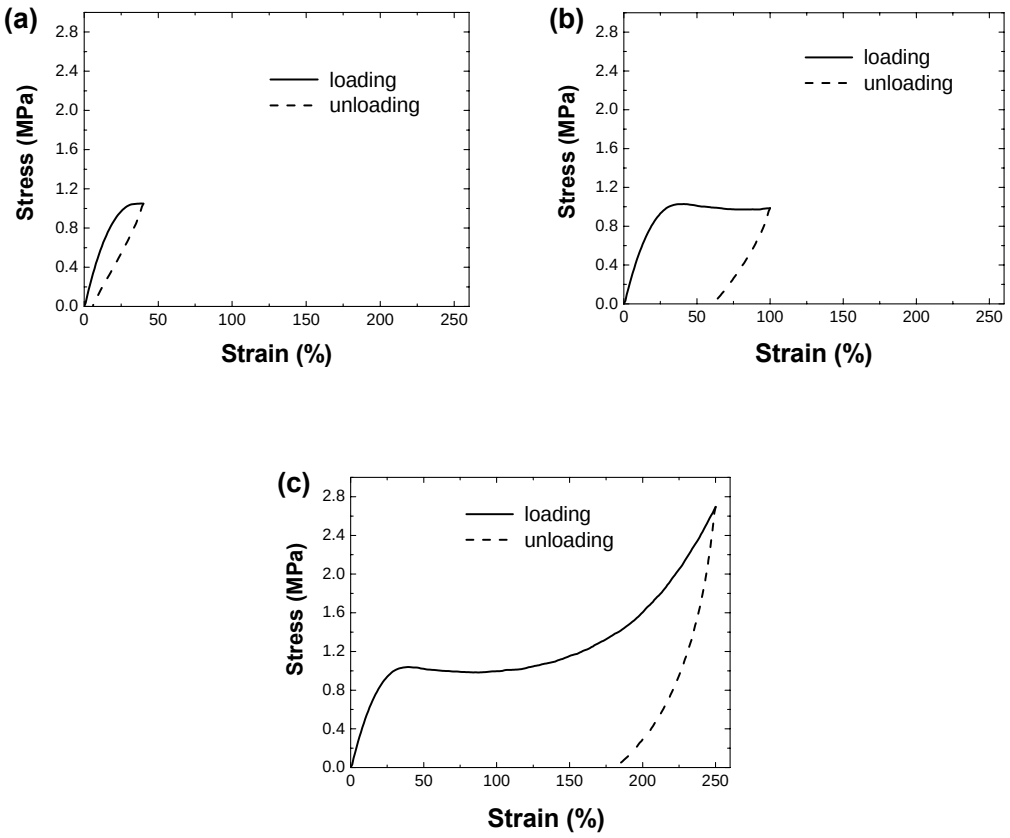

Figure 4-32 Room temperature mechanical hysteresis of C11(MeHQ)Si8XL10 loaded up to various strains: (a) 40%; (b) 100%; (c) 250%.

Figure 4-32 shows the room temperature hysteresis of C11(MeHQ)Si8XL10 with different initial strains. Specimens were loaded up to 40%, 100% and 250%, which locates these strain points before, during and after the *P*-*M* transition. The unloading cycle shows the applied strain of these three specimens recovered 85%, 71% and 27%, respectively. The area of each single cycle or loading-unloading loop can not simply represent the energy dissipated during the process, because the stored energy does not release completely at the ending point (stress = 0 MPa) of each cycle [7, 14]. This was already proven by the strain recovery experiment, which is carried out at zero stress for a long period of time. The recovered strain from strain recovery experiment of C11(MeHQ)Si8XL10 is 53%, which is much higher than 27% recovered strain from the hysteresis measurement.

The influence of the strain rate on hysteresis was also examined under the same experimental conditions, as illustrated in Figure 4-33.

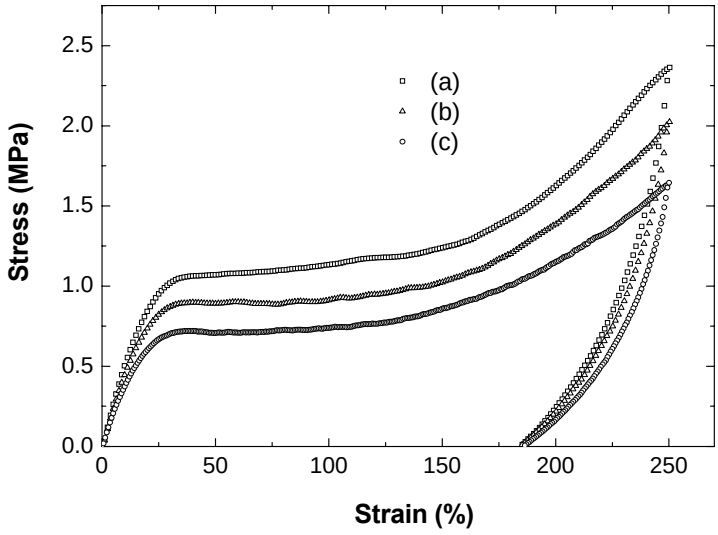

Figure 4-33 Mechanical hysteresis of C11(MeHQ)Si8XL10 at different strain rates: (a) 5×10^{-2} s^{-1}; (b) 5×10^{-3} s^{-1}; (c) 5×10^{-4} s^{-1}.

For the specimen deformed at higher strain rate, the area of the loop is apparently larger than those deformed at lower strain rate, which indicates more energy being stored in the specimen deformed at higher strain rate. But at the point of zero stress, all the specimens return almost to the same strain value. This observation is consistent with what we found in the strain recovery experiments in which the strain rate does not have a much influence on the strain retention under the given experimental condition.

The mechanical hysteresis behavior of LC elastomers with different lateral substituents on mesogenic units are compared in Figure 4-34. The hysteresis loop area of C11(4H)Si8XL10 and C11(4F)Si8XL10 is much larger than that of C11(MeHQ)Si8XL10. It indicates the former two materials dissipate much greater energy than the latter during the loading and unloading cycle. But their recovery of applied strain is similar to each other around 23% to 27%, which is consistent with the results from the strain recovery experiment.

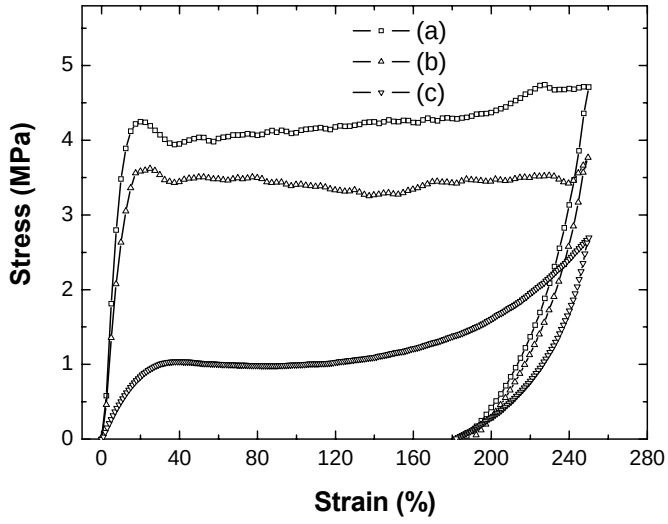

Figure 4-34 Room temperature mechanical hysteresis of LCEs with various lateral substituents on mesogenic unit: (a) C11(4F)Si8XL10; (b) C11(4H)Si8XL10; (c) C11(MeHQ)Si8XL10.

4.7 Stress-strain Behavior of Monodomain MCLC Elastomers

From the previous discussions, we know that a monodomain C11Si8XL10 LCE can be prepared by stretching a material through the *P*-*M* transition (ε >150%). After the removal of load, the deformed specimen always experiences a fast strain recovery followed a slow decay until it is temporally stable at a certain strain level which depends on the value of initial strain. The shape recovery does not significantly affect the macroscopic orientation of domains above 150% strain, since the orientation parameter keeps a value around 0.65 after the applied strain passes 150%. Therefore, 200% extension was given to an unstrained as-cast film in order to prepare a monodomain C11Si8XL10 LCE, as shown in Figure 4-35.

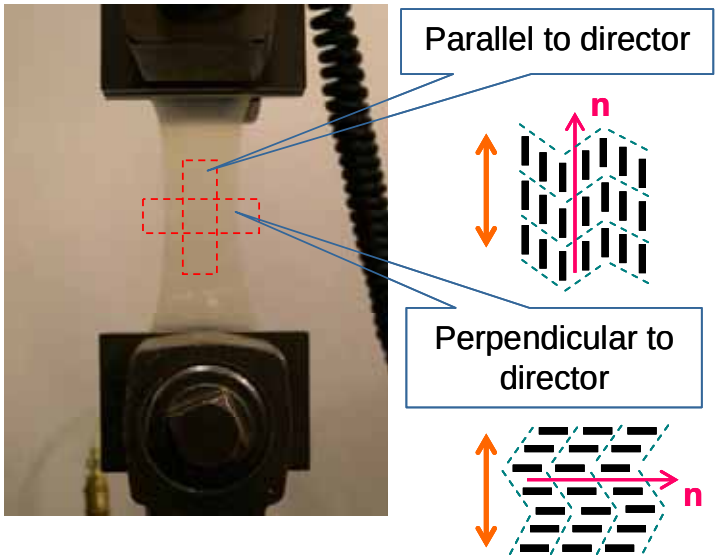

Figure 4-35 Schematic representations of smectic-C C11(MeHQ)Si8XL10 monodomain LC elastomer specimen preparation: Firstly, two wide specimens were stretched to 200% extension; Secondly, one specimen was cut along the director; the other was cut perpendicular to the director.

A monodomain LC elastomer is globally anisotropic compared with a polydomain sample. The mechanical properties of the materials in two directions, parallel or

perpendicular to the stretching direction, should be quite different. A tensile test was performed on two monodomain specimens. Each of them was cut from a wide monodomain specimen obtained by mechanical extension. The specimen cutting directions are perpendicular to each other. One is parallel to the director and the other is perpendicular to the director as illustrated in Figure 4-35.

The stress-strain behaviors of the two monodomain specimens together with that of the corresponding unoriented, as cast polydomain specimen are compared in Figure 4-36. The polydomain specimen behaves in between the two monodomain specimens.

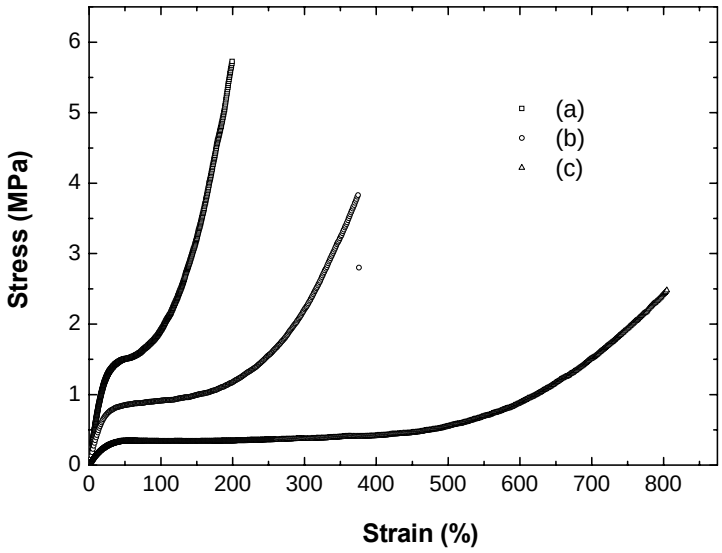

Figure 4-36 Comparison of mechanical properties of unoriented polydomain (as-cast film) and monodomain (with initial 200% elongation) C11(MeHQ)Si8XL10: (a) monodomain specimen stretched parallel to the director (E = 7.2 MPa); (b) polydomain specimen (E = 3.8 MPa); (c) monodomain specimen stretched perpendicular to the director (E = 1.8 MPa).

The Young's modulus of the monodomain sample stretched parallel to the smectic layer normal is roughly two times that of the polydomain sample and as four times as that of the monodomain sample stretched perpendicular to the director. The

monodomain sample stretched perpendicular to the director can have up to ~800% elongation. The elongation at break of the polydomain specimen and the monodomain specimen being stretched parallel to the director are ~ 400% and ~ 200%, respectively. The monodomain specimen stretched perpendicular to the director has a very small threshold stress (0.3 MPa) to the *P-M* transition, which covers from ~ 50% to ~ 450% applied strain in the form of plateau. This observation is of great significance since it illustrates the effect of soft elasticity in smectic-C type of main-chain LC elastomers.

The similar soft elastic plateau was also observed in a monodomain C11(MeHQ)Si8XL10 with 20 mol% **TR3**. From DSC and relaxation experiment of C11(MeHQ)Si8XL10 with 20 mol% **TR3**, we know that introduction of transverse rods into parent C11(MeHQ)Si8XL20 LCE decreases the resulting LCE's liquid crystallinity.

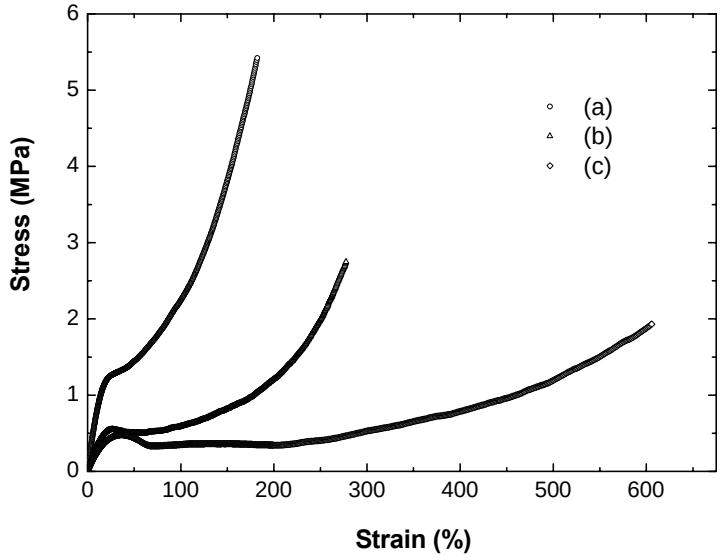

Figure 4-37 Comparison of the mechanical properties of polydomain and monodomain C11(MeHQ)Si8XL10 with 20 mol% TR3: (a) monodomain specimen stretched parallel to smectic layer normal (E = 9.3 MPa); (b) polydomain specimen (E = 4.5 MPa); (c) monodomain specimen perpendicular to smectic layer normal (E = 3.0 MPa).

The ability of LCEs with **TR3** to keep an anelastic deformation is less than that of LCEs

without **TR3**. However, a *P-M* transition still exists in LCEs with **TR3**. By stretching the monodomain LCE with 20 mol% **TR3** in two directions, one parallel to the smectic layer normal and the other perpendicular to the smectic layer normal, a pair of stress-strain curves of monodomain specimen was obtained in Figure 4-37. The specimen (a) stretched parallel to smectic layer normal has higher Young's modulus, higher tensile strength, and shorter elongation at break than its polydomain analogue. The specimen (c) stretched perpendicular to smectic layer normal has lower Young's modulus, lower tensile strength, and longer elongation at break than its polydomain analogue. The unique phenomenon for specimen (c) is the yield point shown in its stress-strain curve, which does not exist in the monodomain specimen without transverse rod stretched perpendicular to the smectic normal.

"Soft elasticity" was first introduced into the field of LC elastomers by Warner and Terentjev. This term describes the phenomenon – "deformation is developed without resistance" [46]. The corresponding plateau region is due to the rotation of individual domain towards the mechanical field. The energy involved with the domain rotation towards the stretching direction is very low.

Softness is a delicate phenomenon and could be partially lost if the mixture of polymer chains in the network have various anisotropies. One population with different anisotropy from the other could cost extra energy if it is deformed along the trajectory selected for the second population. In real experiments, this was always reflected by a small slope before the plateau and the plateau is not completely flat [47]. Therefore, the term "semi-softness" was chosen to describe this phenomenon [1].

4.8 "Poisson's Ratio" of MCLC Elastomers

As introduced in Chapter 1, Poisson's ratio describes the dimensional change when a material is under a tensile or compression force. Its value can be evaluated by the ratio of the lateral strain ($\varepsilon_{lateral}$) to the longitudinal strain ($\varepsilon_{longitudinal}$) measured in a uniaxial tensile test. For conventional materials, Poisson's ratio ranges from 0.2 ~ 0.5. Poisson's ratio is often regarded as a constant for a material since the measurement is carried out within very small strain range. In this elastic region, most materials are macroscopically isotropic. However, strains exceeding those of the elastic region make the sample more and more anisotropic. Under this circumstance, the "Poisson's ratio" of a material is no longer a constant. In this case, we will use *strains ratio* to describe the dimensional change at large strains.

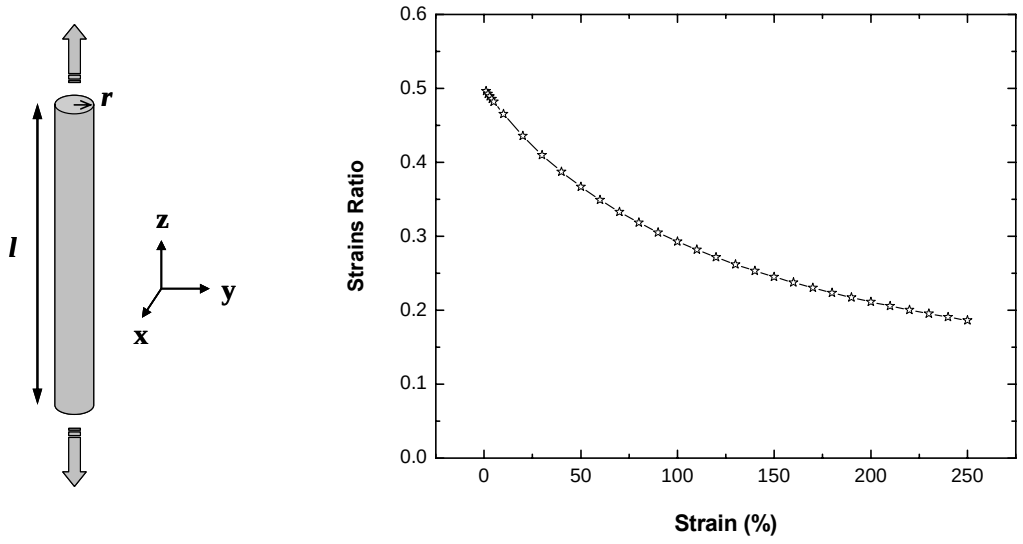

(a) (b)

Figure 4-38 Numerical calculation of strains ratio of ideal rubber: (a) cylindrical specimen; (b) strains ratio as a function of strain**.**

Before discussing the effect of chemical structure on strains ratio of our LC

elastomers, the variation of strains ratio of an ideal rubber (in Figure 4-38) with strain will be calculated numerically based on several assumptions as follows. First of all, the ideal rubber is originally isotropic; Secondly, the ideal rubber is incompressible, i.e. no volume change occurs during deformation ($\Delta V=0$ or $V_0=V$). For simplifying the calculation, a cylindrical specimen is chosen for strains ratio calculation as shown in Figure 4-34 (a). In this diagram, *r* and *l* refer to the instantaneous radius and length of the cylindrical specimen, respectively. And the subscript "0" used here represents the original state of that parameter.

From the geometry, we have

$$r = r_0(1+\varepsilon_x) \tag{4-14}$$

$$l = l_0(1+\varepsilon_z) \tag{4-15}$$

$$V_0 = \pi r_0^2 l_0 \tag{4-16}$$

$$V = \pi r^2 l \tag{4-17}$$

Since

$$V_0 = V \quad \text{i.e.} \quad \pi r_0^{\,2} l_0 = \pi r^2 l$$

Therefore,

$$\pi r_\theta^2 l_0 = \pi r_0^{\,2}(1+\varepsilon_x)^2 l_0(1+\varepsilon_z) \tag{4-18}$$

Then we have

$$1 = (1+\varepsilon_x)^2(1+\varepsilon_z) \tag{4-19}$$

Since we know by definition

$$\nu = -\frac{\varepsilon_x}{\varepsilon_z},$$

strains ratio can be obtained by replacing ε_x with $-\varepsilon_z \nu$. After being expanded and rearranged, strains ratio can be expressed by Equation 4-20, which only involves longitudinal strain ε_z.

$$\nu = \frac{1}{\varepsilon_z}\left(1 - \frac{1}{\sqrt{1+\varepsilon_z}}\right) \tag{4-20}$$

According this equation, strains ratio of an ideal elastomer is 0.5 or near 0.5 only when it undergoes very small strain (within the elastic region). With increasing strain, strains ratio is not a constant any more, but decreases gradually as shown in Figure 4-38 (b).

4.8.1 Effect of Crosslinker

There are five C11(MeHQ)Si8 LC elastomers with various crosslinker contents, from 5 mol% to 25 mol% that were examined for the effect of crosslinker on the strains ratio. In Figure 4-39, it can be seen that strains ratio is especially sensitive to measurement error at small strain, because the axial displacement is comparable to the displacement resolution at the small strain region. This situation improves when the strain exceeds 25%. The elastomer with 5 mol% crosslinker shows a gradual decrease in strains ratio with increasing strain that found in which is analogous to ideal rubber, although its absolute values are smaller than that of ideal rubber. By increasing the crosslinker to 10mol%, the strains ratio *versus* strain plot changes into a convex curve. For the other elastomers, the convexity of the curve becomes larger. Their strains ratio increases abruptly with strain in the small strain region (<50%) and begins to decrease when the strain passes about 55%. It was also found that strains ratio has its highest value in the LC elastomer with the highest crosslinker content.

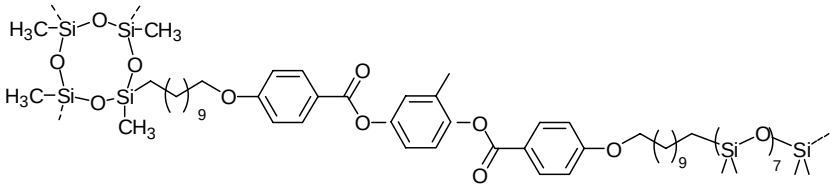

4a - 4e

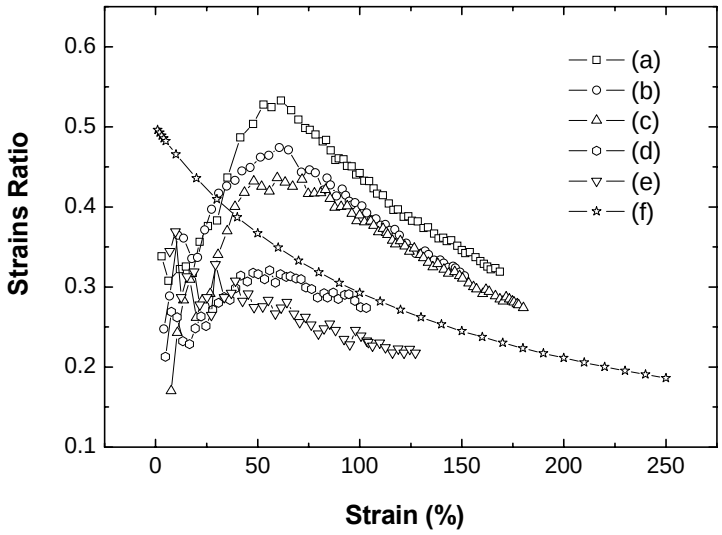

Figure 4-39 Strains ratio of C11(MeHQ)Si8 LC elastomers with various crosslinker content: (a) 25 mol%; (b) 20 mol%; (c) 15 mol%; (d) 10 mol%; (e) 5 mol%; (f) ideal rubber.

The maximum of strains ratio for some of these LC elastomers even exceeds 0.5, possibly because of the anisotropy induced by the large elongation of the network [48]. Lakes found that cell size of polyurethane foam greatly affected the Poisson's ratio which increased with decreasing cell size [48]. Because there is no length scale limit in the theory of elasticity, the factors influencing Poisson's ratio at the macroscopic level also should hold at the molecular level. Increasing crosslinking in the network is analogous to decreasing cell size in a macroscopic foam. In our work, we found that strains ratio increases with increasing crosslinking in LC elastomers, which is similar to the effect of

cell size on Poisson's ratio observed by Lakes. The greater the network connectivity, the greater the anisotropy of LC elstomers. Before a critical strain, LC elastomers with higher crosslinking density have a higher value of strains ratio. After passing a critical strain, the materials have been significantly deformed and the decrease in lateral strain is slower than the increase in longitudinal strain. Therefore, strains ratio begins to decrease with increasing axial strain.

4.8.2 Effect of Non-mesogenic Transverse Rigid Rod

C11(MeHQ)Si8XL10 elastomer was chosen to be the parent system to study the effect of non-mesogenic terphenyl transverse rod (**TR3**) on strains ratio. Four LC elastomers were synthesized by varying the loading of **TR3** in the parent elastomer.

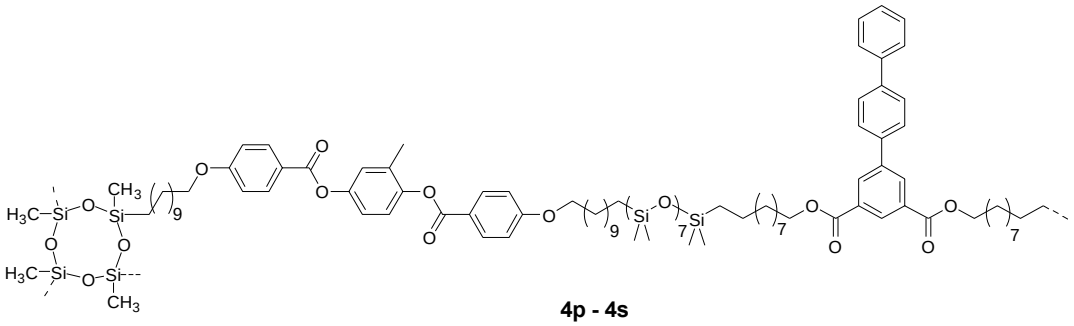

4p - 4s

The value of strains ratio in Figure 4-40 (a) is calculated using the raw data of strain in width and length. Again, as found previously, there was much noise in the curves in the small strain region due to the displacement resolution comparable to the axial displacement. The value of strains ratio is very sensitive to the experimental error at small strain. Smoothed curves in Figure 4.36 (b) were obtained by fitting the original width with length. As discussed at the beginning of section 4.7, the strains ratio of ideal rubber decreases continuously with an increase of strain. However, none of C11(MeHQ)Si8XL10 elastomers with **TR3** follows the same trend. Figure 4-40 shows

a general trend that strains ratio increases with strain when strain is small (<50%).

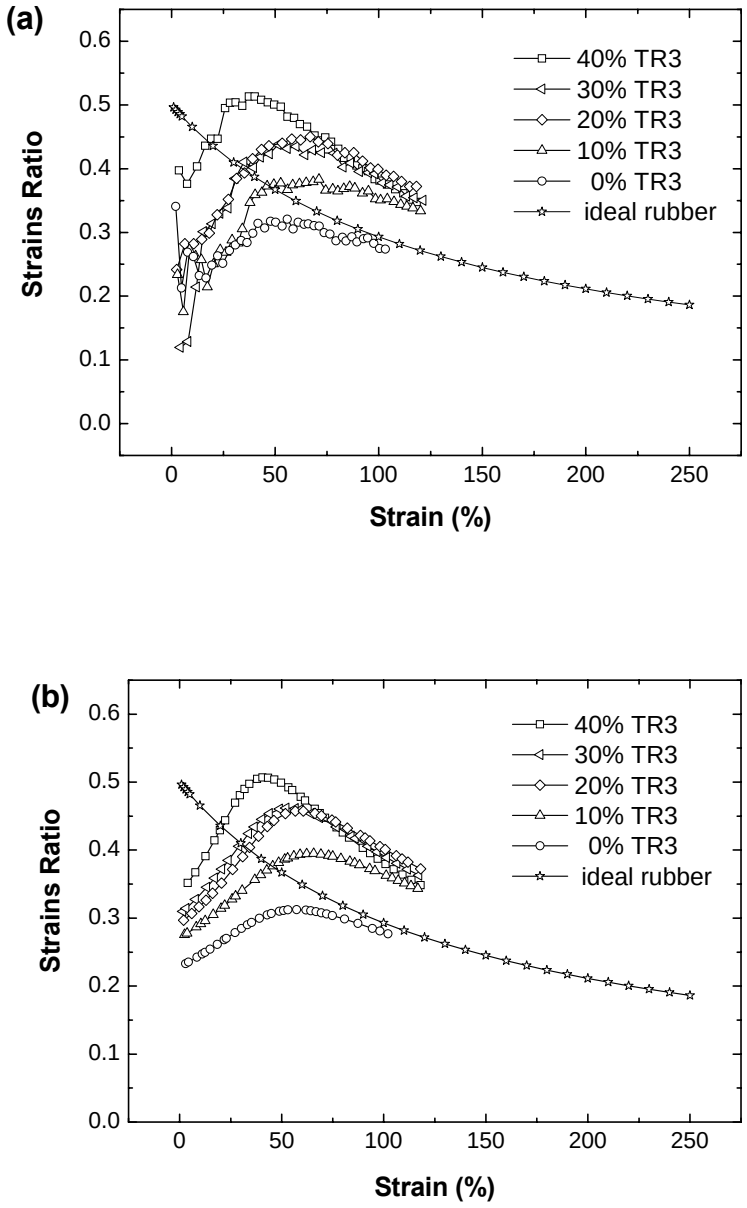

Figure 4-40 Effect of **TR3** on the strains ratio of C11(MeHQ)Si8XL10 LCEs: (a) experimental data before curve fitting; (b) experimental data after curve fitting**.**

Further stretching of the sample leads to decreases in strains ratio. The higher the **TR3** loading in LC elastomer results in a higher strains ratio. This result is comparable to the

observation in previous section. Increasing the amount of transverse rod in the network increases the network anisotropy at small strains. We found the LCE with 20 mol% **TR3** showed special stress-strain behavior compared with other LCEs during the mechanical test. However, this sample didn't show any special and different behavior from the others in this strains ratio measurement. The purpose of introducing transverse rod into C11(MeHQ)Si8XL10 was to examine the "Poisson's ratio" (strains ratio) effect of possible site-connectivity driven rigid rod re-orientation mechanism. Thermal and X-ray analysis showed the presence of a smectic C mesophase at room temperature due to the strong self-segregation of the siloxane spacer, hydrocarbon spacer and rigid mesogenic rods for these LCEs. The reason for that no negative values could be observed for strains ratio by incorporating **TR3** could be that the necessary rotation of **TR3** rod were hindered by the smectic layer structure. The siloxane-based MCLCE system may not be an ideal parent system to achieve the auxetic effect in LCEs.

4.8.3 "Poisson's Ratio" of Monodomain LC Elastomers

It was found that the monodomain state of C11(MeHQ)Si8XL10 has zero Poisson's ratio at small strains (< 10%) when the specimen was deformed in the direction perpendicular to the director n as shown in Figure 4-41.

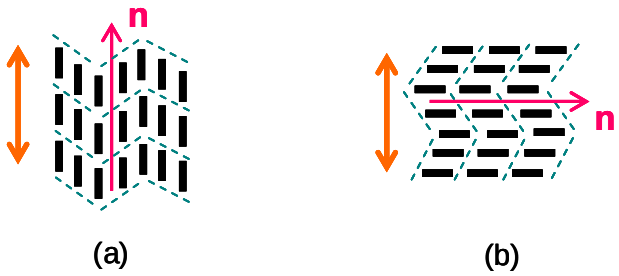

Figure 4-41 Schematic representation of stretching a monodomain smectic LCE along the direction (a) parallel to the director **n**; (b) normal to the director **n.**

It was also found that Poisson's ratio measured in the direction parallel to the director began at about 0.5 and then decreased with increasing strain, the same way as in the strains ratio of polydomain specimen at high strain. A similar observation was found in the monodomain C11(MeHQ)Si8XL10 with 20 mol% **TR3**. The "Poisson's ratio" (strains ratio) versus strain curves of both materials were plotted in Figure 4-42.

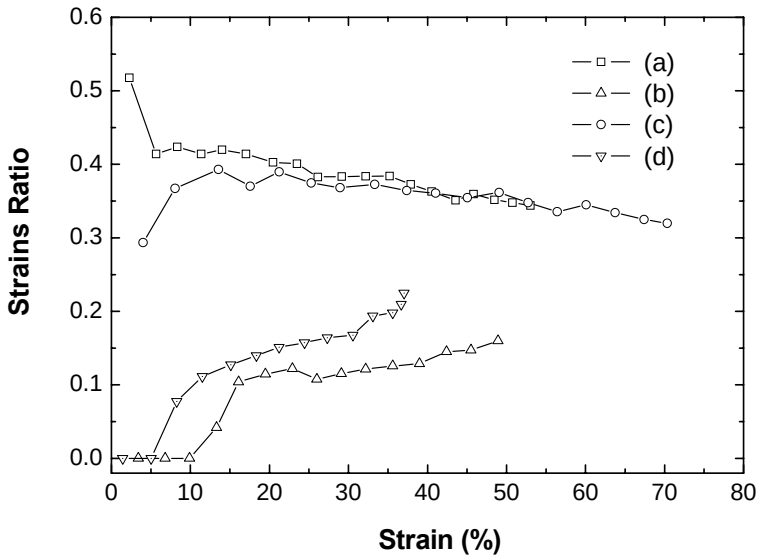

Figure 4-42 Strains ratio of monodomain C11(MeHQ)Si8XL10 with and without 20 mol% **TR3**: (a) 0 mol% **TR3** parallel to the director; (b) 0 mol% **TR3** perpendicular to the director; (c) 20 mol% **TR3** parallel to the director; (d) 20 mol% **TR3** perpendicular to the director.

Zero Poisson's ratio means there is no lateral dimension change when the sample undergoes longitudinal deformation. A similar observation has been reported in a smectic-A liquid single crystal side-chain LC elastomer by Finkelmann *et al*. [49]. They found that their sample kept its full width up to 80% extension when it was deformed in the direction parallel to the layer. The constant dimension in the direction parallel to the layer means that no molecules transfer between smectic layers and no changes in layer

thickness occur upon stretching. The shrinkage in the thickness direction with constant width during deformation indicates the mesogenic units move in the width-thickness plane inside the layers [49]. The in-plane flow of mesogenic units within smectic layers could also help explain the reason for the constant width under extension observed in our monodomain LC elastomers. However, Zentel *et al.* reported their observation of smectic layer thickness change in LCE films upon stretching by optical reflectometry and small angle X-ray scattering studies and claimed the Poisson's ratio is close to 0.5 [50].

4.9 A MCLC Elastomer with Pentaphenyl Transverse Rod (TR5)

As discussed in the previous section, no obvious auxetic effect was observed by introducing terphenyl transverse rod (**TR3**) into our main-chain LC Polymers and LC elastomers. One reason could be that terphenyl transverse rods are not sufficiently long and strong enough (no enough torque developed) to push the neighboring chains away upon stretching. Another reason could be the disrupting nature of non-mesogenic terphenyl transverse rods to the intrinsic liquid crystallinity of the parent LCE system. Therefore, in the unstretched state, the transverse rods may not be aligned well with mesogenic units so that it becomes difficult to observe the lateral expansion in the bulk material by stretching. Ringsdorf *et al.* synthesized and examined phase behavior of main chain LC polymers with laterally linked mesogens previously [51]. A specially designed *p*-pentaphenyl transverse rod (**TR5**) was synthesized in our lab in the purpose of resolving these potential problems. *p*-Phenylene transverse rods with different substituents were synthesized previously [52-55]. A siloxane-based MCLCE, TR5Si3XL10, with *p*-pentaphenylene rods was synthesized with the three components as shown in Figure 4-43.

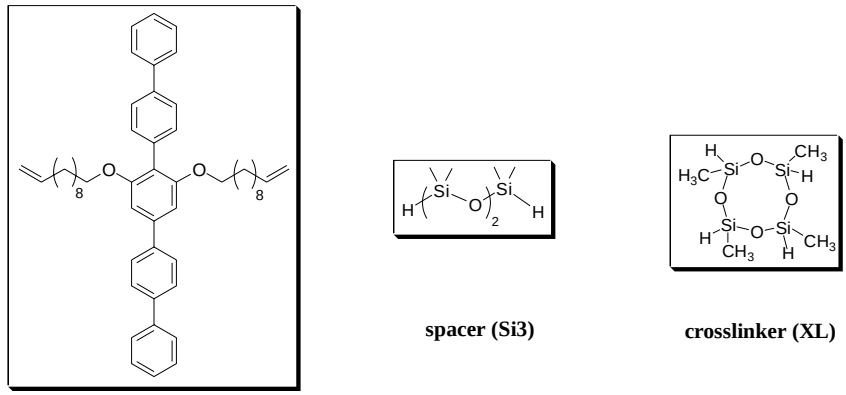

Figure 4-43 Chemical components of TR5Si3XL10 LC elastomer.

This *p*-phenylene transverse rod consists of five para-attached phenyl rings extended at the 2,6- positions from the central benzene ring by an alkenyloxy chain. The purpose of this architecture was to combine the transverse rod's potential 90° rotation upon stretching with the self-alignment feature of liquid crystals. The room temperature stress-strain curve (Figure 4-44) of TR5Si3XL10 was measured at a strain rate of 5×10^{-3} s^{-1}. The nominal stress of an as-cast specimen without thermal treatment increases rapidly to about 15 Mpa and then begins to decrease ($\varepsilon = \sim 7\%$) quickly until reaching about 9 MPa. After that point, nominal stress increases again to about 10 Mpa until the strain reaches about 40%. Almost no further increase in stress occurs with strain after that. Eventually, this specimen fails at about 250% strain. Young's modulus of this specimen (E = 296 Mpa) is calculated in the linear stress-strain region. When the yield point appears on the stress-strain curve, necking occurs on the specimen under extension. The rapid decrease in stress after yield points indicates that some strong local intermolecular interaction is disrupted at this applied load. The irregular nature of the curves was thought likely intrinsic to the material not to instrumental slip.

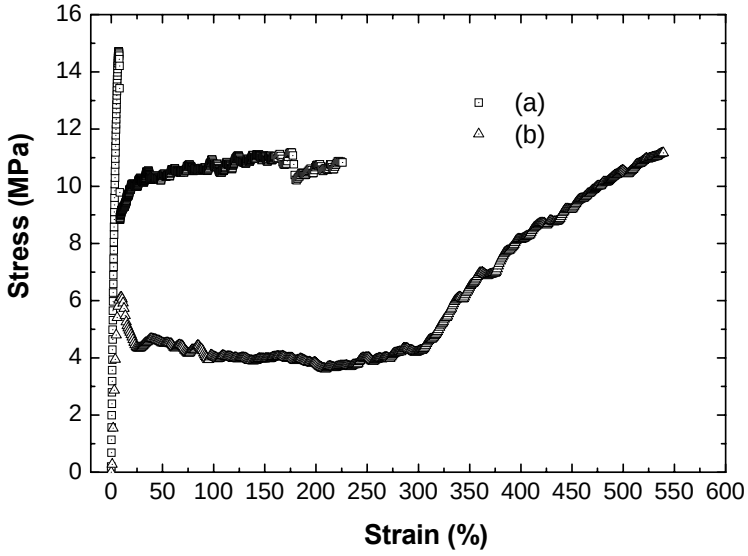

Figure 4-44 Stress-strain curve of unoriented as-cast TR5Si3XL10 at room temperature: (a) without annealing (as-cast); (b) with annealing.

The originally opaque specimen became transparent in the necking region, which corresponds to a characteristic *P-M* transition of a LC elastomer. For the as-cast specimen, there is no strain hardening phenomenon observed before it breaks at about 250% elongation. The stress-strain curve of another specimen having been annealed at 70°C for minutes (15°C above its first order transition temperature by DSC in Figure 4-46) is also reported in Figure 4-44. After annealing, the Young's modulus decreases to 133 MPa. Similar to the unstrained sample, yielding also occurs but at much a lower stress (~ 6MPa). Compared with the sample without thermal treatment, annealing makes the sample much more extendable. After being extended to 300% strain, the specimen began to show strain hardening. The annealed sample can be elongated to 550% without breaking.

A mechanical hysteresis experiment performed on this material by loading up to

300% seen in Figure 4-45. Necking occurs during stretching which corresponds to the observed yield point on the stress-strain curve. Before yielding, the material was rigid at room temperature. After yielding, the necking part became soft. After softening, it turned to rigid again quickly. This rigidification was detected by the unloading cycle of a mechanical hysteresis experiment. The unloading curve was as smooth as that observed in other soft LC elastomers at the beginning. But, with increasing time after unloading, some irregularities (bumps) began to appear in the unloading curve.

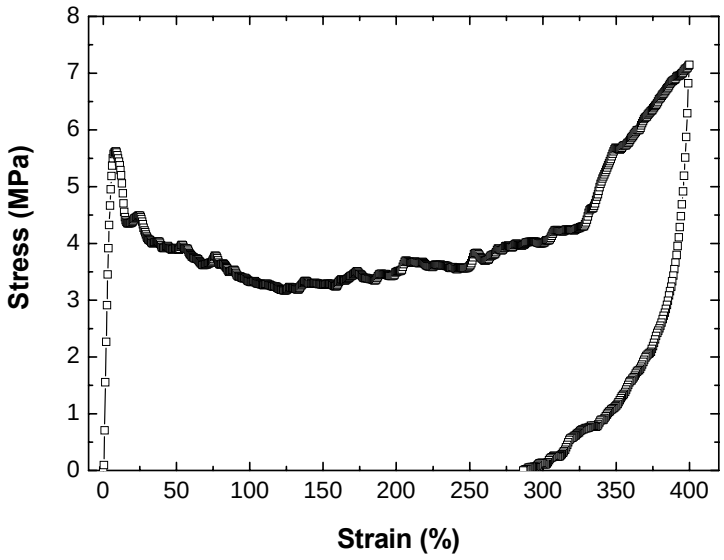

Figure 4-45 Mechanical hysteresis of TR5Si3XL10 with annealing at the rate of 5×10^{-3} s^{-1}

An apparent increase in stress was seen at a strain corresponding to about 2 minutes since the unloading cycle started. This phenomenon likely indicates the presence of strong internal interactions or self-assembly driven reconstructive forces within the network. The DSC profile of TR5Si3XL10 in Figure 4-46 shows a first order transition with peak maximum at 52 °C (ΔH = 11.5 J/g) on the heating cycle and a peak maximum at 29 °C (ΔH = 7.5 J/g) on the cooling cycle. More than 20ºC displacement of the phase transition

peak in the cooling cycle compared with that in the heating cycle likely indicates a crystalline or highly ordered LC structure rather than a normal more fluid LC structure. No apparent glass transition can be detected by DSC, which also indicates the polymer chains are well organized in the material.

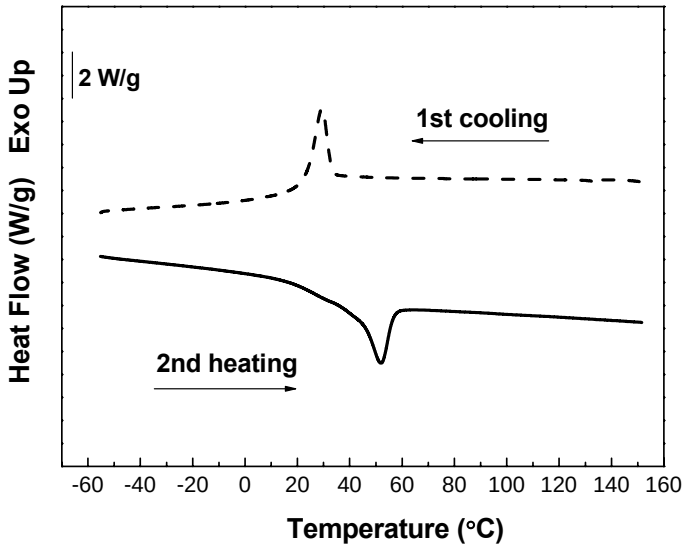

Figure 4-46 DSC profile (1st cooling and 2nd heating at a rate of 10 °C/min) of TR5Si3XL10

Although it was difficult to identify the phase type of this material by DSC, smectic A-like scattering pattern was found in a stretched specimen by wide-angle X-ray diffraction measurement as shown in Figure 4-47. The smectic layer spacing of as-cast specimen was estimated as 30.9 Å (15.2 Å for the second order) and that of a stretched sample was 30.2 Å (15.0 Å for the second order and 10.0 Å for the third order). The measured layer spacing matches the corresponding measurement from a CPK molecular model (~ 30 Å). The diffraction pattern shown in the meridian does not consist of perfect spots but rather short and narrow arcs. Therefore, each smectic layer normal is not

perfectly parallel to the stretching direction. There is a distribution of slightly tilted layer structure in the stretched sample, which makes the average layer spacing decreased about 1 Å compared with that in the as-cast sample. For a stretched TR5Si3XL10 specimen, a series diffraction arcs at low angles located on the meridian indicates the highly ordered lamellar structure of a smectic A phase.

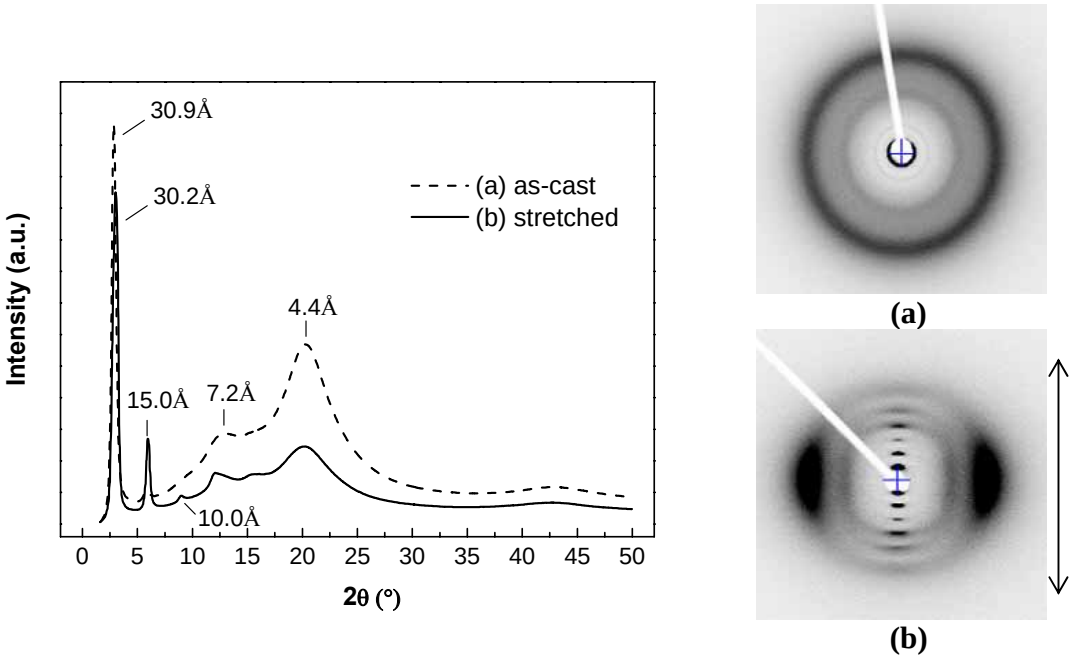

Figure 4-47 Room temperature WAXD intensity profiles and patterns of TR5Si3XL10 after being heated above its clearing temperature and cooled down to room temperature: (a) unstretched; (b) stretched.

An azimuthal scan at a small angle region (2θ = 5.7° - 5.9°) confirmed that the diffraction intensity maxima located at the azimuthal angle χ of 180° and 360° was on the meridian seen in Figure 4-48.

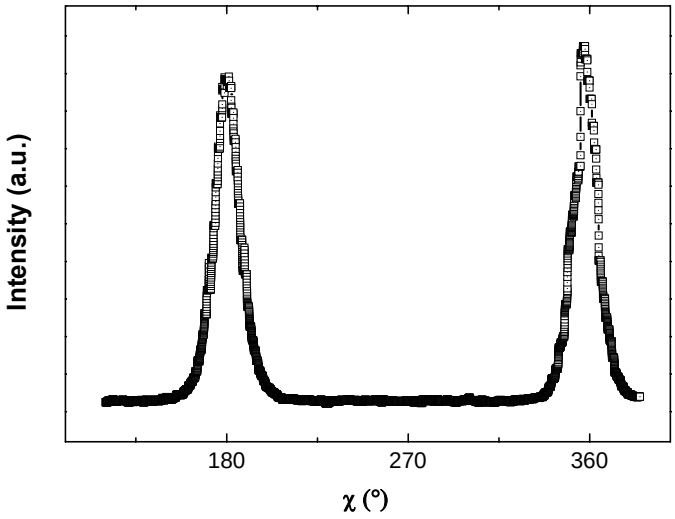

Figure 4-48 Azimuthal intensity profile of second order small angle (2θ = 5.7° ~ 5.9°) diffraction of oriented TR5Si3XL10.

The azimuthal intensity maximum at a wide-angle region located at the equator (90° and 270°) in Figure 4-49 indicates that laterally attached hydrocarbon chains are macroscopically aligned along the stretching direction with an average interchain packing distance of 4.4 Å. This is the characteristic value of hydrocarbon interchain packing distance in polymeric materials. No increase in interchain packing distance was found in the stretched TR5Si3XL10 under these experimental conditions. From the azimuthal scan at the wide-angle region (2θ = 18° - 23°) in Figure 4-49, the order parameter (S = 0.76) reflecting the average orientation of long molecular axes with regard to the stretching direction was determined.

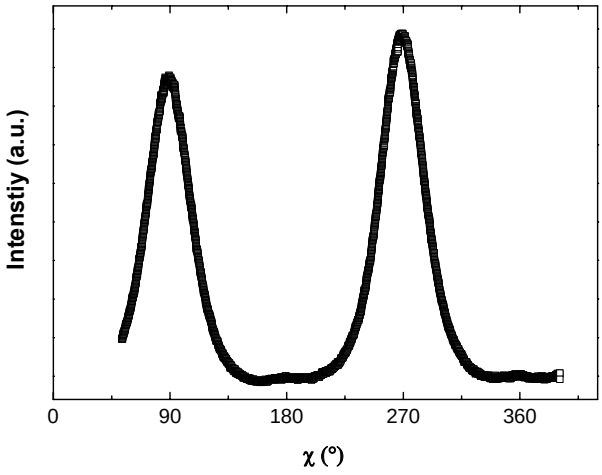

Figure 4-49 Azimuthal scan of wide angle diffraction (2θ = 18° - 23°) of oriented TR5Si3XL10.

WAXD studies were performed on TR5Si3XL10 specimens with various thermal and mechanical treatments as shown in Figure 4-50. In the wide angle region (2θ, ~20º), the as-cast specimen fabricated directly from the reaction solution shows a narrow and sharp diffraction peak. After a thermal treatment, the diffraction peak maximum of the unstretched specimen has a small shift (< 0.5 º) and the peak broadens as well. The reason is, compared with specimens cooled down from the mesophase or the isotropic state, the rigid rod and flexible chain can move more freely and form more ordered structure from a solution environment. The as-cast film is originally rigid and can not bear large extension without brittle failure. Thermal treatment reduces the as-cast film less rigid and more extendable.

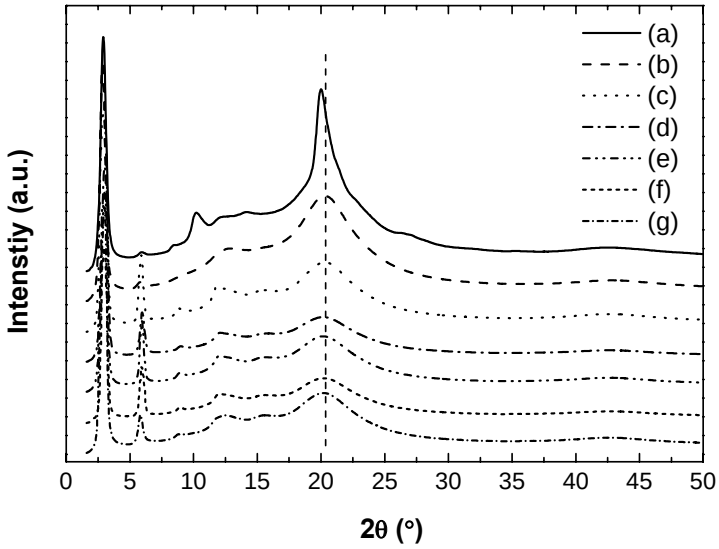

Figure 4-50 Room temperature WAXD intensity profiles of TR5Si3XL10 with various thermal and mechanical treatments: (a) as-cast from reaction solution; (b) heated above clearing temperature and cooled down to room temperature, unstretched; (c) heated above clearing temperature and cooled down to room temperature, stretched (d) stretched in its mesophase and cooled down in the air; (e) stretched in mesophase and cooled down in ice water; (f) stretched in isotropic state and cooled down in air; (g) stretched in isotropic state and cooled down in ice water.

Therefore, the specimens were always given a thermal treatment before mechanical extension. It was found that there are no significant changes in diffraction patterns of the specimens being stretched under different conditions. This indicates the packing structure of transverse rods and backbone prefers a specific organization regardless of the thermal and mechanical treatments.

Based primarily on information from X-ray analysis, a possible arrangement of the *p*-phenylene transverse rods in the network is proposed and is shown in Figure 4-51.

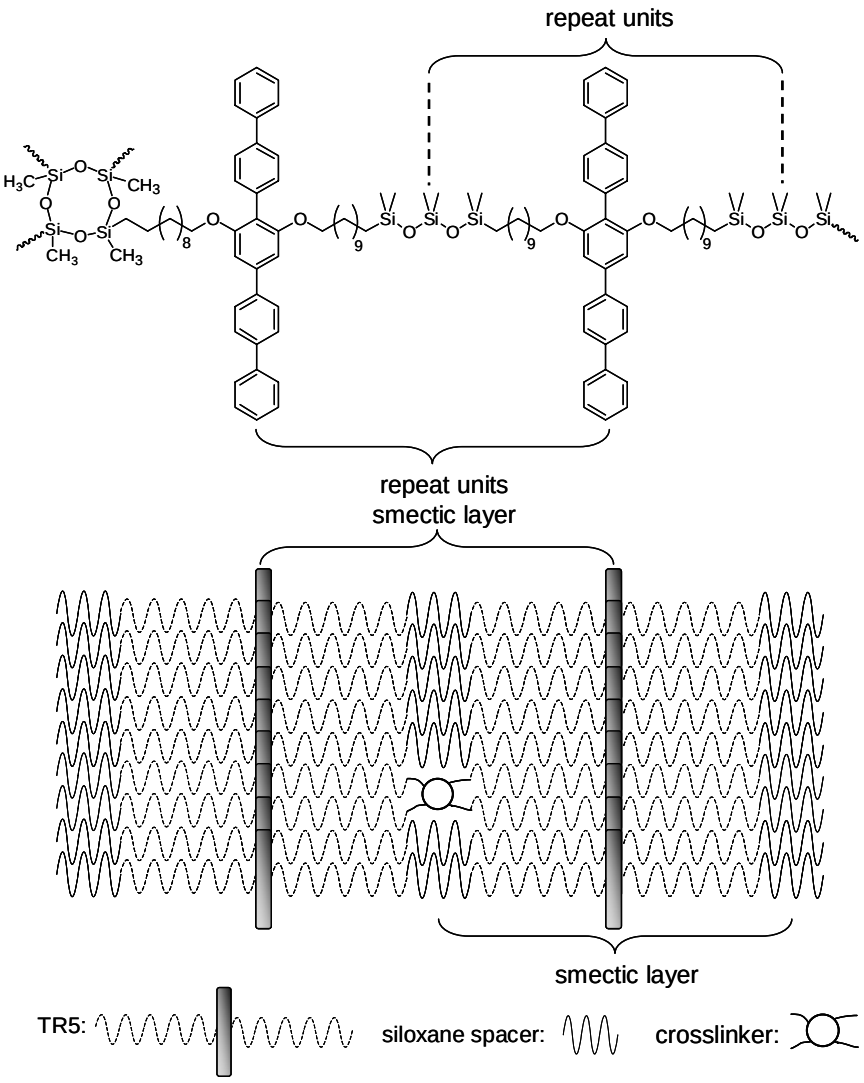

Figure 4-51 Schematic representation of arrangement of *p*-phenylene transverse rods within a stretched TR5Si3XL10 specimen

In this model, the transverse rod is joined to the polymer main chain near the center of the rod and the backbone is extended away from the rod first by a hydrocarbon spacer and then by a siloxane spacer. Neighboring backbones are connected occasionally through a tetrafunctional crosslinker. Due to the mutually strong segregation tendency of siloxane spacers, alkyl spacers and rigid rods, a partially overlapped, stacked transverse rods occurs. This also provides an efficient space filling by alkyl spacers around the

transverse rods. In this structure, smectic A layers form naturally. The CPK moleuclar model indicates layer spacing determined either from a **TR5** to **TR5** layer or a siloxane to siloxane layer matches the observed layer spacing (~30Å) measured by WAXD. Since little characteristic π-π stacking diffraction was detected in this material, the rigid rods may not overlap on top of each other perfectly as shown in the model.

Another two possible packing structures of p-phenylene transverse rods are shown in Figure 4-52.

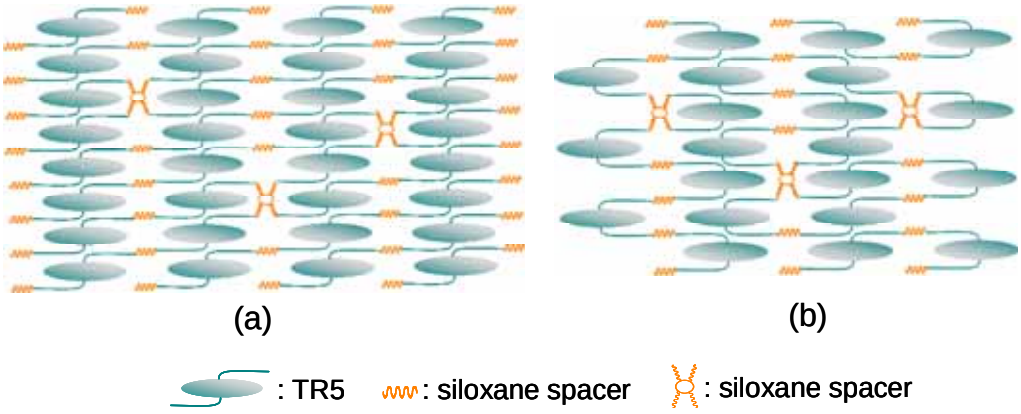

Figure 4-52 Schematic representations of two other possible arrangements of TR5 in TR5Si3XL10: (a) two hydrocarbon spacers pointing to the opposite directions along the rod; (b) two hydrocabon spacers pointing to the same direction along the rod generating a hairpin.

The similar packing structure as that in Figure 4-52 was proposed previously by He *et al.* for their LC copolymers containing p-phenylene transverse rods capable of 60° rotation [54]. In our case, if the *p*-phenylene transverse rods originally arrange themselves along the lateral hydrocarbon spacers, there should be some detectable diffractions coming from transverse rods next to each other side by side. And, if that configuration exists, the interchain distance between lateral hydrocarbon chains on two neighboring transverse rods should be larger than 4.4 Å. However, no diffraction related to these arrangements has been detected. In fact, the configuration of transverse rod in these two arrangement

also makes the segregation of alkyl chain and aromatic rigid part poor. Therefore, these two arrangements are thought to be less likely.

4.10 Main-Chain Liquid Crystalline Elastomers with Anthraquinone Monomer

All the elastomers discussed pervously in this work contain rod-like (calamitic) mesogenic units. It is also our interest to synthesize and examine the properties of MCLCEs with non-calamitic mesogens. In this section, a series of elastomers with anthraquinone mesogenic units will be discussed. Anthraquinone (AQ) types of low mass liquid crystals are known for forming a columnar structure due to the flat shape of the molecules and their tendency to π-stacking [56]. Whether introducing AQ mesogens in the MCLCE system can still allow the formation of the columnar structure or other higher ordered structures is the driving force to investigate these AQ-containing LCEs.

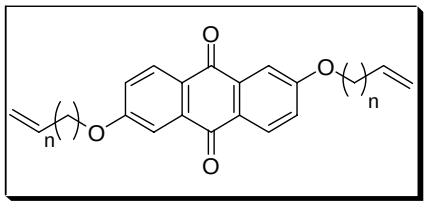

anthraquinone monomers (AQ)

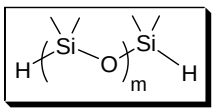

siloxane spacer (Si)

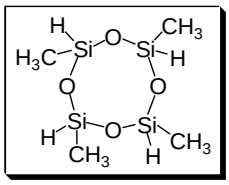

crosslinker (XL)

Table 4-7 Components of anthraquinone type MCLCEs

	n	m	XL (mol%)		n	m	XL (mol%)
AQ5Si3XL10	3	2	10	**AQ11Si3XL10**	9	2	10
AQ5Si8XL10	3	7	10	**AQ11Si8XL10**	9	7	10

With the same crosslinker content (10 mol%), four elastomers were synthesized in our lab by varying the length of hydrocarbon chain on the mesogen and the length of siloxane

spacer. The combination of hydrocarbon chain and siloxane spacer with different lengths is summarized in Table 4-7. Flat-shaped aromatic moieties in AQ molecules tend to stack on top of each other to form a column-like structure. In addition, the siloxane spacers inherently tend to self-segregate, which provides more opportunity for the AQ segments to aggregate. If a columnar mesophase is present in materials, a strong characteristic π-π stacking diffraction peak (25°, 2θ, d-spacing = 3.5 Å) should be detected by WAXD.

Room temperature WAXD patterns of all the unoriented as-cast and stretched AQ specimens are shown in Figure 4-53. Except for AQ11Si8XL10, the other three elastomers showed the characteristic π-π stacking diffraction but with differing intensity. Assuming that π-stacking is necessarily connected to column formation, a preliminary conclusion can be drawn that having an anthraquinone mesogen does not guarantee the formation of columnar structure in LC elastomers. There should be an optimum combination of hydrocarbon chain and siloxane spacer to get a possible columnar mesophase. AQ11Si8XL10, which does not form columns, has a long hydrocarbon chain and a long siloxane spacer. The X-ray pattern of its stretched form showed several spots arranged in a cross shape in the small angle region, indicating a smectic C mesophase at room temperature. The cross shape of the diffraction pattern likely results from the smectic structure arranged in a "chevron" shape in which the smectic layers tilt in two opposing directions and the director points along the stretching direction. The observed smectic layer spacing is around 44 Å in the unoriented as-cast specimen and 40 Å in the stretched one. In the middle angle region, a halo with only slight orientation appears.

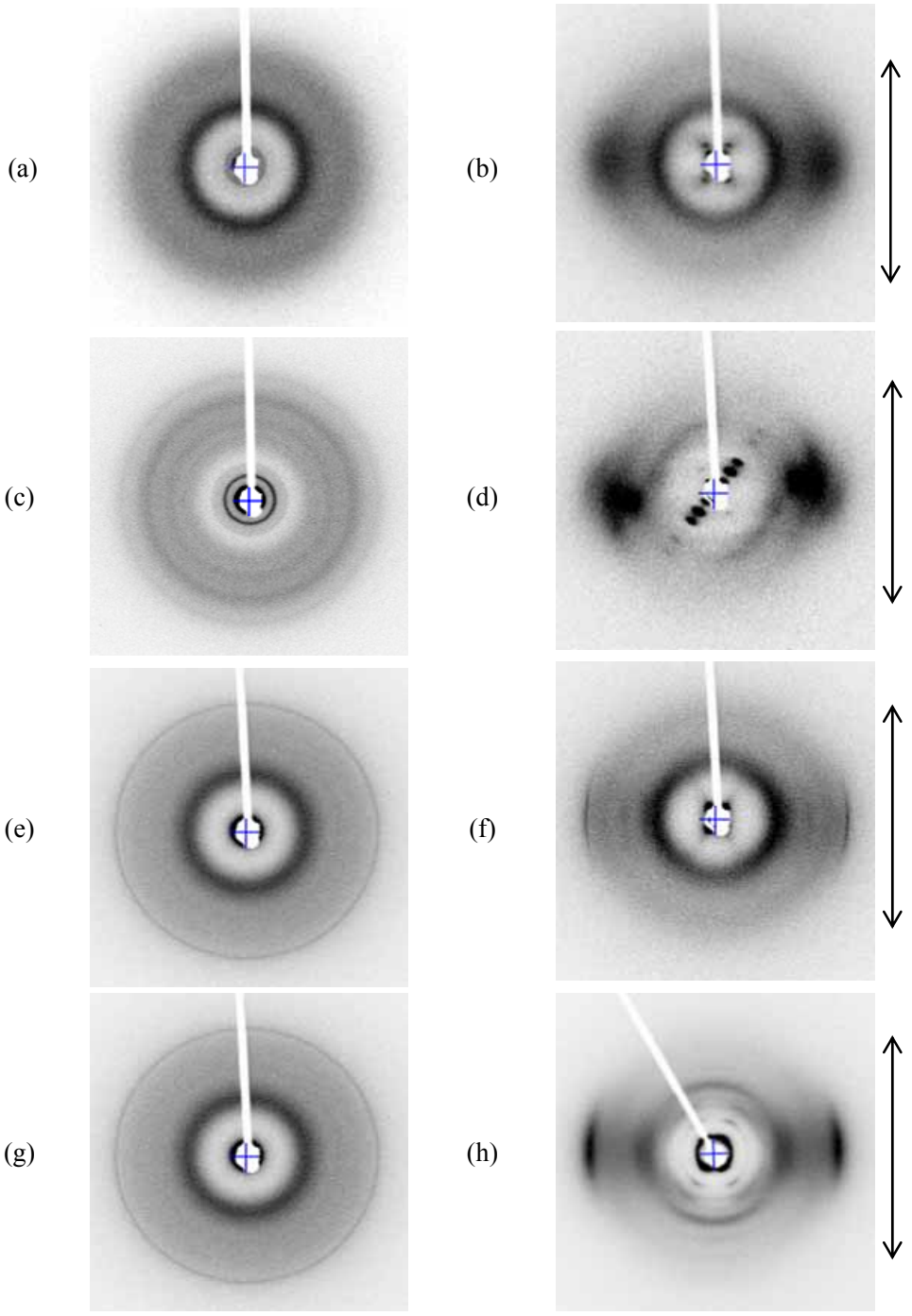

Figure 4-53 Room temperature WAXD patterns of AQ series of LC elastomers: (a) AQ11Si8XL10 (as-cast); (b) AQ11Si8XL10 (stretched); (c) AQ11Si3XL10 (as-cast); (d) AQ11Si3XL10 (stretched); (e) AQ5Si8XL10 (as-cast); (f) AQ5Si8XL10 (stretched); (g) AQ5Si3XL10 (as-cast); (b) AQ5Si3XL10 (stretched).

This diffraction comes from the siloxane spacer and the crosslinker having an interchain

distance around 7.1 Å. In the wide angle region, there are two arcs (*d*-spacing, 4.3 Å) with peak intensity maxima on the equator, which indicates the hydrocarbon chains are partially oriented along the stretching direction.

AQ11Si3XL10 contains a long hydrocarbon chain and a short siloxane spacer. Characteristic π-π stacking diffraction only is seen in its as-cast form. After being stretched, that diffraction cannot be detected. For the stretched specimen, a series of diffractions is observed located mainly along a direction at an angle to the meridian or equator as is seen in Figure 4-53 (d). At the roughly symmetrical position to the direction having strong diffraction intensity, diffraction is still present but it is very weak. This observation means that the majority of smectic layers tilt in one direction with the director pointing along the stretching direction. The smectic layer spacing calculated from the strong diffraction is around 31 Å. The layer spacing corresponding to weak diffraction is around 34 Å. For the unoriented as-cast specimen, the diffractions from these two different layers can not be distinguished. The pattern also illustrates that the siloxane segments are poorly oriented along the stretching direction. In the wide angle region, the different pattern consists of two parts. One part has the diffraction intensity maxima on the equator, which means the hydrocarbon chains are oriented along the stretching direction. The other part of the diffraction has its intensity maxima at an angle to the equator, which indicates some hydrocarbon chains are inclined to the stretching direction.

AQ5Si8XL10 comprises a short hydrocarbon chain and a long siloxane spacer. The characteristic π-π stacking diffraction is detected both in the unoriented as-cast and stretched specimens. A symmetrical cross shaped diffraction pattern is seen at the small

angle region indicating a smectic C mesophase. The smectic layer spacing is around 29 Å. Diffraction at the middle and wide angle region illustrate poor orientation of siloxane and hydrocarbon chains along the stretching direction.

AQ5Si3XL10 contains the short hydrocarbon chain and the short siloxane spacer. A strong characteristic π-π stacking diffraction was detected in both the as-cast and stretched specimens. The Bragg spots at small angle region are arranged in a cross shape indicating the existence of smectic C layered structures.

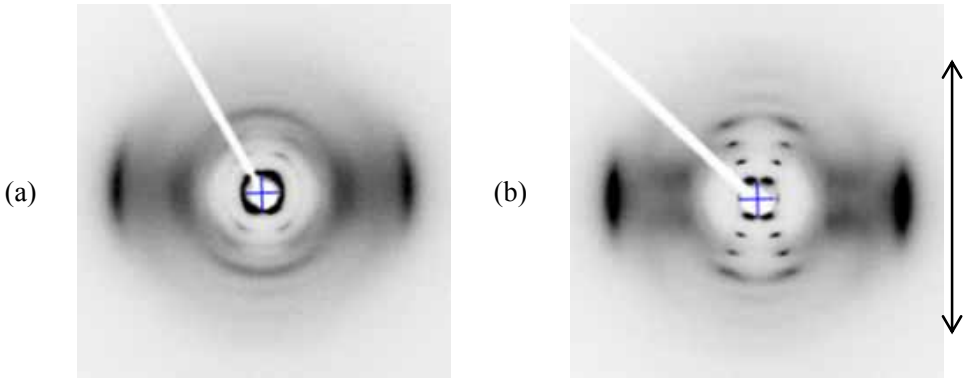

Figure 4-54 Room temperature WAXD patterns of AQ5Si3XL10 specimens: (a) stretched at room temperature; (b) stretched in isotropic phase and cooled down to room temperature**.**

In addition to a specimen being stretched at room temperature, another specimen was stretched in its isotropic phase and cooled down to room temperature for X-ray study. The patterns of these specimens stretched under the two different conditions are shown in Figure 4-54. It is seen that stretching in the isotropic phase resulted in a very ordered structure. Compared with the specimen stretched at room temperature seen in Figure 4-54 (a), the diffraction of the specimen stretched in the isotropic phase is very different in Figure 4-54 (b). For instance, the primary diffraction is clearly split into four spots. All its high-order diffraction spots become very sharp. Even the fourth order diffraction can be distinguished. An important observation is that the scattering regions that normally

show characteristic diffractions between hydrocarbon chains and between siloxane chains exhibit only very weak and smeared patterns. This could result from a special arrangement of AQ molecules. A possibility is that the columns are formed by alternatively crossed AQ molecules [57] as illustrated in Figure 4-55.

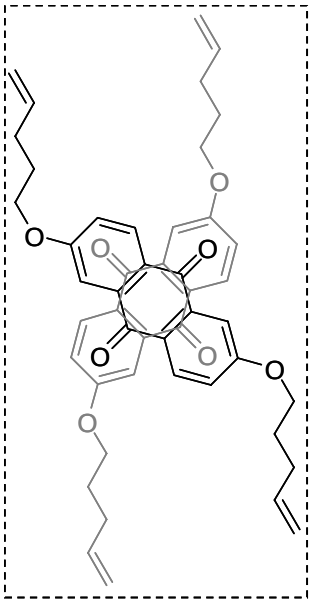

Figure 4-55 AQ cores are stacked in an alternatively crossed style to form columnar structure**.**

Thermal analysis used to examine these AQ samples. Their DSC profiles are compared in Figure 4-56. Among them, the LCEs with short siloxane spacer (**Si3**), AQ5Si3XL20 and AQ11Si3XL20, show stable mesophase to isotropic phase transitions.

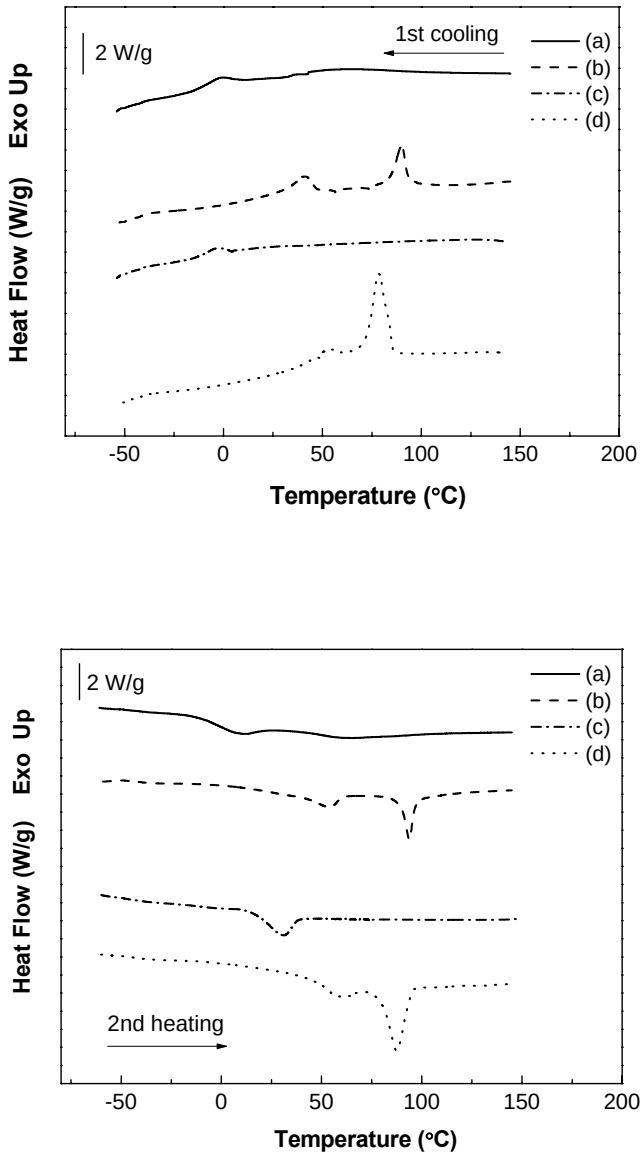

Figure 4-56 DSC profiles (2nd heating) of AQ series of LCEs: (a) AQ11Si8XL10; (b) AQ11Si3XL10; (c) AQ5Si8XL10; (d) AQ5Si3XL10**.**

For AQ5Si3XL20, there are two pairs of transition peaks in a full thermal cycle. On the heating run, one peak is at 59 °C (ΔH = 2.7 w/g) and the other is at 87 °C (ΔH = 10.9 W/g). In cooling run, one peak is at 53 °C (ΔH = 1.5 w/g) and the other is at 78 °C (ΔH = 11.3 W/g). For AQ11Si3XL20, there are also two pairs of transition peaks in a full

thermal cycle, but with the peaks further seperatred. In its heating run, one peak is at 54 °C (ΔH = 4.8 W/g) and the other is at 94 °C (ΔH = 8.3 W/g). In its cooling run, one peak is at 41 °C (ΔH = 3.8 W/g) and the other is at 90 °C (ΔH = 8.5 W/g). For LCEs with the long siloxane spacer (**Si8**), a weak mesophase to isotropic transition was observed in AQ11Si8XL10 and an almost room temperature mesophase was found in AQ5Si8XL10. This result further proves that an optimum combination of the length of hydrocarbon spacer and length of siloxane spacer is necessary to form a stable mesophase. It appears that the short hydrocarbon spacer in AQ monomer and the long siloxane spacer are the worst combination for mesophase formation and LC stability at room temperature.

WAXD of AQ5Si3XL10 and AQ5Si8XL10 indicated the existence of π-π stacking in these materials. Tensile testing of this group of LCEs can also help examine the strong intermolecular interactions between AQ mesogens.

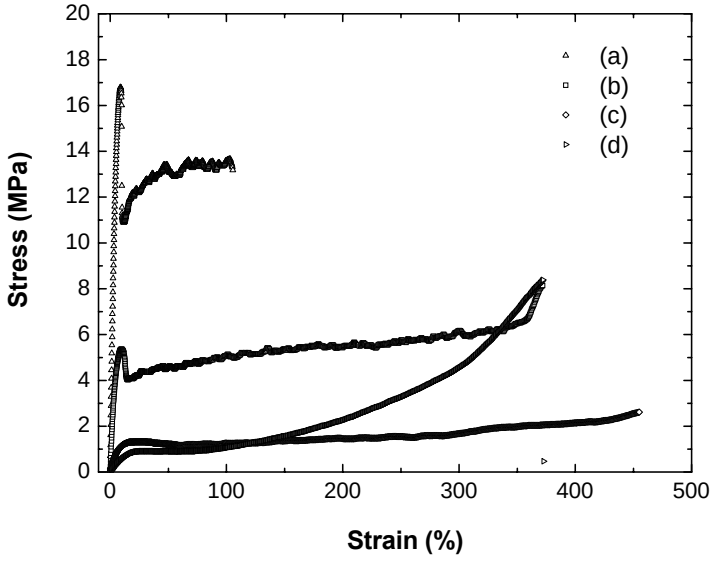

Figure 4-57 Stress-strain curves of AQ series of MCLCEs: (a) AQ5Si3XL10 (E = 314 MPa); (b) AQ11Si3XL10 (E = 110 MPa); (c) AQ5Si8XL10 (E = 19 MPa); (d). AQ11Si8XL10 (E = 6 MPa).

In Figure 4-57, both AQ5Si3XL10 and AQ11Si3XL10 show a yield point on their stress-strain curves. The higher value of yield stress for AQ5Si3XL10 compared to that of AQ11Si3XL10 likely indicates the intermolecular interactions in AQ5Si3XL10 are stronger than those in AQ11Si3XL10. Because a weak π-π stacking diffraction was only observed in the unoriented as-cast AQ11Si3XL10, it indicates that a long hydrocarbon spacer in an AQ mesogen is not favorable for π-π stacking. As for AQ11Si8XL10 and AQ5Si8XL10, both of them have relatively low values of Young's modulus and low yield stress which indicates long siloxane spacers are also not favorable for π-orbital overlap. Because the melting point of AQ5Si8XL20 is about 30 °C, which is very near to room temperature, its stress-strain response looks like a viscous flow. AQ11Si8XL10 has a broad mesophase to isotropic phase transition with peak maximum temperature (68 °C) higher than room temperature. Therefore, at room temperature, it does not behave like a viscous material but more like a typical LCE with an obvious strain hardening phenomenon at high strains. Although the as-cast AQ5Si3XL10 has the highest modulus in this family, it also has the lowest elongation at break. After annealing in the isotropic phase for five minutes, the specimen is much more extendable. It can bear more than 450% extension. In Figure 4-58, the modulus of the specimen with annealing decreases from 314 MPa to 222 MPa. But it is still higher than the modulus of all the other AQ elastomers. The less flexible short hydrocarbon chains permit ordering of the π-systems of the AQ mesogens and the short siloxanes are not sufficiently disordering as to prevent good π-stacking organization. The greater flexibility of either spacer at longer lengths is detrimental to this π-stacking arrangement.

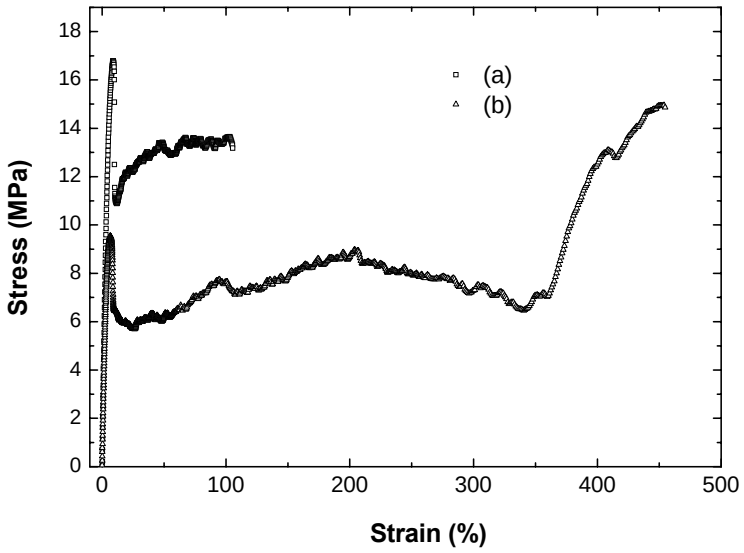

Figure 4-58 Nominal Stress-strain curve of AQ5Si3XL10: (a) without annealing (E = 314 MPa); (b) with annealing (E = 222MPa).

4.11 Results and Discussions

In this chapter, we have discussed the influence on mechanical properties of main-chain LC elastomers in a polydomain state by varying chemical structures, such as crosslinker content, siloxane spacer length, hydrocarbon spacer length, lateral substituents on the mesogenic core and in-chian loading of a non-mesogenic terphenyl transverse rod. The effects of experimental conditions, such as temperature and strain rate, on mechanical properties were also discussed. The mechanical property studies include stress-strain behavior, strain recovery, stress relaxation, mechanical hysteresis and Strainsratio.

A general trend was observed in C11(MeHQ)Si8 elastomers by varying crosslinker content from 5 mol% to 25 mol%. The higher crosslinker content results in

higher Young's modulus, higher threshold stress to polydomain-to-monodomain (*P-M*) transition plateau (or yield stress), shorter plateau region and lower elongation at break. Compared with the linear LC polymer C11(MeHQ)Si8, crosslinking imparts additional restrictions on polymer chain movement. When the crosslinking density is as low as 5% - 10 mol%, mesogens on the polymer backbone can still move relatively freely and self-organize to form an ordered structure. With increasing amount of crosslinker, perturbations from mesogen mobility become significant. A numerical calculation relates the average number of mesogens between netpoints to the crosslinker content. With lower crosslinker content, a small change in crosslinker content decreases the number of mesogens between netpoints dramatically. When crosslinker content exceeds 10 mol%, the change in the number of mesogens between netpoints is slower. This non-linear relation between these two parameters was consistent with the average molecular weight between netpoints calculated from the mechanical experiments.

In this work, C11(MeHQ)Si8XL10 was chosen as the parent LCE and given intensive studies on its mechanical properties. It shows a typical three-region stress-strain curve of LC elastomers. At small strains, the material is fully elastic and deformation occuring in this region can be recovered quickly. The second region begins with a threshold stress to the *P-M* transition region. After overcoming this threshold stress, the curve enters a plateau region. A unique polydomain-to-monodomain transition takes place in these regions, which involve the rotation of individual domains following a low energy soft deformation path towards the stretching direction. It is macroscopically reflected by the flat shape of the curve in this region. In this way, domains originally only having locally preferred orientation become oriented macroscopically. Optically,

the polydomain specimen is originally opaque because of the misalignment of the refractive index of domains. Upon stretching, domains rotate towards stretching direction so that their refractive indices have a preferred orientation and the specimen becomes transparent gradually during this process.

According to Warner and Terentjev, the threshold stress to the *P-M* plateau and the length of the plateau region are related to the chain anisotropy. The higher chain anisotropy of a network results in a higher threshold stress. The length of the plateau, therefore, also depends on the chain anisotropy. Main-chain LC elastomers normally have higher chain anisotropy than side-chain LC elastomers. C11(MeHQ)Si8XL10 is a main-chain LC elastomer. Compared with ordinary side-chain LC elastomers, it has a higher threshold stress (of 1.2 MPa) and a longer plateau region (from 40% - 120%). The dependence of both the threshold stress and the length of *P-M* plateau on the chain anisotropy were consistent with by stress-strain measurements at elevated temperature. A fast decrease both in threshold stress and length of plateau was found in stress-strain measurements of C11(MeHQ)Si8XL10 LCE at elevated temperatures. The polymer main chain of LCE gets less anisotropic when the temperature gets higher. When the temperature is above the clearing temperature, the LC elastomer becomes isotropic and behaves the same as a conventional elastomer.

The dependence of stress-strain response of LCEs on strain rate was investigated by varying the strain rates from 5×10^{-2} s^{-1} to 5×10^{-4} s^{-1}. At the small strain region (< 1%), the stress response is less dependent on strain rate. It becomes more dependent on strain rate at the large strain region. Both C11(MeHQ)Si8XL10 (with long siloxane spacer) and C11(MeHQ)Si3XL10 (with short siloxane spacer) show lower Young's modulus, lower

threshold stress to *P-M* transition and a flatter plateau region at lower strain rate than that at higher strain rate.

Three siloxane spacers were chosen to investigate their influences on the mechanical properties of LC elastomers. They are 1,1,3,3,5,5-hexamethyl-trisiloxane (**Si3**), polydimethylsiloxane (**Si8**) and 1,4-bis(dimethylsilyl)benzene (**Siph**). It was found that the Young's modulus of LCEs with relatively shorter spacer **Si3** and **Siph** is higher than the LCE with longer spacer **Si8** at room temperature. DSC analysis showed the glass transition temperature with different spacer follows **Si8** < **Si3** < **Siph**, which is consistent with the Young's moduli of these materials. Among these three LCEs, C11(MeHQ)**SiPh**XL10 with a stiffer spacer structure has the shortest P-M transition plateau but the highest tensile strength. All of the LCEs could undergo more than 300% elongation.

It was found that both hydrocarbon spacer and siloxane spacer lengths determine the integrity of the LC elastomer films. The combination of short hydrocarbon chain **C3** and long spacer **Si8** always results in a tacky product. But, replacing **C3** with **C5** can produce a non-sticky and integral film. The film **C11**(MeHQ)Si8XL10 with the longest hydrocarbon spacer **C11** among these variations is always smooth and well formed. As-cast film of **C3**(MeHQ)Si3XL10 is less tacky than **C3**(MeHQ)Si8XL10 but it becomes tacky gradually with time. **C5**(MeHQ)Si3XL10 and **C11**(MeHQ)Si3XL10 are both able to be fabricated into smooth and robust films. It was found that LC elastomers with shorter spacer **Si3** always have higher stress response than those with the longer spacer **Si8** when undergoing uniaxial extension. However, the effect of hydrocarbon spacer on the stress-strain behavior of LC elastomers with **Si3** spacer is different from those with

Si8 spacer. For elastomers with short spacer **Si3**, a short hydrocarbon spacer **C5** gives the material a higher Young's modulus, a higher yield stress, a higher tensile strength but a short *P-M* transition plateau than the one with **C11**. When **Si8** was used as spacer, an opposite effect was found when varying the hydrocarbon spacer. In general, **C5**(MeHQ)Si8XL10 exhibits lower Young's modulus, threshold stress to *P-M* transition, elongation at break and tensile strength than **C11**(MeHQ)Si8XL10.

A small chemical modification of the mesogenic units of LC elastomers can results in a quite different mechanical properties. In addition to C11(**MeHQ**)Si8XL10 with a methyl substituent on the central aromatic ring, two other LC elastomers C11(**4H**)Si8XL10 and C11(**4F**)Si8XL10 were studied. C11(**4H**)Si8XL10 has no substituents on the central benzene ring. C11(**4F**)Si8XL10 has the central benzene ring fully substituted by fluorine atoms. This modification makes these two elastomers have different symmetry and steric effect of the mesogenic units and different secondary interaction strengths between chains compared with C11(**MeHQ**)Si8XL10. The LCE C11(**MeHQ**)Si8XL10 shows the lowest stress response to the external force among these elastomers, mainly because its less symmetrical mesogenic core, great breadth due to the lateral methyl group, results in poor intralamellar packing. The other two elastomers having symmetrical mesogenic units show much stronger mechanical properties. Their Young's modulus is almost an order of magnitude higher than that of C11(**MeHQ**)Si8XL10. They also exhibit an observable necking of the specimen upon stretching, which is not the case for C11(**MeHQ**)Si8XL10. In addition, C11(**4F**)Si8XL10 has higher stress response than C11(**4H**)Si8XL10. Although the steric effect of fluorine substituents could disrupt the lamellar packing, the strong polarity of C-

F bonds induces strong intermolecular interactions between fluorine substituents enhancing the lamellar organization.

Incorporating the laterally attached non-mesogenic transverse rod **TR3** generally decreases the properties of the parent LCE C11(MeHQ)Si8XL10. Although the LCE with 10 mol% **TR3** shows similar stress-strain response to that of its parent, LCEs with 30 mol% **TR3** and 40 mol% **TR3** behave much like ordinary elastomers with low Young's modulus and an almost unobservable P-M plateau. The LCE with 20 mol% **TR3** behaves differently from the others. After a linear region similar to the parent LCE, it shows an observable yield point and then enters a plateau region. The stress increases rapidly after a short plateau and then is followed by a failure at relatively lower elongation (< 300%). The 20 mol% **TR3** was thought possibly to be a critical loading for the auxetic effect. Below 20 mol% **TR3** loading, the number of transverse rods might be too low and the rotation of transverse rods to the chain normal might be surpressed. Above 20 mol% **TR3** loading, liquid crystalline order is weak or non-existant so it is difficult to obtain a good pre-alignment of transverse rods along the polymer backbone which is needed for the site-connectivity driven transverse rod rotation mechanism to achieve auxetic effect at the molecular level.

Room temperature strain recovery studies were performed on our main-chain LC elastomers to investigate their strain retention capability in connection to potential shape memory effects. C11(MeHQ)Si8XL10 was again chosen as the parent LCE for this study. All the shape recovery curves show a fast decay within one minute and then a slower recovery. A significant dependence of strain retention on initial imposed strain was found. Only the specimen with 50% initial strain can fully recover of its deformation by

itself after removal of load. All other specimens with higher strain always retain some amount of strain. The specimen with larger initial strain exhibits larger final strain retention (or residual strain). The monodomain smectic structure was thought to lock in the deformation. Higher initial strain induces more monodomain structure in the specimen. Therefore more deformation can be retained by the more perfect monodomain. The greater capacity to retain specimen deformation with higher initial strain was consistent with the results from LCE thermal analysis having different initial strains. A continuous upward shift in the clearing transition temperatures and a broadening in peak area with increasing initial strain were observed in the first heating cycle by DSC. Compared with the unstretched specimen, there is about a 4 °C upward shift in mesophase to isotropic phase transition temperature in the specimen with 350% initial strain (the highest applied strain), although the corresponding transition peak was much broaden and less sharp compared with that of the unstretched specimen. A second stress-strain measurement of specimens having been given different initial strains and then been allowed to partially relax illustrated the effect of retained strain on the mechanical properties of LC elastomers. It was found that larger the initial stain leads to higher Young's modulus, shorter plateau region, smaller elongation at break and larger tensile strength. In addition, the strain retention was found to be independent of strain rate, although the strain rate has an apparent effect on the stress-strain behavior on LC elastomers. A full dimensional recovery of the deformation was observed for a sample heated to a temperature located at the onset of the mesophase to isotropic phase transition.

The effect of crosslinker content on the shape recovery behavior was examined by giving the specimen 150% and 180% initial strain. For these two given initial strains, it

was found that residual strains of LC elastomers have litter dependency on crosslinker content.

The effect of chemical variations on the strain recovery behavior of LC elastomers was investigated by giving a series of LCEs 250% initial strain. It was found that the strain retention ability of the LCEs with different siloxane spacers follows **Si3** > **Siph** > **Si8**, which matches the sequence of their clearing temperatures. For a fixed siloxane spacer **Si3** or **Si8**, LC elastomers with long hydrocarbon spacer could always retain more strain than the one with short hydrocarbon chain. The former has a higher clearing temperature than the latter. A higher the clearing temperature translates to the presence of a more stable mesophase at room temperature. With the combination effect of hydrocarbon spacer and siloxane spacer, it is obvious that the mesophase stability of LC elastomers plays a very important role in the strain retention. The contribution of mesophase stability on the shape retention is further confirmed by studying the strain retention of C11(MeHQ)Si8XL10 with various amount of **TR3**. A continuous decrease in strain retention with increasing **TR3** loading was observed. DSC analysis has already showed the disrupting nature of **TR3** to the mesophase stability. In addition, it was also found that the effect of the lateral substituents of mesogenic units on the strain retention ability is not as significant as it is on the stress-strain behaviors of these LC elastomers.

Monodomain LC elastomers can be obtained by a secondary crosslinking of pre-aligned LC elastomers or by a mechanical extension. Our C11(MeHQ)Si8XL10 monodomain specimens were prepared by following the latter method. Mechanical properties were examined in two directions. One direction is parallel to the director. The other is perpendicular to the director. The monodomain specimens being stretched in

these two directions show very different mechanical properties. The Young's modulus of the monodomain sample being stretched parallel to the smectic layer normal is roughly four times that of the monodomain sample being stretched perpendicular to the director. The most impressive observation is that the monodomain sample stretched perpendicular to the director can undergo ~800% elongation with a long plateau region ranging from ~ 50% to ~ 450% applied strain. This observation is of great significance since it illustrates the predicted soft elasticity phenomenon in smectic-C type of main-chain LC elastomers. C11(MeHQ)Si8XL10 with 20 mol% **TR3** monodomain specimens show similar properties to that of its parent LC elastomer in a similar experiment.

"Poisson's ratio" (strains ratio) of LC elastomers was investigated over a wide strain region by examining the effects of crosslinking and **TR3**. A numerical calculation showed a gradual decrease of Strains ratio with strains in an ideal rubber. Experimentally, the elastomer with 5 mol% crosslinker shows a gradual decrease in strains ratio with strains like an ideal rubber, although its absolute values of Poisson' ratio are smaller than that of the ideal rubber. With increasing the crosslinker to 10 mol%, a convex curve was obtained by plotting strains ratio as a function of strain. For the rest of the elastomers with higher crosslinker content, the convexity of the curves gets larger. In general, strains ratio of these elastomers increases abruptly with strain at the small strain region (<50%) and begins to decrease when the strain goes higher. Strains ratio has a higher value in LC elastomers with higher crosslinker content. A similar trend was observed in C11(MeHQ)Si8XL10 with various amount of **TR3** (10 mol% - 40 mol%) loading. It was found that, for each LCE, strains ratio increases with strain when strain is small (<50%). Further stretching of the sample leads to a decrease in strains ratio. The higher the **TR3**

loading in the LC elastomer results in a larger strains ratio. Lakes *et al*. found that the Poisson's ratio increases with decreasing cell size in polyurethane foam [48]. Because there is no length scale limit in the theory of elasticity, the influential factors on Poisson's ratio at the macroscopic level should also work at the molecular level. In this work, increasing crosslinking loading is analogous to decreasing cell size in polyurethane foams. The effect of crosslinking and **TR3** on the strains ratio follows the same trend observed in Lakes' experiments. Strains ratio begins to decrease after the applied strain passes a critical point. After passing a critical strain, the materials have been significantly deformed and the change in lateral strain cannot follow the change in longitudinal strain any more. One reason for no negative strains ratio was detected by incorporating **TR3** could be that the rotation of **TR3** was hindered by the smectic layer structure. Although no negative strains ratio was found by introducing the terphenyl transverse rod, this result indicates that it is possible to tailor strains ratio of LC elastomers by varying the amount of **TR3**.

An interesting phenomenon was found in strains ratio of monodomain C11(MeHQ)Si8XL10 LCE and C11(MeHQ)Si8XL10 with 20 mol% **TR3**. These LCEs have zero Poisson's ratio at small strains (< 10%) when the specimen was deformed in the direction perpendicular to the director. When stretching the materials in the direction parallel to the director, Poisson's ratio decreases from about 0.5 with increasing strain. Zero Poisson's ratio in the direction perpendicular to the director indicates a constant dimension in the direction parallel to director, which could result from the in-plane flow of mesogenic units within the smectic layers.

A main-chain LC elastomer TR5Si3XL10 with a specially designed *p*-phenylene

transverse rod (**TR5**) was synthesized in our lab. This material is rigid at room temperature. Its as-cast film has a high Young's modulus about 296 MPa but low elongation at break. After annealing, its Young's modulus decreases to 133 MPa and becomes much more extendable (>500% extension). Upon stretching, necking occurs and the sample in that region becomes transparent from its originally opaque state. The necking part also becomes soft but returns to its originally rigid state within a short period of time. Mechanical hysteresis experiments found that it takes about 2 minutes to undergo this soft-rigid transition in the unloading cycle. Although it is difficult to identify the phase type of this material by DSC, a smectic A-like scattering pattern was found in the stretched specimen by wide-angle X-ray diffraction measurement. The unusual molecular architecture of the *p*-pentaphenyl transverse rod provides opportunity for the rod orientation to be either parallel or normal to the main chain under uniaxial tension. The structural model with *p*-phenylene transverse rods normal to the main chain is thought to be the most likely from X-ray analysis. The CPK molecular model showed that the layer spacing measured from **TR5** to **TR5** (or the layer from siloxane to siloxane) matches the layer spacing measured by WAXD.

In addition to LC elastomers with calamitic mesogens, LC elastomers with flat-shaped anthraquinone LC monomers were also studied in this work. Because of the flat-shaped aromatic moieties in AQ molecules, they tend to stack on top of each other to likely form a column-like structure. The specific combination of hydrocarbon chain and siloxane spacer is critical to form a columnar structure. It was found that the combination of short hydrocarbon spacer **C5** and short siloxane spacer **Si3** gives the LC elastomer AQ5Si3XL10 the best possibility to form a columnar structure. This LCE has very

strong characteristic π-π stacking diffraction and a well ordered smectic C mesophase. Compared with the other members in the AQ family, the highest Young's modulus (314 MPa in as-cast film and 222 MPa in annealed film) was found in AQ5Si3XL10, which is consistent with the strong intermolecular interactions between AQ molecules. Since the characteristic diffractions between hydrocarbon chains are very weak and smeared in this material, an alternatively crossed arrangement of AQ molecules in a column could be possible.

4.12 References

[1] M. Warner and E. M. Terentjev, *Liquid crystal elastomers*. Oxford ; New York: Clarendon Press ; Oxford University Press, 2003.

[2] J. Kupfer and H. Finkelmann, "Liquid-crystal elastomers - Influence of the orientational distribution of the cross-links on the phase-behavior and reorientation processes," *Macromolecular Chemistry and Physics*, vol. 195, pp. 1353-1367, 1994.

[3] H. Finkelmann, H. J. Kock, W. Gleim, and G. Rehage, "Investigations on liquid-crystalline polysiloxanes. 5. Orientation of LC-elastomers by mechanical forces," *Makromolekulare Chemie-Rapid Communications*, vol. 5, pp. 287-293, 1984.

[4] P. J. Flory, *Principles of polymer chemistry*. Ithaca,: Cornell University Press, 1953.

[5] F. Rodriguez, *Principles of polymer systems*, 4th ed. Washington, DC: Taylor & Francis, 1996.

[6] I. M. Ward and D. W. Hadley, *An introduction to the mechanical properties of solid polymers*. Chichester ; New York: J. Wiley & Sons, 1993.

[7] C. Ortiz, M. Wagner, N. Bhargava, C. K. Ober, and E. J. Kramer, "Deformation of a polydomain, smectic liquid crystalline elastomer," *Macromolecules*, vol. 31, pp. 8531-8539, 1998.

[8] J. Schatzle, W. Kaufhold, and H. Finkelmann, "Nematic elastomers - the influence of external mechanical-stress on the liquid-crystalline phase-behavior," *Makromolekulare Chemie-Macromolecular Chemistry and Physics*, vol. 190, pp. 3269-3284, 1989.

[9] S. M. Clarke, E. Nishikawa, H. Finkelmann, and E. M. Terentjev, "Light-scattering study of random disorder in liquid crystalline elastomers," *Macromolecular Chemistry and Physics*, vol. 198, pp. 3485-3498, 1997.

[10] S. V. Fridrikh and E. M. Terentjev, "Order-disorder transition in an external field in random ferromagnets and nematic elastomers," *Physical Review Letters*, vol. 79, pp. 4661-4664, 1997.

[11] M. He, W. Chen, and X. Dong, *Polymer physics*. Shang Hai, China: Fu Dan University Press, 1991.

[12] B. Donnio, H. Wermter, and H. Finkelmann, "Simple and versatile synthetic route for the preparation of main-chain, liquid-crystalline elastomers," *Macromolecules*, vol. 33, pp. 7724-7729, 2000.

[13] S. M. Clarke, E. M. Terentjev, I. Kundler, and H. Finkelmann, "Texture evolution during the polydomain-monodomain transition in nematic elastomers," *Macromolecules*, vol. 31, pp. 4862-4872, 1998.

[14] M. Giamberini, P. Cerruti, V. Ambrogi, C. Vestito, F. Covino, and C. Carfagna, "Liquid crystalline elastomers based on diglycidyl terminated rigid monomers and aliphatic acids. Part 2. Mechanical characterization," *Polymer*, vol. 46, pp. 9113-9125, 2005.

[15] S. V. Fridrikh and E. M. Terentjev, "Polydomain-monodomain transition in nematic elastomers," *Physical Review E*, vol. 60, pp. 1847-1857, 1999.

[16] N. R. Barnes, F. J. Davis, and G. R. Mitchell, "Molecular switching in liquid-crystal elastomers," *Molecular Crystals and Liquid Crystals*, vol. 168, pp. 13-25, 1989.

[17] F. J. Davis, A. Gilbert, J. Mann, and G. R. Mitchell, "Liquid-crystal elastomers - Synthesis and characterization," *Journal of Polymer Science Part a-Polymer Chemistry*, vol. 28, pp. 1455-1472, 1990.

[18] A. Hotta and E. M. Terentjev, "Long-time stress relaxation in polyacrylate nematic liquid crystalline elastomers," *Journal of Physics-Condensed Matter*, vol. 13, pp. 11453-11464, 2001.

[19] N. Assfalg and H. Finkelmann, "A smectic A liquid single crystal elastomer (LSCE): Phase behavior and mechanical anisotropy," *Macromolecular Chemistry and Physics*, vol. 202, pp. 794-800, 2001.

[20] S. M. Clarke and E. M. Terentjev, "Slow stress relaxation in liquid crystal elastomers and gels," *Faraday Discussions*, pp. 325-333, 1999.

[21] I. A. Rousseau, "Development of soft polymeric networks showing actuation

behavior: from hydorgels to liquid crystalline elastomers," *PhD Thesis, University of Connecticut*, 2004.

[22] M. A. A. Cortes, "Synthesis and physical properties of unsymmetric main-chain liquid crystal elastomers," *PhD Thesis, University of Exeter*, 2006.

[23] G. B. Crevoisier, P. Fabre, J. M. Corpart, and L. Leibler, "Switchable tackiness and wettability of a liquid crystalline polymer," *Science*, vol. 285, pp. 1246-1249, 1999.

[24] P. J. Collings and M. Hird, *Introduction to liquid crystals : chemistry and physics*. London ; Bristol, PA: Taylor & Francis, 1997.

[25] A. M. Donald and A. H. Windle, *Liquid crystalline polymers*. Cambridge [England] ; New York: Cambridge University Press, 1992.

[26] G. W. Ehrenstein and R. P. Theriault, *Polymeric materials : structure, properties, applications*. Munich Cincinnati, OH: Hanser ; Hanser Gardner Publications, 2001.

[27] R. Quinson, J. Perez, M. Rink, and A. Pavan, "Components of non-elastic deformation in amorphous glassy polymers," *Journal of Materials Science*, vol. 31, pp. 4387-4394, 1996.

[28] O. B. Salamatina, S. N. Rudnev, T. V. Paramzina, M. A. Kravchenko, V. P. Shantarovich, and E. F. Oleinik, "Plastic deformation of the copolyester Vectra A (TM) in the glassy mesomorphic state," *Polymer Science Series A*, vol. 46, pp. 1093-1107, 2004.

[29] E. F. Oleinik, S. N. Rudnev, O. B. Salamatina, S. V. Shenogin, M. I. Kotelyanskii, T. V. Paramzina, and S. I. Nazarenko, "Energy storage in cold non-elastic deformation of glassy polymers," *E-Polymers*, 2006.

[30] O. A. Hasan and M. C. Boyce, "Energy-storage during inelastic deformation of glassy-polymers," *Polymer*, vol. 34, pp. 5085-5092, 1993.

[31] T. M. Kung and J. C. M. Li, "Recovery processes in amorphous polymers," *Journal of Materials Science*, vol. 22, pp. 3620-3630, 1987.

[32] L. David, R. Quinson, C. Gauthier, and J. Perez, "The role of anelasticity in high stress mechanical response and physical properties of glassy polymers," *Polymer Engineering and Science*, vol. 37, pp. 1633-1640, 1997.

[33] A. Pegoretti, A. Guardini, C. Migliaresi, and T. Ricco, "Investigation of nonelastic response of semicrystalline polymers at high strain levels," *Journal of Applied Polymer Science*, vol. 78, pp. 1664-1670, 2000.

[34] T. Ricco and A. Pegoretti, "Energy storage and strain-recovery processes in highly deformed semicrystalline poly(butylene terephthalate)," *Journal of Polymer Science Part B-Polymer Physics*, vol. 40, pp. 236-243, 2002.

[35] D. R. Uhlmann and J. B. Park, "Recovery of deformed polymers. 2. Repeated cold drawing of polycarbonate, polyethylene, and polypropylene," *Journal of Applied Physics*, vol. 42, pp. 3800, 1971.

[36] J. B. Park and D. R. Uhlmann, "Recovery of deformed polymers .1. Retraction of cold-drawn polycarbonate, polyethylene, and polypropylene," *Journal of Applied Physics*, vol. 41, pp. 2928, 1970.

[37] J. B. Park and D. R. Uhlmann, "Recovery of deformed polymers. 3. Thermal properties," *Journal of Applied Physics*, vol. 44, pp. 201-206, 1973.

[38] K. Urayama, S. Honda, and T. Takigawa, "Slow dynamics of shape recovery of disordered nematic elastomers," *Physical Review E*, vol. 74, 2006.

[39] I. A. Rousseau and P. T. Mather, "Shape memory effect exhibited by smectic-C liquid crystalline elastomers," *Journal of the American Chemical Society*, vol. 125, pp. 15300-15301, 2003.

[40] M. Warner, K. P. Gelling, and T. A. Vilgis, "Theory of nematic networks," *Journal of Chemical Physics*, vol. 88, pp. 4008-4013, 1988.

[41] F. J. Davis and G. R. Mitchell, "Liquid crystal elastomers: controlled crosslinking in the liquid crystal phase," *Polymer*, vol. 37, pp. 1345-1351, 1996.

[42] R. Zentel, "Shape variation of cross-linked liquid-crystalline polymers by electric-fields," *Liquid Crystals*, vol. 1, pp. 589-592, 1986.

[43] B. Wunderlich, *Thermal analysis of polymeric materials*. Berlin: Springer, 2005.

[44] Y. P. Liu, K. Gall, M. L. Dunn, and P. McCluskey, "Thermomechanics of shape memory polymer nanocomposites," *Mechanics of Materials*, vol. 36, pp. 929-940, 2004.

[45] C. Ortiz, C. K. Ober, and E. J. Kramer, "Stress relaxation of a main-chain, smectic, polydomain liquid crystalline elastomer," *Polymer*, vol. 39, pp. 3713-3718, 1998.

[46] M. Warner, P. Bladon, and E. M. Terentjev, "Soft elasticity - Deformation without resistance in liquid-crystal elastomers," *Journal De Physique II*, vol. 4, pp. 93-102, 1994.

[47] S. M. Clarke, A. Hotta, A. R. Tajbakhsh, and E. M. Terentjev, "Effect of cross-linker geometry on equilibrium thermal and mechanical properties of nematic elastomers," *Physical Review E*, vol. 64, pp. 061702 (1-8), 2001.

[48] Y. C. Wang, R. Lakes, and A. Butenhoff, "Influence of cell size on re-entrant transformation of negative Poisson's ratio reticulated polyurethane foams," *Cellular Polymers*, vol. 20, pp. 373-385, 2001.

[49] E. Nishikawa, H. Finkelmann, and H. R. Brand, "Smectic A liquid single crystal elastomers showing macroscopic in-plane fluidity," *Macromolecular Rapid Communications*, vol. 18, pp. 65-71, 1997.

[50] V. Aksenov, J. Blasing, R. Stannarius, M. Rossle, and R. Zentel, "Strain-induced compression of smectic layers in free-standing liquid crystalline elastomer films," *Liquid Crystals*, vol. 32, pp. 805-813, 2005.

[51] S. Berg, V. Krone, and H. Ringsdorf, "Structural variations of liquid-crystalline polymers - Cross-shaped and laterally linked mesogens in main chain and side group polymers," *Makromolekulare Chemie-Rapid Communications*, vol. 7, pp. 381-388, 1986.

[52] J. K. Kallitsis, K. G. Gravalos, A. Hilberer, and G. Hadziioannou, "Soluble polymers with laterally attached oligophenyl units for potential use as blue luminescent materials," *Macromolecules*, vol. 30, pp. 2989-2996, 1997.

[53] L. Larios-Lopez, D. Navarro-Rodriguez, R. J. Rodriguez-Gonzalez, B. Donnio,

and D. Guillon, "Liquid crystalline properties of penta(p-phenylene)s modified with short lateral and long terminal alkoxy chains," *Liquid Crystals*, vol. 33, pp. 549-554, 2006.

[54] X. H. Lu, C. B. He, P. W. Liu, and A. C. Griffin, "Structures and properties of liquid-crystalline polymers based on laterally attached oligo p-phenylenes," *Journal of Polymer Science Part A - Polymer Chemistry*, vol. 43, pp. 3394-3402, 2005.

[55] C. B. He, P. W. Liu, A. C. Griffin, C. W. Smith, and K. E. Evans, "Morphology and deformation behaviour of a liquid crystalline polymer containing laterally attached pentaphenyl rods," *Macromolecular Chemistry and Physics*, vol. 206, pp. 233-239, 2005.

[56] H. Kelker, R. Hatz, and C. Schumann, *Handbook of liquid crystals*. Weinheim ; Deerfield Beach, Fla.: Verlag Chemie, 1980.

[57] S. Mery, D. Haristoy, J. F. Nicoud, D. Guillon, S. Diele, H. Monobe, and Y. Shimizu, "Bipolar carrier transport in a lamello-columnar mesophase of a sanidic liquid crystal," *Journal of Materials Chemistry*, vol. 12, pp. 37-41, 2002.

CHAPTER 5

Conclusions and Future Work

5.1. Conclusions

In this work, a number of MCLCPs and MCLCEs with a wide range of chemical variations were successfully synthesized via a standard hydrosilylation reaction. In addition to the ordinary chemical variations, e.g. siloxane spacer length, hydrocarbon spacer length, crosslinker content, lateral substituents on mesogenic monomers, additional chemical variations, such as terphenyl transverse rods, pentaphenyl transverse rod and flat-shaped anthroquinone type of mesogenic monomers, were specially incorporated into MCLCEs and MCLCPs.

We developed an effective approach to fabricate MCLCE free-standing thin films at room temperature by modifying Finkelmann's one-pot method. The reaction time in the flask, a Teflon-coated flat substrate and a slow evaporation of solvent were found critical to obtain a smooth and integral LC elastomer thin film.

The structure-property relationships of our main chain LC polymers and elastomers were established by thermal, X-ray and mechanical analysis. Because of the strong segregation tendency of the siloxane spacer, hydrocarbon spacer and rigid mesogenic segments, most of our MCLCEs and MCLCPs show smectic C type of mesophase. Incorporating terphenyl transverse rods does not change the smectic C mesophase, although they apparently decreased the clearing temperature and broadened the clearing transition peak. The smectic layer structures are thought to hinder the

required rotation and reorientation of the terphenyl transverse rod to achieve the auxetic effect.

The typical three-region stress-strain curve and a polydomain-to-monodomain transition were observed in most of our MCLCEs at room temperature. It was found that short hydrocarbon spacer, short siloxane spacer, high crosslinking content and mesogenic monomer with symmetrical structure generally resulted in stiffer materials associated with higher Young's modulus, higher threshold stress, shorter polydomain-to-monodomain transition region, shorter elongation at break and higher tensile strength.

Specifically, strain recovery experiments of MCLCEs showed a significant dependence of strain retention on the initial maximum strain. The oriented smectic C layered structure or monodomain structure in the MCLCE is thought to be the reason for strain retention. Although chemical variations greatly affect the typical mechanical properties of MCLCEs, these variations do not show great influence on the strain retention abilities of their corresponding LCEs. This observation indicates that strain retention and typical mechanical properties are determined by different molecular mechanisms.

The MCLCE with a pentaphenyl transverse rod showed a highly ordered smectic A mesophase at room temperature associated with a much higher stiffness than ordinary MCLCEs. An interesting soft-to-rigid phenomenon was found in the yield section (originally soft) after removal of the load. This could be described as a self-assembly driven reconstruction process. Three possible molecular models were proposed to describe the arrangement of pentaphenyl transverse rod in the network structure. Among

them, the model with the transverse rod orthogonal to the polymer main chain was thought to be most likely due to X-ray study.

The mechanical properties of MCLCEs with anthraquinone monomers exhibit a great dependence on the combination of hydrocarbon spacer and siloxane spacer. AQ5Si3XL10 with both short hydrocarbon spacer and siloxane spacer shows much higher Young's modulus than the other AQ LCEs. These spacers were thought to contribute to facile and strong π-π stacking between AQ LC monomers detected by X-ray study. A columnar mesophase was probably formed in AQ5Si3XL10.

Poisson's ratio measurement was performed on our MCLCEs with various crosslinker contents and on MCLCEs with various loadings of terphenyl transverse rod in a wide strain range. An increase in Poisson's ratio at small strains and a decrease in Poisson's ratio after a certain strain were found in both systems. Poisson's ratio has a higher value in the LCEs with higher crosslinker content. It also has a higher value in LCEs with higher terphenyl transverse rod loading.

A zero Poisson's ratio was found in the monodomain C11(MeHQ)Si8XL10 and the monodomain C11(MeHQ)Si8XL10 with 20 mol% terphenyl transverse rods when the specimen was deformed in the direction perpendicular to the director at small strain (< 10%). The zero Poisson's ratio could result from the in-plane flows of mesogenic units within the smectic layers.

5.2. Recommendations for the Further Work

Fiber-forming parent LC polymers and LC polymers with transverse rod were synthesized in this project to study the potential auxetic effect. 1,3-substitution was found to be the right substitution pattern of transverse rod. The presence of smectic layer

structure induced by the segregation of siloxane segment prohibits the effective transverse rod rotation upon stretching. In the future, non-siloxane components, such as ether or ester segment, will be used in order to obtain non-layer LC phase. Therefore, the transverse rod rotation will occur more easily.

Strain recovery experiments showed a significant dependence of strain retention on the initial maximum strain. The deformation was thought to be retained due to the monodomain smectic C layered structures. The higher the fraction of monodomain structure results in the higher strain retention. A real time x-ray diffraction measurement of a continuously stretched specimen is suggested to follow the evolution of monodomain structure so that the direct connection between domain structures and strains can be established.

Strain retention and shape recovery are two main parameters to evaluate shape memory effect of a material. They were investigated separately in our work. A full cycle to measure the shape retention and shape recovery of our MCLCEs is suggested. The full cycle consists of heating up the sample, deforming, cooling the sample and heating up the sample again. A three dimensional figure can be plotted with all the collected data [1]. This diagram will show the stress-strain curve at a constant temperature, the strain-temperature curve at a constant stress and the stress-temperature curve at a constant strain. The shape fixing and shape recovery of the materials can be more accurately evaluated by this measurement.

Our Poisson's ratio measurement is good to study Poisson's ratio in a wide strain range. But the experimental error is very sensitive to small strains. More accurate measurements of Poisson's ratio are suggested to compare with our data [2].

In order to determine the arrangement pentaphenyl transverse rods (TR5) in the TR5Si3XL10 network structure, X-ray diffraction measurement is suggested to carry out not only in the x-y plane (width and length plane) but also the other two planes: x-z plane (width and thickness plane) and y-z plane (length and thickness plane). Polarized UV-visible and fluorescence spectroscopy are two other potential methods to identify its structure due to the strong anisotropic polarisability and fluorescence effect of the pentaphenyl transverse rod. A real time X-ray study of the specimen being continuously stretched is suggested to follow the LC structure development during extension.

AQ5Si3XL10 LCE shows strong π-π stacking diffraction by X-ray and large stiffness by mechanical measurements. Whether a columnar mesophase is formed in AQ5Si3XL10 or not still needs to be proved by further X-ray analysis.

5.3. Reference:

[1] I. A. Rousseau and P. T. Mather, "Shape memory effect exhibited by smectic-c liquid crystalline elastomers," *Journal of the American Chemical Society*, vol. 125, pp. 15300-15301, 2003.

[2] M. A. A. Cortes, "Synthesis and Physical Properties of Unsymmetric Main-Chain Liquid Crystal Elastomers," *PhD Thesis, University of Exeter*, 2006.